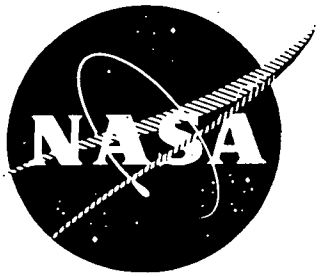

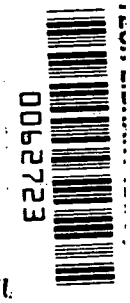

FABRICATION AND VERIFICATION TESTING OF ETM 30 CM DIAMETER ION THRUSTERS

FINAL REPORT

APRIL 1977

BY

ION PHYSICS DEPARTMENT STAFF

HUGHES RESEARCH LABORATORIES
A DIVISION OF HUGHES AIRCRAFT COMPANY
3011 MALIBU CANYON ROAD
MALIBU, CALIFORNIA 90265

PREPARED FOR

NATIONAL AERONAUTICS AND SPACE ADMINISTRATION
NASA LEWIS RESEARCH CENTER

CONTRACT NAS 3-17803

JAMES S. SOVEY, PROGRAM MANAGER

1. Report No.	2. Government Accession No.	3. Recipient's Catalog No.
NASA CR-135193		

4. Title and Subtitle	5. Report Date
FABRICATION AND VERIFICATION TESTING OF ETM 30 CM DIAMETER ION THRUSTERS	April 1977
	6. Performing Organization Code
7 Author(s)	8. Performing Organization Report No.
C. Collett	
9. Performing Organization Name and Address	10. Work Unit No.
Hughes Research Laboratories 3011 Malibu Canyon Road Malibu, CA 90265	11. Contract or Grant No. NAS 3-17803
	13. Type of Report and Period Covered Final Report Mar. 14, 1974-Sept. 15, 1976
12. Sponsoring Agency Name and Address NASA-Lewis Research Center 21000 Brookpark Road Cleveland, OH 44135	14. Sponsoring Agency Code

15. Supplementary Notes

16. Abstract

The original objectives of this program were to (1) fabricate and acceptance test six of the 800-series engineering-model 30 cm electron-bombardment thrusters developed at Hughes Research Laboratories, (2) conduct a 1000 hr verification test of one of the six thrusters, and (3) modify a GFE test console so that the test console could be used to conduct the 1000 hr verification test.

These objectives were modified when it was decided to continue under this contract the endurance test of the first 30 cm engineering-model S/N 701, which had begun under Contract NAS 3-15523. As a result, 7300 hr of the 10,000 hr test were funded under this contract (NAS 3-17803). The entire test is described, as are the results of an extensive post-test analysis of thruster 701.

The 10,000 hr test of thruster 701 demonstrated that ion sputtering within the discharge chamber was a serious life-limiting problem. A joint NASA/Hughes effort results in a package of design changes to minimize this problem. These modifications were available in time for only half of the six thrusters built under this contract. The 800 series design is described first, and then the differences which were incorporated in the 900 series thrusters are identified. Acceptance test results for both 800 series and 900 series thrusters are presented.

17. Key Words (Selected by Author(s))	18. Distribution Statement
Electric Propulsion Ion Propulsion 30-cm Ion Thrusters Testing	

19. Security Classif. (of this report)	20. Security Classif. (of this page)	21. No. of Pages	22. Price*
UNCLASSIFIED	UNCLASSIFIED	281	

*For sale by the Clearinghouse for Federal Scientific and Technical Information, Springfield, Virginia 22151.

Page
Intentionally
Left Blank

TABLE OF CONTENTS

Page
Intentionally
Left Blank

LIST OF ILLUSTRATIONS

PREFACE

The work described herein was performed by personnel of the Hughes Research Laboratories, Malibu, California, and the Space and Communications Group of Hughes Aircraft Company, El Segundo, California. The work at Hughes Research Laboratories was performed in the Ion Physics Department managed by J. H. Molitor; the 10,000 hr endurance test was conducted at Hughes Space Simulation Laboratory managed by H. Allgauer.

This report describes the technical effort conducted under Contract NAS 3-17803 monitored by Mr. James S. Sovey of NASA Lewis Research Center, Cleveland, Ohio. Major technical contributors to this effort were C. R. Collett, Hughes program manager; T. W. Masek, Thruster Project manager; W. E. Schnelker, thruster fabrication; J. J. Caldwell, test facility supervision; and R. L. Poeschel, thruster 701 post-test analysis.

Page
Intentionally
Left Blank

SUMMARY

The original objectives of this program were to (1) fabricate and acceptance test six of the 800-series engineering-model 30 cm electron-bombardment thrusters developed at Hughes Research Laboratories, (2) conduct a 100 hr verification test of one of the six thrusters, and (3) modify a government-furnished test console so that the test console could be used to conduct the 1000 hr verification test.

These objectives were modified when it was decided to continue under this contract the endurance test of the first 30 cm engineering-model thruster S/N 701, which had begun under Contract NAS 3-15523. As a result, 7300 hr of the 10,000 hr test were funded under this contract (NAS 3-17803). The entire test is described, as are the results of an extensive post-test analysis of thruster 701.

The 10,000 hr test of thruster 701 demonstrated that ion sputtering within the discharge chamber was a serious life-limiting problem. A joint NASA/Hughes effort resulted in a package of design changes to minimize this problem. These modifications were available in time for only half of the six thrusters built under this contract. The 800-series design is described first, and then the differences which were incorporated in the 900-series thrusters are identified. Acceptance test results for both 800-series and 900-series thrusters are presented.

Page
Intentionally
Left Blank

SECTION 1

INTRODUCTION

Hughes Research Laboratories (HRL) under NASA sponsorship is actively engaged in developing a 30 cm electron-bombardment ion thruster suitable for prime propulsion systems, both for interplanetary vehicles and orbit raising of synchronous satellites. The original objectives of the program described in this report were to (1) construct and acceptance test six 800-series engineering model (EM) 30 cm ion thrusters, (2) conduct a 1000 hr verification test of one of these thrusters, and (3) upgrade a test console built under a previous endurance test contract so the test console could be used to conduct the 1000 hr verification test.

The 1000 hr verification test was to be conducted in the test facility where the first EM 30 cm thruster (S/N 701) was being endurance tested under Contract NAS 3-15523. When the test of thruster 701 reached 2,700 hr, the number contracted for under NAS 3-15523, NASA decided to continue the test under this contract (NAS 3-17803) and delete the 1000 hr verification test. Thruster 701 was ultimately tested for 10,000 hr, 7300 hr of which were funded under NAS 3-17803. For completeness, the results from the entire test and the details of an extensive post-test analysis of thruster 701 are included in this report.

The endurance test of thruster 701 identified ion sputtering within the discharge chamber as a major wearout mechanism in the first EM 30 cm thruster series. Excessive sputtering creates two problems. First, it erodes discharge-chamber components. Second, sputtering deposits sputtered material which can short out insulators or spall and form large flakes of conductive material. As a result of a joint NASA/ Hughes development and test effort, several design changes were selected as a means of alleviating this problem. These changes were introduced into the 30 cm thruster design midway in the fabrication effort being conducted under this contract. Consequently, three 800

M11326

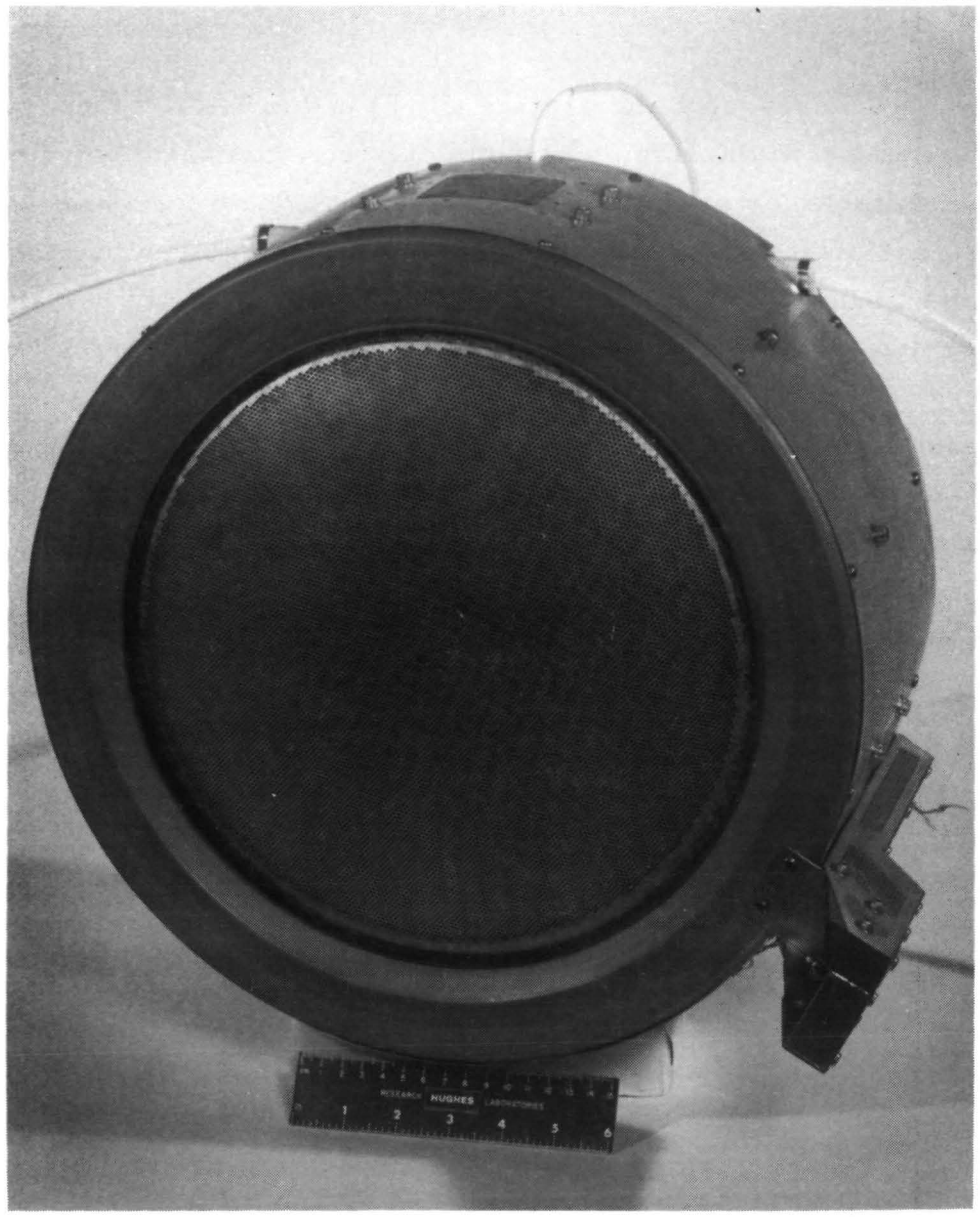

Figure 1. 30 cm EM thruster—900 series.

series and three 900-series thrusters were produced. The first of the 900-series thrusters is shown in Figure 1. This report describes the design of the 800 series and then identifies how the design of the 900 series differs from it. Acceptance test results for these thrusters are also presented.

Page Intentionally Left Blank

SECTION 2

THRUSTER FABRICATION

Six EM 30 cm thrusters were fabricated under this contract. The first three of these had the 800-series configuration, which was developed under NAS 3-16528. The final three had the 900-series configuration, which was developed under this contract. The 800 and 900 series both evolved from the design of the original EM thruster, the 700 series. The design of the 700-series thruster represented a significant step in the development of the 30 cm thruster. Characteristics of that design are discussed in the final report[1] of Contract NAS 3-16528. The 800-series designation was assigned to the configuration created when modifications were introduced to eliminate mechanical problems revealed by the vibration test of thruster 702.

A 10,000 hr endurance test of EM thruster 701 was conducted concurrently with the fabrication of the first 800-series thrusters. As described in Section 3, this test revealed a life-limiting problem in the 30 cm EM thruster—discharge-chamber erosion. The modifications incorporated to minimize this problem resulted in the 900-series thrusters. These modifications were first evaluated in thruster 804. The 800-series thruster design and how it differs from the 900-series design are discussed below.

A. ENGINEERING MODEL THRUSTER DESIGNS

The EM thrusters fabricated under this contract were designed to meet the general specifications listed in Table 1, plus other special requirements. The most important of these additional requirements was that the thruster module should have sufficient structural integrity to meet the launch conditions when mounted at two points to a gimbaling system. A second additional requirement was that the thruster thermal design must not require heat rejection in the direction of the spacecraft or solar array to maintain components within permissible operating temperatures.

Table 1. EM Thruster Design Specifications: 700 and 800 Series

Maximum input power	2.63 kW
Electrical efficiency	84%
Propellant efficiency	86%
Overall efficiency	71.5% ±1%
Effective specific impulse	3000 ±10 sec
Net acceleration voltage	1100 V
Thrust	0.128 ± 0.002 N
Beam current	2 A
Thruster anode diameter	30 cm
Maximum thruster weight	7.8 kg
Throttling capability	2630 to 1140 W input
Lifetime goal	10,000 hr
Maximum thruster envelope	40 cm diameter
Efficiencies and specific impulse are corrected for doubly charged ions and beam divergence.	

T2116

1. 800-Series Design

a. Structural Design

The design of the EM thruster provides a two-point thruster mounting configuration (180° apart) compatible with thruster system designs in which thrust vectoring is achieved by rotating the thruster about an axis normal to the thrust axis. The gimbal shafts are constrained in the axial direction on one side only, thereby imposing large transverse loads on the thruster assembly during launch. It is desirable to provide mounting pads for the gimbal shafts which are accurately positioned and parallel. This will minimize the shimming and remachining required to align the gimbal shafts with respect to each other and

orthogonal to the thrust axis. Other important mechanical constraints are a 7.8 kg weight goal, flexibility in neutralizer and cable exit locations, and additional mounting pads (in case it is desired to mount the thruster from three or more points). The design shown in Figure 2 was conceived from a consideration of all these requirements.

The basic structural element of this design is a cylindrical frame consisting of two annular rings supported by 12 box-type columns. The annular rings are channel-shaped sections located both at the backplate of the thruster and at the ion optics mounting interface. The rings are designed to carry loads in the transverse direction (in the plane of the ring). They have narrow flanges to resist twisting moments which may occur along the gimbal axis. The flanges also resist in-plane twisting and bending forces which could be expected during vibration parallel to the thrust axis. The box-shaped columns strongly resist axial and bending forces.

A tubular cross structure is attached to the backplate of the thruster at the outer edges and to the cathode-isolator-vaporizer (CIV) mounting flange in the center. This serves to support the backplate with CIV, main isolator-vaporizer (MIV), propellant distributor, baffle assembly, and magnets during vibration parallel to the thrust axis. The gimbal mounting brackets are attached to the frame through six insulators. The bolt holes and two locating dowel holes are accurately positioned on each bracket with respect to the grid alignment holes by drilling in a precision fixture after final assembly has been completed. To minimize thruster weight, the entire discharge chamber, including anode, frame support assembly, propellant distributor, backplate, outer shell, and gimbal mounts, is made of titanium and assembled by tungsten inert gas welding (TIG) and spotwelding methods. The ground screen, rear shield, and perforated outer shield are made of aluminum alloy (type 6061) and the downstream mask is made of titanium.

b. Discharge Chamber Assembly

The prime function of the discharge-chamber assembly of an electron-bombardment ion thruster is to ionize the neutral propellant

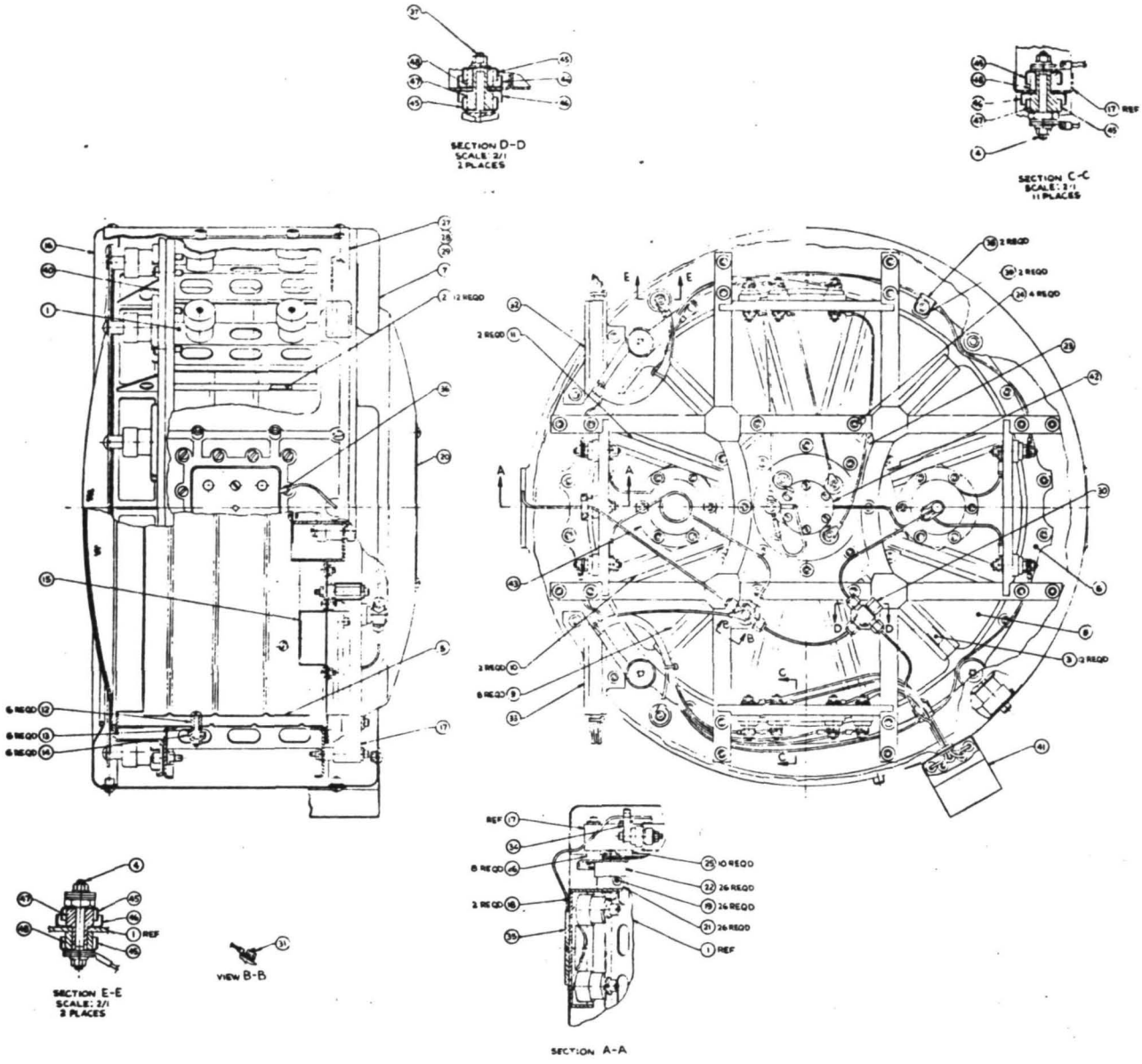

Figure 2. 800-series thruster design.

gas. The design of the discharge chamber is based on the crossed-field or Penning-discharge principle. An electrical discharge is maintained at relatively low internal pressure by restricting the flow of electrons from cathode to anode with an appropriate magnetic field. Components of the discharge-chamber assembly include the thruster shell (which contains the neutral propellant gas), a propellant distributor, permanent magnets and iron pole pieces (for providing the electron-containing magnetic field), an electron emitter, and an electron collector or anode.

As described above, the basic structural element of this design is a cylindrical frame consisting of two annular rings supported by 12 box-type columns. The annular rings and vertical supports were fabricated by a vendor using the precision forming dies equipped with heaters necessary for successful forming of the titanium parts. These parts were assembled at HRL in a special assembly fixture as shown in Figure 3. The parts were positioned in the fixture, clamped, and spot-welded before being TIG welded in a large, dry argon welding facility by the same vendor. The parts were left in the fixture during drilling to assure precision hole location and repeatability.

The structure was then removed from the fixture and the ion optics interface ground to assure a flat mounting surface. The axial magnet retainers were then TIG welded to the frame. The outer housing was completed by spotwelding the outer shell, axial magnets, and magnetic rings in an argon atmosphere. The downstream pole was attached to the downstream magnetic ring by TIG welding at several places around the periphery. The assembly, which at this point weighed 1290 g, is shown in Figure 4.

The 12 radial magnets were then attached by spotwelding to the backplate using 0.02 cm thick titanium magnet retainers. These magnet retainers were formed in the form die shown in Figure 5.

c. Ion Optical System

The ion optical system is the most critical thruster assembly in terms of thruster stability, efficiency, and lifetime. To meet these thruster requirements adequately, the optics must have the following characteristics:

M10027

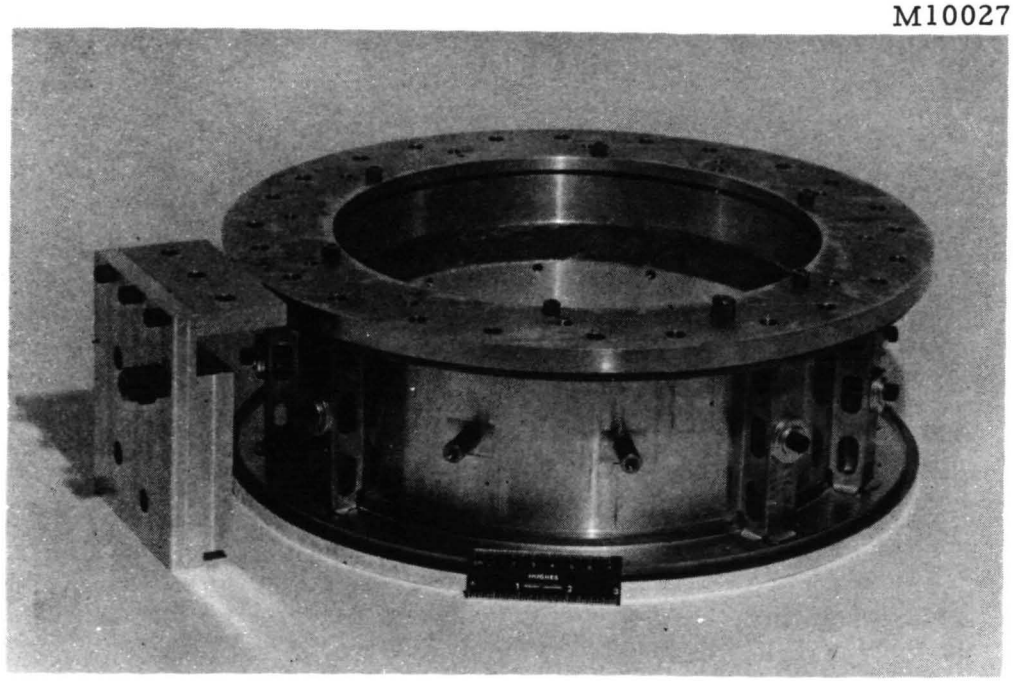

Figure 3. Thruster shell structure welding and drilling fixtures.

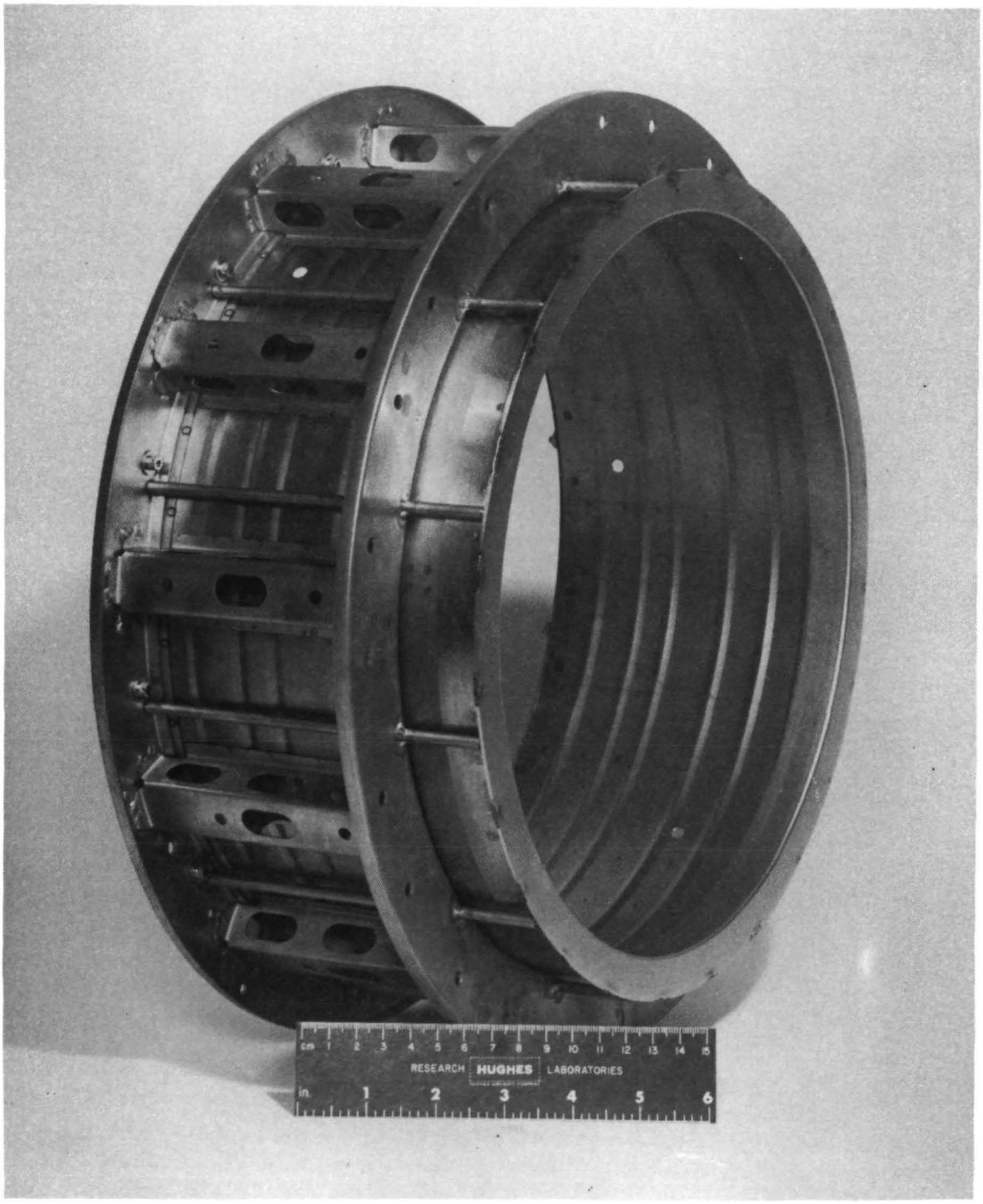

Figure 4. 700- and 800-series thrusters basic structure.

M10029

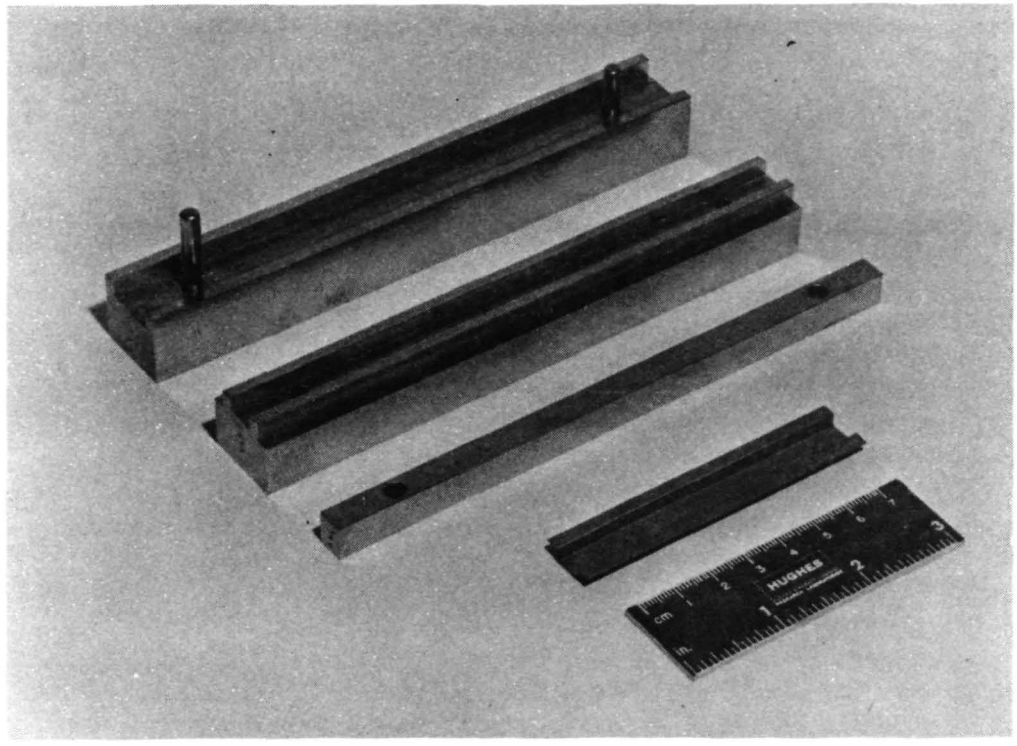

Figure 5. Radial magnet retainer forming die.

- Design life in excess of 10,000 hr
- Structural stability and mechanical reproducibility
- High ion-extraction efficiency
- Low beam divergence
- Light weight.

The ion optical (or ion extraction) system is basically a pair of thin (~0.5 mm) molybdenum plates perforated with 10^4 small (~2 mm diameter) matching apertures. These plates must be positioned parallel to each other, with ~0.5 mm interelectrode spacing. The upstream or screen electrode defines the plasma boundary in the discharge chamber, while the electric field produced between the electrodes accelerates and focuses a beam of positive ions from the plasma through each pair of screen-accelerator apertures.

As a result of tests performed under contracts NAS 3-16528,[1] NAS 3-16949,[2] and NAS 3-15523[3] and of concurrent work at NASA LeRC, an ion optical system design was selected for the 800-series EM thruster. The important dimensions of this subassembly are given in Table 2.

(1) Dished Grid Compensation — Ion thrusters with dished grids are subject to significant thrust losses due to the divergence of

Table 2. Ion Optical System Dimensions

Electrode	Electrode Thickness, cm	Aperture Dimensions	
		Diameter, cm	CTR-CTR Spacing, cm
Screen	0.038	0.190	0.221
Accelerator	0.051	0.152	0.221
Screen electrode compensation = -0.4%.			
Dish depth = 2.1 cm.			
Interelectrode spacing = 0.051 cm.			

T2117

the ion beam.[4] This divergence is a consequence of the relative displacement in the centerlines of screen grid and accelerator apertures. This displacement results from both the geometry of the dished grids and the techniques used to fabricate them. Figure 6 shows the effective beamlet vectoring, which results in beam divergence and associated thrust loss. A change in the aperture center-to-center spacing pattern of one of the electrodes would be needed to vector the individual beamlets to provide paraxial trajectories. A change of less than 0.5% in the center-to-center aperture spacing would converge the beam sufficiently to eliminate such thrust losses. Such a change in spacing is called "compensation."

A dished grid set can be compensated by fabricating the screen grid with a slightly smaller center-to-center aperture spacing pattern than that of the accelerator. This reduction, which is done photographically, produces an offset, as shown in Figure 7. The offset is made so that each beamlet is deflected back parallel to the thruster axis to eliminate the divergence associated with dishing. Screen reduction is based on displacement of peripheral apertures to vector these beamlets by an angle ϕ_{max} given by

$$\phi_{max} \cong \sin^{-1} \frac{r_a}{R_a} \quad , \tag{1}$$

where r_a is the radius of the accelerator aperture pattern and R_a is the radius of curvature of the accelerator grid. Figure 8 illustrates the percent of photographic reduction or compensation factor required for a selected aperture and grid spacing as a function of dish depth (radius of curvature). For the 2.1 cm dish depth, ϕ_{max} is approximately 17^{o}. The electrode aperture pattern adopted for the EM thruster produces direct interception at angles slightly greater than ϕ_{max}. A screen reduction of approximately 0.5% compensates the trajectories for grid curvature. To allow for some misalignment in assembly procedures, a compensation of 0.4% has been specified.

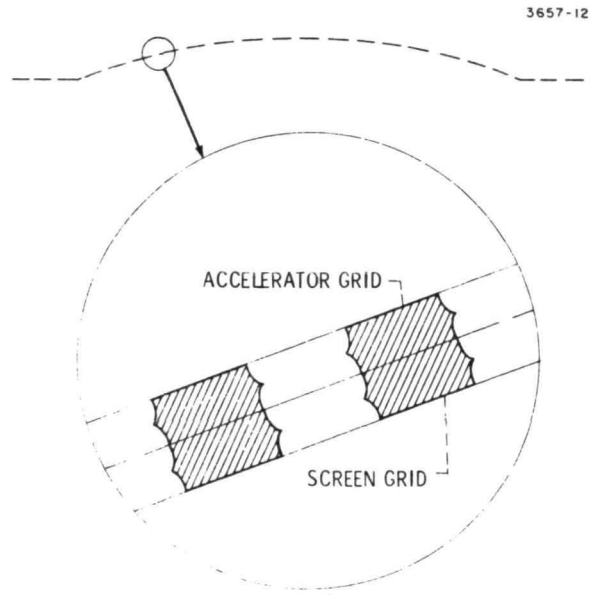

(a) AFTER HYDROFORMING AND STRESS RELIEVING.

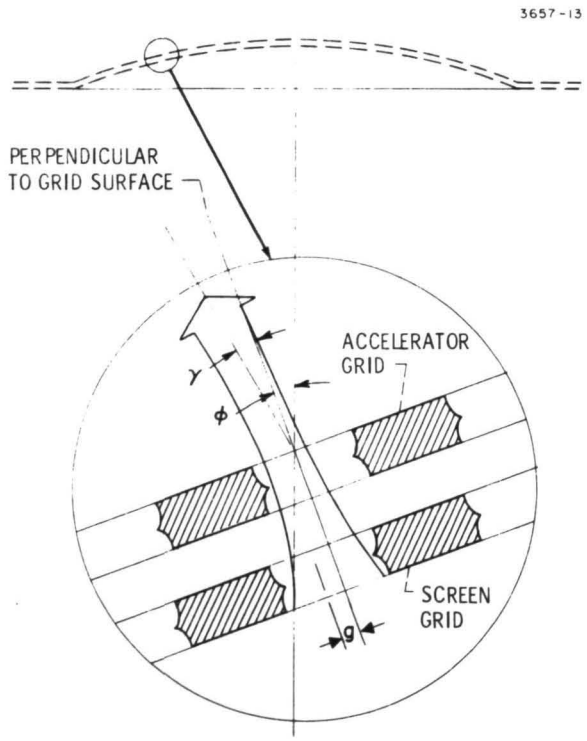

(b) AFTER SETTING GRID SPACING AND DURING OPERATION.

Figure 6.
Beamlet divergence due to aperture alignment.

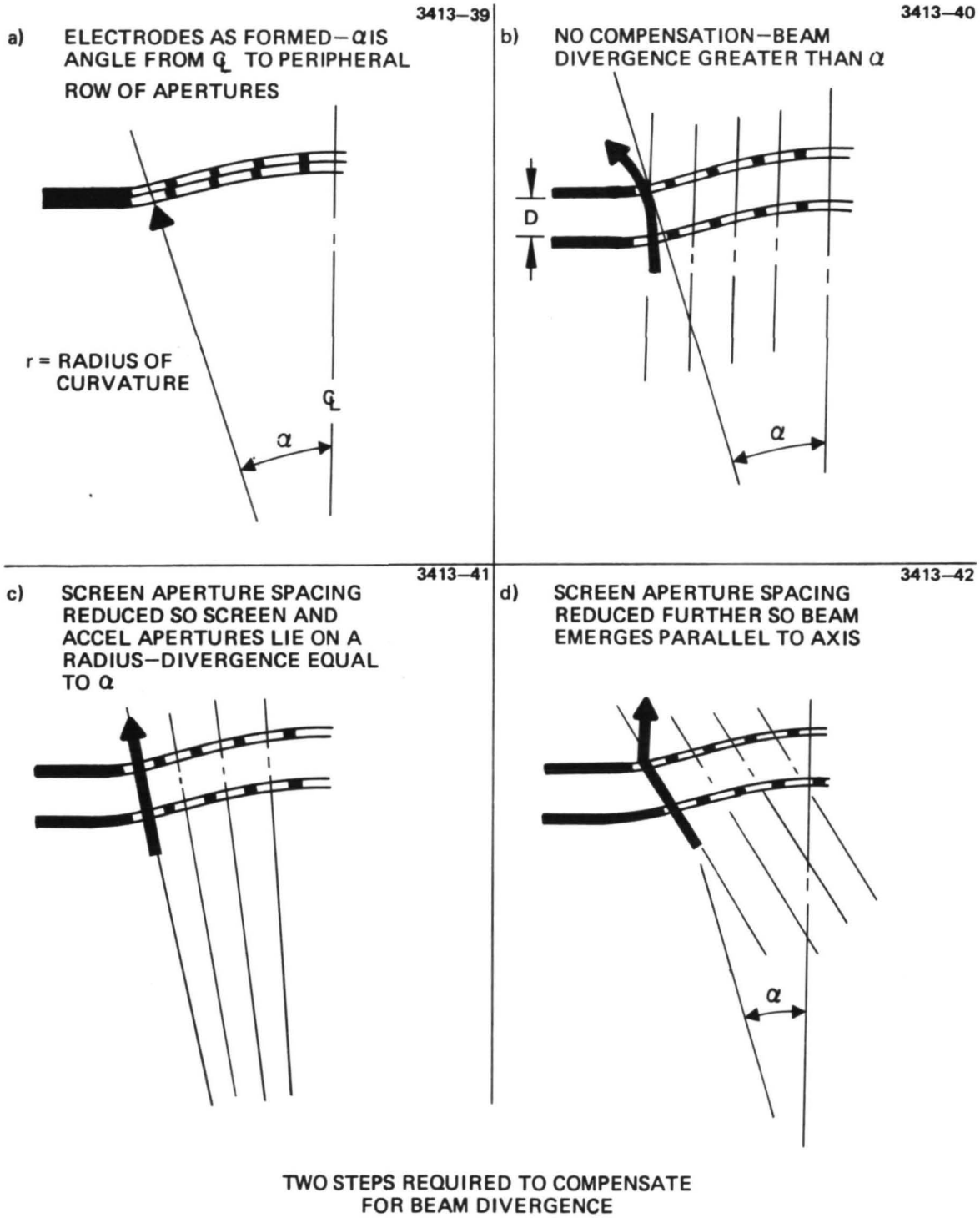

Figure 7. Steps required to offset screen-aperture pattern to compensate for beam divergence.

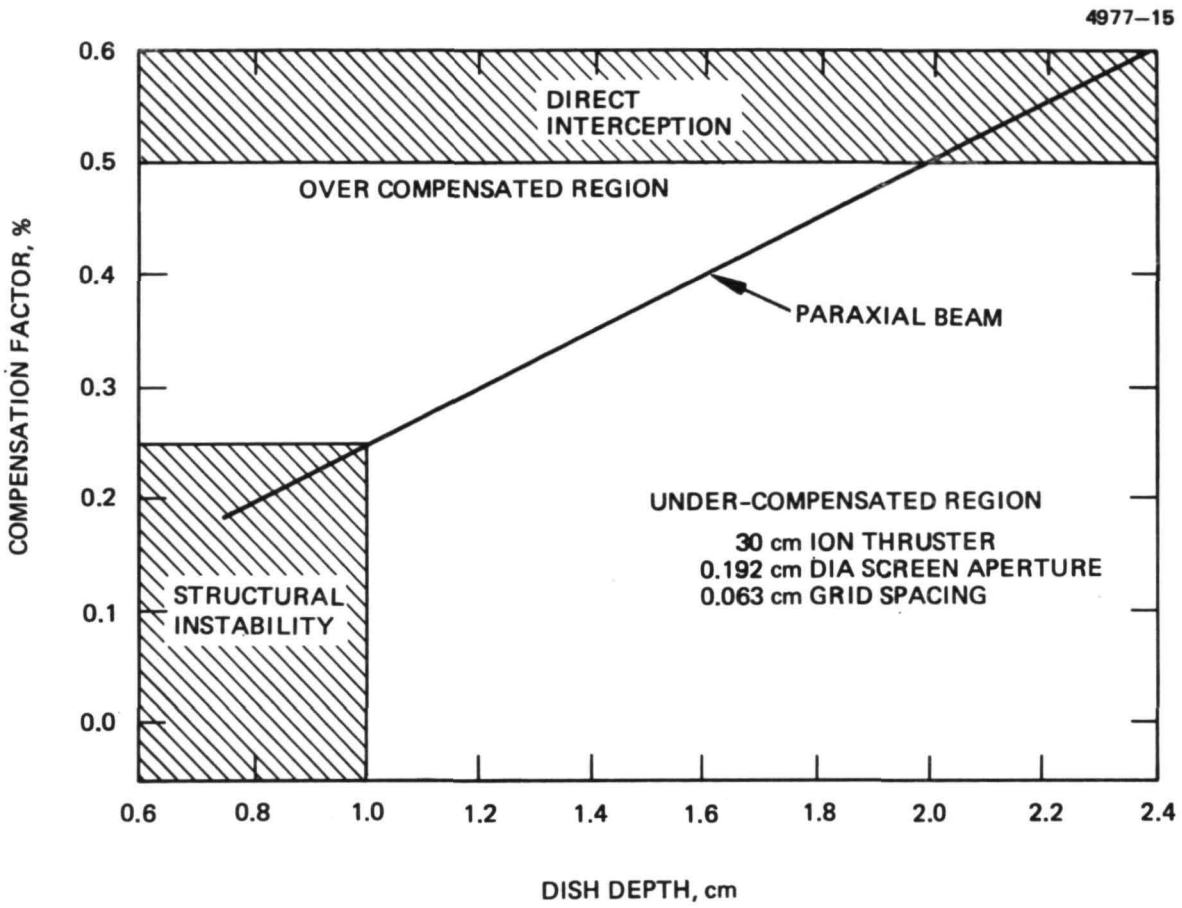

Figure 8. Data for determining dished grid compensation.

(2) Perveance — Typical perveance characteristics of the selected ion optical system design are shown in Figure 9. The minimum voltage for the 800-series grid design is in the range of 1100 to 1200 V for a beam of 2.0 A. The minimum voltage varies slightly among grid sets because of assembly tolerances and uncertainties in thruster operating parameters. Figure 9 also compares methods of measuring perfeance. The normal method maintains constant discharge current and allows the beam current to vary with total voltage. The alternate method maintains constant beam current by adjusting the discharge current. The constant beam current method probably provides a more accurate evaluation of the capability of the ion optical system.

(3) Mechanical Design of the Ion Optical System — The ion optical system is a complicated assembly which requires precise mechanical alignment and stability to assure proper electrical performance and long operating lifetime. During operation, the heat load (which is greater at the center than at the periphery), coupled with the relatively poor thermal conduction of the perforated structure, causes the temperature at the center of each grid to be 50 to 100°C higher than the temperature at the edge. Thermal stresses, therefore, naturally cause a dishing (or "oil-canning") effect.

Several support structures, including interelectrode supports, were evaluated in an attempt to produce a stable configuration with flat electrodes; in all cases these were unreliable. The final solution was to hydroform the electrodes into a dished configuration. Although the fabrication and assembly of this subsystem is still very critical, it is now possible to reliably and reproducibly fabricate ion extraction systems of this design. The final alignment and spacing procedure has been empirically established so that the relative positions of the screen and accelerator electrodes are correct at the operating temperature.

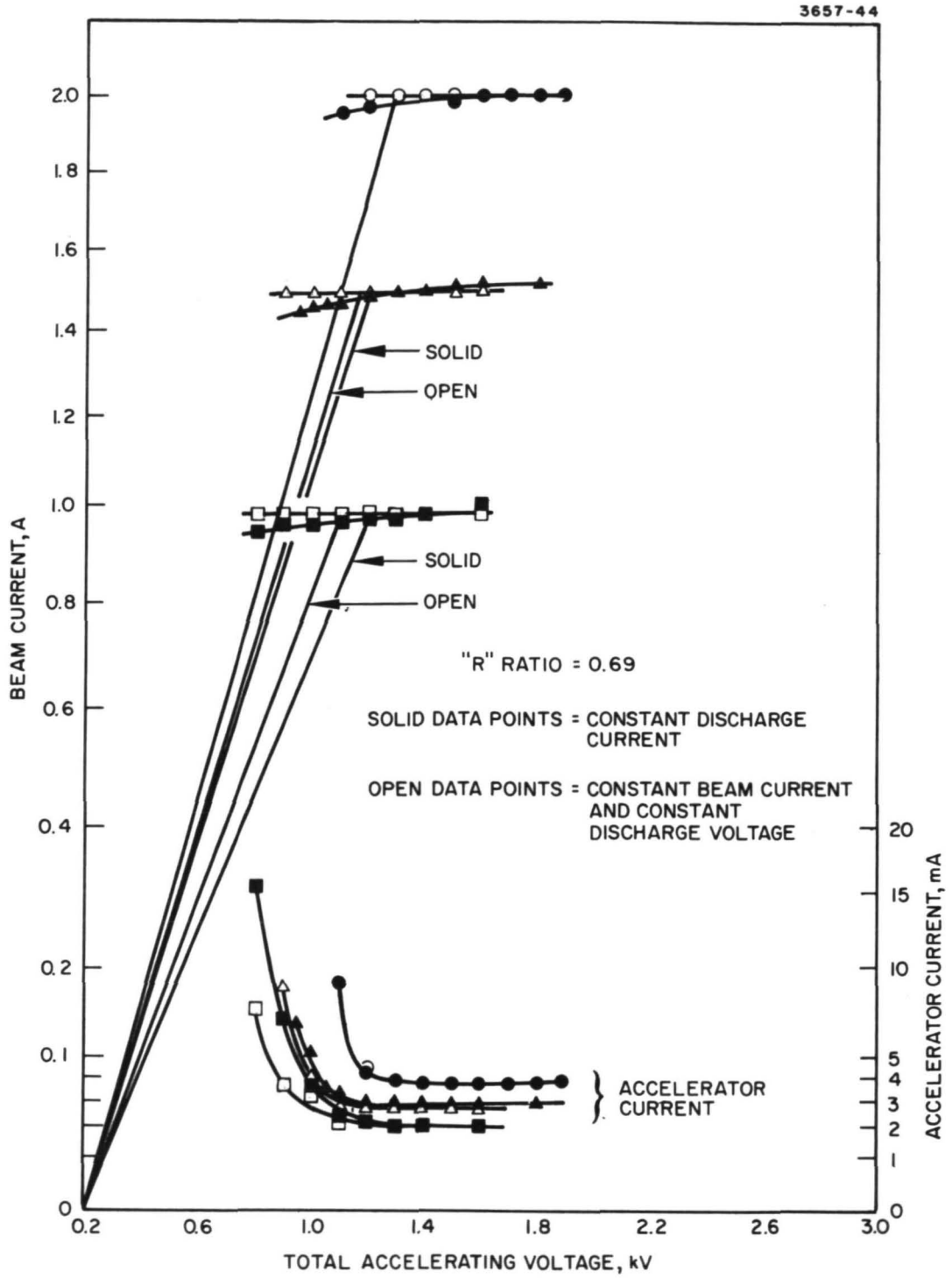

Figure 9. Perveance characteristics of the ion optical system for 700/800-series thruster.

(4) Grid Fabrication Procedure — The screen and accel electrodes are fabricated from low-carbon molybdenum sheets. The blank sheets are first imprinted on both sides with photoresist by a vendor. The printed blanks are returned to HRL to be formed in the special fixture and large hydraulic press shown in Figure 10. The accelerator and screen electrodes are dished by simultaneous hydrostatic forming at a clamping force of 9800 psi around the grid periphery. The press is instrumented with pressure gauges, heater controls, thermocouples, and a digital readout which measures the depth of the formed dish while the process takes place. The grids are formed by pumping hydraulic oil from a separate system into the top of the forming fixture until the desired free-form shape is achieved.

Since molybdenum is known to be more readily formed at temperatures above the ductile-brittle transformation temperature of ~100°C, heaters are provided to warm the forming fixture and grids. The grids, after being formed, are returned to the vendor for final etching of the hole pattern.

The grids are then stress relieved in the fixture shown in Figure 11. The grid set is carefully centered in the fixture and clamped by twelve 1.27 cm bolts at the outer edge. The unclamped center plug is weighted with a 34 kg molybdenum mass. Then the entire assembly is loaded into a large vacuum furnace, and the fixture is fired in vacuum at 1000°C for 3 hr.

After stress relieving, the grids are set up in the assembly fixture shown in Figure 12, which aligns the hole pattern with respect to the grid stiffening rings. Holes are drilled in each grid for subsequent alignment on the mounting structure.

(5) Main Support Ring, 800-Series Thruster — Although the support rin of the 300- to 700-series optics provided relatively good structure characteristics, an improved design was developed for the 800-series thruster. The new design (illustrated in Figures 13 and 14) simplifies assembly, improves grid flatness, and provides more rigid structural properties.

M8550

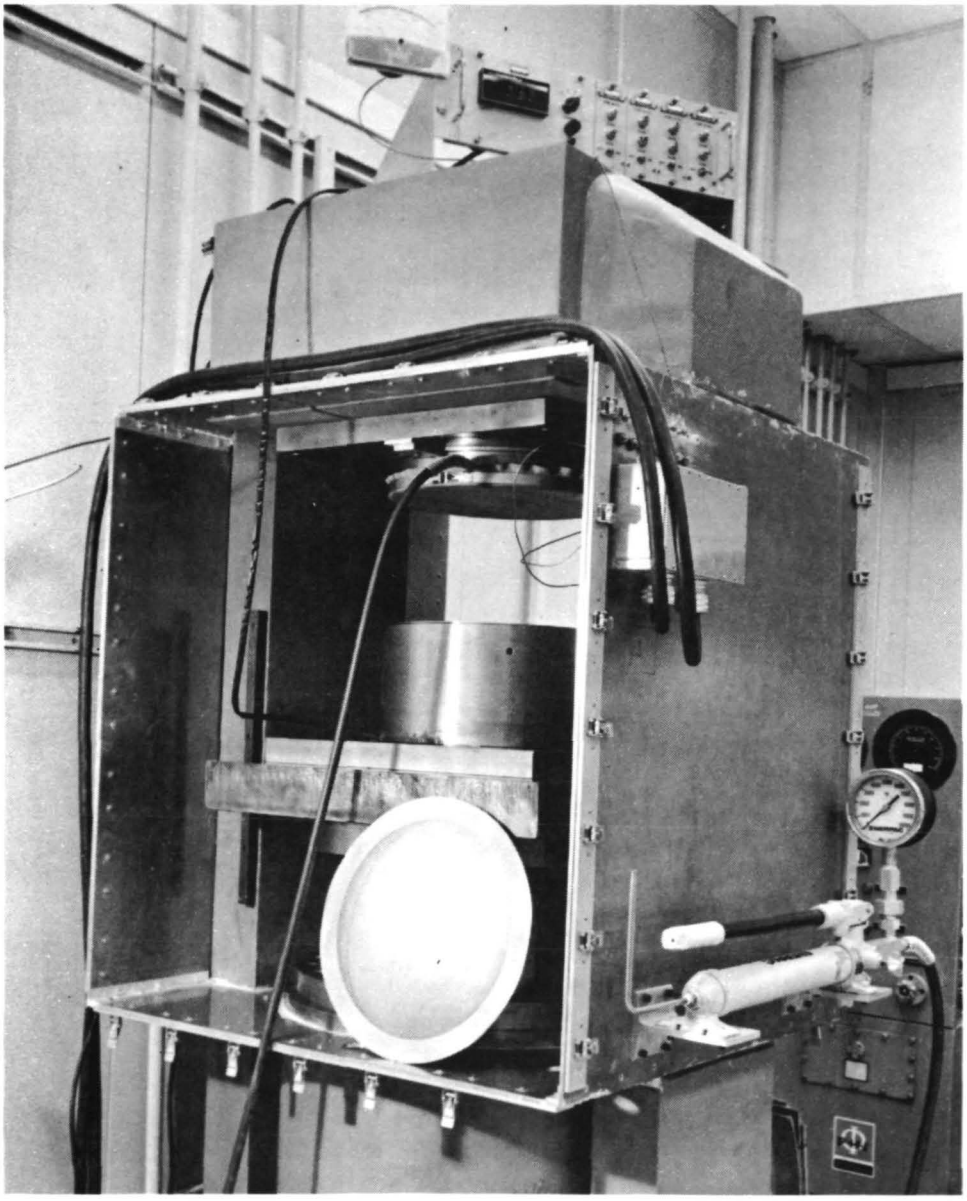

Figure 10. 30 cm dished-grid hydroforming press and fixture.

M10026

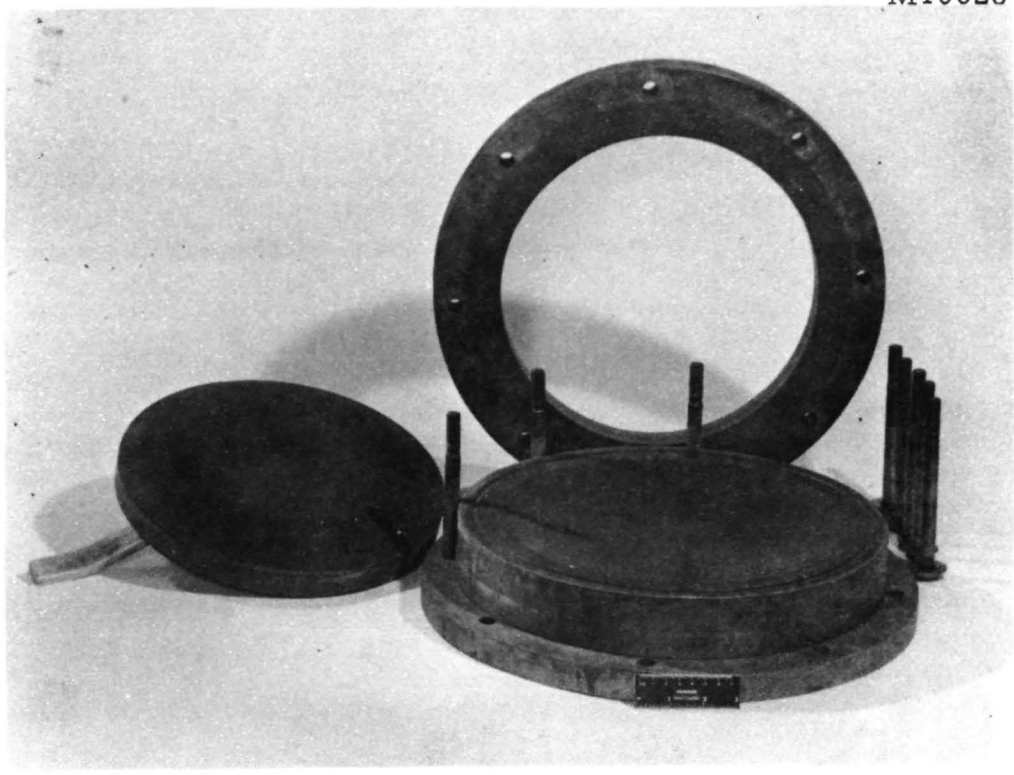

Figure 11. Dished-grid stress relieving fixture.

M10028

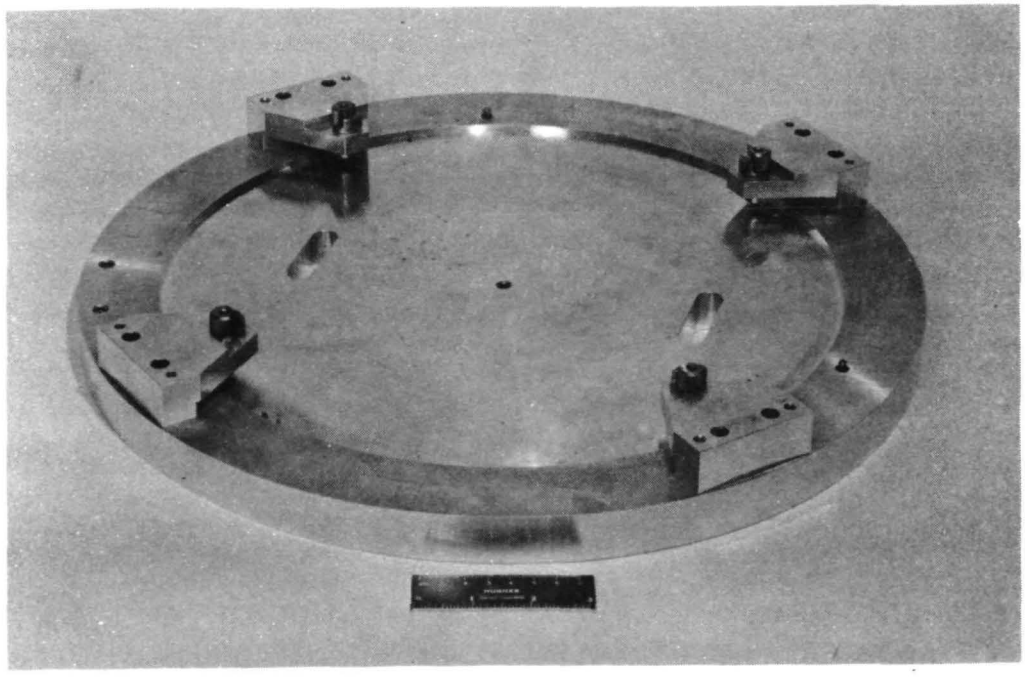

Figure 12. Dished-grid alignment fixture.

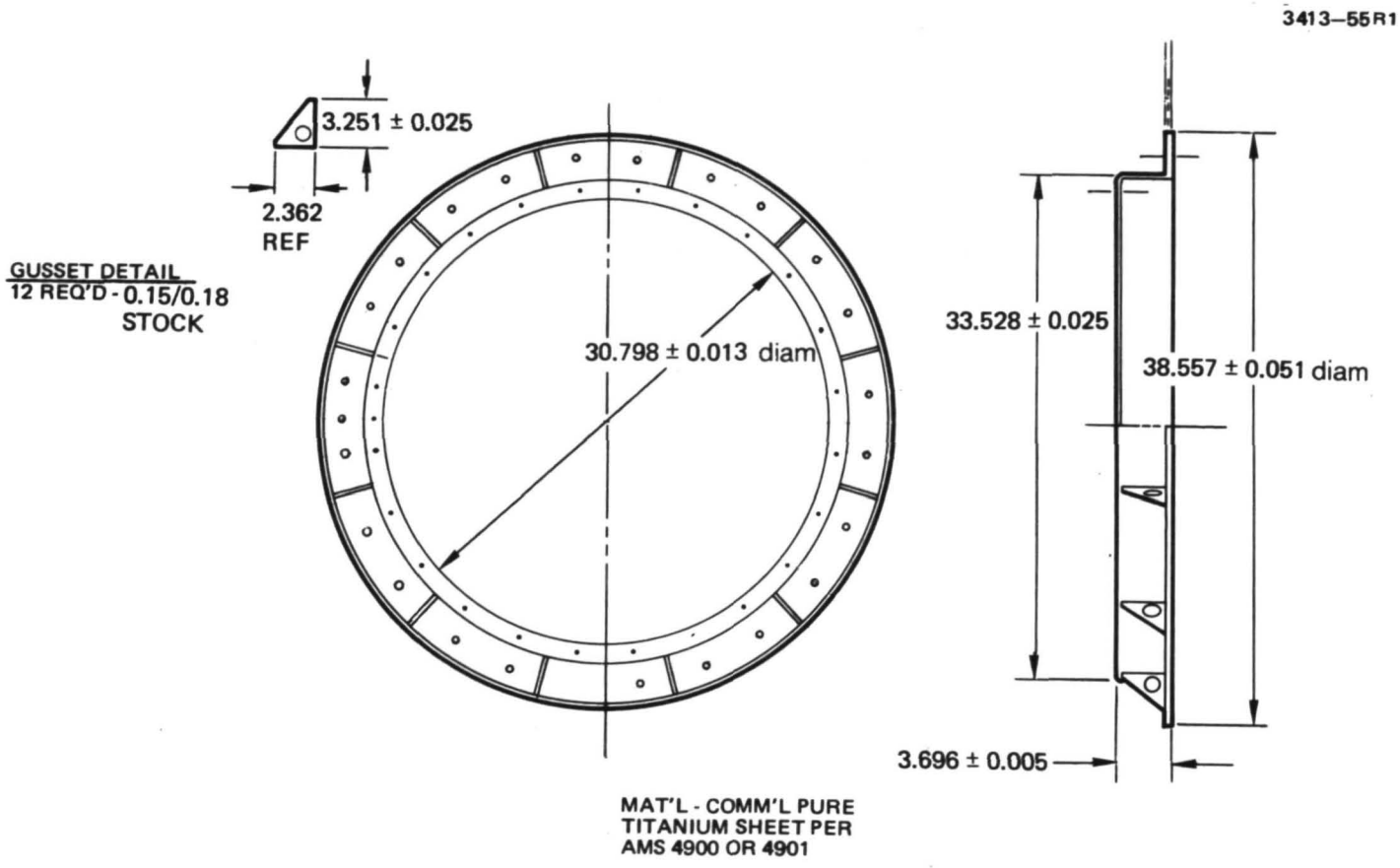

Figure 13. Electrode support ring design for 800-series thruster.

M10403

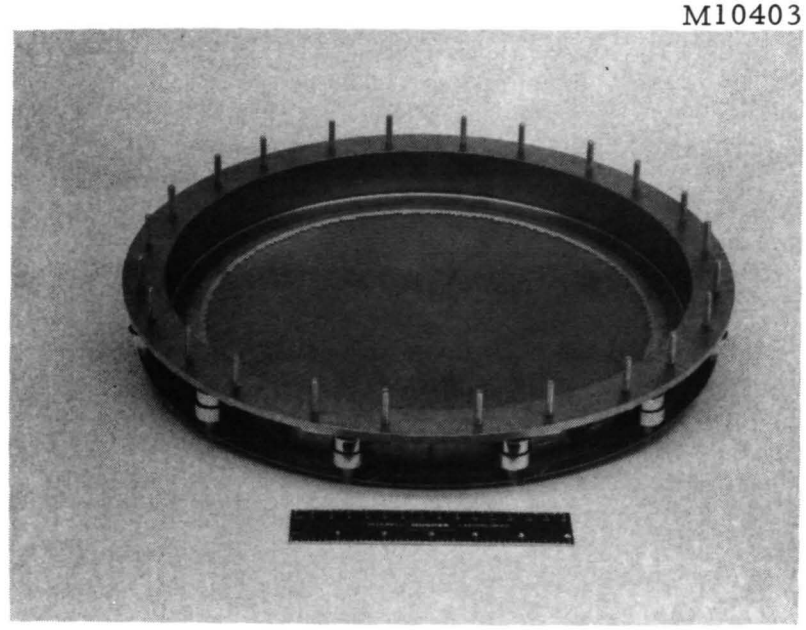

(a) Downstream view

M10404

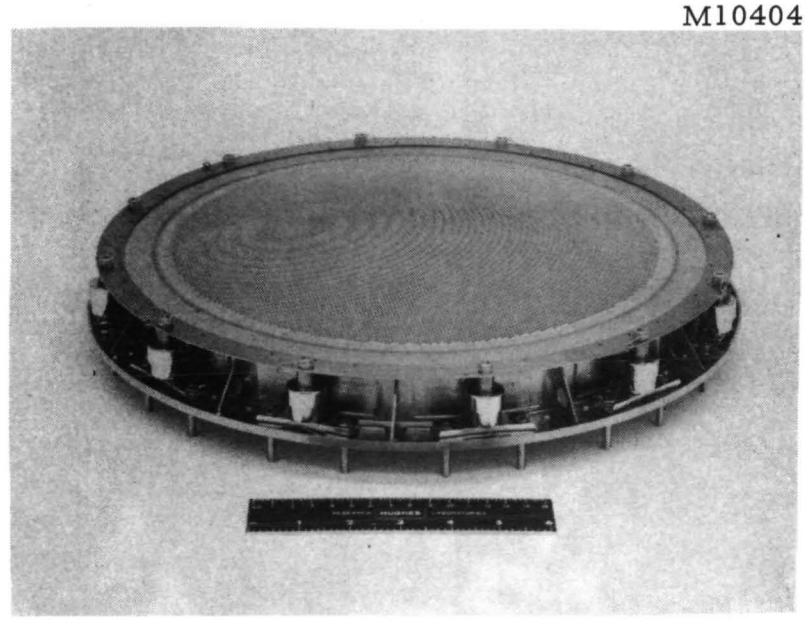

(b) Upstream view

Figure 14. Ion optical system assembly using titanium support ring.

The support ring is fabricated from commercially pure titanium plate. After the ring is rough machined, the 12 gussets are welded into position. Final machining, with rigidity added by the gussets, achieves accurate parallelism between the screen and accelerator mounting surfaces and also achieves precision flatness. The solid cylindrical web design eliminates the screen-grid mounting brackets and provides a "sealed" discharge chamber.

The titanium support ring design uses 0-80 screws to mount the screen grid directly to the machined flange. The accel grid is mounted to a molybdenum grid support ring in a similar manner. The grid support ring is then attached to the titanium ring through 12 shielded insulators. This technique eliminates the time consuming brazing, heat-treating, and aperture-alignment processes used in the previous design.

The assembly shown in Figure 14 was developed as part of a Hughes-funded program. Shake testing of this optics assembly was conducted under Contract NAS 3-18334 to verify its suitability for the 800-series thruster. This first assembly was also used in the vibration test of thruster S/N 702-A.

(6) Accel Insulator Fabrication — The accel insulators are ground from prefired Wesgo AL300 high-purity alumina, and the ends are metallized by conventional techniques. These processes are done at the Electron Dynamics Division of Hughes Aircraft Company, Torrance, California. The end caps are then brazed with OFHC pure copper in a hydrogen atmosphere. The insulator assembly is then ground flat on each end, ultrasonically cleaned, and grit blasted with high-purity alumina (Al_2O_3) prior to final assembly. The grit blasting unit used was purchased especially for this operation; it is also used for final cleaning of the high-voltage isolators of the MIV and CIV assemblies.

(7) Ion Optical System Finaly Assembly — During the final assembly of the ion optical system, it is ciritical that the grids are attached to the mounting structure in a stress-free condition. This is necessary to prevent the thermal stresses placed on the assembly during normal operation from causing shorting or unpredictable

performance. Accurate grid alignment and spacing is essential to long-term stability and lifetime. The grid-mounting planes are carefully checked for flatness and height uniformity at each mounting point before the screen and accelerator assemblies are attached. These surfaces are required to be flat within 0.005 cm for successful grid performance. Numerous measurements are taken at each assembly step and recorded in the assembly log book. Finally, grid spacing is measured at several points across the surface and recorded on a data sheet, as shown in Figure 15.

(8) Bench Checkout Procedure – A thermal simulator was constructed to examine the structural integrity of the grids during bench testing. This simple device consists of a series of flat circular electrical heaters arranged concentrically, similar to an electric stove element. These were placed inside an insulated cylinder large enough to hold the electrode system. By independently controlling the power to each ring, a wide range of thermal conditions can be simulated. Test temperatures are measured either with attached thermocouples or contact thermocouples or are estimated from precalibration of the thermal simulator. Electrical properties are typically monitored during the test with an electronic "megger" (1000 Vdc) which reads to 1000 MΩ yet does not damage the grids under short-circuit conditions.

d. Cathodes

Two hollow cathodes are used in the 30 cm EM thruster: one in the discharge chamber and one in the neutralizer. The cathode design selected for the 800-series EM thruster was based on a Hughes study[5] and on work performed concurrently at NASA LeRC.[6] The thermal criteria used for cathode designs are (1) tip temperature of 1100°C maximum, (2) insert temperature of 850°C maximum and 600°C minimum, (3) main cathode maximum input power of 75 W up to ignition, and (4) neutralizer cathode maximum input power of 50 W up to ignition.

30 cm OPTICS ASSEMBLY RECORD
SCREEN ACCELERATOR SPACING CHART

DATE: 4-13-76
TECH: H. T.

MOUNTING RING ASSEMBLY S/N 818
ACCELERATOR ELECTRODES S/N 818
NOTES:

SCREEN ELECTRODES S/N 818
NOTES:

TYPE	2.108 Dished
DRAWING NO.	D1026138
APERTURE dia	0.152
SPACING CTR/CTR	0.221
THICKNESS	0.051
DRAWING NO.	D1026137
APERTURE dia	0.191
SPACING CTR/CTR	0.221
THICKNESS	0.038
REDUCTION (%)	0.4

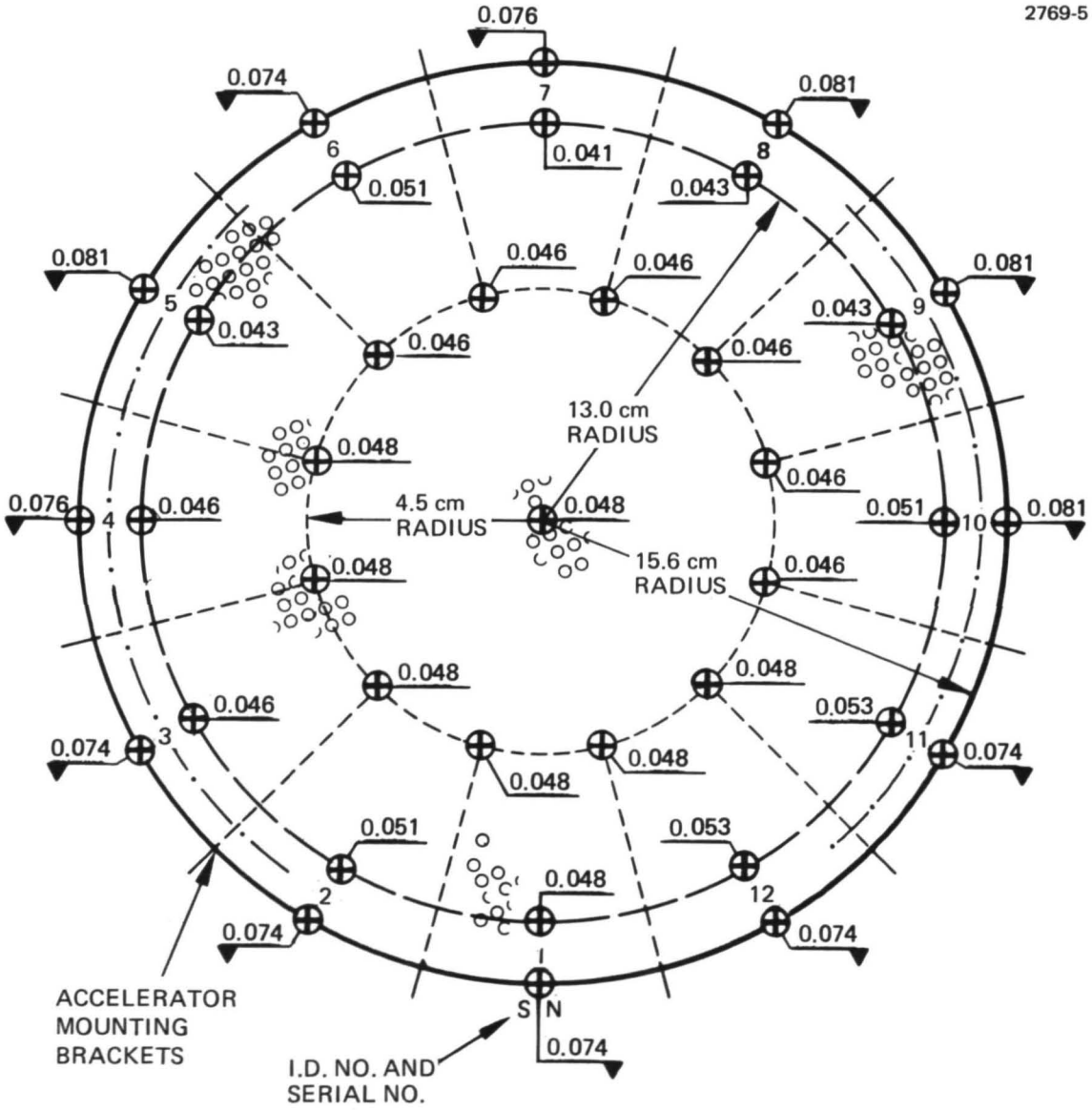

Figure 15. Grid-spacing data sheet.

A thermal analysis of the cathode showed that the heat loss is predominantly by radiation from the incandescent tip, with conduction down the tube playing a minor role. Therefore, it is possible to control the operating temperature range by adjusting the radiating area of the tip. The thermal profile of the main cathode final design is illustrated in Figure 16 for startup and operating conditions. The axial position of the insert was chosen so as not to exceed the maximum insert temperature criterion. The heat shields are necessary to improve heater efficiency in the startup mode.

The hollow-cathode assembly, shown in Figure 17, uses a flame-sprayed heater configuration. The first step in the fabrication is to apply a 0.013 cm thick tungsten coating to the heater area of the cathode tube. A 0.025 cm thick Al_2O_3 coating is then sprayed over the tungsten. Two 0.013 cm by 0.075 cm Mo/Re straps are electron-beam (E-beam) welded to the tube, and the heater coil is attached by E-beam welding to the straps and heater lead (as shown in Figure 17). The heater lead and clamp is then OFHC copper brazed to the tube, and the final coating of alumina is sprayed to a thickness of about 0.025 cm. The final assembly steps depend on whether the cathode is to be used as a main cathode or as a neutralizer cathode.

For main cathodes, an orifice disk (as shown in Figure 18) and a radiating flange are E-beam welded in place. The tube is cut to length and E-beam welded into the cathode mounting flange. The heater terminal is brazed to the lead by rf brazing in a bell jar. Finally, the heat shields and insert are installed to complete the assembly, as shown in Figure 18.

The neutralizer cathode requires only 50 W for ignition and does not have a tip radiator. Thus, after installing the heater elements in the basic cathode assembly, a neutralizer cathode is made by E-beam welding the orifice disk into place and brazing on the heater terminal. The cathode orifice disk is 0.15 cm thick with a straight 0.038 cm diameter hole. Additional details of the neutralizer assembly are presented in Section 2.A.e.(3).

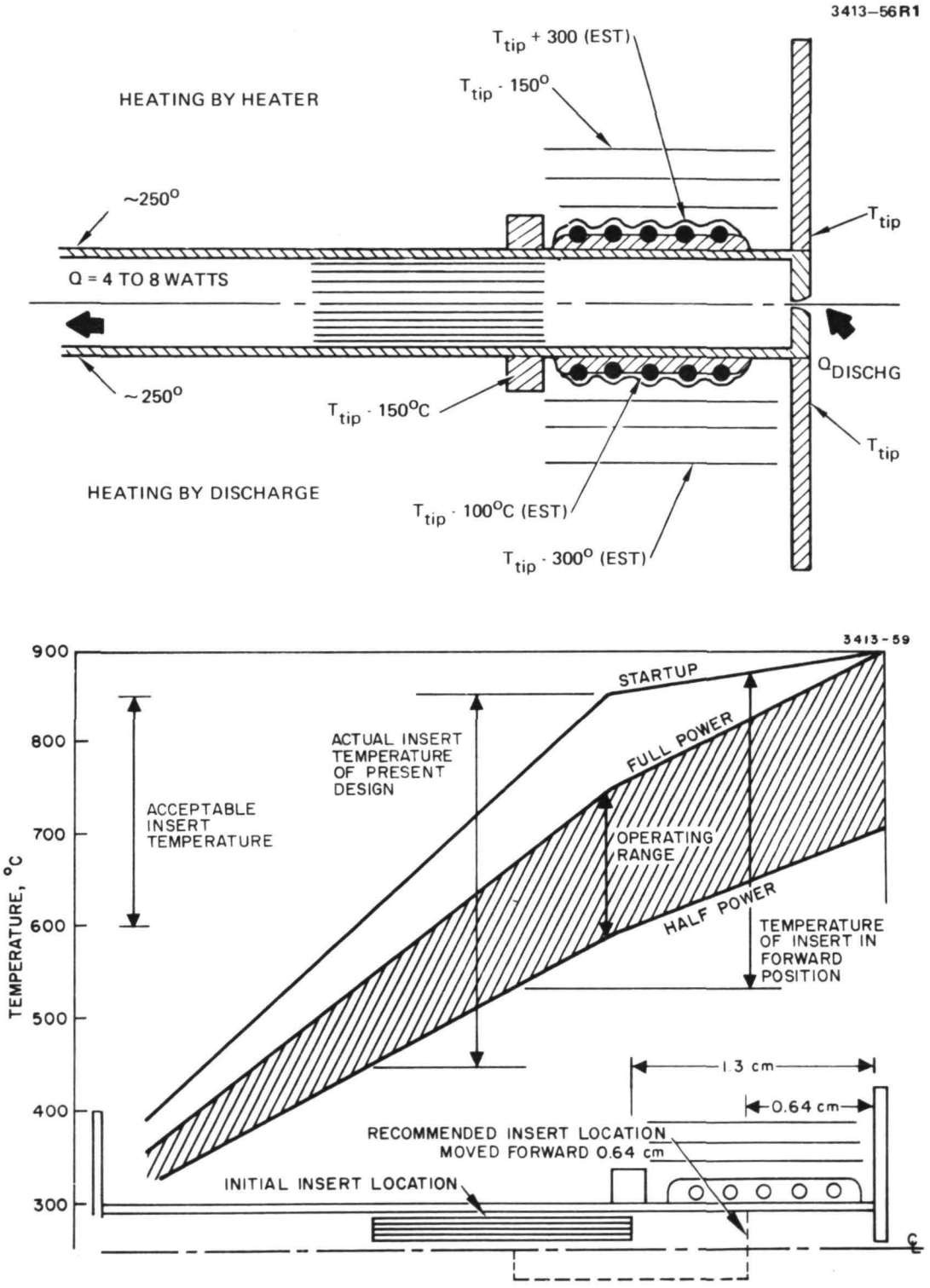

Figure 16. Cathode thermal model and predicted temperature profiles.

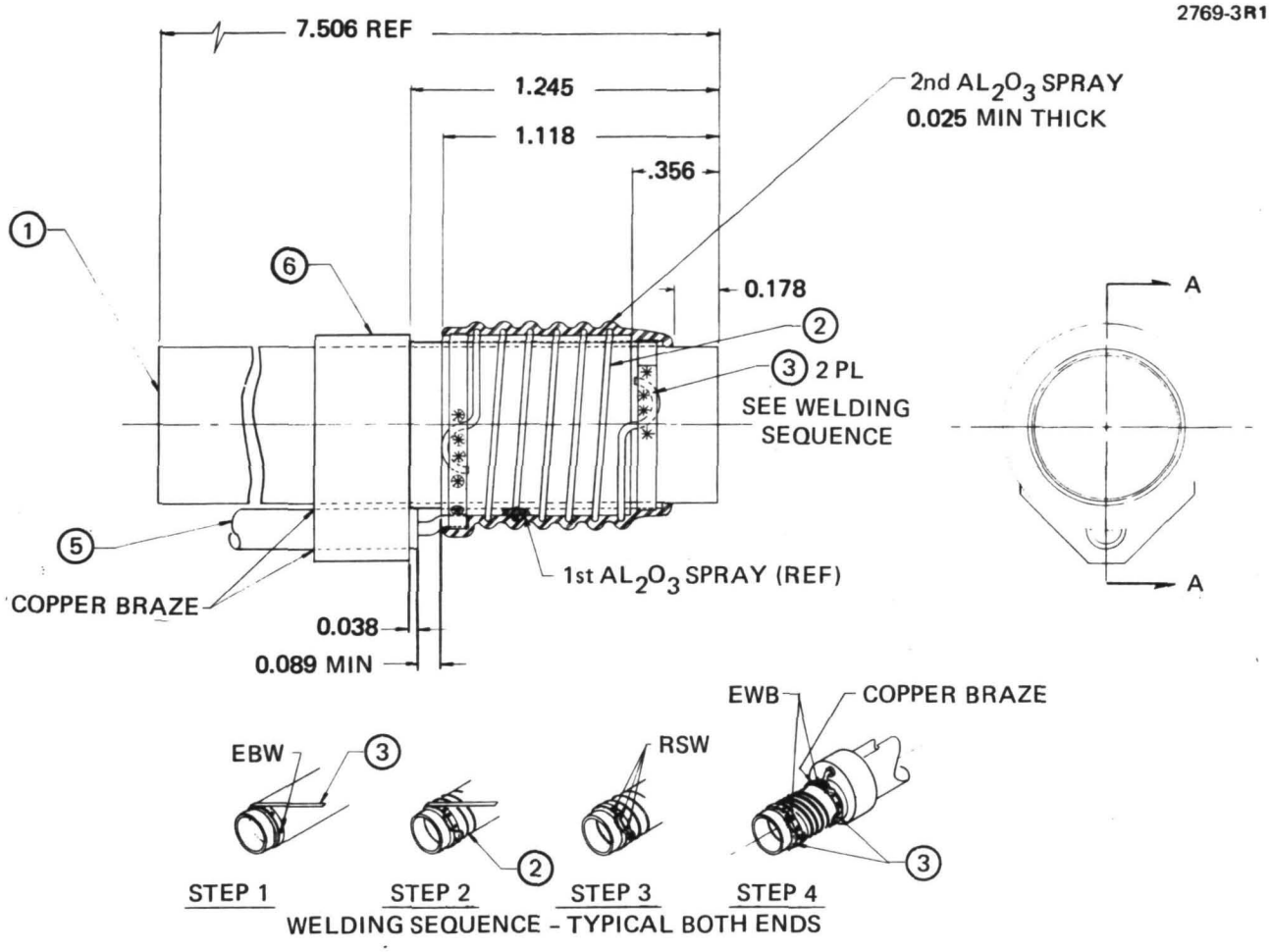

Figure 17. Basic cathode with sprayed heater.

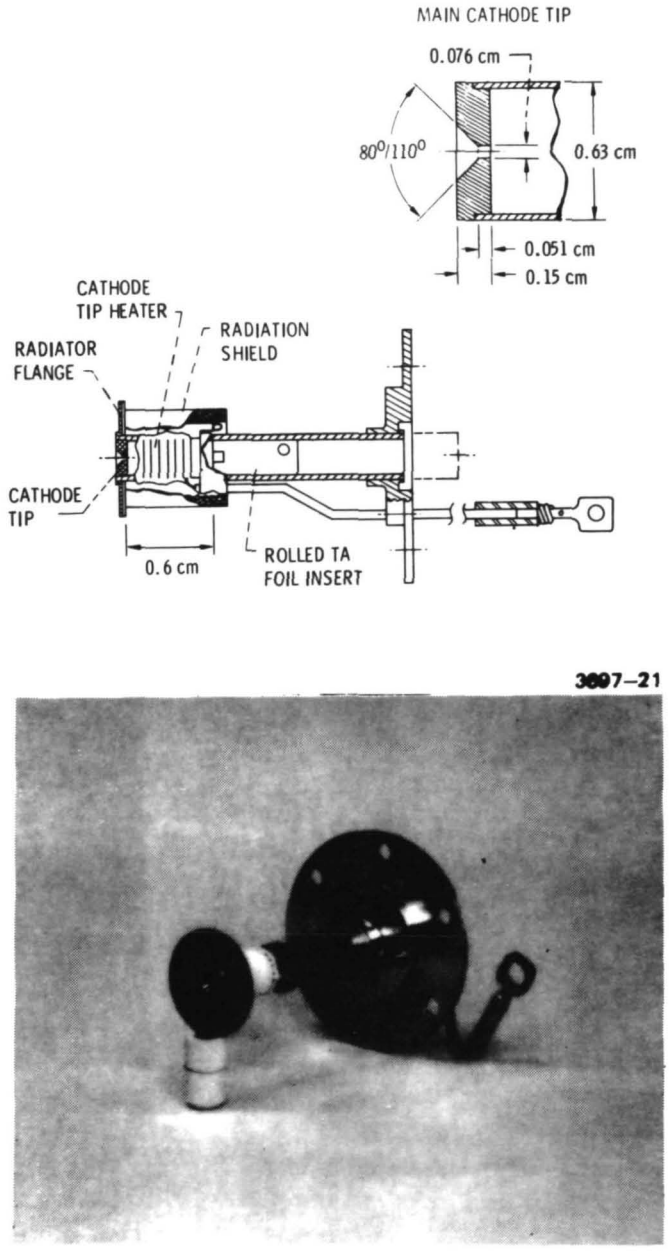

Figure 18. Main cathode assembly.

e. Isolator-Vaporizer Assemblies

Isolators are used in each of the three propellant feed lines (main, cathode, and neutralizer) to provide electrical isolation between thruster voltages and the grounded propellant system. The isolator, placed downstream of the vaporizer in each line, must withstand the voltage difference (1100 V for main and cathode isolators, 100 V for the neutralizer) and conduct mercury vapor. The principle involved in the feedline electrical isolators requires the propellant vapor to flow through a series of "chambers" across which the voltage drop is below the Paschen maximum for mercury. These chambers are formed by spacing optically dense metallic screens in a ceramic tube that connects the vaporizer with the cathode or discharge chamber being supplied. Since the isolator and vaporizer designs are closely associated, the combined isolator-vaporizer assemblies for the three applications are discussed in this section.

(1) Main Isolator Vaporizer Assembly — The previous discussion characterized the basic isolator portion of the main isolator vaporizer (MIV) assembly shown in Figure 19. The vaporizer is a porous tungsten disc E-beam welded into a tantalum housing. The housing is attached to the upstream end of the isolator. A coaxial heater is brazed with Nicrobraz 135 to the vaporizer assembly. The isolator heater is also brazed to the downstream flange with Nicrobraz 135, and this unit is TIG welded to one end of the alumina isolator assembly. Heater specifications for the MIV are shown in Table 3.

An outside vendor fabricates the isolator by OFHC copper-brazing Kovar flanges to the WESGO AL 300 alumina insulator tube. After joining the isolator and the flange, the isolator is loaded with the alumina rings and wire mesh separating screens, and the vaporizer subassembly is TIG welded in place. The stainless-steel mounting flange is then TIG welded to the downstream flange, and the completed assembly is nickel plated (0.0005 cm maximum thickness). Finally, the outer surface of the alumina insulator is grit blasted, and the nickel plated sputter shields are attached. Thermal constraints for the MIV assembly are:

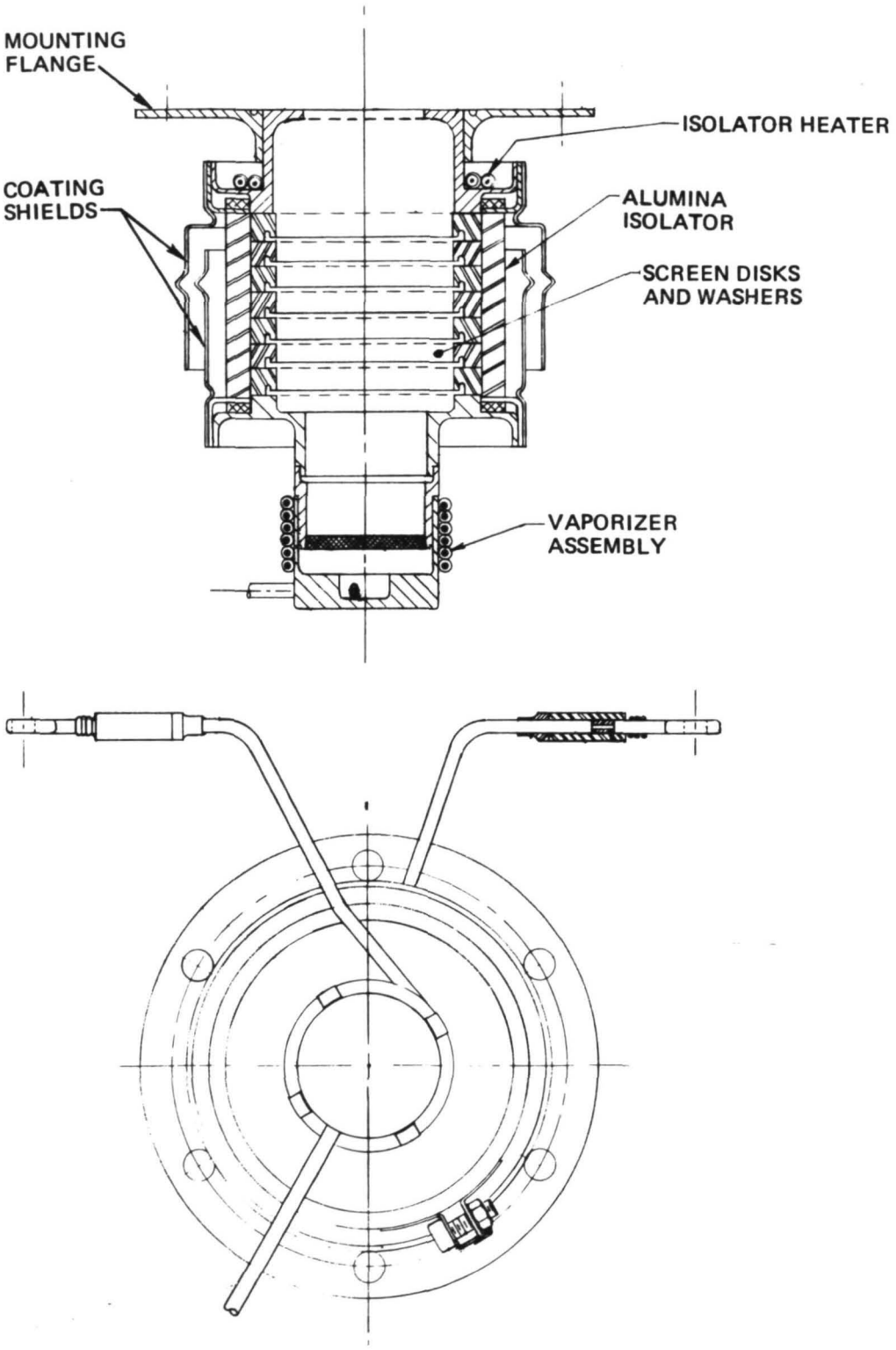

Figure 19. Main isolator vaporizer (MIV) assembly.

- Isolator temperatures
  - (a) 200°C minimum to prevent mercury condensation
  - (b) Minimum temperature rise during operation to ensure long lifetime ($T_{max} \sim 350°C$)
- Vaporizer temperature: Controllable in the range 280 to 340°C to adjust mercury flowrate.

Table 3. MIV Heater Specifications

Item	Main Isolator	Main Vaporizer
Part number	B1025330	B1024917
Conductor material	Nichrome V	Nichrome V
Conductor diameter, cm	0.025	0.025
Sheath material	Inconel	Inconel
Sheath diameter, cm	0.100	0.100
Insulation material	MgO	MgO
Number of turns (approx.)	2	6
Resistance, Ω	4.65 ± 0.23 at 25°C	6.50 ± 0.32 at 25°C

T408

(2) CIV Assembly — Initially, the cathode isolator was mechanically (and therefore thermally) integrated with the cathode itself on the thruster centerline. At full-power operation, even the modest amount of power (~8 W) conducted along the cathode tube heated the cathode isolator to >400°C. At this temperature, several isolator failures were observed. In the first EM thruster (700-series), the operating temperature was lowered by moving the cathode isolator to a location on the thruster backplate diametrically opposite the main isolator. At this location, the operating temperature of the cathode isolator is approximately the same as that of the main isolator. Mercury from the isolater is carried to the cathode through a small tube. This

tube is initially heated by the isolator heater, and its temperature is maintained by thermal conduction from the discharge chamber when the thruster is operating.

The isolator-vaporizer design, shown in Figure 20, is fabricated and assembled in a manner similar to that described for the MIV, except that an additional feed tube and flange are added to direct the mercury flow to the cathode tube. The 0.240 cm diameter by 0.05 cm wall mild steel tube is brazed to the isolator flange and to the stainless-steel feed-tube flange. This subassembly is shown in the special brazing fixture in Figure 21. A portion of the isolator heater is also brazed to the feed tube to preheat the tube during startup. Heater specifications for the CIV are shown in Table 4.

Table 4. CIV Heater Specifications

Item	Cathode Tip	Vaporizer
Part number	B1025262	B1025330
Conductor material	Tungsten/26% rhenium	Nichrome V
Conductor diameter, cm	0.025	0.025
Sheath material	N/A	Inconel
Sheath diameter, cm	N/A	0.100
Insulation material	Al_2O_3 [a]	MgO
Number of turns (approx.)	8	2
Resistance, Ω	1.15 ± 0.05 at 25°C	2.86 ± 0.14 at 25°C

[a] Flame sprayed.

T2127

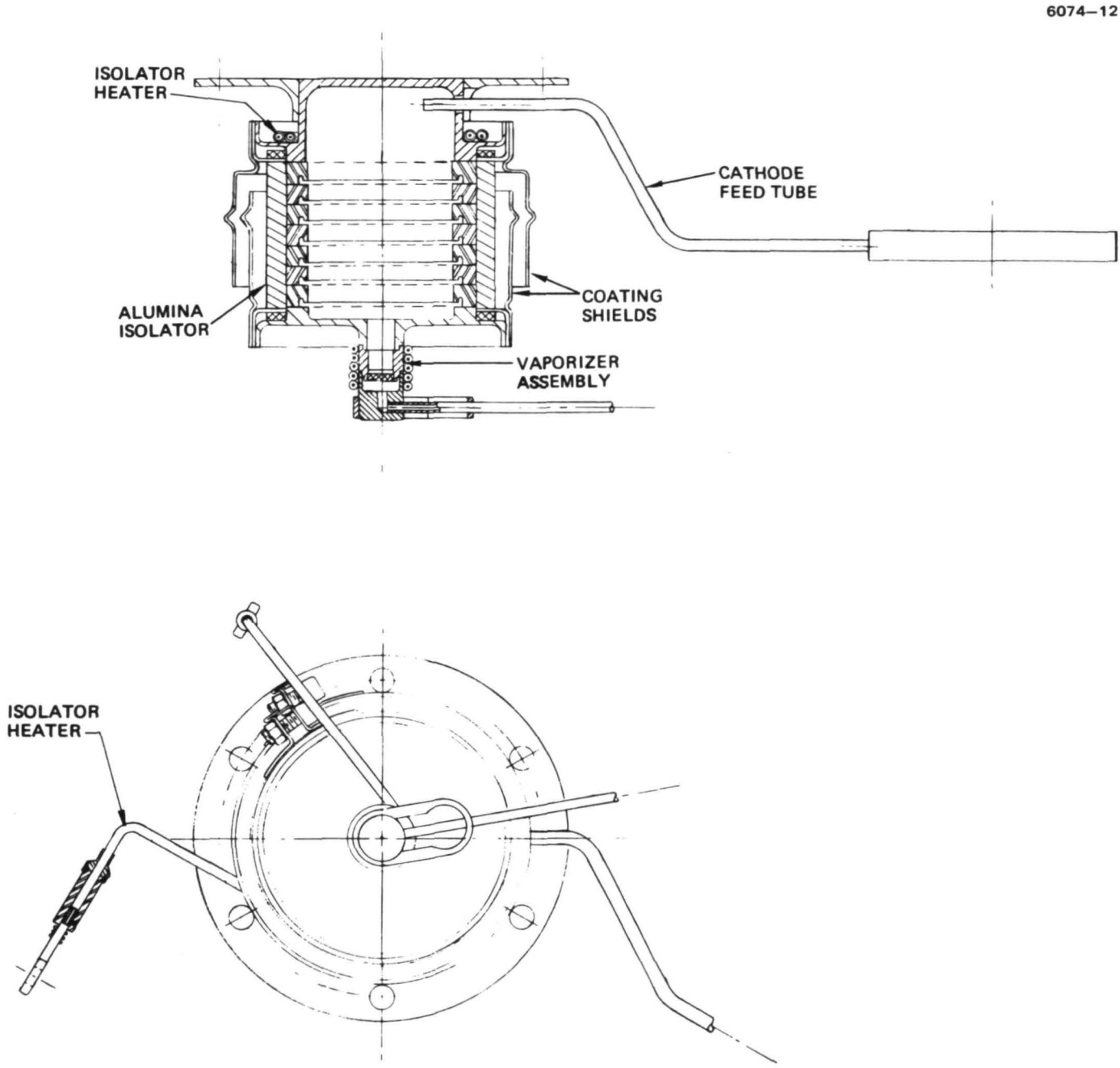

Figure 20. 800-series thruster cathode isolator-vaporizer assembly.

M10030

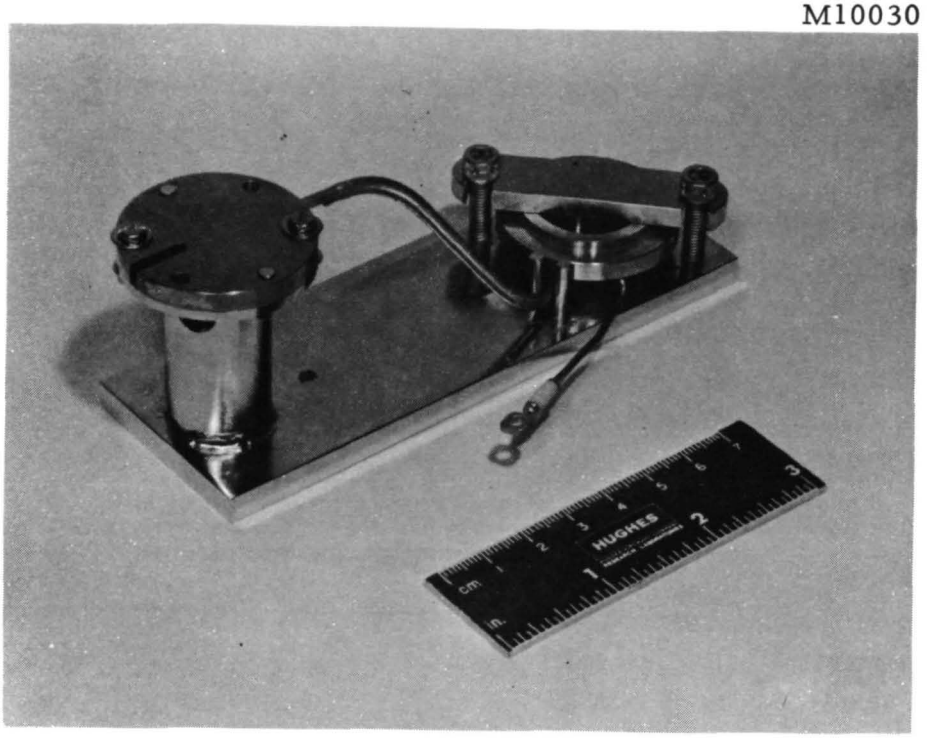

Figure 21. CIV feed tube and cathode flange brazing fixture.

The isolator-vaporizer subassembly is then joined to the cathode assembly (Figure 18) with a 0.01 cm thick annealed tantalum seal. The cathode, isolator, and vaporizer are installed in a baffle subassembly. This total CIV assembly is shown in Figure 22.

(3) Neutralizer Isolator Vaporizer Assembly — The neutralizer tube subassembly, excluding keeper, brackets, and mounting hardware, is shown in Figure 23. The isolator section is first assembled by OFHC copper brazing the tantalum shield and vaporizer housing to the ends of an Al-300 alumina tube. Screen baffles, as used in the CIV and MIV, are not required because the voltage level is low. The vaporizer plug and feed tube are E-beam welded in place and the vaporizer heater is brazed to the housing. Heater specifications for the neutralizer-isolator-vaporizer (NIV) assembly are shown in Table 5.

Table 5. Neutralizer Heater Specifications

	Cathode Tip	Vaporizer
Part number	D1026367C	B1024543
Conductor material	Tungsten/26% rhenium	Nichrome V
Conductor diameter, cm	0.025	0.025
Sheath material	N/A	Inconel
Sheath diameter, cm	N/A	0.100
Insulation material	Al_2O_3 [a]	MgO
Number of turns (approx.)	8	5
Resistance, Ω	1.15 ± 0.05 at 25°C	2.86 ± 0.14 at 25°C

[a] Flame sprayed.

T2128

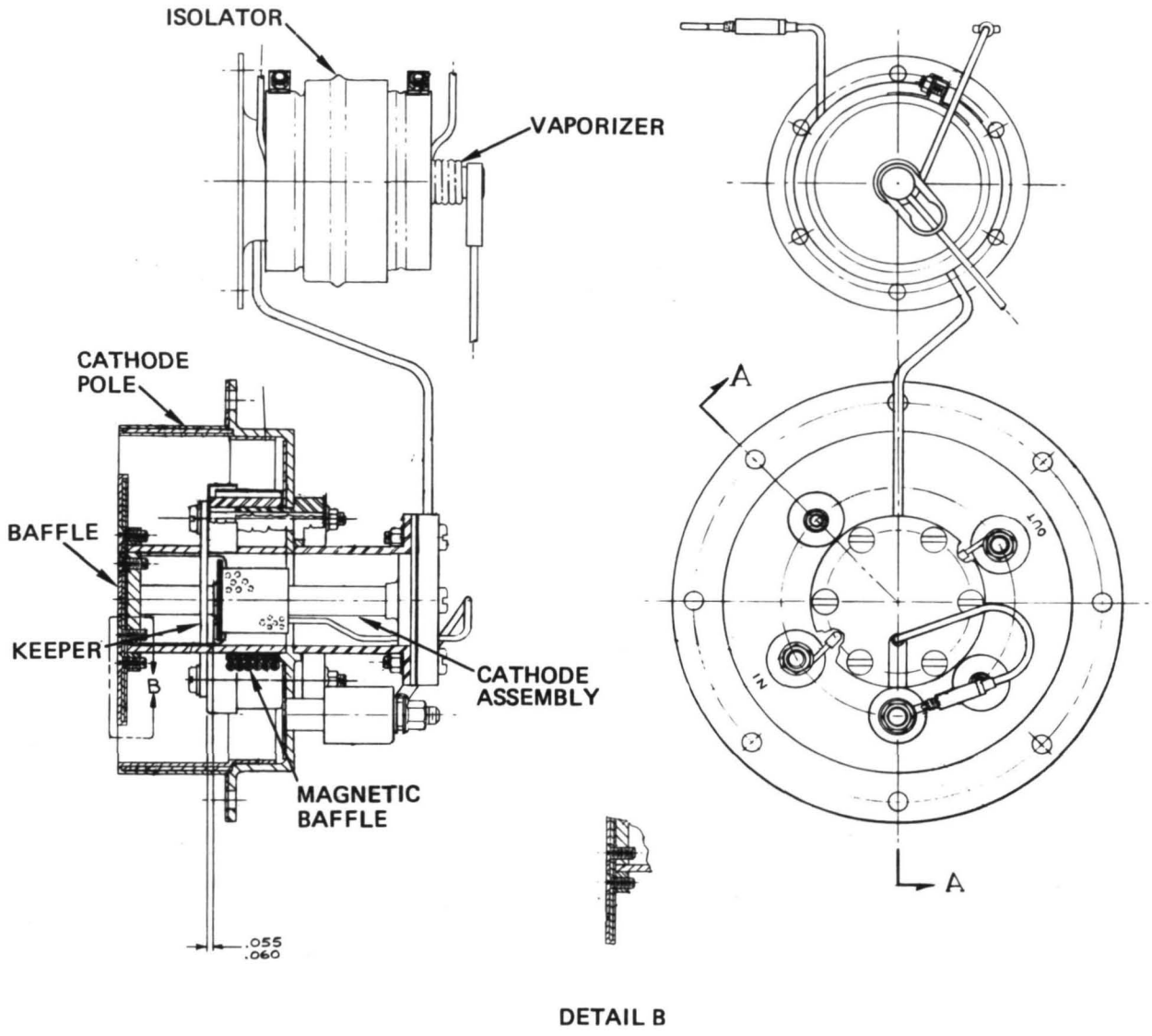

Figure 22. Drawing of CIV assembly, including cathode pole and magnetic baffle.

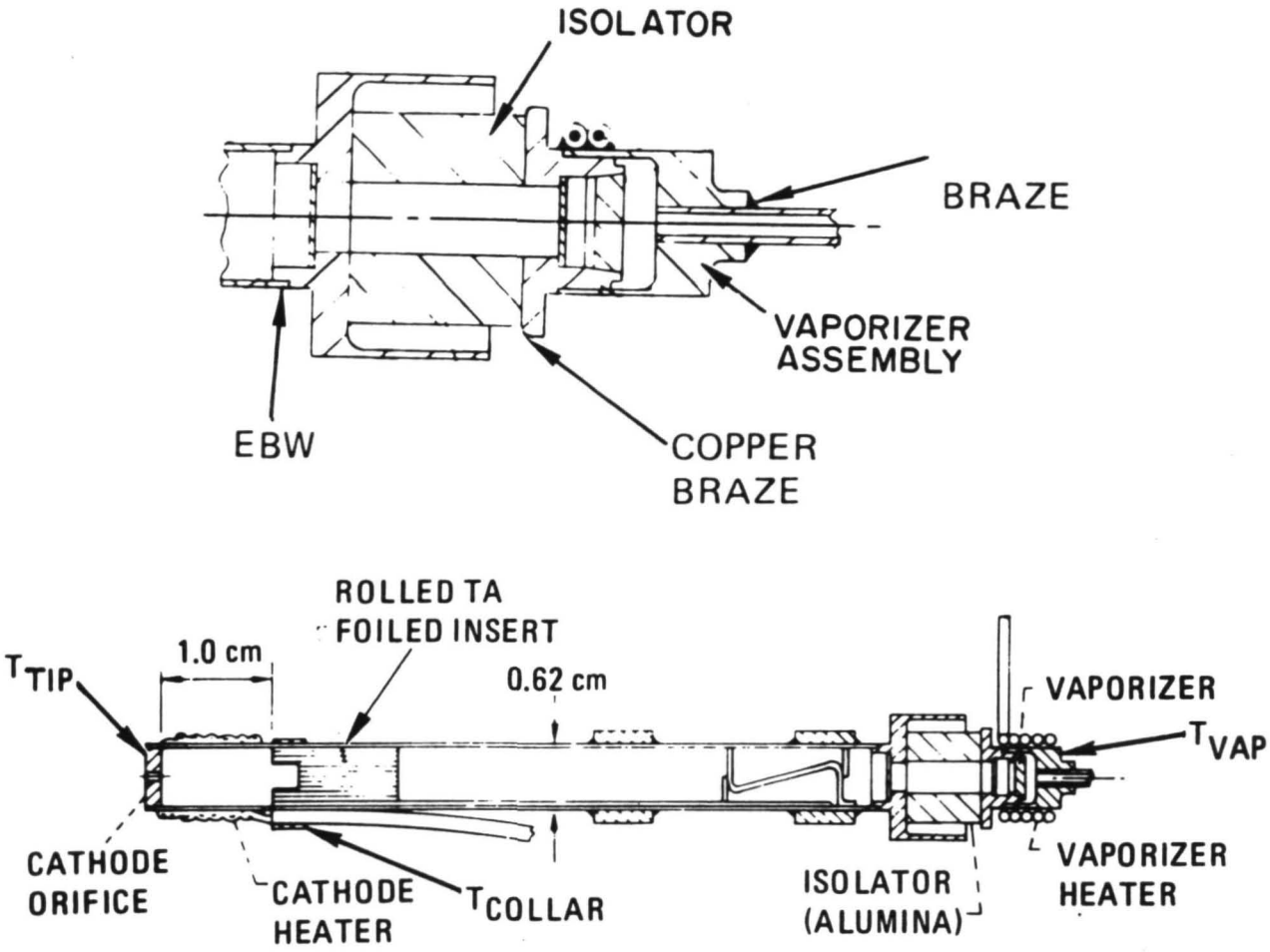

Figure 23. Drawing of neutralizer tube assembly.

The neutralizer cathode design and fabrication technique is the same as used for the main-cathode assembly, and no differentiation is made in the assembly procedures until the orifice is welded in place. The two tube supports are copper brazed to the cathode tube; the cathode insert and baffle are installed, and the tube and isolator sections are E-beam welded together to complete the tube assembly. The keeper, insulators, shields, and mounting brackets are mated with the tube subassembly to complete the entire NIV assembly, as shown in Figure 24.

f. Complete Thruster Assembly

The subassemblies (described in the preceding sections) are assembled to form the complete thruster, which is shown in Figure 25. The four hollow titanium cross beams (1.27 cm by 1.9 cm) stiffen the backplate and support the cathode, isolator, and phenum assemblies. To minimize the length of unsupported tubing, the single input feedline is connected to manifolds at two stations near the main and CIV subassemblies, as shown in Figure 25. The propellant manifolds are supported by double shadow-shielded insulators. Provision for a temperature sensor is made on one surface of the inlet manifold. The aluminum rear cover has four dip-brazed caps at the periphery to provide clearance between the cross braces and cover. The rear shield can be easily removed without disturbing the feed lines or the wiring harness. Individual thruster wires (e.g., heater, anode, magnetic baffle) connect to the input power cable harness at terminals which are grouped on brackets attached to the cross braces near the edge of the thruster in a relatively cool environment. The harness exits the thruster through two cable clamps.

2. 900-Series Design

Between March 1974 and May 1975 the first 30 cm EM thruster was endurance tested for 10,000 hr. This test identified two life-limiting problems: discharge-chamber erosion and the resultant deposition and spalling of sputtered material. Most of the differences between the 800-series and 900-series designs are changes which were

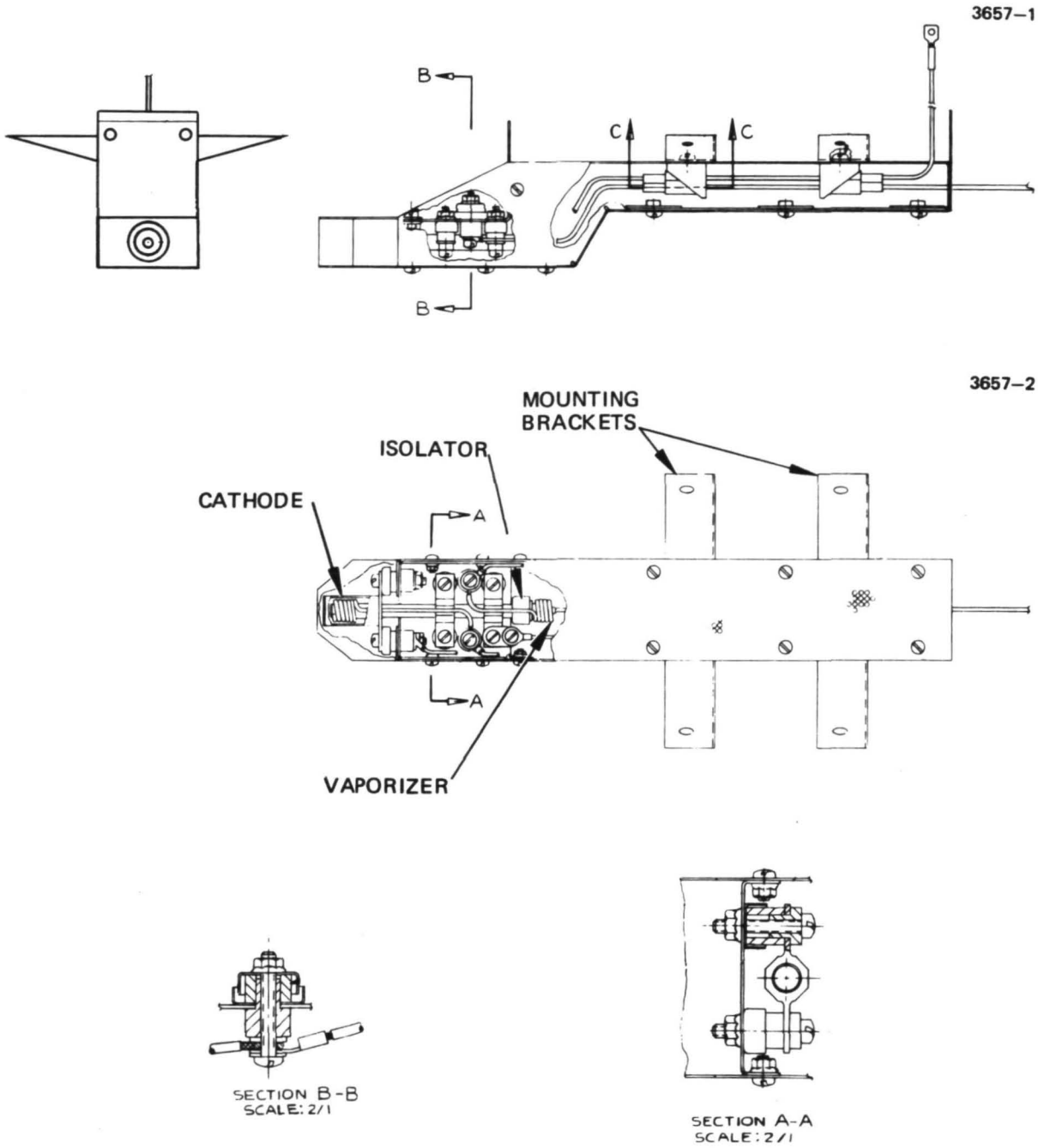

Figure 24. Neutralizer assembly, including keeper.

M10536

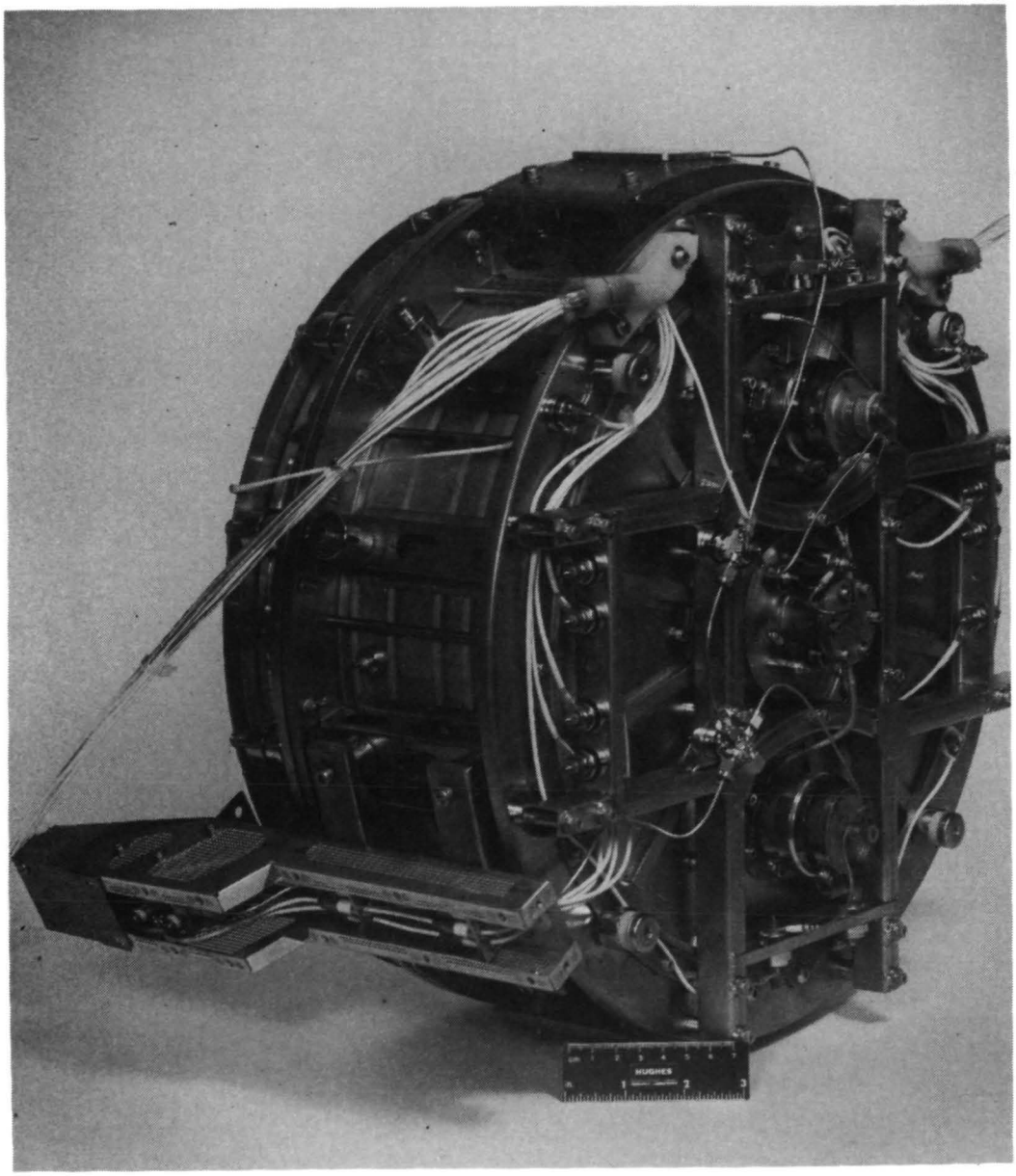

(a)

Figure 25. Photographs of 800 series thruster with ground screen and rear cover removed.

M10543

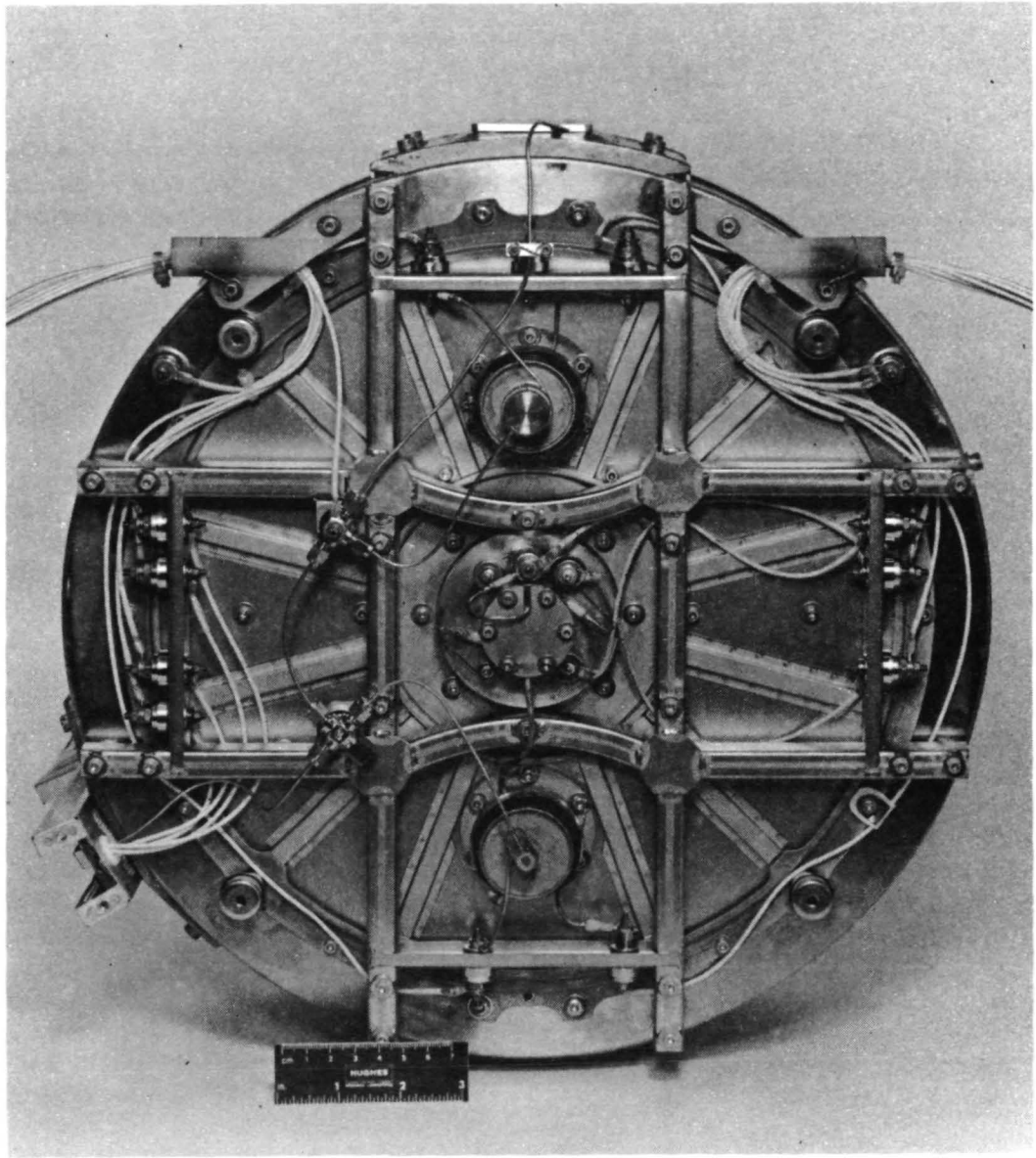

(b)

Figure 25. Continued.

incorporated to overcome these erosion-related problems. Joint efforts between NASA LeRC and Hughes have resulted in thruster modifications which, based on short-term erosion monitoring and double-ion measurements, show evidence of significantly reducing discharge-chamber erosion. These modifications were intended to

- Reduce erosion by reducing the ratio of doubly to singly charged ions
- Reduce erosion by covering the most erosion-sensitive surfaces with a low-sputter-yield material
- Prevent spalling of sputter-deposited flakes by grit blasting or covering the deposition sites with fine wire mesh.

Additional changes included in the 900-series design are (1) shadow shields on the anode insulators, (2) impregnated porous tungsten inserts in the cathodes to replace the rolled foil insert, (3) sheathed coaxial heaters substituted for the flame sprayed cathode tip heaters, (4) a layer of graphite on a section of the neutralizer bracket, (5) a demountable neutralizer-vaporizer assembly, and (6) improved neutralizer insulator shielding. Each change is described below.

a. Discharge Chamber

The majority of the differences between the 800-series and 900-series thrusters are in the discharge chamber. These changes were introduced to overcome the effects of discharge-chamber erosion. As described in Appendix A, the post-test analysis of the 10,000 hr endurance test thruster (S/N 701) established three erosion sites in the discharge chamber:

- Cathode pole piece
- Baffle
- Screen electrode.

The following deposition sites in the discharge chamber were identified:

- The thruster backplate and innermost wall of the propellant distribution plenum

- The central 7.6 cm of the anode
- The upstream boundaries of the interior and exterior surfaces of the cathode pole-baffle subassembly.

There were several locations in the discharge chamber that were neither appreciably eroded nor covered with deposits:

- The downstream surface of the plenum
- The upstream and downstream edges of the anode (about 1.3 to 2 cm)
- The screen pole piece.

Two approaches were taken to reduce discharge-chamber erosion. Since doubly charged ions are believed to be the major source of erosion, one approach was to reduce the percentage of doubly charged ions created within the discharge chamber. Short-term erosion-rate tests conducted at NASA LeRC indicated that the amount of erosion was influenced by the geometry of the baffle support structure.[7] Subsequent tests with a collimated ExB mass separator probe at HRL confirmed that the generation rate of doubly charged ions could be reduced by changing the dimensions of the baffle support, as shown in Figure 26.

The second approach to reducing discharge-chamber erosion was to cover the erosion sites, where possible, with tantalum (a more sputter-resistant material). This solution was applied to the baffle, the legs of the baffle support, the inner and outer surfaces of the cathode pole, and the interior of the CIV flange. The thickness of the tantalum cover for each surface is itemized in Table 6.

A second deterimental effect of discharge-chamber erosion experienced in the endurance test of thruster 701 was spalling of the material which had been sputter deposited on surfaces not subjected to erosion. The deposited material spalled off in flakes of sufficient size to bridge the interelectrode gap of the optics, thus shorting out the ion-extraction voltage.

Tests at NASA LeRC have demonstrated that the number and size of flakes spalled from sputter-deposited surfaces can be significantly reduced by roughening the surface on which the sputtered material is

6074-1R1

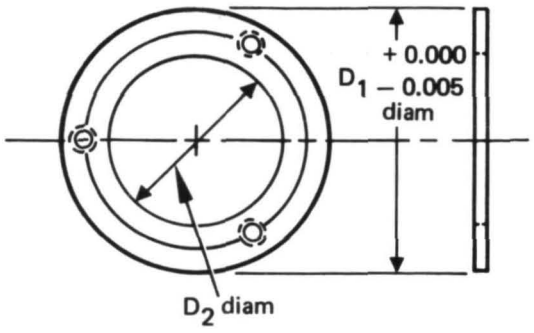

	D_1	D_2	D_3
900 SERIES	3.175	2.223	2.858
800 SERIES	2.029	1.143	1.588

6074–2R1

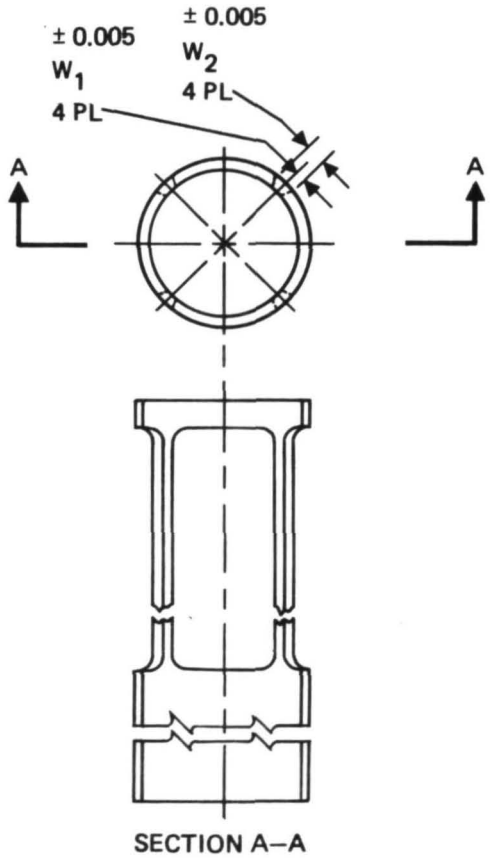

	"W_1"	"W_2"
900 SERIES	0.318	0.635
800 SERIES	0.157	0.318

Figure 26. Dimensions of baffle support in 800 series and 900 series thruster designs.

deposited. This can be done in two ways: grit blasting and covering the surface with a fine stainless-steel wire mesh. Both techniques were used in the 900-series thruster. Table 7 itemizes the sites where these flake-control methods were applied within the discharge chamber. Figure 27 illustrates how the stainless-steel mesh was added to various components.

The fourth (and final) change in the discharge chamber was also a consequence of the 10,000 hr endurance test. During the post-test disassembly of thruster 701, it was discovered that two of the six anode insulators had suffered damage. After an extensive investigation, including scanning electron microscope photography and K_α X-ray analysis, it was concluded that the damage to the anode insulators was a direct result of the deposition of sputtered material (see Appendix A). Therefore, in the 900-series thrusters, shadow shields have been placed over the anode end of the anode insulators. Insulator material was also changed from Al-300 to Lucalox.

Table 6. Discharge-Chamber Surfaces Covered with Tantalum to Reduce Erosion

Surface	Tantalum Thickness, cm
Baffle—upstream side	0.036-0.041
Baffle—downstream side	0.076-0.089
Cathode polepiece—inside	0.074-0.089
Cathode polepiece—outside	0.070-0.090
CIV flange—interior	0.038-0.051
CIV flange—exterior	0.076-0.089
Baffle support legs	0.025
Plug—baffle support	0.254

T2118

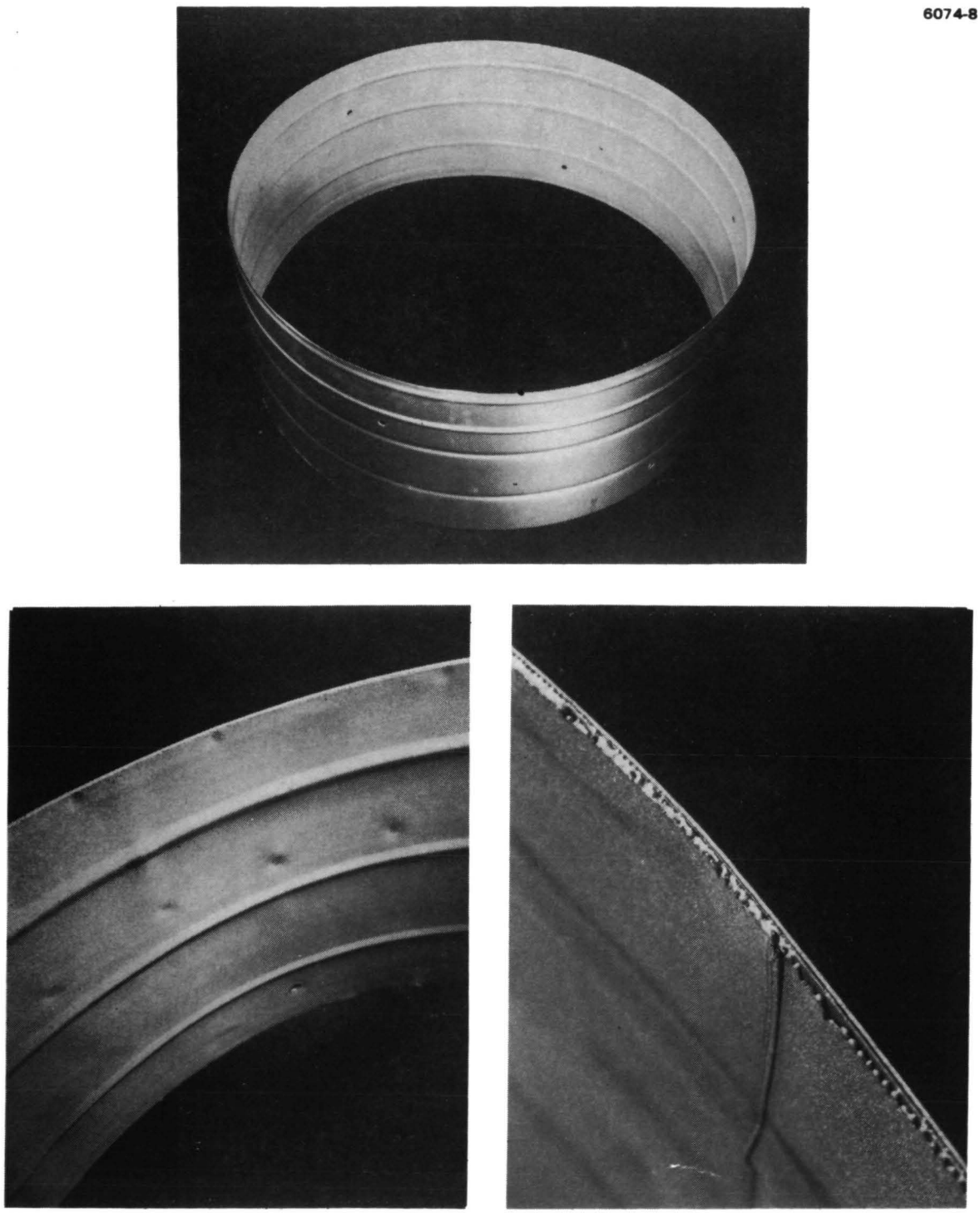

(a) Anode

Figure 27. Discharge chamber surfaces covered with stainless-steel mesh to reduce spalling.

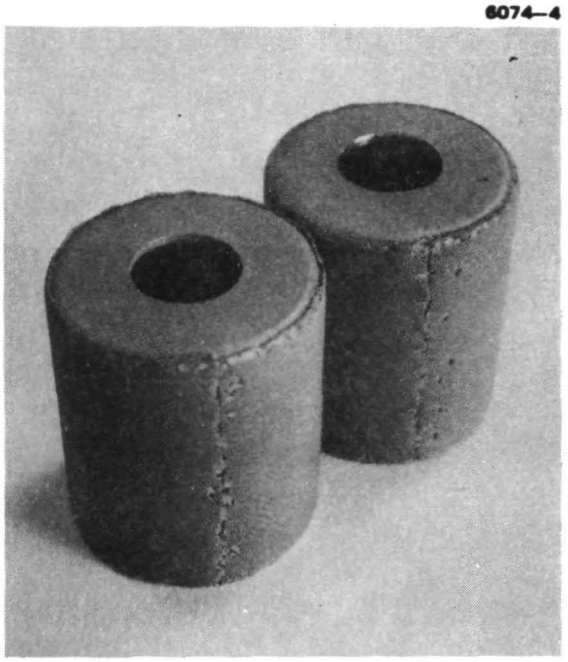

(b) Keeper shield

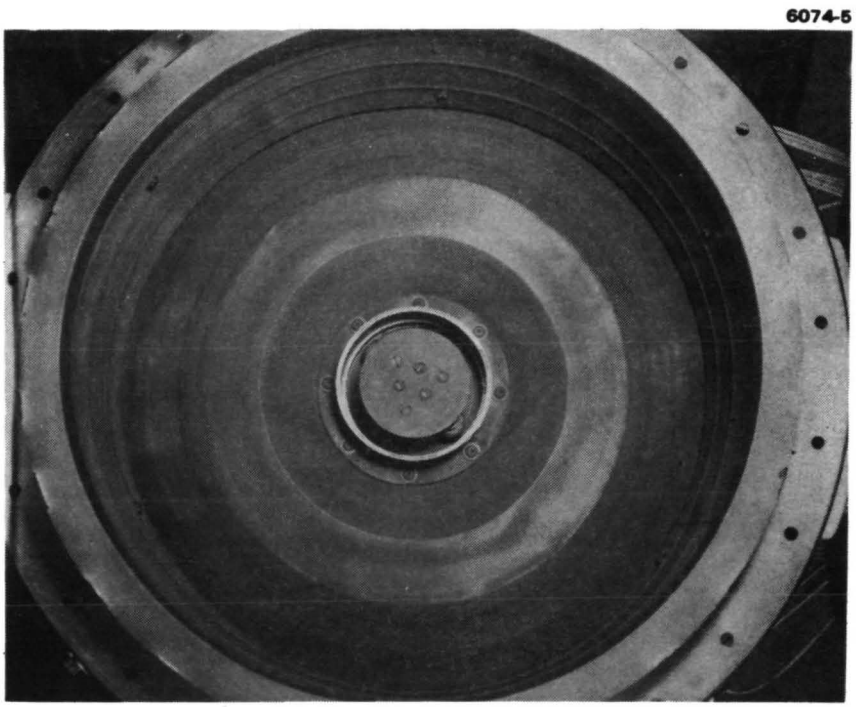

(c) Discharge-chamber backplate and anode

Figure 27. Continued.

Table 7. Locations where Wire Mesh and/or Grit Blasting Were Used to Reduce Spalling of Sputter-Deposited Material

Surface	Covered by Wire Mesh	Grit Blasted
Anode	X	X
Backplate and plenum	X	X
CIV flange Ta cover		X
Screen pole—inner diameter		X
Screen electrode—inactive area		X
Main keeper		X
Magnetic baffle coil		X
Mask		X
Keeper insulator shields	X	X
CIV exterior flange	X	X
Outer shell—interior upstream and downstream ends (~2.5 cm)		X

T2129

b. Cathodes

In the 900-series thrusters, two changes from the 800-series design were made in both the main and neutralizer cathodes. First, impregnated porous tungsten inserts replaced the rolled tantalum foil inserts. Second, sheathed coaxial heaters replaced the flame sprayed ceramic encapsulated tip heaters.

The insert previously used was made of rolled tantalum foil, coated with a barium-calcium carbonate material. The carbonate compound activates to form a low-work-function barium oxide coating. This

type of insert has provided long life and stable operation under controlled conditions, but it is sensitive to exposure to water vapor. As described in Section 3, a variation in neutralizer operation was experienced during the 10,000 hr endurance test. This may have been due to the neutralizer insert. Also, the oxide coating will react with the tantalum foil rather severely at operating temperatures greater than $1000^{\circ}C$.

Although the rolled foil insert has operated satisfactorily, its vulnerability to contamination and embrittlement, and consequently to failure, led to its replacement by a porous tungsten insert with impregnated barium aluminate. This type of insert is considered to be less vulnerable to high-temperature excursions, contamination by atmospheric exposure, and mechanical damage than the rolled tantalum foil insert.[8] The insert material now in use is 84% dense porous tungsten and contains approximately 0.2 g of $4\ BaO \cdot CaO \cdot Al_2O_3$ impregnant. This insert is formed in the shape of a cylindrical shell with 2.54 cm length, 0.533 cm outside diameter, and 0.381 cm inside diameter.

During the development of the 30 cm thruster, the cathode heater experienced several evolutionary changes. Initially, swaged coaxial-type heaters were used, primarily for convenience; these were held in place only by the spring action of the heater coiled around the cathode tube. When it was necessary to consider vibrational qualification, the heater was brazed to the cathode tube. Difficulties were then encountered with a tantalum–braze-material interaction. Primarily because a ceramic-encapsulated cathode heater had been successfully used in the SERT II thruster, an effort was made to scale this type of heater to the 0.635 cm diameter cathodes used in the 30 cm thruster rather than to attack the braze interaction problem. After several iterations on heater design and fabrication procedures, it was determined that the quality-control required to successfully fabricate the aluminum encapsulated heaters in a reliable manner was too costly and time consuming to be feasible. Consequently, the coaxial, swaged heater design was reinstituted; the heater is now held in place mechanically with an E-beam

tack weld between the outer conductor of the coaxial heater material and a bracket fastened to the cathode tube.[9] The sheathed heater on the main cathode of thruster 901 is shown in Figure 28.

c. Neutralizer

In addition to the insert and tip heater changes described in the previous section, three other modifications were incorporated in the 900-series neutralizer assembly: (1) a layer of graphite added to the forward section of the neutralizer bracket, (2) a demountable vaporizer assembly, and (3) improved shielding of the wiring feed-through insulators.

As shown in Figures A-102 and A-103 (Appendix A), the downstream edge of the inboard surface of the neutralizer cover was eroded through during the 10,000 hr endurance test. Since energetic ions with trajectories at angles up to 75° have been measured under the 2.5 kW Advanced Technology Ion Thruster Program (NAS 3-17831), relocating the neutralizer to avoid interception by all beam ions is not practical. To reduce the amount of erosion and ensure the required lifetime, a 1.3 mm thick layer of graphite was added to the three surfaces of the neutralizer bracket shown in Figure 29. Graphite was selected because of its low sputter yield.

The NIV assembly was modified to provide a demountable isolator-vaporizer subassembly. Mating flanges were added to the neutralizer cathode (Figure 30(a)) and to the downstream end of the isolator (Figure 30(b)). The two subassemblies were then clamped together as shown in Figure 30(c). This configuration permits separate replacement of the neutralizer cathode, insert, or isolator-vaporizer subassembly.

The need for improved shielding of the wiring feed-through insulators was determined after the 10,000 hr endurance test. If the neutralizer is to be isolated from the spacecraft, then the surfaces of the insulators that support the NIV and the associated wiring must be kept clean. After the endurance test, the insulators that support the NIV wiring showed considerable darkening from coating. In the 900-series design, a solid piece of titanium has been positioned over the wiring feed throughs to act as a sputter shield. The shield is secured in place under the standard perforated neutralizer cover.

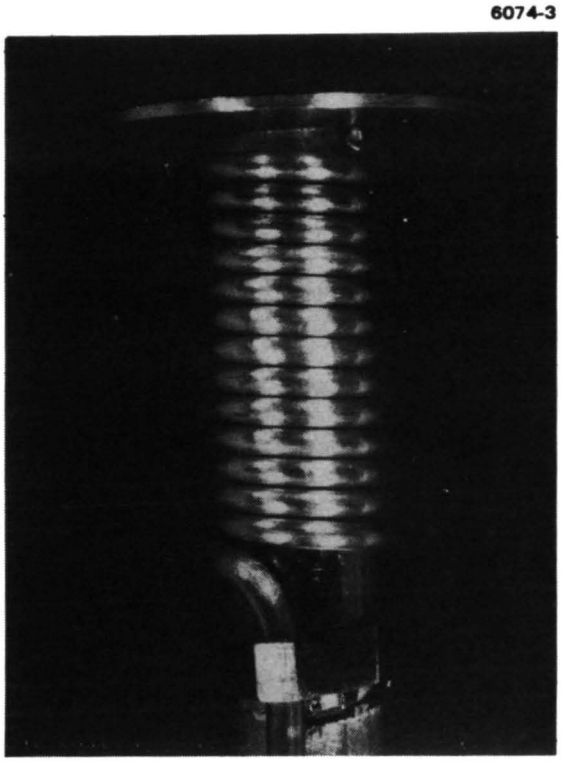

Figure 28. Main cathode of thruster 901 showing sheathed heater used in 900 series design.

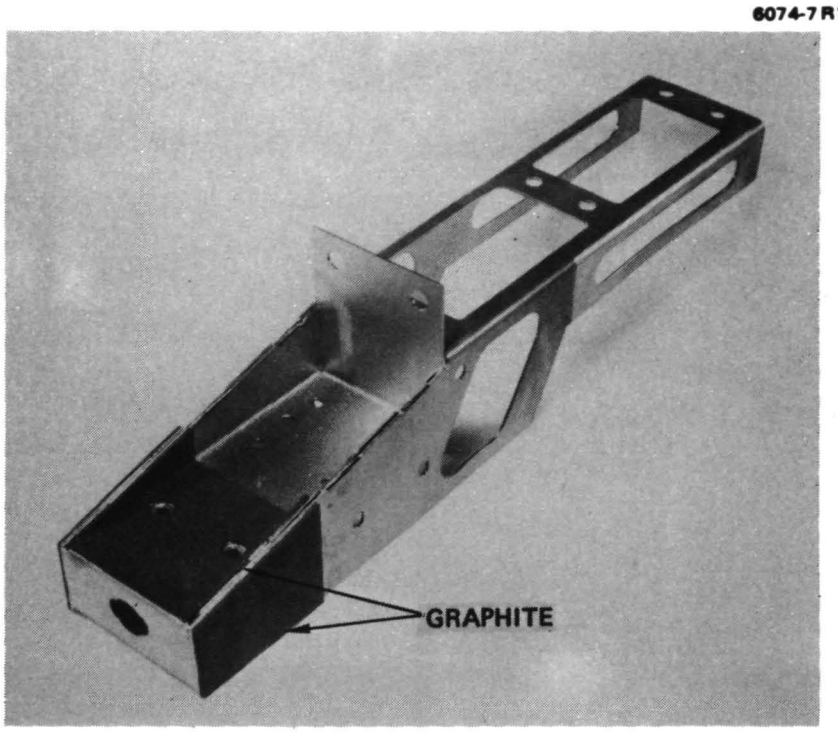

Figure 29. 900-series neutralizer bracket showing graphite added to reduce erosion.

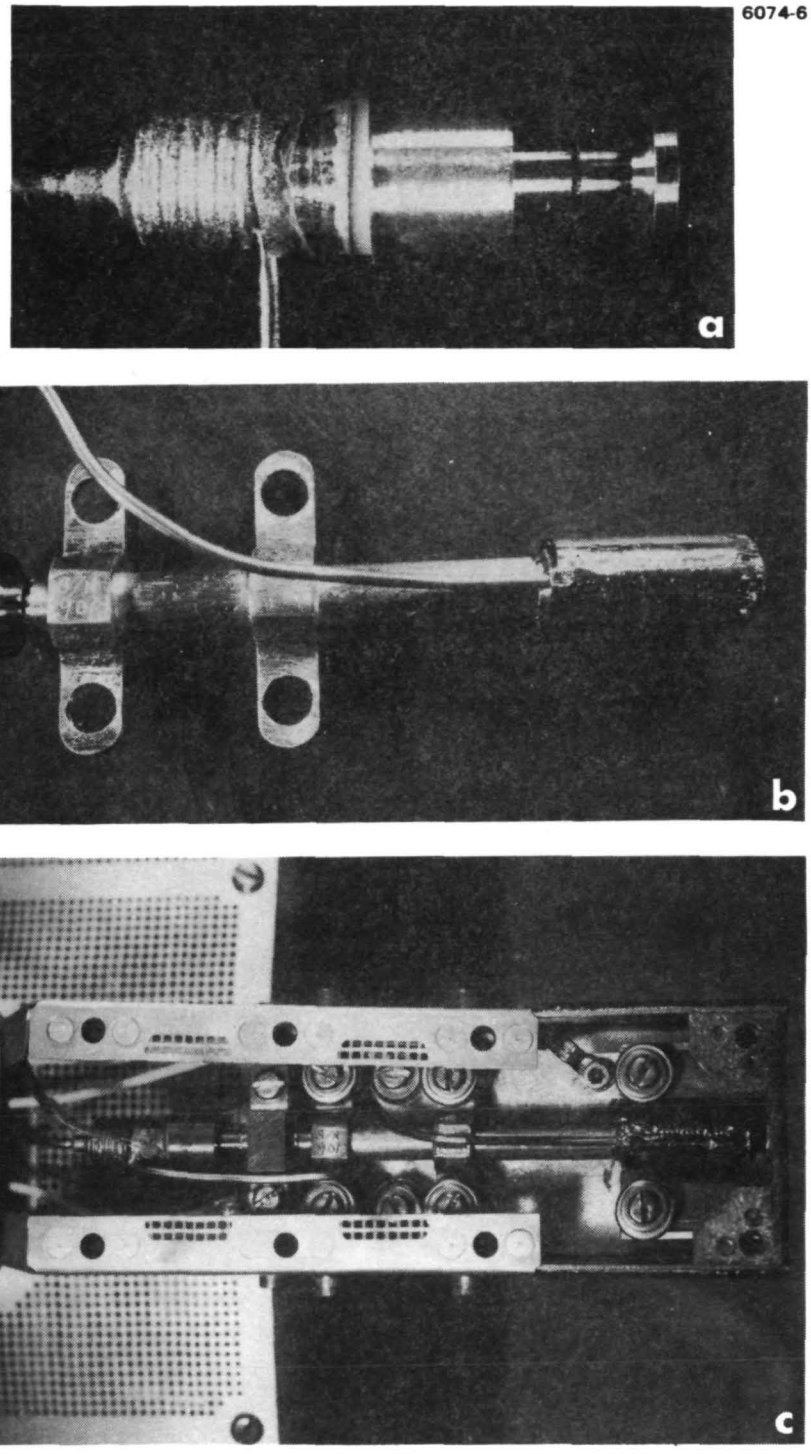

Figure 30. 900-series neutralizer assembly showing demountable isolator-vaporizer sub-assembly.

B. THRUSTER ACCEPTANCE TESTS

Six 30 cm EM thrusters were fabricated under this contract: three 800-series (S/N 801, 802, 804) and three 900-series (S/N 901, 902, 903). The differences between the 800-series and 900-series designs are described above. Five of the six thrusters were acceptance tested at Hughes prior to delivery. In accordance with the NASA program manager's directions, thruster 903 was shipped to LeRC without being tested.

Pre-delivery acceptance testing was performed to confirm proper electrical operation and propellant utilization. Electrical operating performance was determined by measuring all input voltages and currents required to start and operate the thruster. Propellant utilization was determined by measuring the rate of mercury flow through the main, cathode, and neutralizer vaporizer, converting the flowrates to an equivalent electrical current, and dividing the measured beam current by the total mercury flowrate equivalent electrical current.

All five thrusters were tested at the rated beam current of 2 A and the specified net accelerating voltage of +1100 V as part of the acceptance test procedure. The results of the acceptance testing are summarized in Table 8. The first four thrusters tested (801, 802, 804, and 901) were operated at 185 eV/ion. S/N 902 was tested at 198 eV/ion to compare its performance with that of S/N 901, which was then being endurance tested at 198 eV/ion.

After completing acceptance testing, two of the 800-series thrusters were modified and tested as prototypes of the 900-series design. Thruster 802 was modified and tested at NASA LeRC; thruster 804 was modified and tested at HRL. Results of the tests of 802-M and 804-M as well as endurance test results for thruster 901 are included in Table 8 for comparison purposes. To facilitate the comparison of discharge-chamber efficiencies, a constant 30 mA equivalent flow through the neutralizer was used for the data presented in Table 8. The correction factors for doubly charged ions and beam divergence were developed from beam probe measurements made under Contract NAS 3-17831.

Table 8. 30 cm EM Thruster: Performance Comparison

Thruster	ev/Ion	Electrical Efficiency, %	Propellant Efficiency, %	α[a]	F_T[b]	Total Efficiency, %	Test Location	Remarks
801	185	83.8	92.2	0.9556	0.983	68.2	HRL	
802	185	83.8	95.8	0.9475	0.983	69.2	HRL	
804	185	83.8	93.6	0.9533	0.983	68.9	HRL	
802-M	185	83.8	91.2	0.9592	0.983	67.9	LeRC	Prototype for 900 series, modified at LeRC
804-M	185	83.8	90.7	0.9603	0.983	67.7	HRL	Prototype for 900 series, modified at HRL
901	185	83.8	92.1	0.9570	0.983	68.3	HRL	
901	185	83.8	90.8	0.9602	0.983	67.8	SSL[c]	Endurance test
901	198	83.0	94.7	0.9501	0.983	68.6	SSL	Endurance test
902	198	83.0	94.7	0.9501	0.983	68.6	HRL	

[a]Correction factor for doubly charged ions.

[b]Correction factor for beam divergence of 0.4% compensated optics.

[c]Hughes Space Simulation Laboratory, El Segundo, CA.

T2120

Very little performance dispersion was found during acceptance testing of the ETM thrusters. Variations in total efficiency for 800- and 900-series thrusters ranged from 67.7 to 69.2%.

Page
Intentionally
Left Blank

SECTION 3

THE 10,000 HR ENDURANCE TEST OF THRUSTER 701

From March 1974 until May 1975, the first EM 30 cm thruster (S/N 701) was endurance tested for 10,000 hr. This test was the culmination of an endurance test program conducted under Contract NAS 3-15523, which included several shorter duration tests. The final 7300 hr of the 10,000 hr test and the post-test analysis of thruster 701 were performed under the Fabrication and Verification Testing of ETM 30 Centimeter Diameter Ion Thrusters contract (NAS 3-17803). In the interest of completeness, this report includes the results of the full 10,000 hr test and of the complete post-test analysis.

By the time the 10,000 hr test was to start, the first EM 30 cm thrusters (S/N 701) being developed under contract NAS 3-16528 had been assembled and tested. The EM thruster development had been occurring in parallel with the early part of the endurance test program. Thus, the thruster changes which had been adopted as solutions to the problems identified by the shorter term tests had been incorporated in thruster 701. The availability of thruster 701 provided an opportunity to endurance test a new thruster in which all the life-extending changes had been made.

A. TEST RESULTS

1. Thruster Performance

The endurance test as initially contracted was to be run for 6000 hr at a beam current of 1.5 A. Subsequent contract modifications provided for increasing the beam current in steps to 2 A and extended the test duration to 10,000 hr. The number of hours accumulated and the performance achieved at each beam current level is summarized in Table 9; the discharge voltage was held at 37 V. More detailed performance data is presented in Tables 10 and 11. When the effects of baffle erosion (described below) became evident while operating at

Table 9. Summary of Thruster Performance During 10,000 hr Test

Test Period, hr	Beam Current, A	Accel Current, A	High-Voltage Trip/Rate No./Hr	eV/Ion	Total Power, kW	Propellant Efficiency (Meter Value), %	Electrical Efficiency (Meter Value), %	Total Efficiency (Corrected),[a] %	Effective Specific Impulse,[a] sec	Thrust (Corrected),[a] N	Remarks
100 to 2110	1.50	0.0030	0.14	185	2.03	88.0	83.3	65.7	2800	0.098	
2110 to 2750	1.61	0.0033	0.19	185	2.17	89.8	83.6	67.0	2850	0.104	
2750 to 3000	1.71	0.0034	0.36	185	2.30	92.3	83.6	68.6	2920	0.111	
3000 to 6050	1.75	0.0038	0.21	185	2.36	93.3	83.5	69.2	2950	0.113	Flakes on optics at hour 4530. Hole in baffle at hour 5845.
6050 to 7300	1.51	0.0029	1.21	214	2.08	93.1	81.3	67.8	2960	0.098	Baffle edge erosion at hour 6845. Cryoshroud LN_2 leak at hour 7197.
7300 to 7500	1.00	0.0017	0.42	278	1.47	87.3	76.7	61.0	2800	0.066	
7500 to 8130	1.00	0.0025	1.35	240	1.43	90.4	78.5	64.8	2900	0.066	Chamber pressure on 10^{-5} Torr scale until LN_2 leak eliminated at hour 8036.
8130 to 8380	1.01	0.0018	0.29	253	1.46	85.7	78.2	61.2	2750	0.066	
8380 to 9000	1.01	0.0018	1.24	278	1.48	85.7	76.9	60.0	2750	0.066	
9000 to 9300	1.01	0.0020	2.00	296	1.50	83.9	76.0	58.8	2690	0.066	
9300 to 10000	0.51	0.0010	0.41	370	0.82	70.5	69.8	46.6	2300	0.034	

[a]Correction factors for doubly charged ions and beam divergence were developed from beam probe measurements made under Contract NAS 3-17831. Correction factors used were for 185 ev/ion operation.

T1852

Table 10. Performance Summary of 10,000 hr Test of Thruster 701

Time Period, hr	J_S, A	J_A, mA	V_I, V	V_{CK}, V	V_{NK}, V	V_G, V	$\dot{m}_M$, eq. A	$\dot{m}_C$, eq. A	$\dot{m}_N$, eq. A	η_{m_D}, %	η_{m_T}, %	Arcs, No./hr
100 to 250	1.503	2.90	37.55	7.47	14.19	11.88	1.580	0.108	0.029	88.9	87.4	0.14
200 to 300	1.503	2.94	37.55	7.62	14.43	12.44	1.580	0.110	0.034	88.8	87.0	0.14
300 to 400	1.505	3.04	37.55	7.73	14.78	12.58	1.591	0.111	0.033	88.2	86.6	0.16
400 to 500	1.499	3.06	37.38	7.60	14.32	12.58	1.570	0.109	0.038	89.1	87.1	0.08
500 to 600	1.497	3.09	37.15	7.44	14.36	12.56	1.568	0.108	0.036	89.1	97.3	0.11
600 to 700	0.495	3.11	37.09	7.40	14.52	12.58	1.561	0.103	0.037	89.7	97.7	0.12
700 to 800	1.484	3.12	37.03	7.30	14.25	12.61	1.553	0.108	0.037	89.2	97.2	0.22
800 to 870	1.475	3.08	36.92	7.19	14.18	12.60	1.523	0.105	0.037	90.4	89.4	0.22
870 to 1000	1.498	2.95	36.97	7.51	14.90	12.79	1.584	0.106	0.036	88.5	86.6	0.27
1000 to 1100	1.495	3.16	36.90	7.35	13.72	13.20	1.556	0.106	0.046	89.8	87.4	0.14
1100 to 1240	1.504	3.19	36.90	7.34	14.10	12.86	1.570	0.106	0.038	89.6	87.6	0.10
1250 to 1300	1.502	3.05	37.15	7.31	13.97	12.70	1.560	0.095	0.035	90.6	88.7	0.15
1340 to 1400	1.496	2.99	37.35	7.25	13.88	12.78	1.547	0.096	0.038	90.9	88.8	0.11
1540 to 1600	1.508	2.79	37.25	7.63	14.01	13.00	1.583	0.099	0.054	89.5	86.7	0.09
1600 to 1700	1.508	3.01	37.23	7.44	14.51	13.01	1.542	0.100	0.035	91.7	89.7	0.07
1700 to 1800	1.508	3.05	37.08	7.39	14.54	13.11	1.554	0.098	0.035	91.1	89.2	0.12
1800 to 1910	1.508	3.05	37.02	7.33	14.51	13.16	1.556	0.097	0.036	91.0	89.1	0.06
1930 to 2000	1.508	3.05	36.96	7.31	14.51	13.21	1.559	0.095	0.036	91.0	89.0	0.10
2000 to 2110	1.509	3.04	37.05	7.36	14.51	13.25	1.541	0.097	0.037	91.9	89.9	0.15
100 to 2100	1.500	3.03	37.16	7.41	14.30	12.79	1.562	0.103	0.037	89.9	88.0	0.14
2130 to 2200	1.609	3.30	36.55	7.38	15.69	14.46	1.670	0.095	0.036	91.0	89.2	0.10
2200 to 2270	1.608	3.37	36.55	7123	15.52	13.60	1.667	0.096	0.029	91.0	89.6	0.13
2280 to 2400	1.612	3.26	36.46	7.40	14.52	13.10	1.680	0.093	0.032	90.8	89.1	0.14
2130 to 2400	1.610	3.31	36.51	7.34	15.15	13.60	1.674	0.094	0.032	90.9	89.3	0.13
2400 to 2500	1.613	3.42	36.49	7.25	14.49	13.20	1.678	0.094	0.034	90.8	89.1	0.22
2500 to 2600	1.618	3.35	37.07	7.17	14.44	13.23	1.654	0.091	0.033	92.6	90.8	0.17
2600 to 2700	1.617	3.34	37.04	7.15	14.42	13.54	1.653	0.090	0.036	92.6	90.7	0.28
2700 to 2750	1.614	3.20	37.11	7.56	15.29	13.66	1.655	0.093	0.038	92.1	90.2	0.28
2130 to 2750	1.613	3.33	36.73	7.29	14.82	13.47	1.666	0.093	0.034	91.5	89.8	0.19
2750 to 2800	1.708	3.41	36.94	6.68	15.42	14.20	1.719	0.092	0.033	94.1	92.4	0.42
2800 to 2900	1.707	3.42	37.06	6.66	15.45	14.32	1.712	0.091	0.037	94.5	92.6	0.21
2900 to 3000	1.714	3.50	37.16	6.81	15.42	14.42	1.730	0.087	0.041	94.1	92.1	0.49
2750 to 3000	1.710	3.45	37.08	6.72	15.43	14.34	1.721	0.090	0.038	94.3	92.3	0.36
3000 to 3100	1.761	3.69	37.06	6.62	15.88	15.04	1.778	0.086	0.044	94.2	92.1	0.24
3100 to 3200	1.760	3.66	37.34	6.56	16.30	15.42	1.768	0.087	0.049	94.7	92.2	0.37
3200 to 3300	1.760	3.68	37.28	6.54	16.47	15.36	1.756	0.088	0.058	95.3	92.4	0.18
3300 to 3400	1.760	3.66	37.26	6.52	17.92	14.38	1.772	0.087	0.026	94.5	93.2	0.18
3400 to 3500	1.759	3.68	37.30	6.50	17.94	14.65	1.768	0.086	0.027	94.6	93.3	0.19
3500 to 3600	1.761	3.69	37.27	6.48	17.96	15.16	1.770	0.087	0.032	94.6	93.1	0.19
3600 to 3700	1.762	3.69	37.26	6.45	17.96	14.97	1.764	0.086	0.030	95.0	93.5	0.14
3700 to 3800	1.763	3.66	37.31	6.44	17.84	14.32	1.761	0.086	0.031	95.2	93.7	0.19
3800 to 3900	1.756	3.69	37.22	6.55	17.82	14.86	1.759	0.086	0.031	95.0	93.4	0.27
3900 to 4000	1.752	3.66	37.14	6.46	17.78	14.35	1.755	0.085	0.028	95.0	93.6	0.18
4000 to 4100	1.749	3.70	37.14	6.64	15.68	12.32	1.742	0.086	0.027	95.4	94.1	0.25
4100 to 4200	1.749	3.68	37.10	6.72	15.64	12.50	1.763	0.086	0.028	94.3	92.9	0.12
4200 to 4300	1.747	3.64	37.02	6.58	15.54	12.60	1.760	0.084	0.028	94.5	93.0	0.41
4300 to 4400	1.744	3.60	37.10	6.48	15.44	12.80	1.748	0.083	0.030	95.0	93.5	0.25
4400 to 4500	1.750	3.62	37.02	6.36	15.44	13.16	1.756	0.083	0.031	94.9	93.4	0.21
4500 to 4600	1.750	3.65	(a)	6.36	15.42	13.88	1.759	0.082	0.035	94.9	93.1	0.32
4600 to 4700	1.748	3.98	37.21	6.40	17.22	14.64	1.758	0.080	0.035	94.9	93.1	0.21
4700 to 4800	1.753	4.06	37.22	6.42	16.87	15.52	1.744	0.084	0.040	95.7	93.6	0.17
4800 to 4900	1.755	4.14	37.06	6.32	17.86	17.06	1.750	0.080	0.069	95.7	92.2	0.16
4900 to 5000	1.752	4.12	37.16	6.28	17.48	15.20	1.754	0.081	0.048	95.3	92.8	0.27
5000 to 5100	1.753	4.16	37.36	6.28	17.16	15.44	1.751	0.080	0.035	95.5	93.7	0.15
5100 to 5200	1.754	4.14	37.10	6.29	17.19	15.54	1.751	0.079	0.036	95.6	93.8	0.11
5200 to 5300	1.752	4.16	(b)	6.27	17.10	15.36	1.754	0.077	0.035	95.6	93.7	0.02
5300 to 5400	1.751	4.16		6.27	17.10	15.18	1.756	0.076	0.034	95.4	93.6	0.04
5400 to 5500	1.751	4.12		6.22	17.44	16.31	1.750	0.076	0.048	95.7	93.2	0.15
5500 to 5600	1.748	4.10		6.23	17.78	14.70	1.759	0.075	0.028	95.1	93.7	0.04

(a) Data channel failure at hour 4504.8.

(b) Data channel failure at hour 5161, V_i is periodically checked at the bulkhead.

T2130

Table 10. Continued

Time Period, hr	J_S, A	J_A, mA	V_I, V	V_{CK}, V	V_{NK}, V	V_G, V	$\dot{m}_M$, eq. A	$\dot{m}_C$, eq. A	$\dot{m}_N$, eq. A	η_{m_D}, %	η_{m_T}, %	Arcs, No./hr
5600 to 5700	1.744	4.10		6.26	17.83	14.76	1.753	0.076	0.029	95.1	93.6	0.11
5700 to 5800	1.752	4.10		6.37	20.15	20.86	1.734	0.084	0.029	96.1	94.6	0.16
5800 to 5900	1.752	4.08		6.59	15.73	13.69	1.743	0.083	0.031	95.7	94.1	0.04
5900 to 6000	1.753	3.54		6.60	15.70	13.97	1.755	0.083	0.032	95.2	93.5	0.35
6000 to 6050	1.756	3.61		6.59	15.34	13.47	1.642	0.092	0.042	--	--	≥11.1
6050 to 6200	1.510	3.01		6.37	16.82	13.60	1.479	0.081	0.032	96.6	94.7	1.20
6200 to 6300	1.514	3.30		7.29	14.84	12.01	1.532	0.085	0.034	93.4	91.5	0.31
6300 to 6400	1.525	3.14		7.57	14.87	12.10	1.534	0.084	0.034	94.1	92.1	0.20
6400 to 6500	1.524	3.02		7.62	14.90	12.20	1.530	0.081	0.034	94.4	92.5	0.34
6500 to 6600	1.521	3.00		7.77	14.88	12.32	1.528	0.081	0.035	94.3	92.3	0.56
6600 to 6700	1.503	2.87		8.66	14.71	12.56	1.488	0.084	0.038	95.4	93.2	0.34
6700 to 6800	1.502	2.81		8.62	14.79	12.63	1.499	0.080	0.037	94.9	92.8	0.18
6800 to 6900	1.497	2.77		8.68	14.81	12.76	1.486	0.080	0.038	95.4	93.1	0.25
6900 to 7000	1.498	2.79		8.92	14.82	13.09	1.478	0.081	0.040	95.9	93.5	0.20
7000 to 7100	1.499	2.78		9.44	14.80	13.39	1.489	0.083	0.046	95.2	92.3	0.28
7100 to 7200	1.506	2.77		9.25	14.87	13.83	1.473	0.084	0.049	96.5	93.8	0.10
7200 to 7300	1.509	2.63		8.93	15.49	13.97	1.465	0.080	0.041	97.5	95.0	≥0.59
7300 to 7400	1.005	1.68		10.48	16.84	12.70	0.995	0.118	0.039	90.1	87.1	--
7400 to 7500	1.003	1.67		10.28	16.82	12.84	0.980	0.124	0.040	90.7	87.5	--
7500 to 7600	1.005	2.04		10.86	17.14	14.26	0.979	0.117	0.040	91.5	88.3	--
7600 to 7700	1.008	2.01		10.87	17.53	14.02	0.940	0.119	0.044	95.0	91.2	--
7700 to 7800	1.009	2.54		10.19	17.45	13.60	0.920	0.120	0.042	96.7	93.0	--
7800 to 7900	1.008	2.70		10.09	17.48	13.79	0.915	0.121	0.042	97.0	93.2	--
7900 to 8000	1.008	2.89		11.26	17.50	13.99	0.900	0.122	0.048	98.3	93.9	--
8000 to 8120	1.007	2.49		10.28	16.46	11.36	1.101	0.070	0.039	85.7	83.0	0.29
8130 to 8200	1.008	1.79		10.34	16.05	11.63	1.004	0.112	0.039	90.1	87.1	0.10
8200 to 8300	1.008	1.74		10.75	16.03	11.67	1.020	0.109	0.039	89.1	86.1	0.27
8300 to 8380	1.008	1.94		9.41	16.04	11.73	1.087	0.072	0.039	86.8	84.0	0.07
8390 to 8500	1.008	1.77		10.30	16.08	12.04	0.996	0.113	0.041	90.7	87.5	0.31
8500 to 8600	1.008	1.76		10.18	16.02	11.98	1.007	0.112	0.041	89.9	86.7	0.37
8600 to 8700	1.008	1.78		9.94	16.01	12.17	1.011	0.109	0.043	89.8	86.5	0.88
8700 to 8800	1.009	1.84		9.45	16.45	12.69	1.062	0.095	0.043	87.0	93.9	0.70
8800 to 8900	1.010	1.78		9.76	16.61	12.35	1.028	0.108	0.040	88.7	85.7	0.74
8900 to 9000	1.009	1.93		9.50	16.67	13.09	1.075	0.080	0.045	87.2	83.9	0.84
9000 to 9100	1.011	1.98		8.22	16.82	13.64	1.111	0.066	0.048	85.7	82.4	0.81
9100 to 9200	1.010	2.03		8.20	16.99	12.72	1.110	0.060	0.040	86.2	83.3	0.73
9200 to 9300	1.012	2.13		8.10	17.05	12.86	1.079	0.053	0.041	89.2	86.1	0.70
9300 to 9400	0.511	1.18		9.82	17.30	12.02	0.595	0.065	0.050	77.3	71.8	0.08
9400 to 9500	0.511	1.14		9.92	17.27	12.22	0.603	0.064	0.052	76.5	70.9	0.07
9500 to 9600	0.508	1.10		9.86	18.26	13.36	0.601	0.064	0.053	76.2	70.6	0.14
9600 to 9700	0.509	1.12		9.88	18.48	13.90	0.596	0.065	0.058	76.9	70.7	0.11
9700 to 9800	0.509	1.12		9.89	18.22	13.65	0.599	0.064	0.062	76.8	70.2	0.07
9800 to 9900	0.510	1.14		9.94	17.86	13.44	0.600	0.065	0.062	76.5	70.0	0.10
9900 to 10000	0.510	1.16		9.92	18.14	13.92	0.601	0.063	0.068	76.7	69.5	0.29

ⓒ eV/ion increased to 216 from 185 (increased J_I, V_I still at 37 V)
ⓓ eV/ion increased to 278 (increased J_I)
ⓔ eV/ion decreased to 240
ⓕ eV/ion increased to 259 (J_I increased to prevent "low mode")
ⓖ eV/ion increased to 278 (J_I increased to prevent "low mode")
ⓗ eV/ion increased to 296 (J_I increased to prevent "low mode")
ⓘ eV/ion set at 370

J_s ≡ screen current
J_A ≡ accel current
V_I ≡ discharge voltage
V_{CK} ≡ cathode keeper voltage
V_{NK} ≡ neutralizer keeper voltage
V_G ≡ system floating potential
$\dot{m}_M$ ≡ main flow rate
$\dot{m}_C$ ≡ cathode flow rate
m_N ≡ neutralizer flow rate
m_D ≡ discharge mass utilization efficiency
M_T ≡ total mass utilization efficiency

T2130

Table 11. Performance Summary of 10,000 hr Test of Thruster 701

Time Period, hr	Main Vap		Cath Vap		Neut Vap		Neut Cath		Main Cath		Isolators	
	V	A	V	A	V	A	V	A	V	A	V	A
2400 to 2500	5.99	0.97	4.10	1.31	3.20	0.99	0.68	0.24	1.45	0.41	1.18	0.43
2500 to 2600	5.94	0.96	4.07	1.29	3.18	0.99	0.71	0.24	1.44	0.40	1.17	0.42
2600 to 2700	5.93	0.96	4.05	1.29	3.20	1.02	0.69	0.24	1.40	0.40	1.16	0.42
2700 to 2750	5.96	0.96	4.07	1.29	3.17	0.98	0.68	0.24	1.42	0.41	1.17	0.42
2750 to 2800	5.85	0.94	3.96	1.25	3.05	0.94	0.70	0.24	1.40	0.39	1.18	0.42
2800 to 2900	5.89	0.94	3.95	1.25	3.20	1.00	0.67	0.24	1.49	0.41	1.18	0.42
2900 to 3000	5.96	0.95	3.96	1.25	3.17	0.99	0.64	0.23	1.35	0.39	1.16	0.42
2750 to 3000	5.91	0.94	3.96	1.25	3.15	0.98	0.67	0.24	1.42	0.40	1.17	0.42
3000 to 3100	6.00	0.96	3.94	1.25	3.16	0.99	0.62	0.23	1.35	0.39	1.16	0.42
3100 to 3200	6.09	0.99	4.01	1.27	3.21	1.02	0.67	0.23	1.30	0.39	1.16	0.42
3200 to 3300	6.10	0.98	4.01	1.27	3.39	1.04	0.68	0.23	1.31	0.38	1.16	0.42
3300 to 3400	6.11	0.98	4.04	1.28	2.62	0.83	0.66	0.24	1.25	0.39	1.14	0.42
3400 to 3500	6.06	0.98	4.04	1.28	2.64	0.83	0.58	0.23	1.29	0.38	1.14	0.43
3500 to 3600	6.08	0.98	4.04	1.28	2.68	0.86	0.63	0.23	1.32	0.39	1.15	0.42
3600 to 3700	6.12	1.02	4.04	1.28	2.71	0.85	0.70	0.23	1.30	0.38	1.15	0.42
3700 to 3800	6.12	1.04	4.05	1.28	2.59	0.81	0.77	0.24	1.38	0.39	1.15	0.42
3800 to 3900	6.12	1.05	4.04	1.28	2.62	0.82	0.78	0.24	1.36	0.38	1.16	0.43
3900 to 4000	6.10	1.03	4.03	1.28	2.57	0.85	0.80	0.25	1.34	0.39	1.16	0.43
4000 to 4100	6.08	1.03	4.03	1.28	2.84	0.94	0.85	0.25	1.30	0.39	1.16	0.42
4100 to 4200	6.09	1.05	4.02	1.28	2.85	0.91	0.86	0.25	1.29	0.39	1.15	0.42
4200 to 4300	6.05	1.05	4.02	1.27	2.93	0.91	0.78	0.25	1.28	0.40	1.15	0.43
4300 to 4400	6.12	1.04	4.01	1.27	2.90	0.96	0.74	0.26	1.30	0.41	1.16	0.43
4400 to 4500	6.16	1.05	4.00	1.27	2.93	0.94	0.75	0.26	1.31	0.41	1.15	0.43
4500 to 4600	5.99	1.02	4.01	1.27	2.92	0.96	0.78	0.26	1.31	0.41	1.16	0.43
4600 to 4700	6.04	1.04	3.98	1.26	2.84	0.90	0.73	0.25	1.29	0.41	1.15	0.42
4700 to 4800	6.05	1.04	3.98	1.26	2.93	0.94	0.81	0.26	1.32	0.41	1.16	0.43
4800 to 4900	6.01	1.05	3.96	1.25	3.00	0.94	0.78	0.26	1.33	0.41	1.16	0.42
4900 to 5000	6.07	1.04	3.98	1.26	2.78	0.87	0.76	0.25	1.33	0.41	1.15	0.42
5000 to 5100	6.10	1.05	3.97	1.25	2.68	0.85	0.79	0.26	1.32	0.42	1.15	0.42
5100 to 5200	6.10	1.05	3.95	1.25	2.71	0.86	0.77	0.25	1.29	0.41	1.14	0.42
5200 to 5300	6.10	1.04	3.93	1.24	2.71	0.86	0.75	0.25	1.29	0.42	1.14	0.42
5300 to 5400	6.08	1.04	3.93	1.24	2.71	0.86	0.78	0.26	1.29	0.41	1.13	0.42
5400 to 5500	6.06	1.04	3.92	1.24	2.97	0.95	0.82	0.25	1.42	0.42	1.15	0.42
5500 to 5600	5.97	1.03	3.79	1.24	2.56	0.85	0.78	0.25	1.34	0.42	1.13	0.42
5600 to 5700	5.82	0.98	3.90	1.25	2.67	0.86	0.76	0.25	1.33	0.41	1.13	0.42
5700 to 5800	6.14	1.07	4.01	1.27	2.73	0.89	0.84	0.29	1.51	0.48	1.21	0.44
5800 to 5900	6.13	1.05	4.01	1.27	2.62	0.88	0.81	0.25	1.41	0.41	1.16	0.42
5900 to 6000	5.99	1.03	4.01	1.27	2.87	0.96	0.81	0.26	2.32	0.55	1.16	0.44
6000 to 6050	6.00	1.03	3.96	1.30	2.81	0.97	0.84	0.26	2.44	0.57	1.12	0.43
(c) 6050 to 6200	5.66	0.98	3.86	1.22	2.86	0.92	0.84	0.26	2.06	0.51	1.18	0.46
6200 to 6300	5.85	1.02	4.10	1.30	3.05	1.01	0.83	0.26	2.42	0.56	1.18	0.45
6300 to 6400	5.82	1.01	4.08	1.30	2.97	0.98	0.85	0.25	2.49	0.56	1.18	0.45
6400 to 6500	5.83	1.03	4.06	1.29	3.04	0.98	0.90	0.25	2.49	0.56	1.17	0.44
6500 to 6600	5.90	1.02	4.06	1.29	3.02	0.99	0.93	0.25	2.48	0.56	1.17	0.45
6600 to 6700	5.96	1.02	4.06	1.30	2.96	1.01	1.07	0.26	3.85	(j) 1.00	1.16	0.44

(c) eV/ion increased to 216 from 185 (increased J_I, V_I still at 37 V)

(j) New mag amplifier installed at hour 6666.

T2131

Table 11. Continued

Time Period, hr	Main Vap		Cath Vap		Neut Vap		Neut Cath		Main Cath		Isolators	
	V	A	V	A	V	A	V	A	V	A	V	A
6700 to 6800	5.82	1.00	4.01	1.27	3.10	0.99	1.11	0.26	3.84	1.00	1.10	0.47
6800 to 6900	5.80	1.00	4.01	1.28	3.06	0.99	1.16	0.27	4.27	1.19	1.07	0.46
6900 to 7000	5.84	1.01	4.01	1.28	3.16	1.01	1.15	0.27	4.26	1.18	1.07	0.46
7000 to 7100	5.77	1.00	4.01	1.27	3.20	1.05	1.17	0.27	4.22	1.15	0.93	0.53
7100 to 7200	5.81	1.00	4.03	1.28	3.09	1.05	1.17	0.27	4.14	1.14	0.92	0.53
7200 to 7300	5.84	0.99	3.99	1.26	3.20	1.01	1.15	0.26	4.08	1.12	0.91	0.52
(d) 7300 to 7400	5.38	0.92	4.37	1.43	3.30	1.09	1.22	0.28	4.01	1.09	0.89	0.51
7400 to 7500	5.36	0.93	4.42	1.45	3.12	1.09	1.24	0.28	4.02	1.10	0.88	0.51
(e) 7500 to 7600	5.44	0.94	4.46	1.46	3.37	1.10	1.26	0.29	3.85	0.98	0.91	0.52
7600 to 7700	5.50	0.95	4.47	1.46	3.27	1.07	1.25	0.28	3.99	1.09	0.89	0.52
7700 to 7800	5.43	0.94	4.52	1.48	3.18	1.03	1.26	0.29	3.85	1.07	0.89	0.51
7800 to 7900	5.52	0.95	4.50	1.47	3.22	1.06	1.26	0.29	3.81	1.04	0.89	0.51
7900 to 8000	5.46	0.93	4.51	1.47	3.24	1.07	1.23	0.29	3.77	1.02	0.89	0.52
8000 to 8120	5.67	0.97	4.34	1.41	3.20	1.04	1.14	0.28	3.76	1.03	0.83	0.50
(f) 8130 to 8200	5.54	0.95	4.27	1.38	3.28	1.14	1.12	0.27	3.78	1.03	0.84	0.50
8200 to 8300	5.48	0.94	4.40	1.43	3.31	1.08	1.17	0.27	3.71	0.99	0.85	0.49
8300 to 8380	5.65	0.96	4.02	1.27	3.36	1.10	1.09	0.26	3.75	1.00	0.84	0.50
(g) 8390 to 8500	5.41	0.92	4.39	1.42	3.32	1.08	1.12	0.27	3.77	1.01	0.82	0.49
8500 to 8600	5.42	0.92	4.38	1.42	3.28	1.07	1.14	0.27	3.77	1.01	0.83	0.49
8600 to 8700	5.45	0.93	4.38	1.42	3.34	1.05	1.12	0.26	3.79	1.00	0.83	0.49
8700 to 8800	5.49	0.93	4.25	1.37	3.29	1.08	1.10	0.26	3.80	1.03	0.84	0.50
8800 to 8900	5.47	0.92	4.36	1.41	3.34	1.09	1.15	0.27	3.78	1.01	0.84	0.50
8900 to 9000	5.49	0.95	4.49	1.30	3.40	1.12	1.10	0.26	3.79	1.02	0.84	0.50
(h) 9000 to 9100	5.56	0.94	3.88	1.23	3.34	1.10	1.19	0.25	3.78	1.01	0.85	0.50
9100 to 9200	5.46	0.92	3.83	1.15	3.24	1.10	1.09	0.25	3.76	0.99	0.86	0.51
9200 to 9300	5.34	0.89	3.68	1.15	3.14	1.05	1.11	0.24	3.81	0.99	0.86	0.51
(i) 9300 to 9400	5.22	0.88	4.27	1.39	3.51	1.16	1.15	0.25	3.62	0.97	0.83	0.50
9400 to 9500	5.23	0.88	4.28	1.39	3.77	1.17	1.16	0.26	3.64	0.97	0.83	0.50
9500 to 9600	5.21	0.88	4.26	1.39	3.76	1.13	1.21	0.25	3.70	0.98	0.85	0.50
9600 to 9700	5.21	0.88	4.27	1.39	3.80	1.15	1.22	0.26	3.69	0.98	0.85	0.50
9700 to 9800	5.20	0.89	4.27	1.39	3.72	1.16	1.24	0.25	3.66	0.99	0.84	0.50
9800 to 9900	5.22	0.89	4.27	1.39	3.71	1.13	1.22	0.26	3.69	0.99	0.84	0.50
9900 to 10000	5.22	0.88	4.26	1.39	3.75	1.13	1.24	0.26	3.67	1.01	0.83	0.50

(d) eV/ion increased to 278 (increased J_I)
(e) eV/ion decreased to 240
(f) eV/ion increased to 259 (J_I increased to prevent "low mode")
(g) eV/ion increased to 278 (J_I increased to prevent "low mode")
(h) eV/ion increased to 296 (J_I increased to prevent low mode)
(i) eV/ion set at 370

T2131

1.75 A beam current, it was decided to limit the maximum current to 1.75 A.

The test results indicated that all three thruster modifications were successful. The three modifications were improved propellant isolator design, flame-sprayed cathode heaters, and compensated dished grids. In contrast to the previous tests, the cathode feedline high-voltage isolator did not develop any leakage current. The test system wiring was configured so that the cathode and main feedline isolators were continuously stressed with the 1100 V screen voltage. Periodically, a microammeter was inserted in series with each of the high-voltage isolators, and throughout the test neither isolator showed any measurable leakage current (<0.1 μA).

The discharge-chamber erosion, vacuum-chamber problems, and test-console repairs described below made some thruster restarts necessary during the more than one year the test continued. Although not planned, these thruster restarts provided data on the reliability of the plasma-sprayed heaters which had been substituted for the original sheathed heaters on the main and neutralizer cathodes. The cathode heaters are used only when starting the thruster; during normal operation, self-heating maintains the cathodes at the temperature necessary for electron emission. All thruster restarts were uneventful and made with the same heater power supply settings as used for the initial thruster turn on. The longest thruster off time was 70 hr at test hour 8036 when a cryoshroud LN_2 leak made it necessary to turn the discharge off.

Final evaluation of the third modification (compensated dished electrodes in place of the original flat optics with center support) was made when the test was concluded and the optics were available for close inspection. However, thruster performance (i.e., low accel drain current and low arc rate) and the appearance of the optics when viewed in situ through a questar telescope indicated that this modification had also been successful. (Localized erosion due to the flakes described below was visible on the accel electrode). This conclusion was confirmed during the post-test analysis of the optics.

A thruster problem occurred immediately after the test was begun. Liquid mercury had penetrated both the main and cathode vaporizers. The vaporizers were baked out in situ, after which they held back liquid mercury and performed normally for the remainder of the test. Two thruster problems were identified during the test: (1) a variation in neutralizer operating characteristics and (2) discharge chamber erosion. The first problem required a system adjustment at test hour 3310 to raise the neutralizer keeper voltage setpoint and increase the neutralizer keeper current to 1.5 A from 1.3 A. These changes were made to compensate for a shift in the operating characteristics of the neutralizer. One of the three system control loops in the test console adjusts the neutralizer vaporizer flowrate to maintain the neutralizer keeper voltage at a selected value. At this point in the test, the neutralizer mercury flowrate increased above the desired maximum level of 50 mA equivalent flow (0.375 g/hr). This increase in flowrate indicated that the keeper voltage was trying to increase but was being constrained by the vaporizer control loop. The neutralizer was mapped by measuring the keeper voltage range and the range of neutralizer vaporizer temperature over which the control loop would control as the keeper current was varied. The neutralizer control range is bounded at one extreme by neutralizer "decoupling" (i.e., the electron emission decreases to the point where the beam is insufficiently neutralized to maintain an acceptable voltage to ground). The other boundary of the neutralizer control range is identified by vaporizer "runaway" when a setpoint below the minimum achievable keeper voltage is selected.

From the neutralizer mapping, it was determined that the neutralizer keeper voltage versus vaporizer flowrate characteristic had shifted upward. Also, at 1.3 A keeper current, the usable keeper voltage range was only 1.3 V; at 1.5 A, the keeper voltage control range was 3.5 V. Therefore, both the keeper voltage and keeper current were adjusted to provide a satisfactory combination of keeper voltage and flowrates (at hour 6048 the keeper current was raised to 1.6 A).

After the initial shift in neutralizer keeper voltage, there were several other shifts to a lower keeper voltage mode and back to a higher voltage regime. The shift to a lower mode typically followed a thruster restart and may have been caused by the cathode (and insert) heating associated with a thruster restart. The shift to the higher keeper voltage operation happened during thruster operation and was characterized by a gradual increase in flowrate caused by the control loop trying to maintain the selected keeper voltage.

The first evidence of thruster discharge chamber erosion was the observation at test hour 4530 of flakes lying on the upstream side of the screen grid (the thruster was mounted in the vertical vacuum chamber pointing down at a frozen mercury collector). The number and size of flakes varied as the test continued; Figure 31 illustrates this by showing the flakes at test hours 8600 and 10,000. Some of the erosion of the accelerator electrode apertures caused by the flakes is shown in Figure 32. In that figure, the uneroded apertures adjacent to eroded apertures demonstrate the localized nature of the erosion. The source of flakes on the screen electrode is presumed to be spalling of the material which had been sputter eroded from within the discharge chamber and deposited on other discharge chamber surfaces. This theory was substantiated at test hour 5845 when a small hole was observed in the center of the cathode baffle. The cold-rolled steel baffle had originally been 0.075 cm thick. The maximum dimension of this hole when first observed was approximately 0.4 cm. Additional erosion of the cathode baffle than appeared at two locations on the edge (see Figure 31). The two regions of edge erosion began diametrically opposite each other and appeared to be coincident with the axis of the cathode keeper; the cathode keeper is mounted 1.7 cm upstream from the baffle. The condition of the baffle at the conclusion of the 10,000 hr test is shown in Figure 31.

The flakes on the optics did not seem to affect thruster performance by their presence until 1450 hr after they were detected. In fact, the lowest 100 hr average high-voltage trip rate of the test occurred

M10333

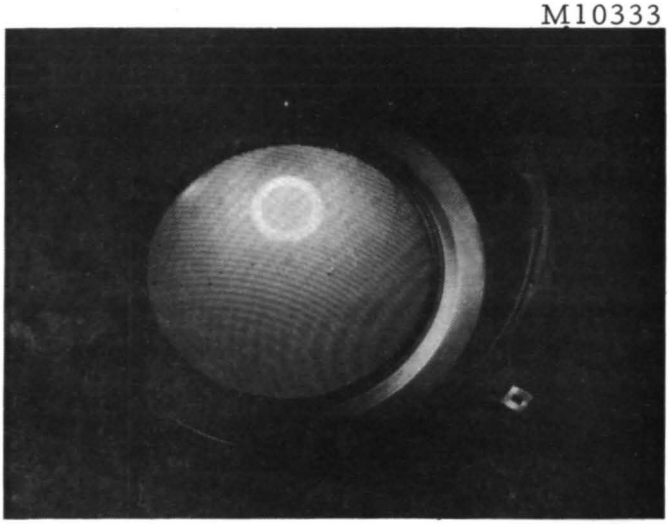

1800 hours

M10882

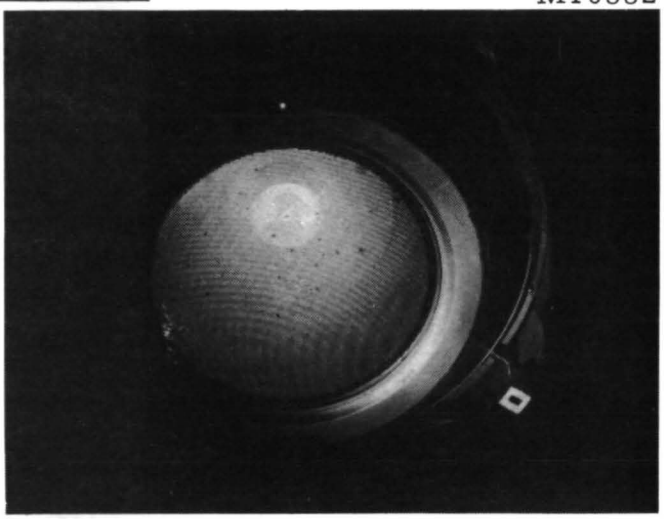

8600 hours

M11009

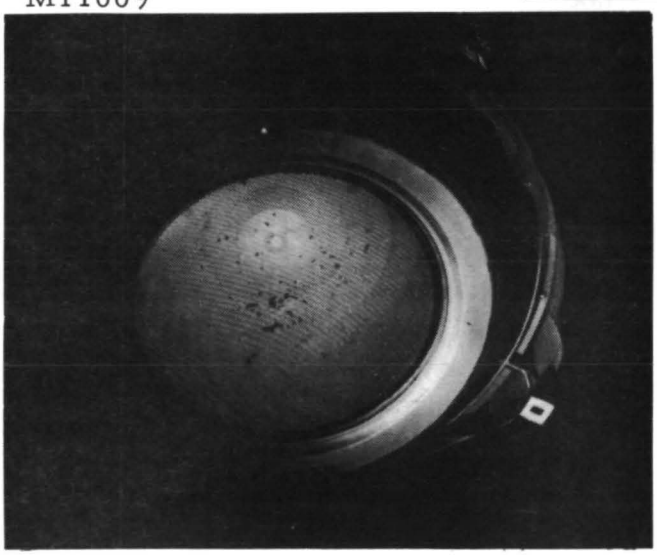

10,000 hours

Figure 31. Thruster at test hours 1800, 8600, and 10,000 showing flakes on the optics and erosion of the baffle.

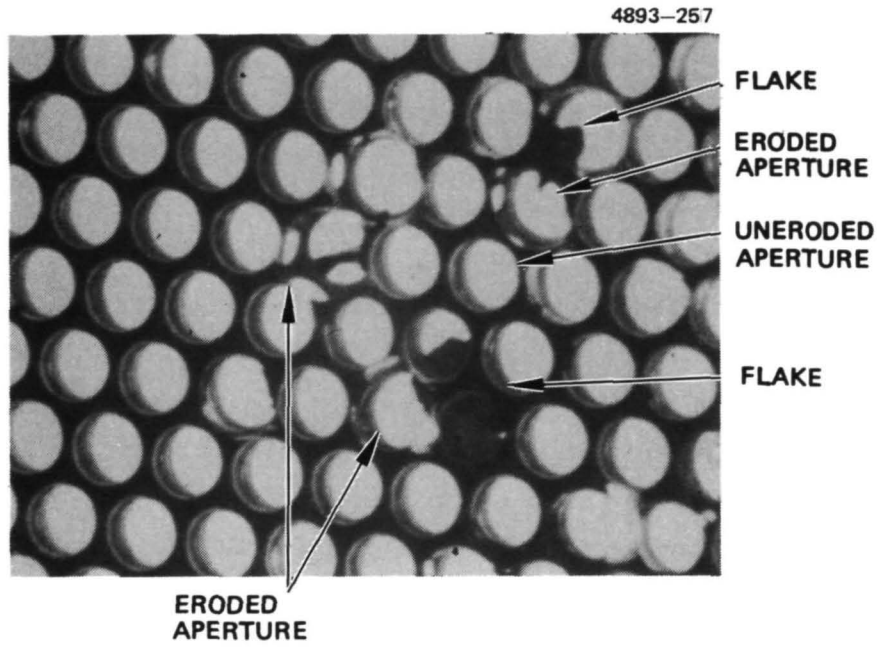

Figure 32. Photograph of optics showing flakes on screen electrode and localized erosion of accelerator electrode apertures caused by flakes. (Accelerator aperture diameter is 0.15 cm.)

after the flakes had first been observed. However, at test hour 5980 while operating at 1.75 A beam, a period of high and erratic trip rate did begin. At hour 6050 it was decided to lower the beam current to the original starting level of 1.5 A. The discharge current was left at 8.75 A, thereby increasing the electron volts per ion from 185 to 214. The high trip rate was attributed to penetration of the 0.06 cm inter-electrode gap by the flakes on the screen electrode. This assumption seemed justified when at test hour 6610 a short developed between the accelerator electrode and the screen electrode. The short was eliminated by discharging a 1 μF capacitor, charged to 600 V, between the accelerator electrode and the screen electrode. After the short was cleared, the beam was re-established and the test continued.

Following the success of the grid-clearing experiment, the system wiring was modified to add a grid-clearing circuit; this circuit was used when an excessive trip rate indicated that a flake had penetrated the interelectrode gap. The circuit consisted of a 1 μF capacitor connected between the shell and system common so that it was charged to the screen voltage (nominally 1100 V). A switch was incorporated so that when the switch was operated, the charged capacitor was connected between the shell and the accelerator electrode.

The flakes created by discharge chamber erosion probably were the cause of a cathode-keeper-to-shell short which developed at test hour 7255. This problem was eliminated by discharging a 1 μF capacitor, charged first to 400 V and then to 600 V, between the cathode keeper and the shell. This particular short occurred only once.

The final effect attributed to discharge-chamber erosion generally and to cathode baffle erosion specifically was a change in discharge operating perameters at hour 7100. Presumably because of reduced cathode baffle area, the discharge began to shift into the "low" mode at beam currents above 1 A and discharge currents below 7.5 A. The low discharge mode was characterized by a low cathode flowrate, low discharge voltage, high main flowrate, and a loss of up to 10% in total mass utilization efficiency. Since increasing the magnetic baffle current did not ensure operation in the normal discharge mode, the beam

was lowered to 1 A. After 9300 hr, the beam current was lowered to 0.5 A. Figure 33 shows the beam current profile for the entire test.

Before removing the thruster at the end of the 10,000 hr test, two brief tests were conducted: the redundant neutralizer was operated and a cold restart of the thruster was made. Neutralizer S/N 415 had not been operated during the more than 14 months the thruster had been in the endurance test vacuum chamber. The last time it had been operated was during the thruster checkout at HRL prior to the endurance test. When the thruster was shut down at the conclusion of the 10,000 hr test, the system wiring was switched so that the appropriate test console supplies were connected to neutralizer S/N 415. Starting power was applied to the tip heater, vaporizer, and keeper. The neutralizer ignited without difficulty and control of the keeper voltage was normal.

The power to the thruster was left turned off for 5.7 hr until all three vaporizer thermocouplers read below $0^{\circ}C$. The automatic start-up sequence of the test console was then used to restart the thruster. Startup through discharge ignition was normal. When the high voltages were applied, the flakes lying on the optics caused 42 high-voltage recycles to occur before the beam was established.

2. Test Console Performance

The portion of the test console of most interest in terms of performance and reliability is the transistorized power processor, which is the predecessor to the thermal vacuum breadboard (TVBB) system developed under contract NAS 3-17223. Operation of the power processor unit (PPU) was relatively trouble free. This test console had accumulated several thousand operating hours during the tests which preceded this endurance test. Only two repairs were made to the power supplies during this test. At hour 4668, the data printout indicated that the screen voltage was 890 V instead of 1100 V. A check of the screen supply revealed that the 250 V line fuse was open in two of

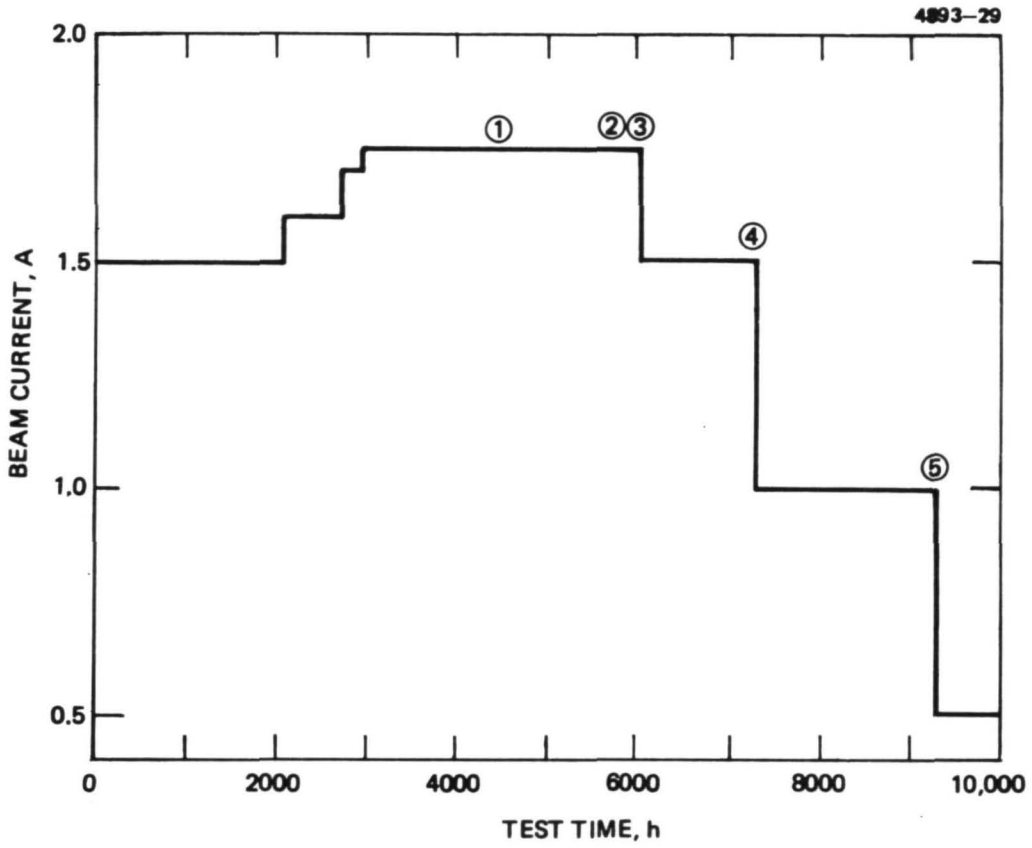

① FLAKES ON OPTICS AT HOUR 4530

② HOLE IN BAFFLE AT HOUR 5845

③ HIGH TRIP RATE DUE TO FLAKES

④ LOW DISCHARGE VOLTAGE MODE DUE TO ERODED BAFFLE

⑤ HIGH TRIP RATE DUE TO FLAKES AND ERODED BAFFLE

Figure 33. Beam current time history profile for 10,000 hr test.

the eight inverter modules. Replacing the fuses restored the supply to normal operation. One of the fuses may have been open before the low voltage was observed, since the screen supply regulator could compensate for the loss of one module. The second power processor failure was a magnetic amplifier in the cathode heater supply which had to be replaced at hour 6667. None of the inverter transistors failed during normal operation even though the PPU was subjected to thousands of high-voltage trips and recycle sequences. (Human error caused the loss of a pair of transistors while the failure of the cathode heater magnetic amplifier was being troubleshot.)

The integrated circuits in the test console controller and data system were not as immune to the adverse transient environment generated by an ion thruster high-voltage arc as the components in the PPU. Integrated circuits had to be replaced on several occasions. When the combination (described below) of flakes on the optics and high chamber pressure caused numerous high-voltage trips, some of the nonessential thruster alarms were disabled to eliminate false alarms. The test console controller contains significantly more logic circuitry than the TVBB to provide the functions of automatic startup, automatic shutdown, and alarm generation.

3. Performance of the Vacuum Test System

The performance of the vacuum system was basically good. The nominal chamber pressure with the thruster beam bombarding the frozen mercury collector was less than 2×10^{-6} Torr at all beam current levels. Two types of difficulties were experienced with the system: problems with the vacuum system components themselves and interruptions in the utility services to the vacuum system.

The most serious of the vacuum system component problems was a leak that developed in the lower of the two LN_2 cryoshrouds inside the vacuum chamber. This leak caused the chamber pressure to rise to the 10^{-4} Torr scale, making it necessary to shut down the thruster for 70 hr at hour 8036. The external piping of the LN_2 system was rerouted to bypass the leaking cryoshroud. With the defective

cryoshroud isolated and evacuated, the chamber pressure returned to less than 2×10^{-6} Torr and the test was resumed. The only other problems with vacuum system components were two incidents of burned-out wires to one of the two 32 in. diffusion pumps and an intermittent flow switch in the diffusion pump cooling water line. None of these problems caused more than a brief interruption in system operation.

As might be expected in a test lasting more than a year, several unanticipated interruptions in system utilities occurred. There were two building circuit-breaker failures. An emergency generator was used when the incoming power lines required preventive maintenance. There were also interruptions in the building cooling-water supply because of a leak and because of problems related to the addition of an annex to the Space Simulation Laboratory. These interruptions provided opportunities to demonstrate the excellent restart capability of the thruster and the value of the automatic startup sequence built into the test console controller.

4. Feed System Performance

The laboratory feed system built for this program performed faultlessly throughout all of the tests which were conducted. The only attention required was periodic filling of the reservoirs with mercury during the test, cleaning of the reservoirs between tests, and calibration of the load cells.

B. POST-TEST ANALYSIS

After the 10,000 hr endurance test, a thorough post-test examination and analysis of thruster 701 was performed. The full details of that analysis are presented in the Appendix, and only the significant findings are summarized in this section.

Analysis of thruster S/N 701 emphasized careful and nondestructive disassembly of the thruster to preserve all possible observable characteristics. The analysis began with an extensive visual inspection and photographic documentation of the thruster to identify both the

damaged and undamaged components. This type of inspection and documentation continued while we removed the outer coverings of the thruster, removed the entire upstream boundary (with all its subassemblies in place), and finally removed and disassembled each subassembly.

Most of the thruster components showed little or no evidence of the long duration of the test. These undamaged components included the main and cathode propellant isolator-vaporizer assemblies, all structural elements, main standoff insulator, and most of the wiring. Components which had been extensively damaged were the accelerator grid (from direct impingement by defocussed ions due to flakes on the screen grid), the cathode pole-piece assembly (includes baffle and baffle support), two of six anode standoff insulators, and the keeper cover of the neutralizer which was operated throughout the test. Components which showed wear but still had considerable useful lifetime included the main and neutralizer cathodes (slight orifice wear), accelerator grid (where not damaged by interception), screen grid (upstream side eroded), thruster anode, and both cathode and neutralizer keepers.

Erosion of the baffle and cathode pole piece by ion sputtering were concluded to be the major problem areas. All major damage could be related to either the removal or deposition of material which results from this process. Precise assessment of erosion sites and erosion rates was not possible because of the almost complete destruction of the baffle and the resultant exposure of the cathode and baffle support members to high-energy discharge ions. Definite erosion sites included the baffle, the cathode pole piece (downstream of the plane of the cathode), and to some extent probably the baffle support structure. Deposition sites included the anode, all thruster boundaries in the plane of or upstream from the cathode, and the cathode keeper. Discharge chamber surfaces which were not obviously eroded or coated included the downstream surface of the propellant distributor and the screen pole piece.

Several dimensional and weight measurements were made for comparison with the pre-test measurements. Some significant findings included:

- There was no significant enlargement of screen or accel grid apertures in areas which were not damaged by beamlet defocussing (from flakes masking parts of the apertures).
- Cathode orifice dimensions were not significantly changed (~0.003 cm).
- Cathode keeper deposits increased the keeper weight by ~10%.
- Edges of cathode pole and remaining baffle had been thinned to knife edge.
- Cathode heaters on both main and neutralizer cathodes showed cracking of flame-sprayed insulation, but none of the insulating coating had been lost.
- Main cathode and neutralizer inserts could be removed and unrolled without destruction and appeared to still have coating over most of the insert surface.
- There was no evidence of excess charge-exchange erosion associated with the neutralizer.
- Charge-exchange ion erosion of the accelerator grid is a secondary factor in life limitation.

SECTION 4

TEST CONSOLE MODIFICATION

As part of the original 30 cm endurance test program (Contract NAS 3-15523), four test consoles were built (one is shown in Figure 34). The first of these test consoles was used to power and control thruster 701 during the 10,000 hr endurance test (described in Section 3). Based on the experience gained during that test and the requirements for a higher power capability to support the planned 1000 hr verification test, a task was included in this contract to modify the fourth test console.

Each test console is a self-contained unit combining a power processor, data acquisition system, and dc bus supply. The power processor portion consists of a control unit and the following supplies: screen, accelerator, discharge, cathode keeper, neutralizer keeper, cathode tip heater, neutralizer tip heater, isolator heater, main vaporizer, cathode vaporizer, and auxiliary heater (used as a neutralizer vaporizer supply). These are transistorized, high-switching-frequency, high-line-voltage (250V), flight-prototype supplies. The control unit contains front panel controls for manual operation of the power supplies plus timing and logic circuits that provide automatic startup, automatic shutdown, overload detection, power-supply cutback, and recycling and annunciation of a variety of alarm conditions. The data acquisition system provides information about the operation of the power supplies (and thruster) in two forms. Telemetry readouts of the voltage and current outputs of all supplies are displayed on panel meters. These panel meters permit quickly assessing the status of the system. Higher accuracy data than provided by the panel meters is available on a digital voltmeter (DVM), which is included as part of the DAS. The voltage and current outputs of all supplies can be viewed serially on the DVM either by selecting an individual channel or by manually initiating a scan of the data channels. The dc voltage input to the power processor from the bus supply simulates the output that would be provided by solar panels in a flight system.

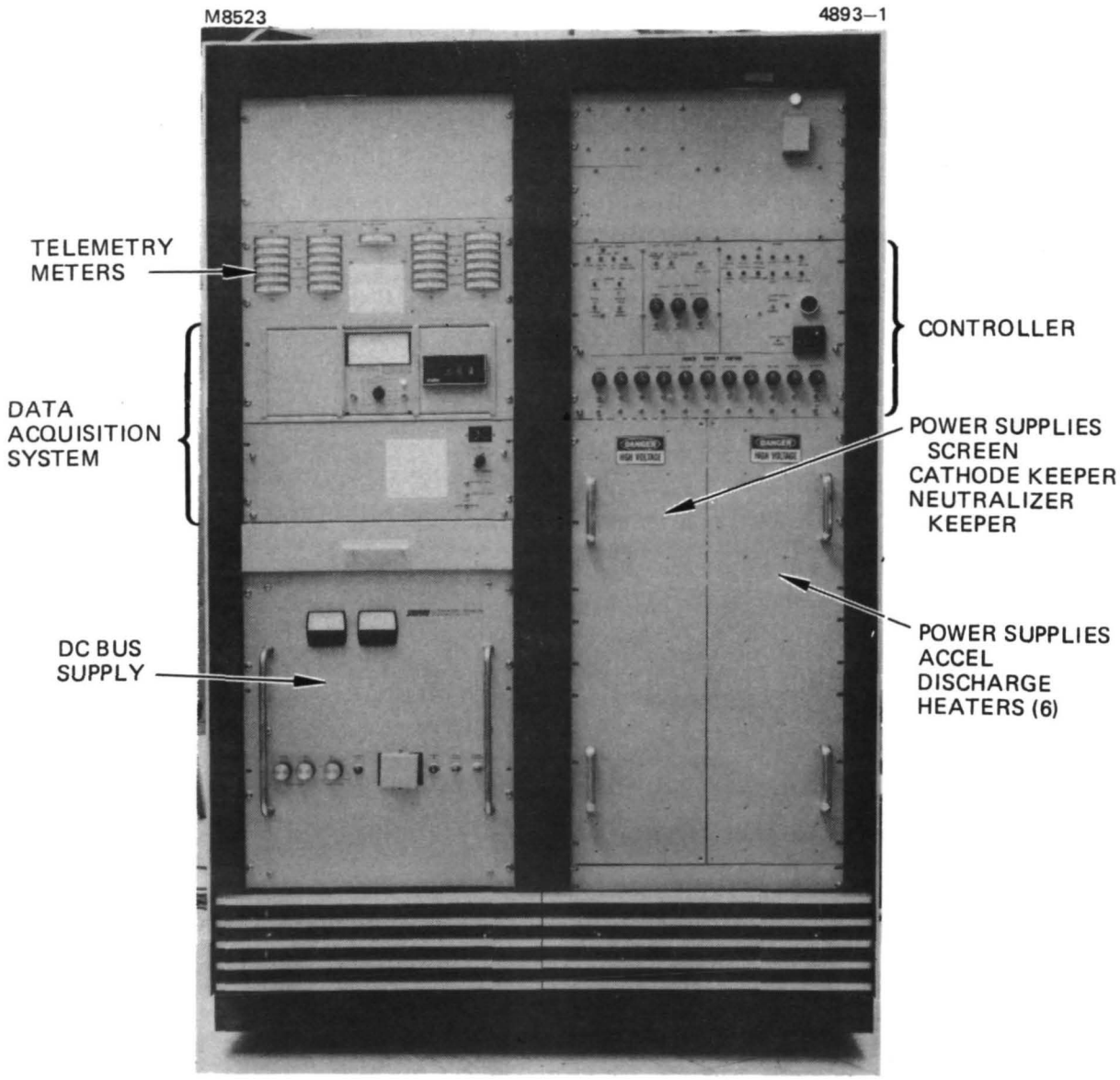

Figure 34. Test console built for 30 cm thruster endurance test program.

Changes to the test console associated with changes in output current and/or voltage requirements resulted in changes to the screen supply, accel supply, and four heater supplies. The nominal output current of the screen supply was increased from 1.5 A to 2.2 A. The maximum output voltage was not changed. The increased power capability required replacing the output bridge rectifiers, relocating the output filter choke to within a forced-air cooling channel, and increasing the speed of the screen supply's internal trip circuit to limit the maximum inverter-transistor collector current. After these modifications were completed, operating temperatures of all critical power dissipating components in the screen supply were determined to be satisfactory at full rated power output.

The change to the accel supply was prompted by a reduction in the nominal operating point of 30 cm thrusters. Through continuing improvement in optics fabrication techniques (e.g., successful implementation of close-spaced dished electrodes), it was possible to lower the accelerator voltage required. Previously, a lower accel output voltage had caused an instability problem. This problem, which was associated with operating the supply at a low-pulse-width duty cycle, was overcome by designing, fabricating, and installing a lower-voltage full-scale output transformer for the accel supply.

The changed heater-supply requirements affected the cathode vaporizer, cathode tip heater, neutralizer tip heater, and isolator heater supplies. The original design philosophy adopted for the test console was to make all six heater supplies identical and satisfy the individual output voltage and current requirements by selecting the appropriate tap on the output transformer. Thus, it was possible to meet the new heater supply requirements by changing transformer taps and adjusting the control-loop responses accordingly.

Experience gained during the endurance test of thruster 701 with the test console demonstrated that both cathode-keeper and neutralizer-keeper operation were more stable if the keeper supply output circuit impedance was inductive rather than capacitive. This change was implemented in test console 4 as part of the modification task.

Several improvements were incorporated into the power processor controller; these included:

- A new recycle circuit which uses adjustable one shots to determine high-voltage off time and the relative time delay between accel and screen turn on following a high-voltage trip. In addition, since the system clock was made to resynchronize itself to the trip, the recycle events are always of the same relative and absolute duration.

- New logic for the neutralizer-heater and neutralizer-vaporizer supplies so that when the neutralizer keeper lights, the tip heater supply turns off and the vaporizer supply automatically servos to control the keeper voltage.

- A modification to allow the cathode vaporizer supply to stay in closed loop and servo around a different value of discharge voltage when a trip occurs and during other beam-off periods as indicated by the screen current being less than 0.5 A.

- Changing the neutralizer keeper logic to command a higher keeper current during a trip or during beam-off periods.

- Changing the cathode keeper logic to command a higher current during a trip.

- Connecting the internal trips of the screen, accel, and discharge supplies to the recycle circuit in the controller so that a current overload in any of these supplies will cause a system recycle.

- Adding maximum loop-limit adjustment potentiometers for all three vaporizers.

- A modification to cutback the discharge current momentarily on initial turn on of the high voltages during startup.

The performance of the modified test console was evaluated in a series of dummy-load and thruster integration tests. The dummy-load test data included waveform photographs, data acquisition system calibration, and power supply ripple and regulation characteristics.

Thruster–test-console integration testing emphasized the ability of the test console to provide proper thruster operation, control in the fully automatic mode, and proper functioning of the high-voltage recycle circuitry. Several automatic cold start ups were routinely performed and overload recycle recovery was excellent. Oscilloscope photographs showed good management of the peak currents in the screen and accel inverters under a wide variety of induced overload conditions (see Figure 35). No component failures were experienced during thruster tests, which included thousands of induced overloads.

At the conclusion of the test console modification effort, there was one problem which had not been completely eliminated. During thruster integration testing, occasional perturbations in the controller logic circuits occurred when thruster overloads were induced by generating high-voltage shorts external to the vacuum system. These perturbations would manifest themselves as false alarms or resets to earlier start-up sequence states. The problem was not evident during smooth thruster operation or naturally occurring arcs. The source of this behavior is thought to be electrostatic coupling between circuits at power processor common and circuits at earth ground. Filtering of logic supply bus voltages and input-output signals did not eliminate the problem.

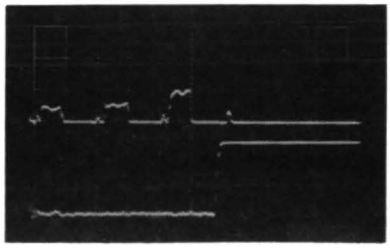

6074–9

UPPER TRACE	SCREEN INVERTER COLLECTOR CURRENT	4A/DIV
LOWER TRACE	SCREEN INVERTER TRIP 279-P20	5V/DIV
SWEEP		50 μsec/DIV
AT	SCREEN SUPPLY SHORT	

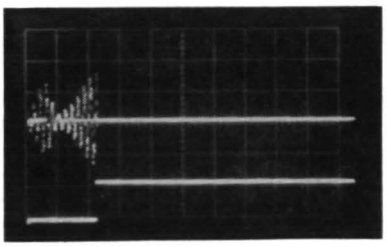

6074–10

UPPER TRACE	ACCEL INVERTER	2A/DIV
LOWER TRACE	ACCEL INVERTER TRIP	10V/DIV
SWEEP		50 μsec/DIV
AT	SCREEN ACCEL SHORT	

Figure 35. Screen supply and accel supply inverter current during overload conditions.

SECTION 5

CONCLUSIONS

The 10,000 hr test of thruster SN 701 has served to identify either the major wearout mechanism or confirm the long lifetime capability of thruster components and subassemblies. The test results showed that the following components or subassemblies could provide operating lifetime in excess of 10,000 hr without any design changes.

- All structural components
- MIV and CIV assemblies
- Discharge and neutralizer cathodes
- All shadow-shielded insulators
- Ion optics assembly.

The major wear mechanism was identified as erosion of discharge-chamber components by ion sputtering. This process also causes secondary damage because the deposits of back-sputtered material either short-out insulators or spall and form large flakes of conducting material. To provide longer thruster lifetime, several design modifications are recommended as follows.

A. INSULATORS

All insulators should be better shadow shielded to prevent deposition of back-sputtered material. Wiring should be routed and/or protected to prevent deposition on wiring insulation, which could form current leakage paths. Specific insulators requiring attention are

- Anode insulators
- Keeper insulators
- Neutralizer support insulators

- Neutralizer isolator insulator
- Neutralizer wiring insulation.

Re-entrant shielding should be used where space permits and/or isolation requirements demand minimum leakage current. It is thought that damage to insulators, such as observed in the case of the anode insulators, will be eliminated by protection from conductive coatings.

B. ERODED COMPONENTS

Three types of erosion were noted in this test: erosion by low-energy discharge-chamber ions, erosion by high-energy beam ions, and erosion by high-energy charge-exchange ions. Erosion of discharge-chamber components by low-energy ions is a strong function of the ratio of multiply charged ions to singly charged ions. Therefore, any modification which reduces the density of doubly charged ions or reduces discharge voltage is recommended as the preferred method of eliminating component erosion of this type. Care must be exercised to ensure that substantial reduction of true propellant efficiency does not accompany any design modification that is incorporated to reduce double ionization, thereby causing more severe charge exchange erosion of the accelerator grid. Rather than eliminating double ionization in the discharge chamber, some of the vulnerable surfaces could be protected with lower sputtering yield materials. If possible, the design of components observed to be heavily eroded ought to be modified so that dimensional changes caused by the expected erosion will not critically affect the operational characteristics of the thruster. Components that could be easily protected are the cathode pole piece, the baffle, and the baffle support. The screen grid electrode of the ion optics assembly is also eroded by discharge ions but cannot be protected without appreciable loss of performance. Therefore, extension of its lifetime must rely on reducing the energy and/or density of doubly charged ions.

Direct erosion by high-energy beam ions occurred on the accel electrode and the neutralizer cover. Erosion of the accel electrode in this test was a consequence of beam deflection caused by flakes of spalled, backsputtered material. This phenomena may be reduced by reducing discharge-chamber sputtering, but can be eliminated only by controlling the formation of metallic flakes. Flake control has been demonstrated by NASA LeRC with 5 cm and 8 cm thrusters either by grit blasting the surfaces where flakes form or by using wire mesh to cover these surfaces. Surfaces where such treatment has been shown to be necessary by the results of this test are:

- The entire upstream discharge-chamber boundary
- The discharge anode
- The keeper electrode and insulator shields.

The neutralizer cover intercepts a small but significant number of ions that emerge from the outermost apertures of the ion optics assembly. The preferred modification would be one that eliminates these trajectories; however, the erosion rate is sufficiently low that an adequate thickness of material can be provided to accept this direct interception and consequent erosion and still prevent penetration of the neutralizer housing. The choice of material for this erosion site should take into consideration the possible sites where the sputtered material will be deposited.

Finally, erosion of the accelerator electrode by charge-exchange ions remains a concern, but is not the major life-limiting factor as determined here. The main recommendations at this point are to

- Reduce accelerator operating voltage (if possible)
- Disallow modifications to the thruster design that appreciably reduce effective propellant utilization.

Charge-exchange erosion as measured in a vacuum chamber is probably more severe than would be experienced in the vacuum of space and, until other wear mechanisms have been reduced, it is of secondary importance to discharge-chamber (screen-electrode) erosion.

The recommendations for design modifications mentioned above are based on the observations and their interpretations as described in Appendix A. Modifications to other assemblies have been implemented to alleviate fabrication, quality-control, operational-control, and structural problems. Design modifications to extend thruster lifetime have already been incorporated into the 900-series thrusters.

REFERENCES

1. H. J. King, et al., "Low Voltage 30 cm Ion Thruster Development," NASA CR-134731, October 1974.

2. R. L. Poeschel, et al., "2.5 kW Advanced Technology Ion Thruster," NASA CR-134687, August 1974.

3. C. R. Collett, et al., "Thruster Endurance Test," NASA CR-135011, May 1976.

4. R. L. Danilowicz, et al., "Measurement of Beam Divergence of 30-cm Diameter Dished Grids," AIAA Paper 73-1051, October 1973.

5. D. Zuccaro, "Mercury Vapor Hollow Cathode Component Studies," AIAA Paper 73-1141, October 1973.

6. M. J. Mirtich, "Investigation of Hollow Cathode Performance for 30-cm Thrusters," AIAA Paper 73-1138, October 1973.

7. M. A. Mantenieks and V. K. Rawlin, "Studies of Internal Sputtering in a 30 cm Ion Thruster," AIAA Paper 75-400, New Orleans, LA, 1975.

8. M. J. Mirtich and W. R. Kerslake, "Long Lifetime Hollow Cathodes for 30 cm Mercury Ion Thrusters," AIAA Paper 76-985, Key Biscayne, Florida, 1976.

9. L. A. Mueller, "High Reliability Cathode Heaters for Ion Thrusters," AIAA Paper 76-1071 Key Biscayne, Florida, 1976.

Page
Intentionally
Left Blank

APPENDIX

POST TEST ANALYSIS OF 10,000-HOUR ENDURANCE TEST THRUSTER

I. INTRODUCTION

This appendix contains a complete description of the post-test examination of thruster serial number 701 (SN 701) after 10,000 hr of testing. Disassembly and documentation procedures are described, and all data and observations considered noteworthy are included. Wherever possible, an attempt has been made to interpret the observed data.

To establish a common basis for discussing the post-test condition of thruster SN 701, the thruster design, its initial assembly, and the test conditions are described as follows. Thruster SN 701 is the first thruster built to meet the "Engineering Model" (EM) thruster design specifications on structural strength, overall efficiency, and total weight. Some features of the EMT design have since been changed to correct structural deficiencies determined by vibration tests or to facilitate fabrication, but, since these modifications have not significantly changed the operating characteristics of the thruster, SN 701 can be considered representative of the 800-series thruster design (Ref. 2). As the first thruster module built to the EMT design specifications, SN 701 was not designated as the endurance test thruster until after construction and initial testing had been sucessfully completed. Consequently, documentation of the detailed history of the thruster components is not as complete as one would desire to perform a detailed quantitative analysis of the effects of long-term testing. Future tests should benefit from improvement in the documentation and assembly procedures that have recently been established for EMT construction. The conduct of the test has been described in Section 3 of this report and will only be outlined briefly here. Initially, the thruster was operated at 1.5 A beam current because contractual agreements had originally specified this value and the peripheral test equipment had to be

modified to permit operation at the nominal EMT level of 2A. After 2000 hours of operation at 1.5 A beam current, the beam current was increased to 1.75 A in several steps. After about 4500 hours of testing, "flakes" were noted on the ion acceleration optics screen grid. These "flakes" are formed by the deposition and spalling of material that is sputtered from cathode potential surfaces by ion bombardment. This sputter erosion and its consequences have been identified as the major wearout mechanism of the 30 cm thruster used in this 10,000 hr test. The consequences of these metallic flakes resting on the screen grid are twofold. The first may be considered specific to the mounting of the thruster in the endurance test such that the beam is directed vertically downward. Consequently, the flakes which spall from anode or other surfaces fall onto the screen grid under the force of gravity and either remain there or fall through the screen apertures. The larger flakes block, or partially block, the screen grid apertures and distort the ion trajectories through these apertures. This results in direct interception of high-energy ions on the accelerator grid and machines away relatively large segments of this grid in short periods of time. The accelerator grid sustained considerable damage from this "flake-initiated" mechanism. The second consequence of "flake" formation could occur equally well in a gravity-free environment. If a flake is small enough to pass through a grid aperture, it can short-circuit the ion optics grids. This may result in a brief arc as the flake is vaporized by the power available from the power processor, but it at least produces a high voltage overload and recycle sequence. If the flake is substantial enough, a more or less permanent short circuit results, and thruster operation can only be restored by using extraordinary means to burn out the flake. A number of these latter types of short circuits between the screen and accelerator grid were removed during the course of the 10,000 hr test by capacitive discharge. It is not known whether any of the observed thruster wear can be attributed to the repeated overload recycling or short removal associated with the atypical operation (due to the flakes) of the ion optics electrodes.

After about 5800 hours of testing, the major consequence of sputtering erosion was evidenced by the appearance of a hole in the baffle (which isolates the cathode plasma from the main discharge plasma). From this point in time until the end of the test, the isolation of the cathode and discharge plasma decreased as the baffle continued to decrease in size. A consequence of this modification to the baffle was a more or less continuous change in thruster control characteristics which had to be compensated by varying the controlled parameters. Eventually this resulted in reducing beam current and operating at an increased ratio of discharge to beam current. Thus, the 10,000 hr of testing was logged at beam currents that varied between 1.75 A and 0.5 A with a weighted average of 1.4 A. The effect of this variation in beam current and/or discharge conditions to compensate for baffle erosion also represents an unknown factor in considering the wear on thruster SN 701 described in this report.

After completion of the test, considerable care was taken in removing the thruster from the test facility and documenting the condition of the thruster. The documentation procedure followed a sequence of visual inspection, photographing, disassembly, and measurement for each major assembly, subassembly, and, finally, component (with some components being dissected and more carefully analyzed). The details of this post-test analysis procedure are described in the next section. The discussion of results is then presented and organized according to the major sub-assemblies and describes the notable observations at all levels of complexity used in the analysis.

II. POST-TEST EXAMINATION AND DOCUMENTATION PROCEDURES

After removal from the test facility, thruster SN 701 was carefully inspected and photographed on the test stand. Flake samples were collected from a number of locations and electrical measurements were made at the vacuum interface terminals. The thruster was then removed from its test facility mounting and carefully inspected, photographed, disassembled, and measured on a step-by-step basis. One goal of this procedure was to gain as much information as possible with minimum alteration of the thruster condition. Initially, the only disassembly performed was the removal of the outer casings, the neutralizer assemblies, and the ion optics assembly. In this phase of the thruster examination, the following measurements and documentations were performed:

- Electrical resistance measurements at thruster terminals
- Close-up photographs of the interior and exterior discharge chamber assembly
- Mapping of the magnetic field strength distribution
- Dimensional checks of critical discharge chamber, ion optics assembly, and neutralizer assembly parameters
- Collection of additional flake and deposition samples
- Close-up photographs of neutralizer and ion optics subassemblies.

During these measurements, the thruster discharge chamber assembly was mounted through one gimbal mount, on a portable stand that facilitated both visual inspection, photography, and handling without disturbing or altering the condition of the thruster. To permit any necessary retakes, further disassembly and documentation was delayed until all photographs were developed and examined.

The next phase of the examination involved the complete mechanical disassembly of the thruster and subassemblies. Before removal of any subassembly or component, visual observations were noted and photographs were taken where indicated. Notes were made during the disassembly and the separated subassemblies were photographed, weighed, or otherwise measured. The order of disassembly was as follows:

- The entire upstream boundary (backplate) including the structural braces, isolators, and cathode pole piece assemblies was removed from the discharge chamber body.
- Damaged anode insulators were examined and removed.
- All components and subassemblies were removed from the upstream boundary (backplate). This includes the propellant distribution plenum, the main and cathode isolators, the support structures, and the cathode pole assembly.
- Subassemblies were disassembled. This includes the neutralizers, the ion optics electrodes and mounting, the cathode pole assembly, and the discharge chamber. During the disassembly, special attention was paid to component orientation, erosion of or depositions on surfaces, and the presence of discoloration or other markings.

Having completed the mechanical disassembly, the next phase of the examination called for dissecting selected components. This action was again delayed until the results of the disassembly documentation were assured. Selection of components to be sectioned for further analysis was restricted to those components that showed evidence of erosion or wear which could not be adequately measured in other ways. (Dental molding techniques were attempted but proved to be unsuccessful because the molding would not release from the eroded surfaces.) Such components included the baffle support mount, the thruster and neutralizer cathodes, the accelerator and screen grids, anode insulators, and the main keeper electrode. Sectioned parts were examined by microscope and microphotographs and in some cases by scanning electron

microscope. The latter procedure provides a detailed analysis of the materials present as well as their distributions in deposited layers.

The most meaningful procedure available in this post-test examination of thruster S/N 701 was visual examination using microscope and magnified photographs of thruster components. Dimensional and weight measurements rely on comparison with pre-test data if meaningful interpretations are to be offered. Without an "a priori" knowledge of what is expected to occur in an endurance test such as this, the initial documentation of the proper parameters to appropriate accuracy is more a question of chance than careful planning. In describing the results of this test in the sections which follow, an interpretation of thruster wear must be based on certain assumptions (which will be stated), since the preparation for and conduct of the test, although carefully planned, were performed without rigid control over many of the conditions that could appreciably affect interpretation of results.

III. POST TEST EXAMINATION OF THRUSTER SN 701 RESULTS AND INTERPRETATIONS

A. Total Thruster Assembly

This section presents the documentation and observations that relate primarily to the complete thruster assembly. Component wear is noted; however, the detailed discussion of such wear is deferred to later sections. A photograph of the thruster taken during the final hours of testing is shown as Fig. A-1. On the ion optics assembly can be seen the damage to the accelerator grid and also the "flakes" of material that partially block screen grid holes. These flakes cause the deflection of the ion trajectories which, in turn, causes the damage. Erosion of the baffle is also visible, and a "severed" portion of the baffle is identified by a circle where it lies on the screen grid. The comparable portion of the opposite side of the baffle has not yet been severed, and is identified by an arrow. The operating neutralizer (SN 701) is seen nearer the top of the figure. In Figs. A-2 and A-3, the thruster is seen as it appeared upon removal from the test facility. The most notable observances on the thruster exterior are the coatings on the downstream surfaces of the thruster's outer case and unused neutralizer, XN 415 (see Figs A-2(c) and A-3(a) and (b)), the machining of the outer case of neutralizer SN 701 (operating neutralizer throughout the test (see Fig. A-2(d)), and the machining of the accelerator grid (see Fig. A-3(d)). Samples of this flake material taken from the locations shown in Fig. A-4 were analyzed to yield the elemental composition listed in Table A-1. Note that the flakes from locations I and II are composed predominantly of iron and also have a high chromium content. These deposits are considered to be constituents of stainless steel sputtered by the ion beam from either the collector during preliminary thruster testing at HRL or the cryowall during the endurance test at SSL. Note that the sample from location III, though similarly located to I and II, is composed predominantly of molybdenum. Location III has a reduced view factor for the cryowall, since it is in the shadow of neutralizer SN 415. Because the view factor for the beam target

M11009

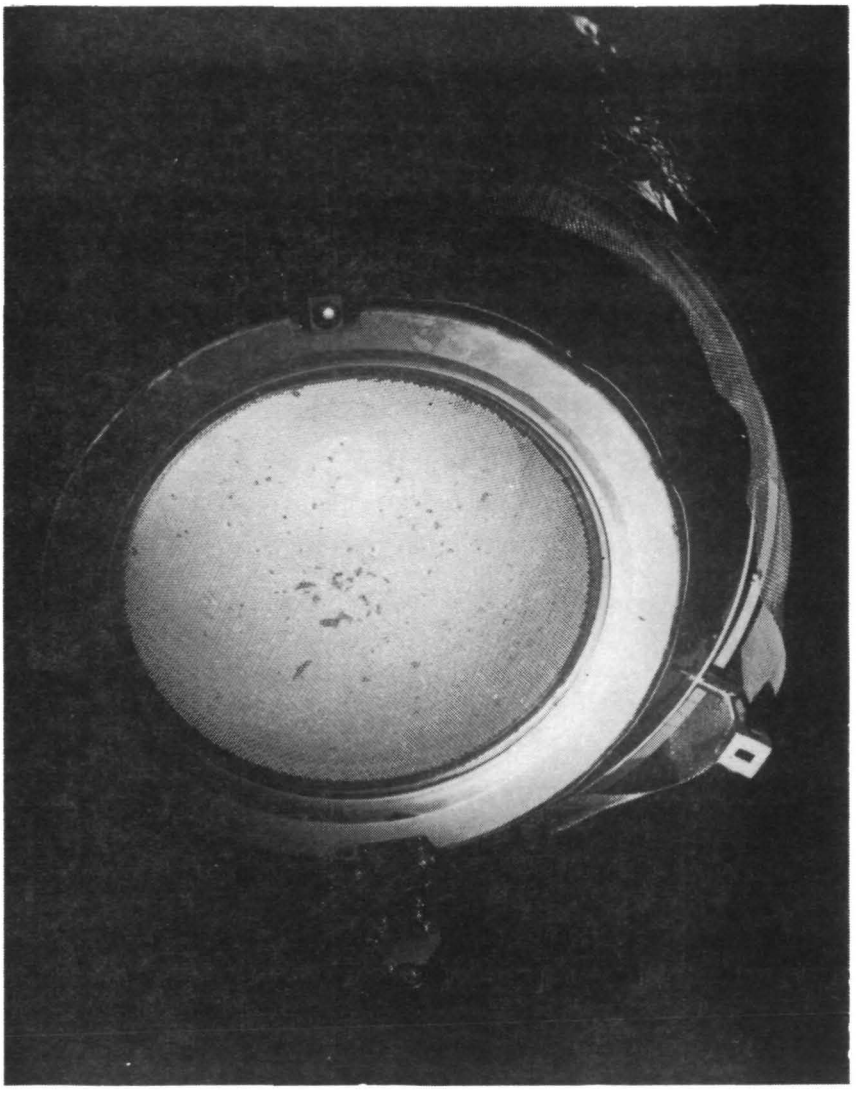

Figure A-1. Thruster during final hours of 10,000 hr test.

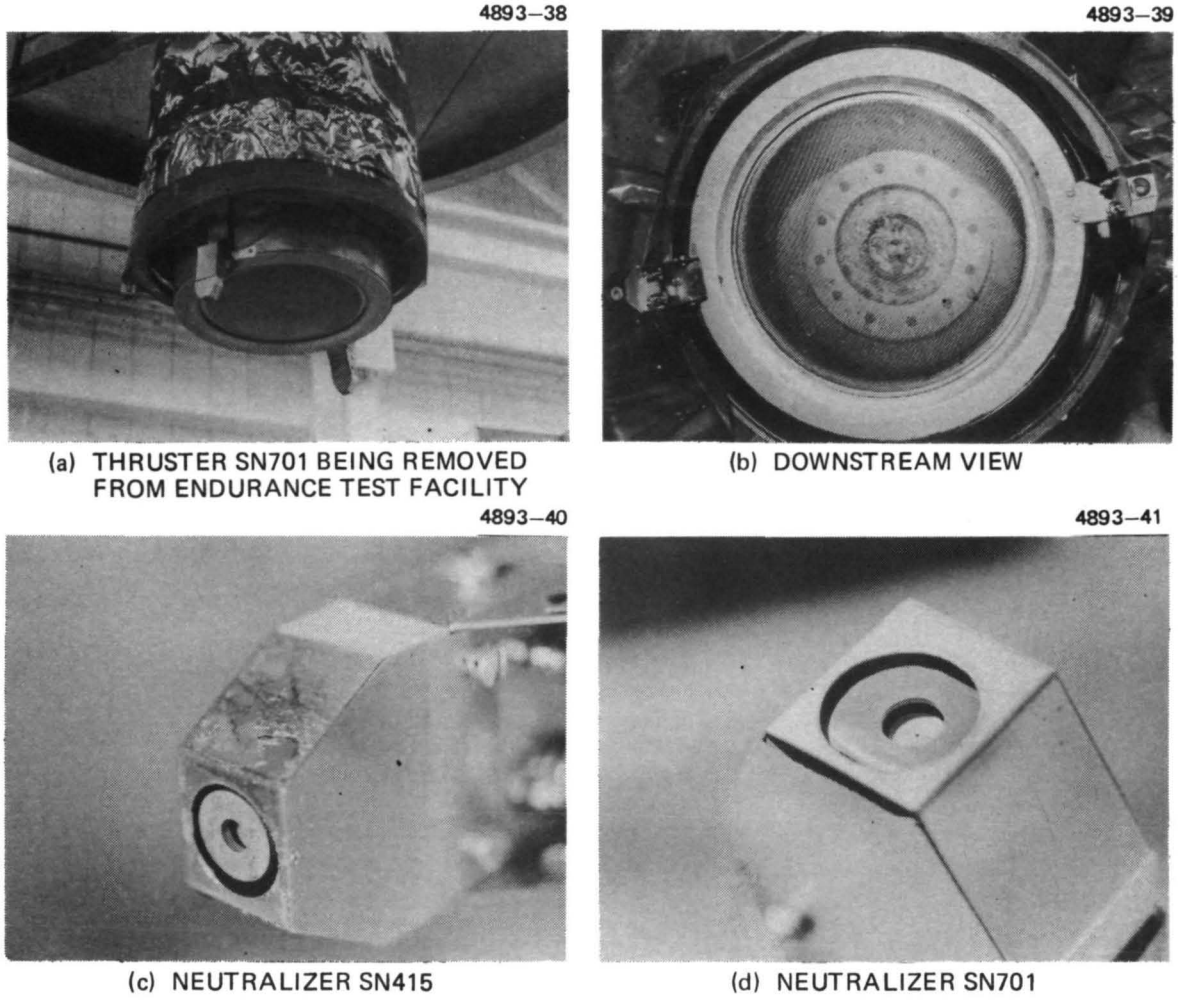

Figure A-2. (a) Thruster SN 701 being removed from endurance test facility. (b) Downstream view. (c) Neutralizer SN 415. (d) Neutralizer SN 701.

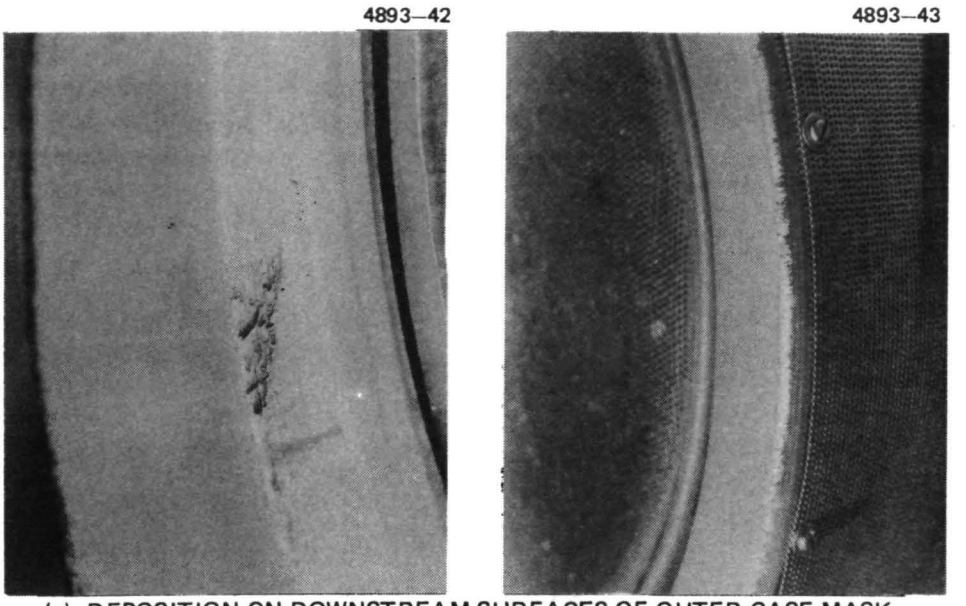

(a) DEPOSITION ON DOWNSTREAM SURFACES OF OUTER CASE MASK

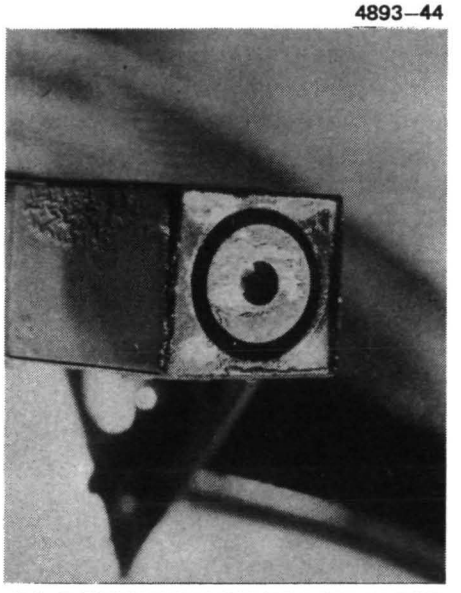

(b) DEPOSITION ON NEUTRALIZER SN 415

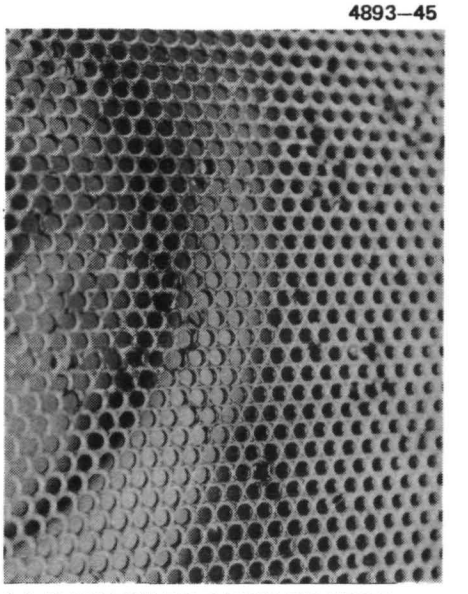

(c) DAMAGE TO ACCELERATOR APERTURES

Figure A-3. (a) Deposition on downstream surface of outer case mask. (b) Deposition on neutralizer SN 415. (c) Damage to accelerator apertures.

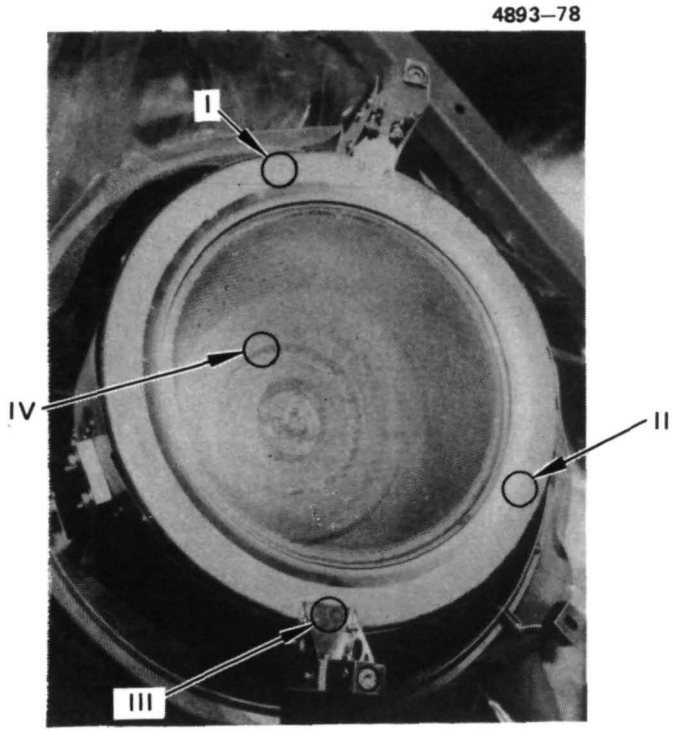

Figure A-4. Location of flake sampler.

Table A-1. Semiquantitative Analysis of Flake Samples

	COMPOSITION			
SAMPLE LOCATION	I	II	III	IV
ELEMENTS				
Fe-	REM	REM	18 %	4.8 %
Cr-	11 %	26 %	5.8	0.14
Ni-	13	12	7.5	0.44
Ti-	12	0.70	4.9	0.21
Mo-	4.3	6.1	REM	REM
Si-	4.3	1.6	4.9	0.040
Mn-	2.8	1.1	0.27	TR < 0.010
Mg-	0.19	0.078	0.080	TR < 0.003
Al-	2.4	0.25	1.3	0.14
Ag-	ND < 0.010	0.0085	0.016	ND < 0.002
Hg-	9.8	0.78	8.4	2.8
Pb-	TR < 0.50	ND < 0.05	ND < 0.50	ND < 0.05
Cu-	0.27	0.22	0.053	0.0051
Co-	TR < 0.10	0.28	ND < 0.10	ND < 0.01
Ca-	0.32	0.092	0.17	ND < 0.002
Sr-	ND < 0.05	ND < 0.005	ND < 0.05	ND < 0.005
Ba-	ND < 5.0	ND < 0.50	ND < 5.0	ND < 0.50
Ta-	ND < 3.0	ND < 0.30	ND < 3.0	ND < 0.30
W-	ND < 4.0	ND < 0.40	ND < 4.0	ND < 0.40
Au-	ND < 0.06	ND < 0.006	ND < 0.06	ND < 0.006
OTHER ELEMENTS	NIL	NIL	NIL	NIL

REM = remainder

T2134

would be essentially equivalent for locations I, II, and III, it is concluded that the deposits of stainless-steel constituents found on the downstream surfaces of the thruster case are caused primarily by ion beam sputtering of the cryowall. Sample IV was a single flake that was lodged in a grid aperture and is seen to be predominantly molybdenum. The molybdenum found in all these samples is presumed to originate from the electrodes of the ion optics assembly. Three forms of erosion of grid material can be observed; a thinning of the screen grid electrode by discharge chamber ions, machining of the accelerator electrode by direct interception, and charge exchange erosion on the accelerator electrode. No technique has been devised, as yet, to determine how much each of these processes contributes to the deposition. The ion optics electrode wear will be discussed in more detail in a later section.

Measurement of electrical resistance (or insulation) was performed and recorded when the thruster was installed in the endurance test facility (2-21-74), after completion of 10,000 hours of testing (5-14-75) and again after the thruster was removed from its test mount. The resistances were measured with a Leeds & Northrup Model 5305 resistance bridge (HAC ID No. 37381) which is calibrated against a primary standard. The values measured have been corrected for test lead resistance and are shown in Table A-2. Although some differences can be seen, the percentage of change is small, and in some cases it is greater for the two measurements made after the test was completed than for the measurements before and after the test. Consequently, it is concluded that the change in resistance of the thruster heaters during the 10,000 hour test was not significant. Leakage resistance across insulators was measured using a high voltage ohmeter ("Megger" insulation tester, James G. Biddle Co.) that applies 1000 V to the terminals in question. Table A-3 gives values of leakage resistance measured before and after the test. The low value of the insulation between the ion optics electrodes (discharge chamber shell to accel electrode) is attributed to "flakes" between the electrodes. The leakage resistance between the thruster outer case and ground represents conductive coatings on mounting insulators (which could be condensed mercury) and reflects on test facility design, rather than thruster design.

Table A-2. Resistance Measurements

Heater	Value Before Test	Value After Test		Δ_{21}^{a}	Δ_{31}	Δ_{32}
	2-21-74 ① ohms	5-14-75 ② ohms	6-3-75 ③ ohms	%	%	%
Cathode Tip	1.216	1.163	1.209	-4.4	-0.6	4.0
Main Isolator	4.060	4.158	4.162	2.4	2.5	0.1
Cathode Isolator	3.835	3.867	3.877	0.8	1.1	0.3
Main Vaporizer	5.563	5.553	5.570	-0.2	0.1	0.3
Cathode Vaporizer	2.528	2.562	2.559	1.3	1.2	-0.1
Neutralizer (701)[b]						
Tip	1.167	1.122	1.190	-3.9	2.0	6.1
Vaporizer	2.507	2.492	2.682	-0.6	7.0	7.6
Neutralizer (415)[c]						
Tip	0.526	0.490	0.563	-6.9	7.0	14.9
Vaporizer	2.160	2.149	2.178	-0.5	0.8	1.3

a. $\Delta_{\alpha\beta} = (\alpha/\beta - 1) \times 100$

b. Neutralizer SN 701 was operated over entire 10,000 hours

c. Neutralizer SN 415 was not operated during the 10,000 hour test

T1853

Table A-3. Insulation Leakage Measurement

Terminals	Leakage	Resistance
	2-21-75	5-14-75
Discharge Chamber Shell-Accelerator	∞	-20 Ω (erratic)
Discharge Chamber Shell-Outer Cover	∞	∞
Discharge Chamber Shell-Cathode Keeper	∞	∞
Discharge Chamber Shell-Anode	∞	5 kΩ
Discharge Chamber Shell-Main Propellant Line (MIV)	∞	∞
Discharge Chamber Shell-Cathode Propellant Line (C-IV)	∞	∞
Outer Cover - Ground	1000 MΩ	260 MΩ
Accelerator - Ground	∞	∞
Accelerator - Outer Cover	∞	∞
Neutralizer Cathode (SN 701) - Neutralizer Propellant Line (NIV)	2 MΩ	130 MΩ
Outer Cover - Neutralizer Keeper (SN 701)	∞	1 MΩ
Outer Cover - Neutralizer Keeper (SN 415)	∞	1.2 MΩ
Outer Cover - Neutralizer Cathode (SN 701)	250 MΩ	9 MΩ
Neutralizer Keeper - Neutralizer Cathode (SN 701)	∞	1.1 MΩ

T1854

Thruster insulators or wiring which show deterioration are the neutralizer and thruster cathode keeper electrodes, the neutralizer isolator and mounting insulators (SN 701), and the thruster anode. The source of of this leakage will be discussed in later sections. It is noteworthy that the propellant isolators (the CIV and the MIV), show no measurable loss of insulation properties (leakage current during operation also remained at a satisfactorily low value throughout the test).

Views of the thruster assembly taken during initial disassembly are shown in Figs. A-5 through A-12. In Fig. A-5, the major wear of the thruster baffle and cathode pole is visible as well as its consequence, the deposition of the sputtered material on the thruster backplate and anode. This wear and its consequences will be discussed in detail in the following sections covering the discharge chamber assembly and the cathode pole/baffle assembly.

Figure A-6 is a side view of the thruster and two observations are noteworthy. First, it can be seen that two of the insulators used to support the outer case have the "shadow shields" removed, exposing the ceramic surfaces. These insulators showed no electrical leakage and the ceramic surfaces are clean and free of any discoloration. Second, on the discharge chamber shell adjacent to the anode terminal seen in the center of the photograph (arrow) a "bright" region can be seen on the metal where the insulator makes contact, surrounded by a darker region. The anode insulator leakage resistance mentioned earlier was a consequence of damage to this and one other anode support insulator. This damage will be discussed in detail in the discharge chamber section with reference made to the coloration noted here. Figure A-7 shows the opposite side of the thruster. The fracture seen in the cover on neutralizer SN 701 is considered a weakness of the prototype cover and support design and a design change has already been incorporated in thruster SN 702A.

M11060 4893–270

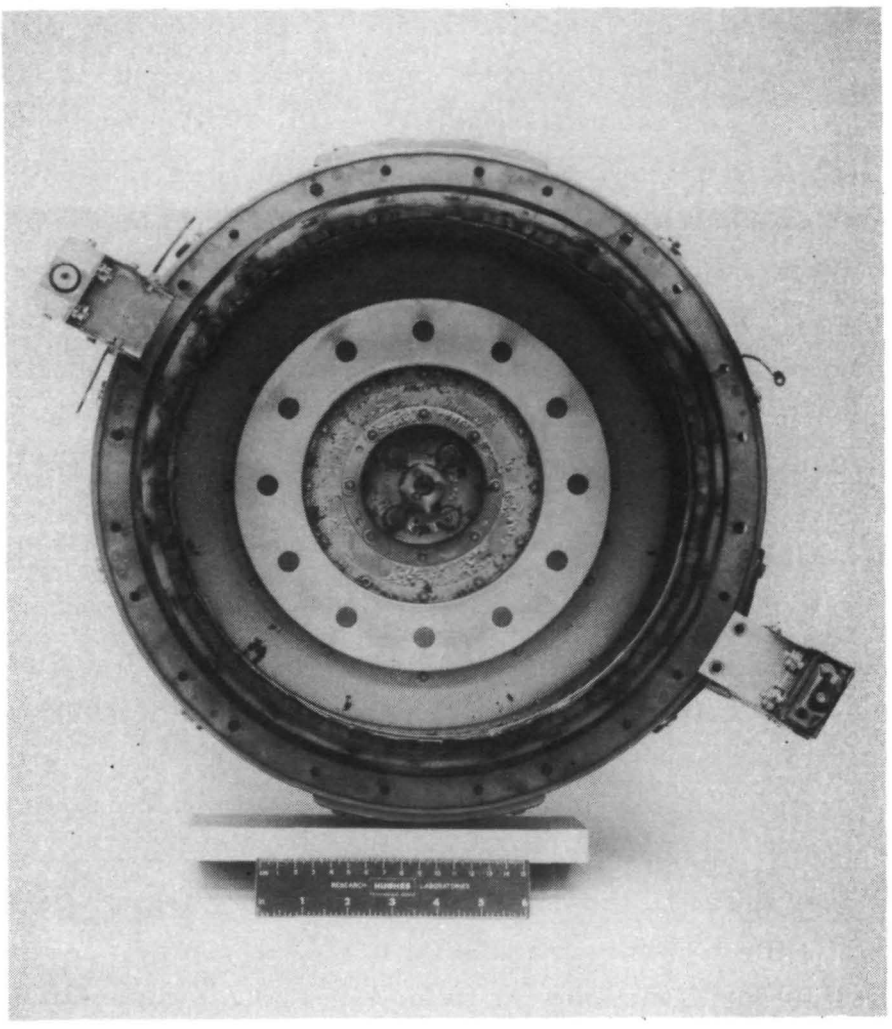

Figure A-5. Thruster 701—front view with optics removed.

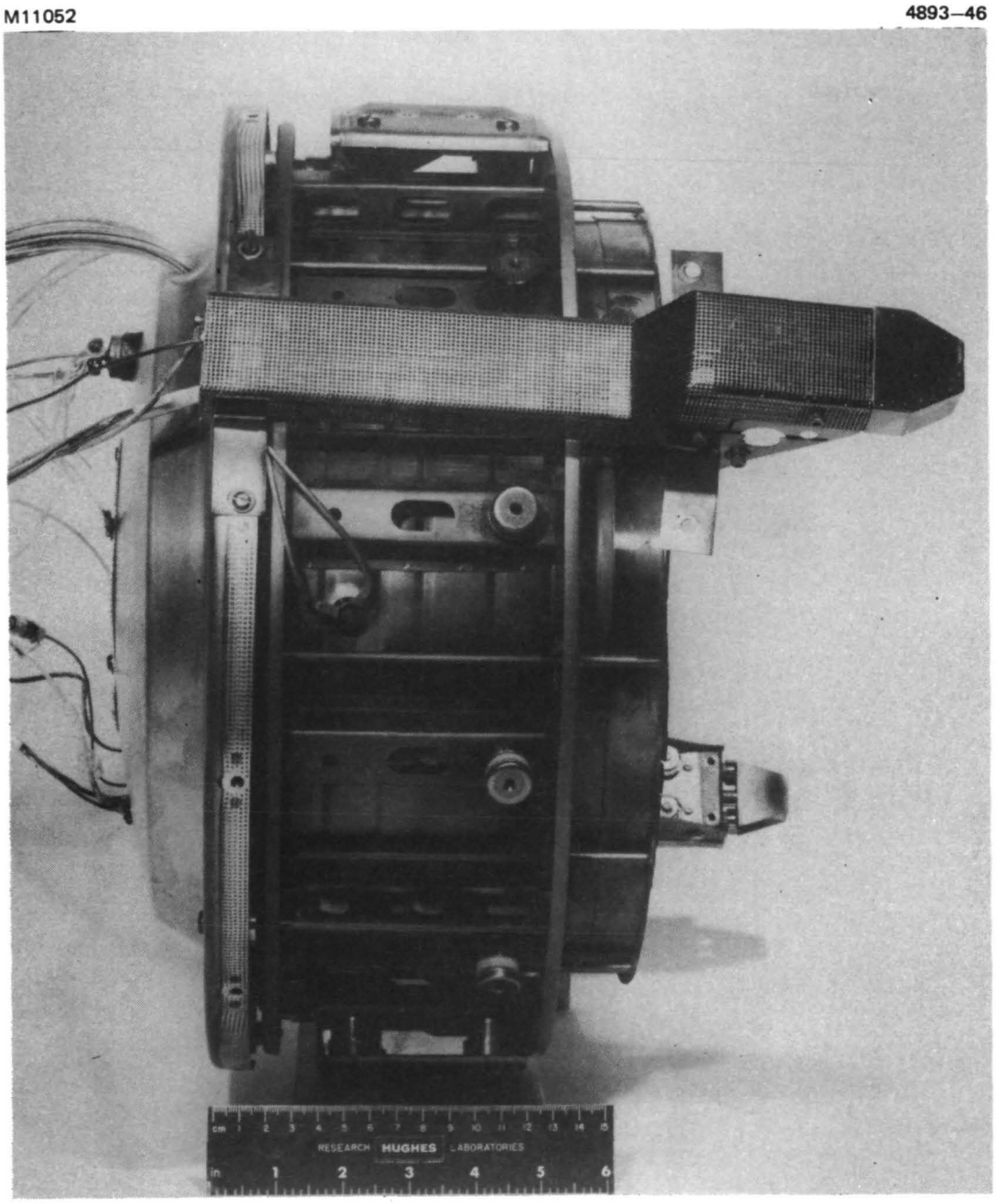

Figure A-6. Thruster 701 — side view with ground screen removed.

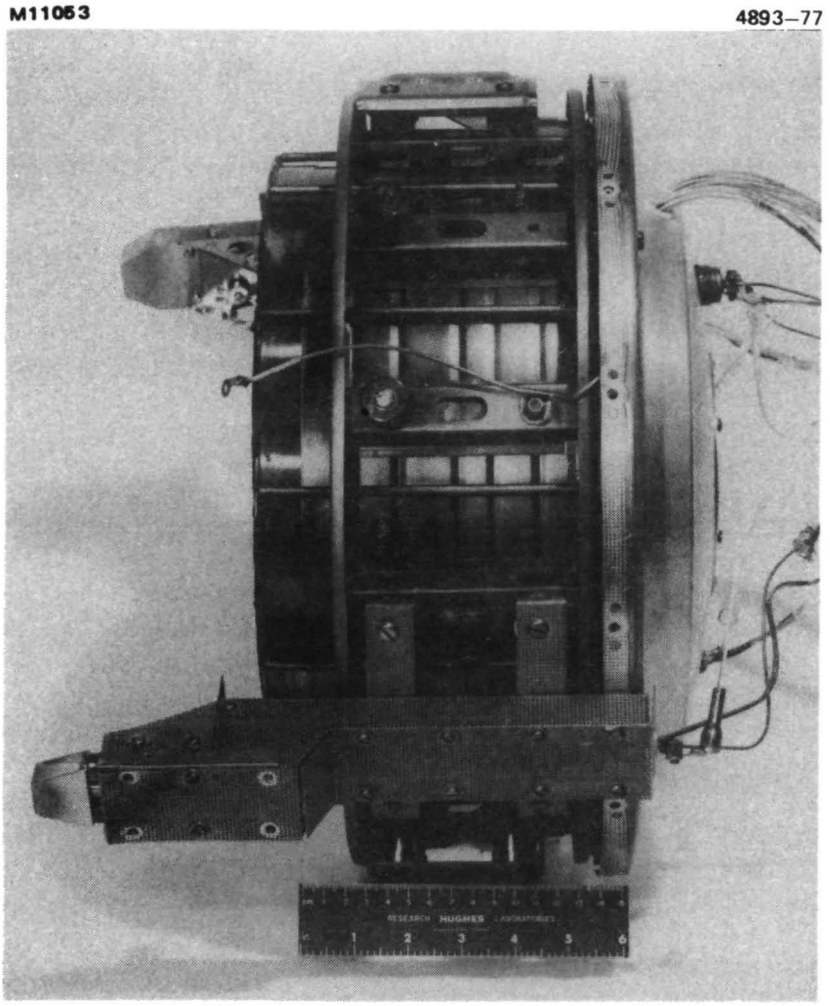

Figure A-7. Thruster 701—side view with ground screen removed.

M11054

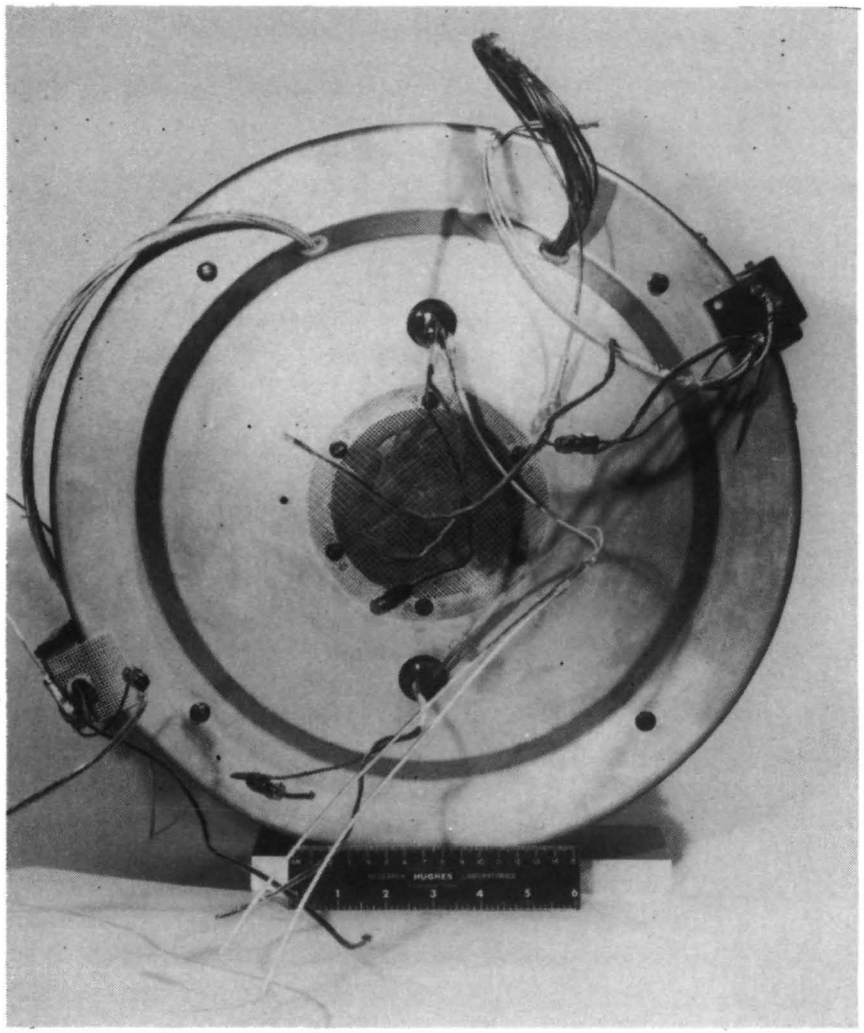

Figure A-8. Thruster 701—rear view.

M11051

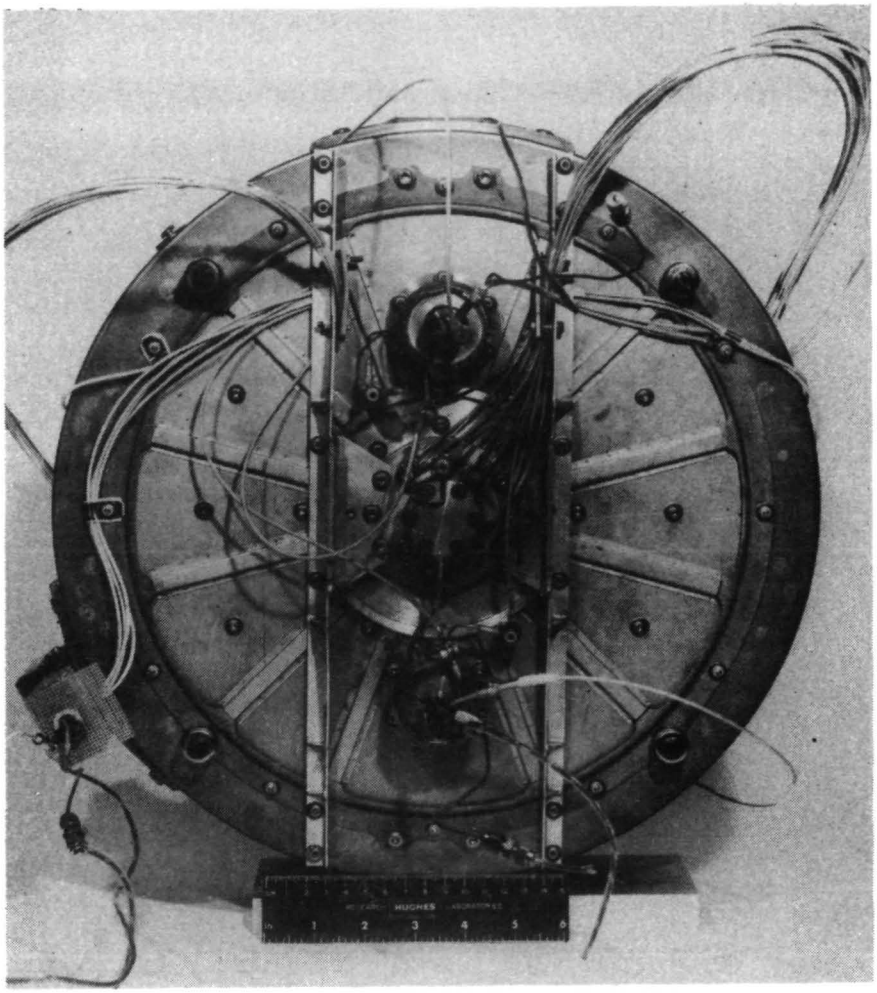

Figure A-9. Thruster 701—rear view with rear cover removed.

M11055 4893–47

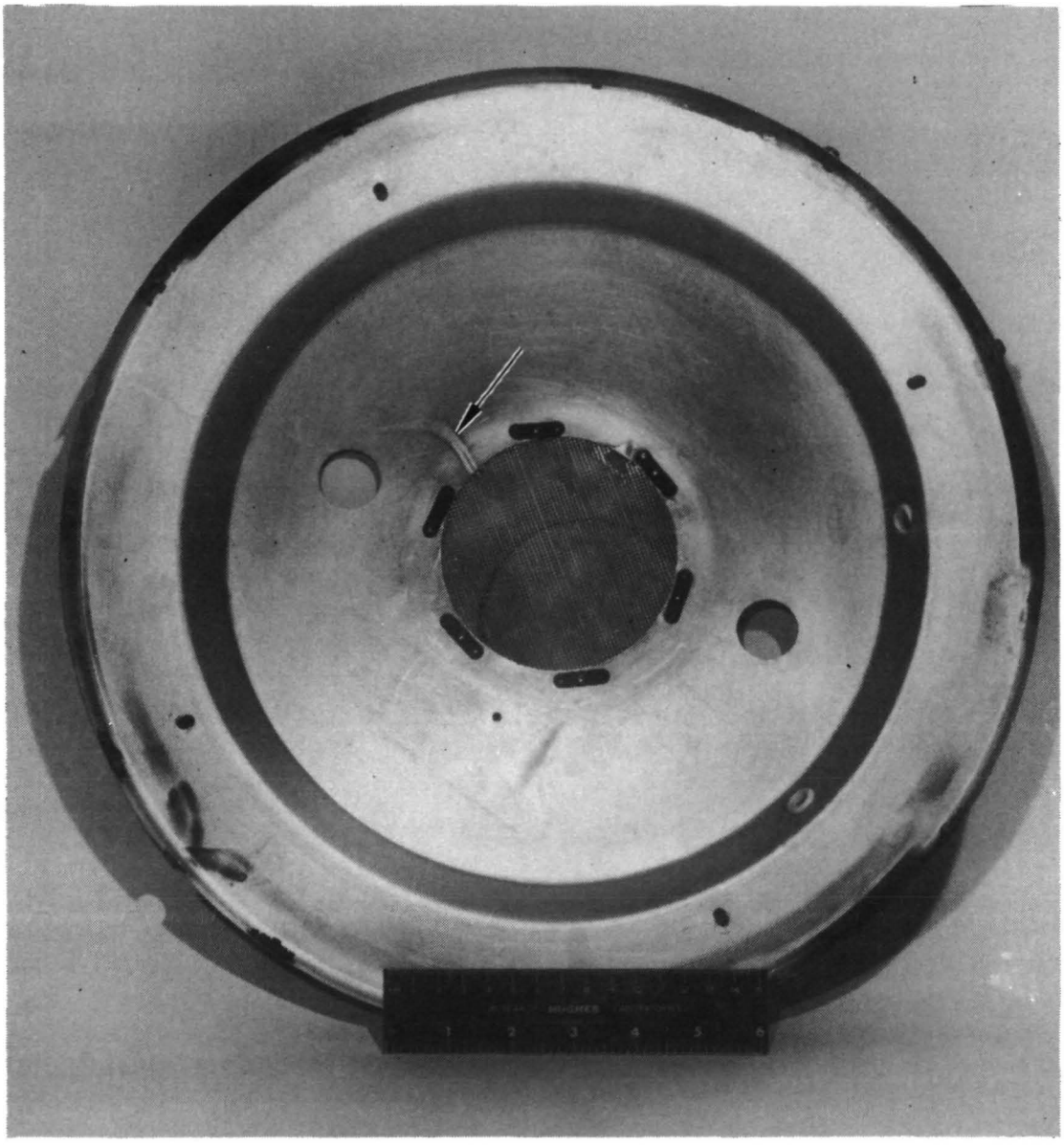

Figure A-10. Inside of rear cover.

M11078 4893–79

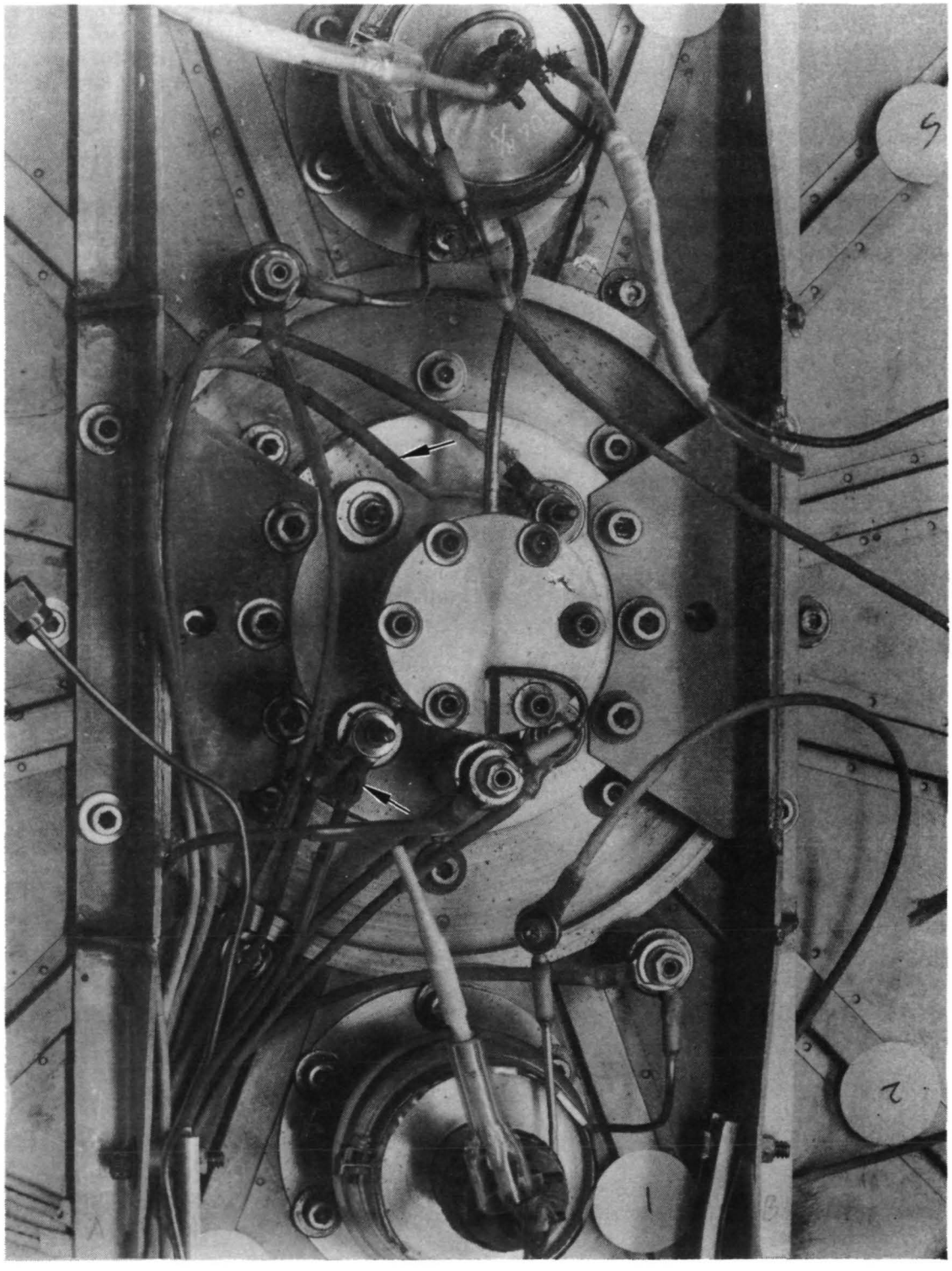

Figure A-11. Closeup of wiring in center region of backplate.

M11010 4893-48

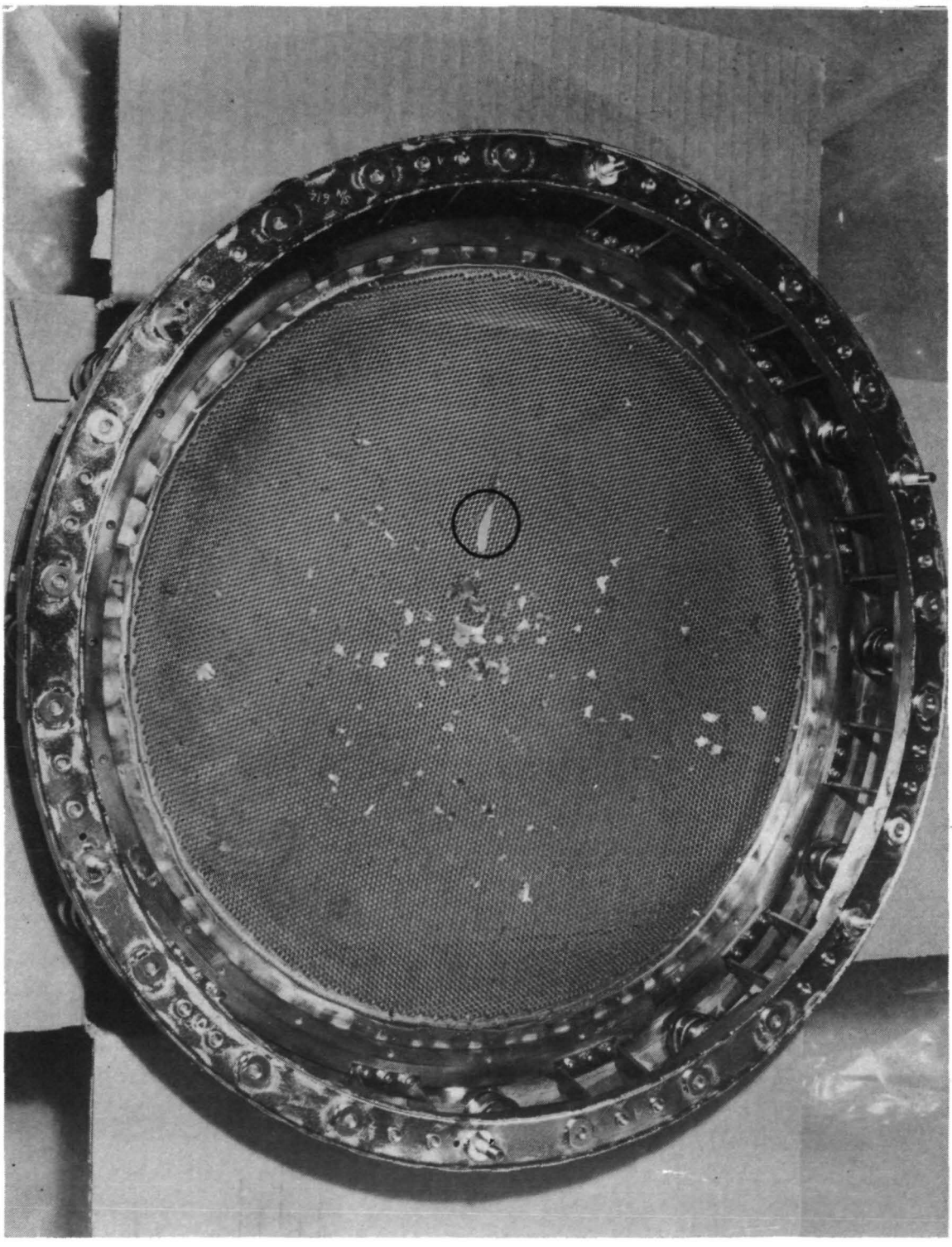

Figure A-12. Optics with flakes on upstream side of screen electrode. Encircled flake is piece of baffle.

Figures A-8 and A-9 show the thruster as viewed from an upstream location, with and without the back outer case. On the basis of what can be seen from these photographs, it would be impossible to estimate how long the thruster has been operated. The slight discolorations seen on the vaporizer and central access plate of the back cover are considered to be a consequence of wiring insulation deterioration. Other evidence of this deterioration is seen in Figs. A-10 and A-11. The wires affected are attached to or are routed very close to components that operate at relatively high temperature (~300°C). Notice also the relatively large number of mercury droplets seen on the thruster surface in Fig. A-11. This mercury is thought to be a consequence of the vacuum chamber venting and thruster dismounting procedures rather than deposits which have condensed during the test.

Figure A-12 shows the upstream view of the ion optics assembly after careful removal to preserve the orientation of the "flakes" resting on the screen grid. The circled "flake" is a portion of the baffle, comparable to the remaining portion seen in Fig. A-5. The markings around the edge of the screen grid are a consequence of the tantalum "gasket" used to cover the gap between the screen grid and screen pole piece. This assembly will be discussed in detail in a separate section.

Before proceeding to the detailed discussion of the thruster subassemblies, it is considered appropriate to point out that a relatively large number of the thruster components show no significant wear or damage and have thereby demonstrated the durability of a number of the component designs. The sections which follow will concentrate on the discussion of damage and wear and although this damage may represent the result of relatively few processes and affect only a relatively small number of parts, the volume of discussion on damage far exceeds that on success.

B. Discharge Chamber Assembly

The discharge chamber assembly is comprised of the following components and subassemblies:

- Discharge chamber shell
- Anode
- Propellant distributor plenum
- Magnets and pole pieces (magnetic circuit)
- Cathode pole-baffle subassembly.

All of these elements (except the last) will be discussed in detail in this section. The cathode pole-baffle subassembly sustained the greatest wear, and its elements will be described in detail in another section. Figures A-13 and A-14 show the extent of this wear. (For comparison, a photograph of a new subassembly is shown as Fig. A-15.) The baffle is eroded almost completely away, exposing the internal components of the subassembly to ion bombardment. Similarly, the pole piece is seen to be thinned to a "knife-edge" at the downstream edge. The material removed from these components is re-deposited on the internal surfaces of the discharge chamber, and, as the coating builds in thickness, the deposited material spalls and forms "flakes." These deposits are evident in Figs. A-13, A-14, A-16, and A-17 primarily on the upstream discharge chamber boundary or backplate and the anode. Samples of these deposits were taken at the locations marked on the photographs in Figs. A-13 and A-16 and analyzed to provide the results listed in Table A-4. Except for the deposit taken from the outboard location on the backplate (L), the samples were comprised predominantly of iron. The sources of this iron are the baffle and the cathode pole which are fabricated from cold rolled electrolytic steel. The other constituents and impurities anticipated to be present in steel are also in evidence.

M11013 4893-49

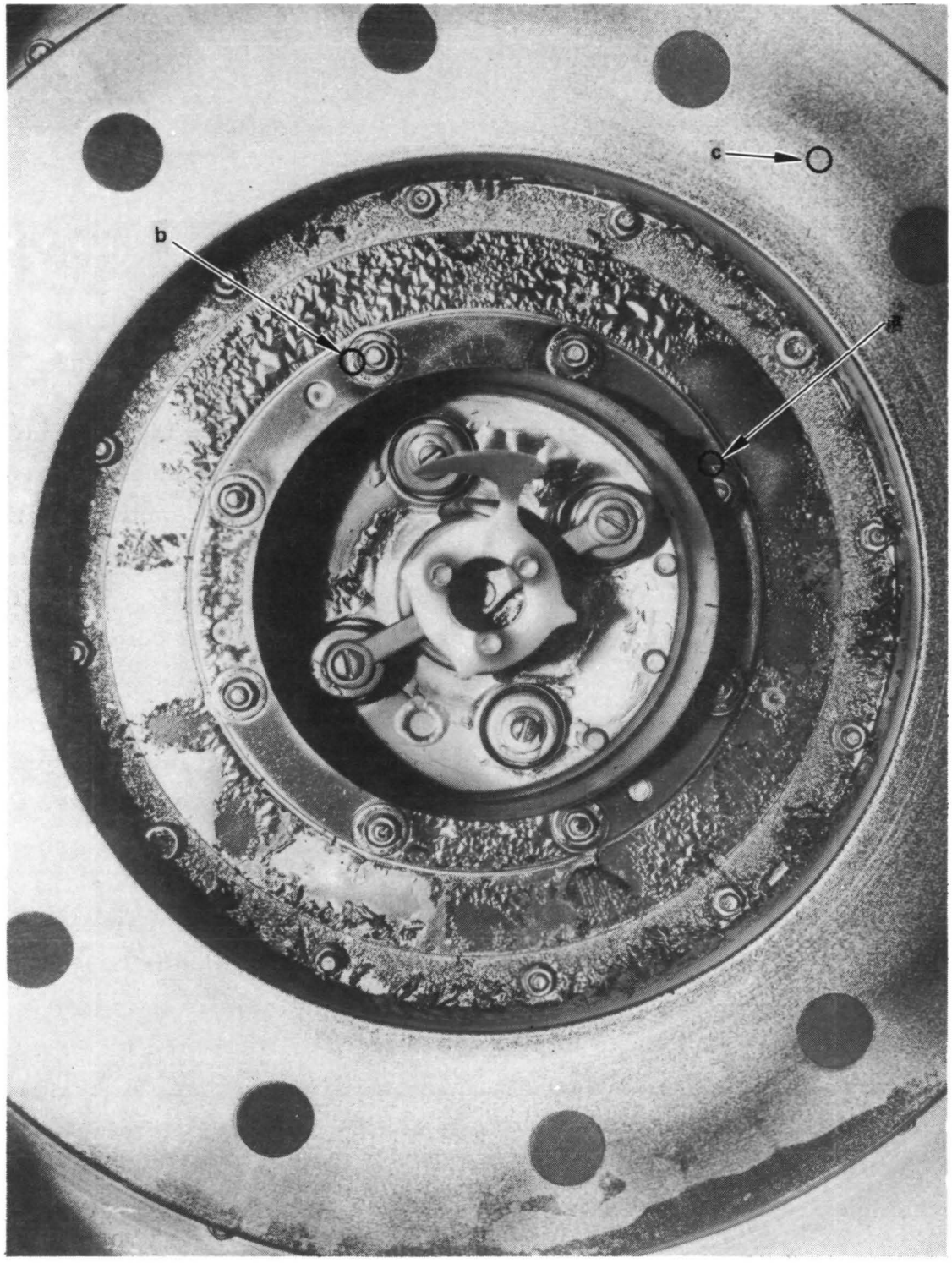

Figure A-13. Cathode pole-baffle region.

M11014

4893–258

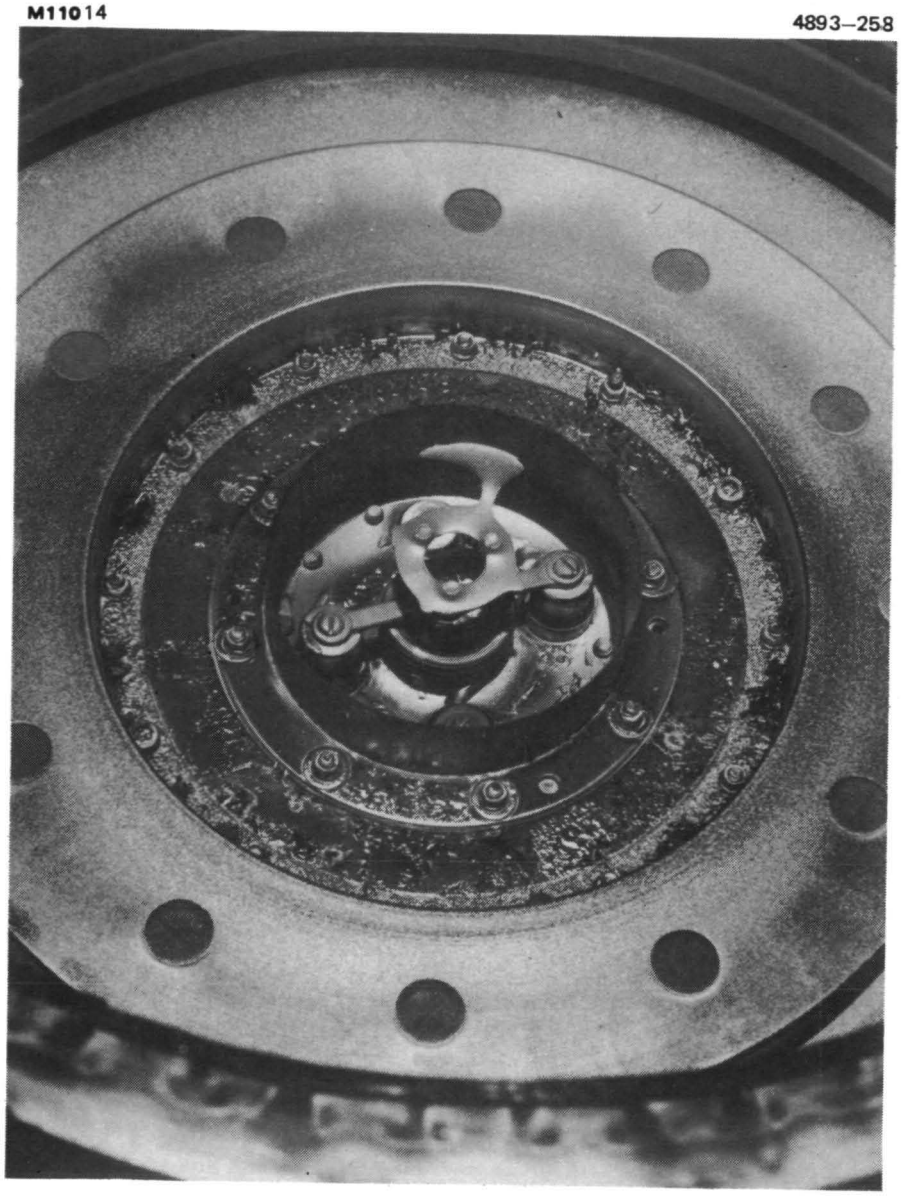

Figure A-14. Cathode pole-baffle region.

M110128 4893–259

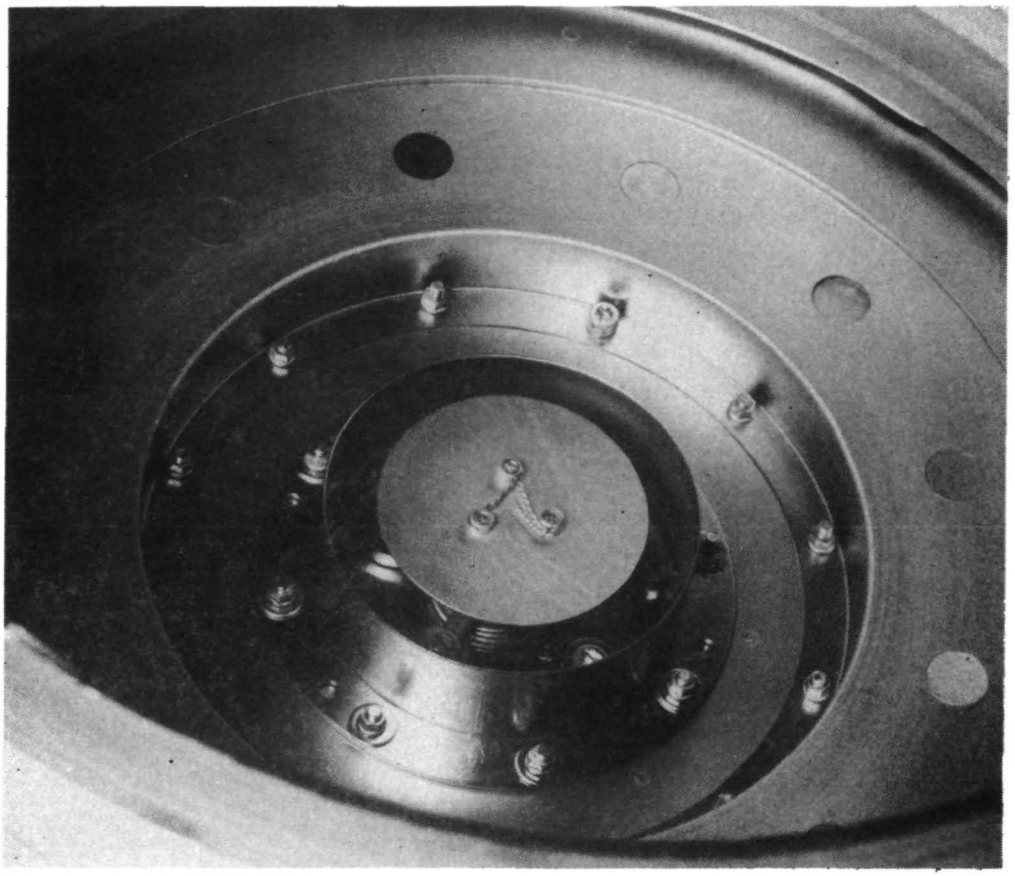

Figure A-15. Cathode pole-baffle region of a new 700-series thruster.

M11012

4893–49A

Figure A-16. Sputter deposition on anode.

M11011

Figure A-17. Sputter deposition on anode.

Table A-4. Semiquantitative Analysis of Discharge Chamber Flake Samples

Sample Location	Composition					
	A	B	E	F	G	L
Elements						
Fe-	Rem.	Rem.	Rem.	Rem.	Rem.	6.8%
Cr-	0.27%	0.52%	0.61%	0.57%	0.61%	1.4
Ni-	11.	22.	4.1	4.4	3.9	6.2
Ti-	0.17	0.61	0.56	0.48	0.66	2.8
Mo-	27.	7.4	25.	16.	16.	Rem.
Si-	ND<0.020	TR<0.020	0.22	0.32	0.15	1.2
Mn-	0.061	0.24	0.46	0.61	0.35	TR<0.020
Mg-	0.0048	0.013	0.025	0.025	0.034	0.12
Al-	0.061	0.048	0.24	0.22	0.18	ND<0.10
Ag-	0.0059	0.018	0.051	0.040	0.032	ND<0.010
Hg-	0.043	0.087	0.92	0.15	0.76	8.4
Pb-	ND<0.05	—	—	—	—	ND<0.50
Cu-	0.019	0.041	0.11	0.11	0.076	0.047
Co-	0.093	0.33	0.087	0.070	0.056	ND<0.10
Ca-	ND<0.002	—	—	—	—	0.13
Sr-	ND<0.005	—	—	—	—	—
Ba-	ND<0.50	—	—	—	—	—
Ta-	ND<0.30	—	—	—	—	—
W-	ND<0.40	—	—	—	—	—
Au-	ND<0.006	—	—	—	—	—
Other Elements	nil					

T1855

Higher concentrations of Ni were found in locations A and B. Locations A and B are near mild steel components which were originally nickel plated. Note that the percentage of molybdenum found in the anode samples decreases with distance from the screen grids. The only molybdenum components are the screen and accelerator electrodes and the keeper electrode. The molybdenum present in the deposit samples is thought to be from the screen electrode. The erosion of this electrode was significant, as will be described in the ion optics assembly section. The locations noted as C, D, and H did not yield any measurable deposit although several attempts were made to dislodge deposits in these locations by thermal shock and also by scraping the surface while observing it under a microscope. These locations do not appear to be erosion sites either. Note also that there is very little titanium in evidence in these samples and therefore it is concluded that there is little or no ion erosion of the propellant distribution plenum or other cathode potential surfaces of the discharge chamber shell.

In the 700-series thruster design, a small gap exists between the screen electrode of the ion optics assembly and the screen pole piece. If left uncovered, this gap allows ions to be accelerated radially outward to impinge on the outer case. Although the number of these ions is small, the outer case and elements of the ion optics support can be detectably sputtered. Consequently, the 700-series discharge chamber design included a thin tantalum gasket that is spotwelded to the screen pole piece and makes slight contact with the screen electrode (see Fig. A-5). No appreciable erosion or deposition could be detected on this tantalum gasket (thickness measured with micrometer). Consequently, the erosion sites in the discharge chamber are

- The cathode pole piece
- The baffle
- The screen electrode

Deposition sites in the discharge chamber are

- The thruster backplate and innermost wall of the propellant distribution plenum

- The central 3 in. (7.6 cm) of the anode
- The upstream boundaries of the interior and exterior surfaces of the cathode pole-baffle subassembly.

Locations in the discharge chamber which are not appreciably eroded or covered with deposits are

- The downstream surface of the plenum
- The upstream and downstream edges of the anode (about 0.5 to 0.8 in.; 1.3 to 2 cm)
- The screen pole piece.

The erosion and deposition sites on the cathode pole-baffle subassembly will be discussed in more detail in a later section.

The radical modification of the baffle and baffle support by sputtering erosion was expected to have modified the magnetic field distribution in the thruster. The axial and radial magnetic field components were measured using a Hall effect probe gaussmeter and probe positioning mechanism that automatically plots field strength versus probe movement on an x-y plot. These measurements are made by moving the probe axially at constant radius from upstream to downstream discharge chamber boundaries. Field distributions of this type were not available from the pre-test data; however, the second 700-series thruster built (SN 702) was measured in this manner. Figures A-18 and A-19 compare the axial and radial field strengths for thrusters SN 701 and SN 702. It is apparent that the field strength in the vicinity of the damaged cathode pole is reduced by about 25% at some radii and less as one moves away from the damaged polepiece-baffle subassembly. The radial magnets were removed and measured in the fixture which has been established as the standard for calibrating and documenting new magnets used in thruster fabrication. Although this type of documentation was not performed in the fabrication of thruster SN 701, the procedure used in magnetizing thruster SN 701's permanent magnets is though to be the same as that used now, and it is reasonable to assume that these magnets originally had the same strength as those being magnetized and measured recently. The standard field strength

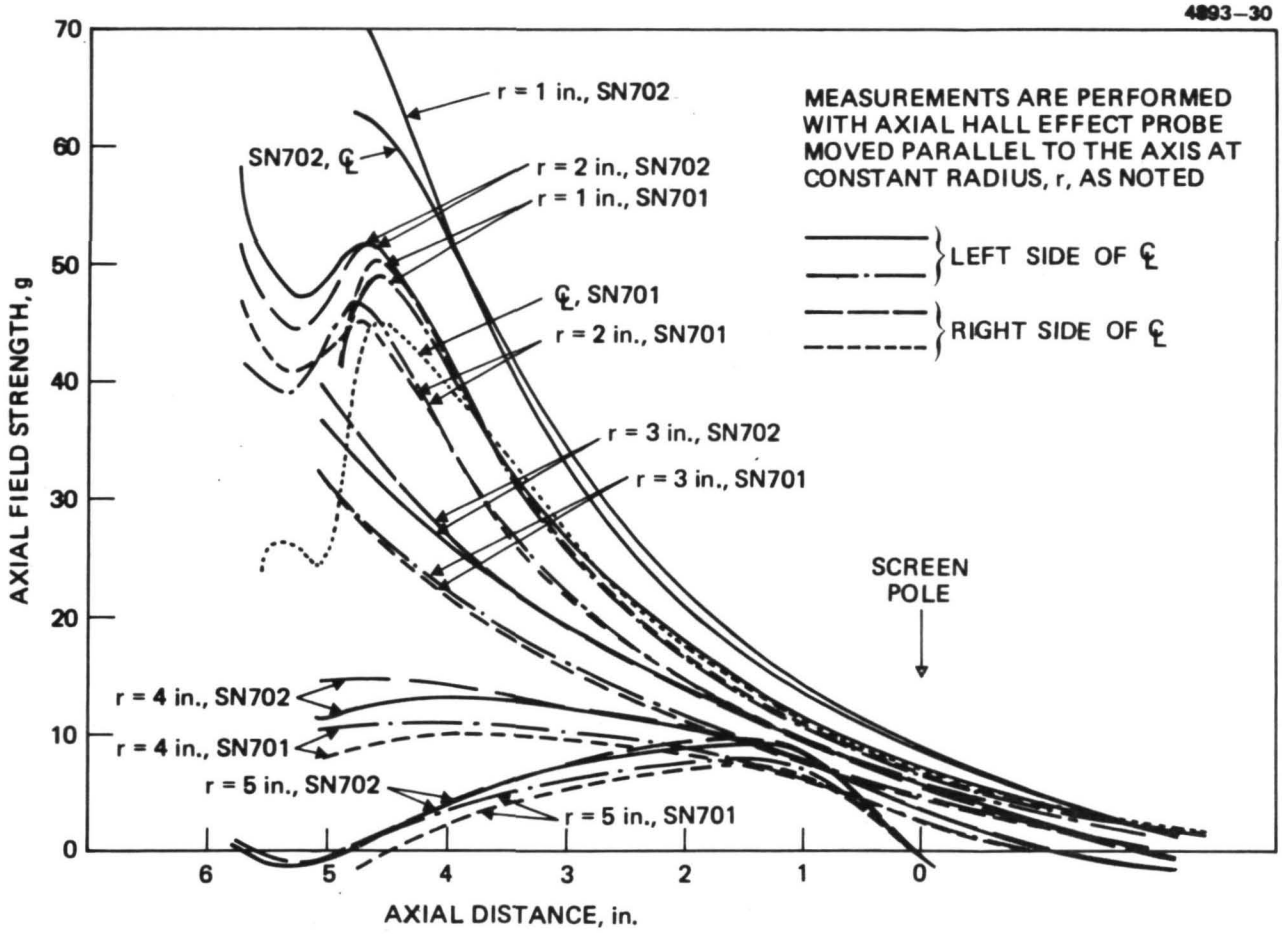

Figure A-18. Comparison of axial magnetic field components of thruster SN 701 after 10,000 hr test with those of thruster SN 702.

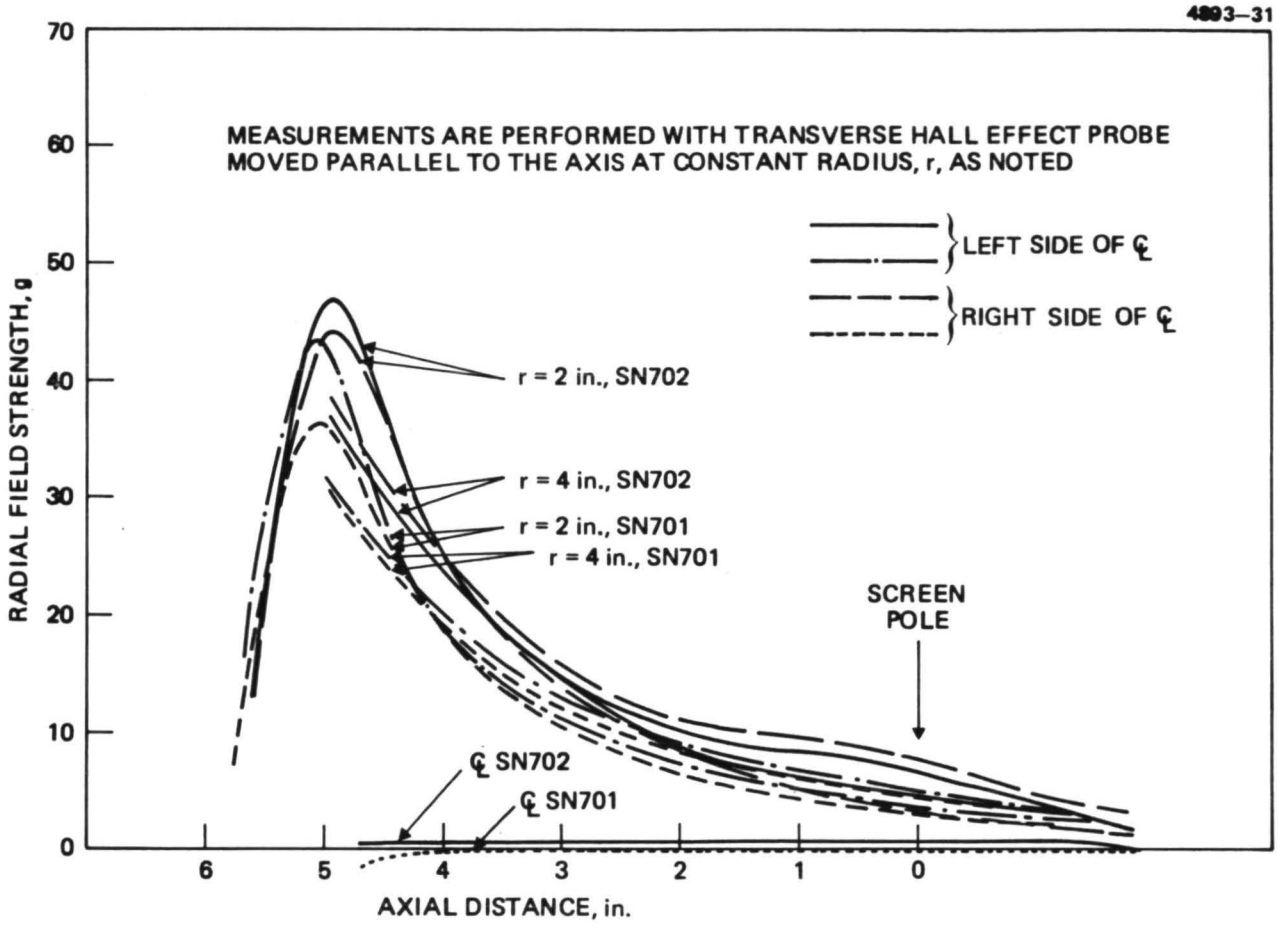

Figure A-19. Comparison of radial magnetic field components of thruster SN 701 after 10,000 hr test with those of thruster SN 702.

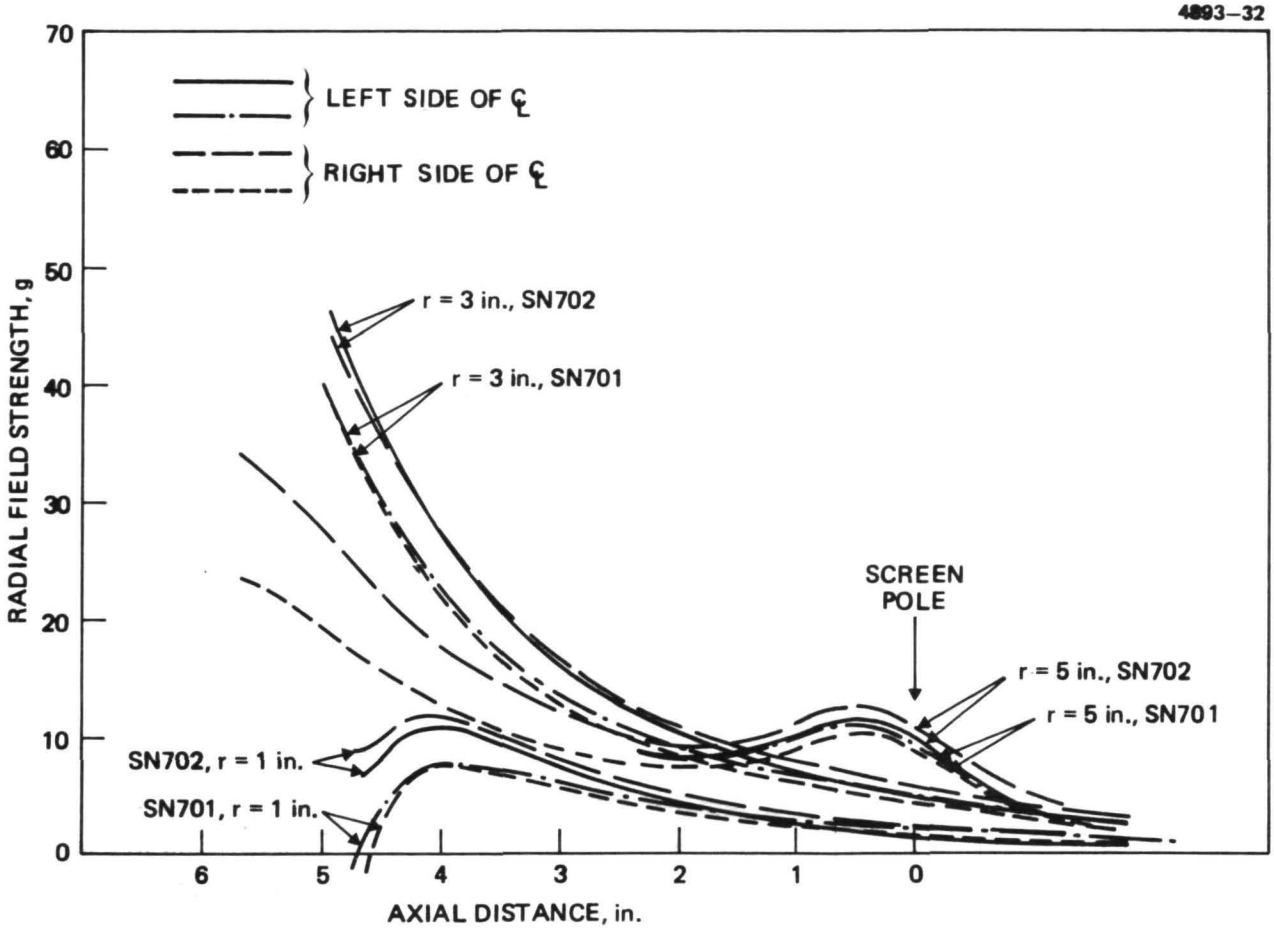

Figure A-19. Continued.

required for each of the radial magnets is 4.8 to 5.0 G, as measured in the calibrating fixture. The measured values of the radial magnets from thruster SN 701 vary in strength between 4.35 and 4.9 with an average value of 4.5. Thus, assuming that these magnets were originally the same as those being used now, the magnetization appears to have decreased by at least 6% below the value considered to be minimum in new thruster fabrication. This decrease in magnetization can account for at least a part of the generally lower magnetic field components of thruster SN 701 as compared to thruster SN 702 in Figs A-18 and A-19.

As mentioned earlier, the anode-to-discharge chamber shell insulation appeared to degrade between removal of the thruster from the test facility mounting and the first measurements taken before beginning disassembly (from 5000 Ω to 350 Ω). The reason for this decrease became evident after removing the discharge chamber backplate, and is shown in Fig. A-20. A flake of magnetic material was held between the screen polepiece and the anode by the thruster magnetic field (see arrow) and was responsible for the low resistance measurement. When the flake was removed, the anode to discharge chamber shell resistance increased to 5000 Ω again.

Another observation that can be seen in Fig. A-20 is the distortion in the downstream edge of the anode. A possible explanation of this distortion is that current surges from shorting by flakes, such as the one seen bridging the gap between the screen pole piece and the anode, caused local heating of the anode, thereby causing the observed distortion. Although the localized current may not be caused by flakes, it is probable that some form of localized heating is responsible for the anode distortion seen in Fig. A-20.

An interaction between the anode and the anode fasteners can be seen on two of the six fasteners which hold the anode in place. The anode supports numbered 1, 3, and 5 were nearer the downstream end of the discharge chamber, while numbers 2, 4, and 6 were located nearer the upstream end. Enlarged photographs of these two fasteners are shown in Figs. A-21 and A-22 (which will be referred to as anode support numbers 6 and 2, respectively). The stainless steel screw of anode

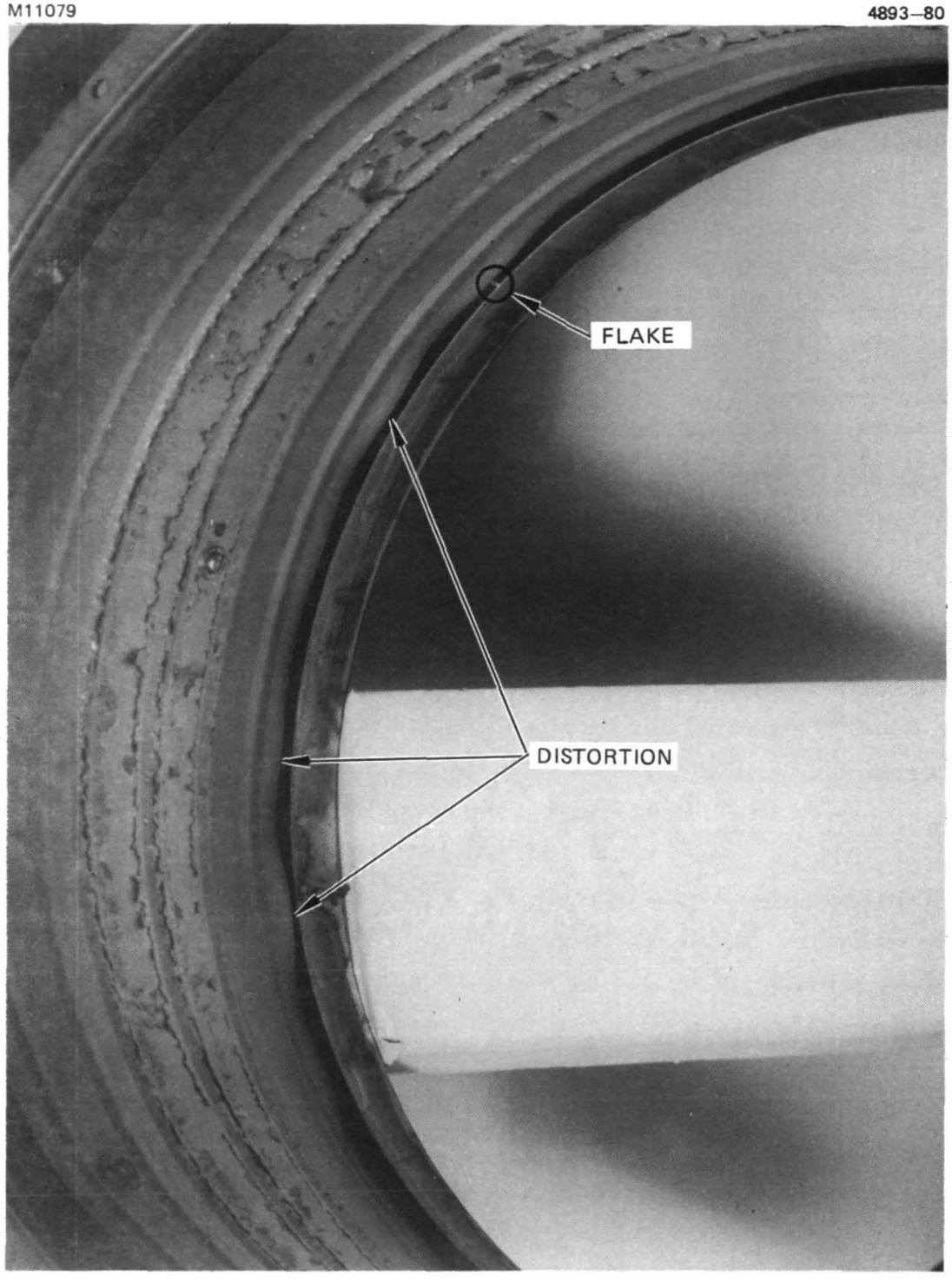

Figure A-20. Part of anode showing distortion and flake.

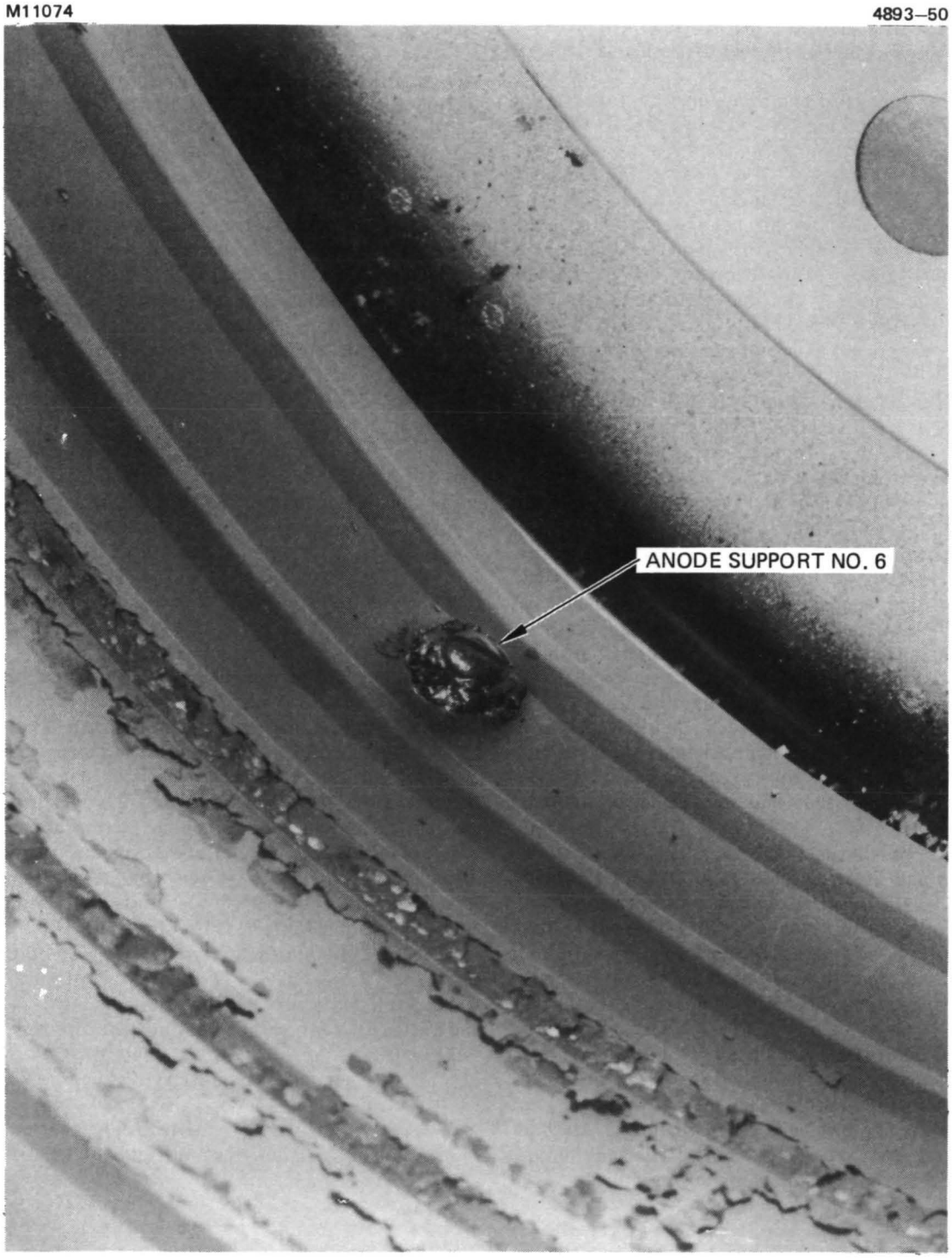

Figure A-21. Part of anode showing damaged anode support No. 6.

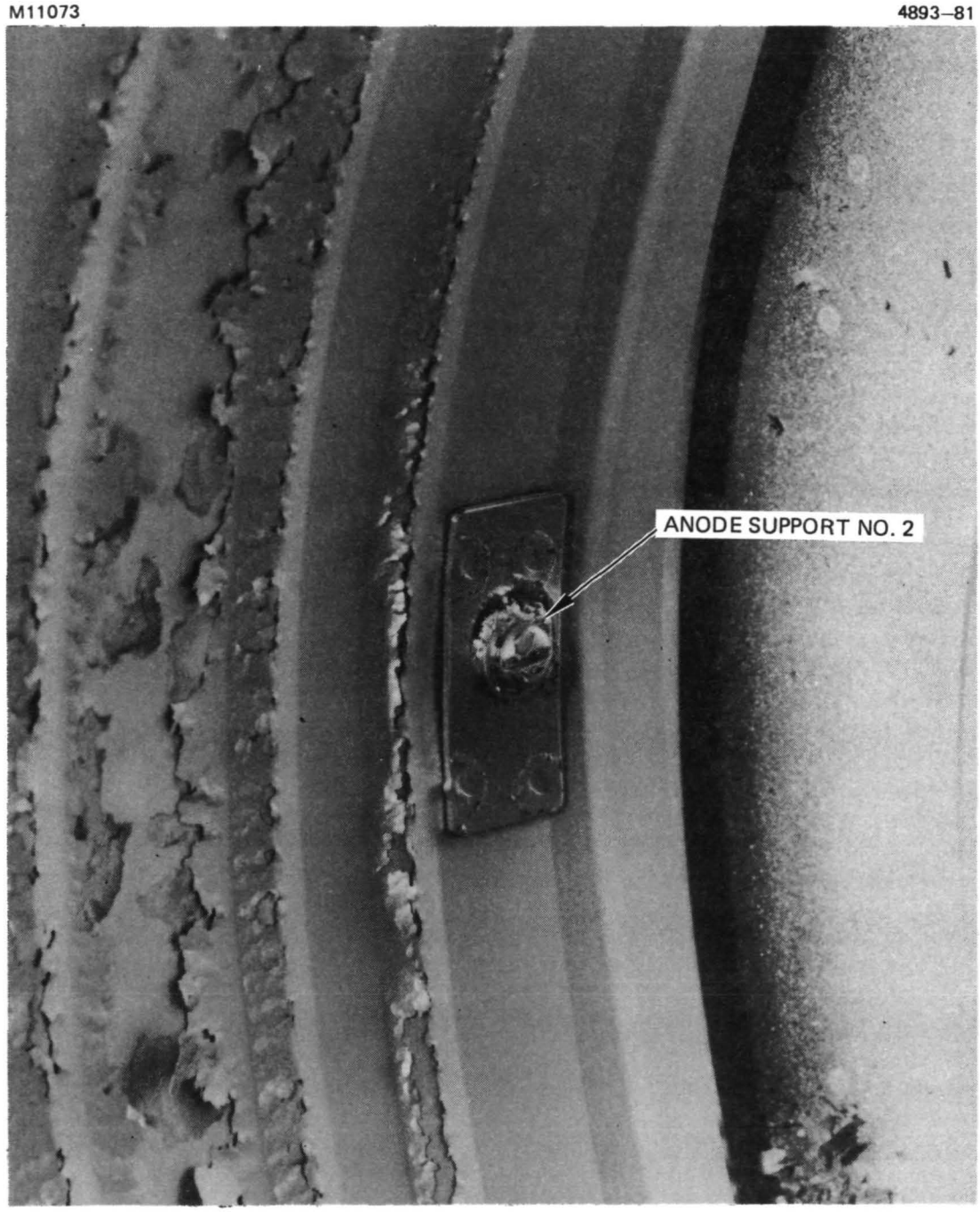

Figure A-22. Part of anode showing damaged anode support No. 2.

support number 2 is the only anode current path and carries the combined beam and discharge currents. After removing all the anode siring, the leakage resistance measured between the anode and the discharge chamber shell was still only 5000 Ω, and these two fasteners and their anode support insulators then became the most probable source of this relatively low leakage resistance.

The thruster backplate was removed to expose these support insulators; upon inspection, the ceramics were seen to have sustained damage, as shown in Figs. A-23 and A-24. The damaged insulators were removed intact by cutting the anode and discharge chamber shell with a high-speed abrasive wheel. Removal of anode support number 2 (current connection) resulted in an increase in the leakage resistance, as measured with the "megger" 1 kV ohmmeter, to 10 kΩ. The megger measurement was seen to fluctuate to readings as high as 25 kΩ. Removal of the other damaged support, number 6, did not appreciably change the leakage resistance. Figures A-25 and A-26 show all sides of the damaged anode supports after removal from the discharge chamber. The leakage resistance measured across these insulators was approximately 10 kΩ. Removal of the third upstream anode support, number 4, by normal disassembly increased the leakage resistance to a value fluctuating between 30 and 200 kΩ; sparking was seen around the downstream insulators. The remaining anode supports were removed with care taken to preserve a record of their orientation. The ceramic insulators removed are shown in Fig. A-27.

The ceramic parts shown in Fig. A-27(a) are the portion of the anode support insulators which are located on the exterior side of the discharge chamber shell, while those shown in Fig. A-27(b) are located between the anode and the shell. The exterior insulators have a shield and are only slightly coated on the downstream surface (arrows seen on insulator tags indicate beam direction). The interior insulators are not shielded, except by means of their location between anode and shell, and are coated more or less uniformly with no indication of the orientation of the source of the deposited material. The nature of this coating will be discussed later. Figure A-27(c) and (d) show the opposite views

M11080 4893–51

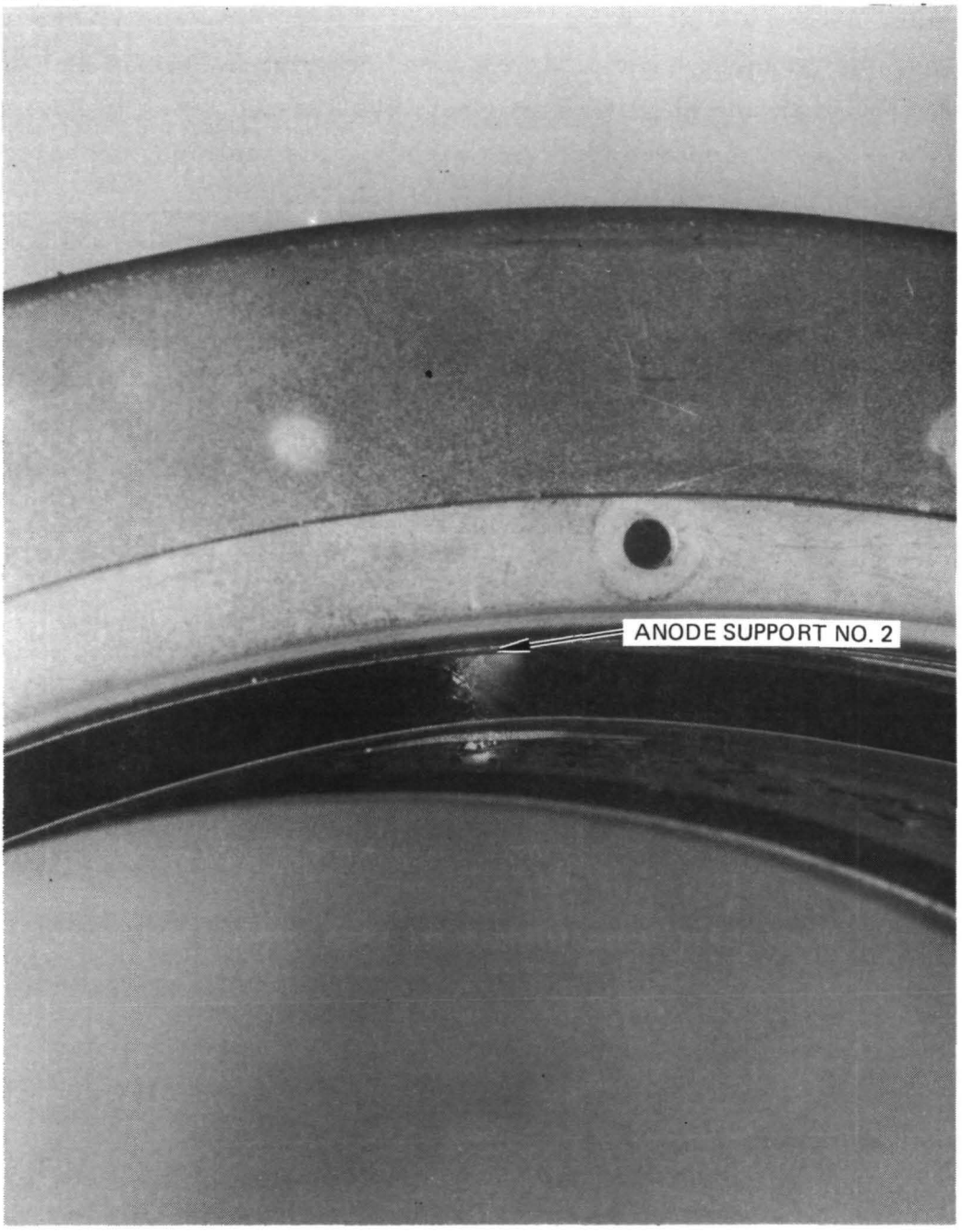

Figure A-23. Anode support No. 2 in place.

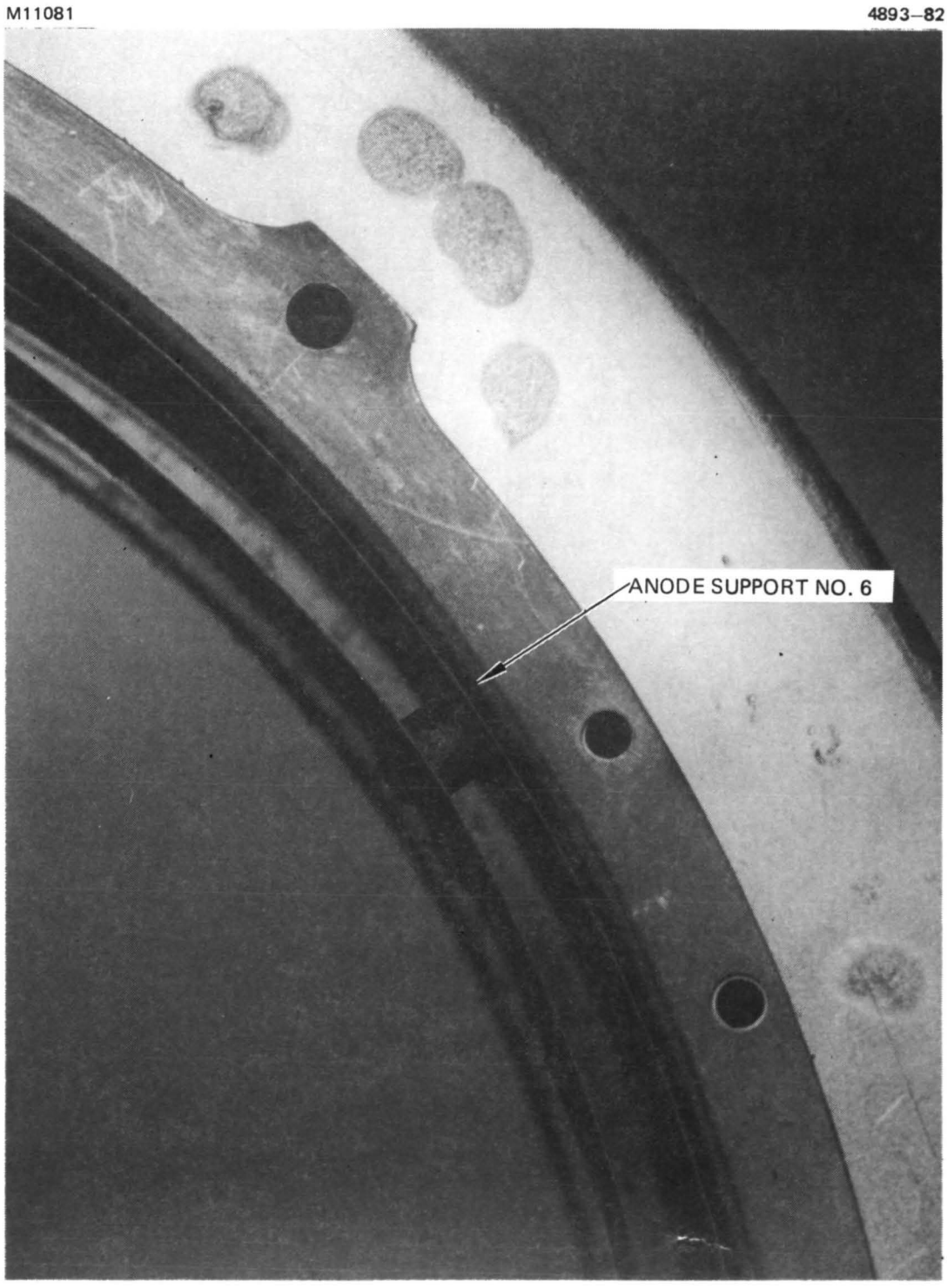

Figure A-24. Anode support No. 6 in place.

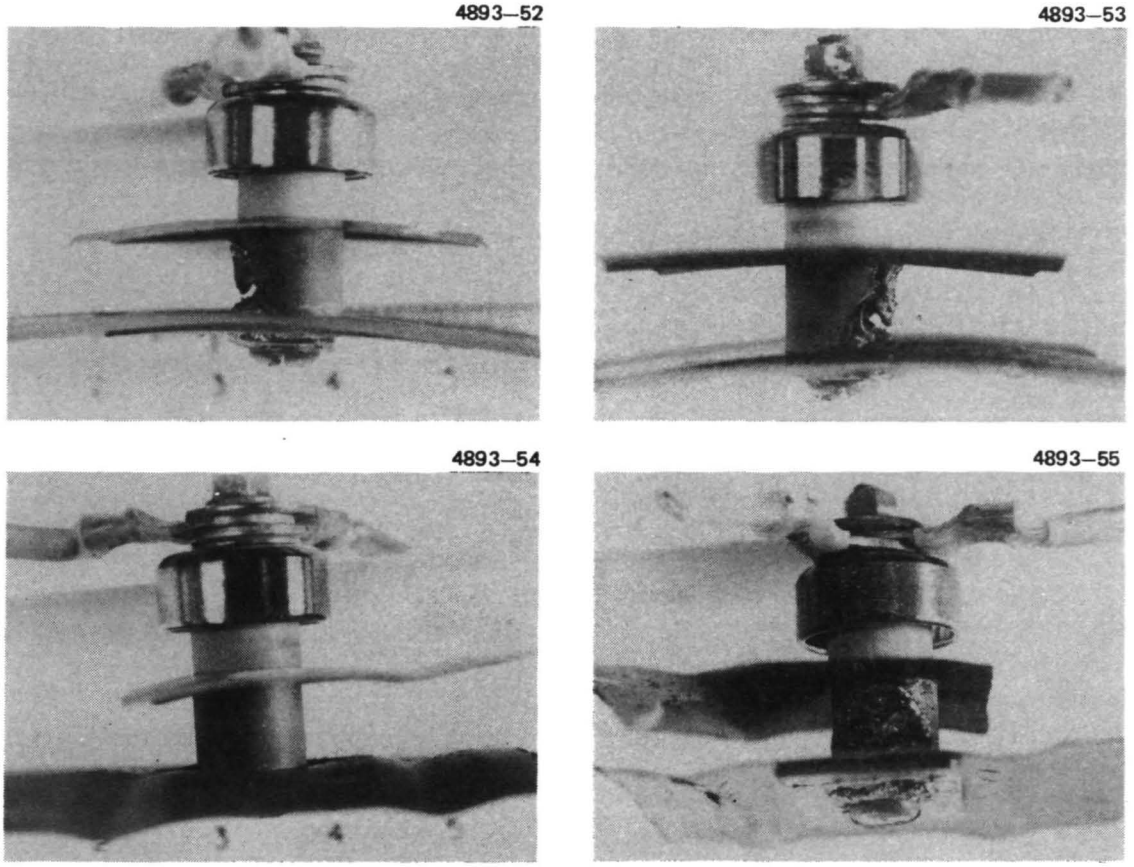

Figure A-25. Damaged anode support No. 2.

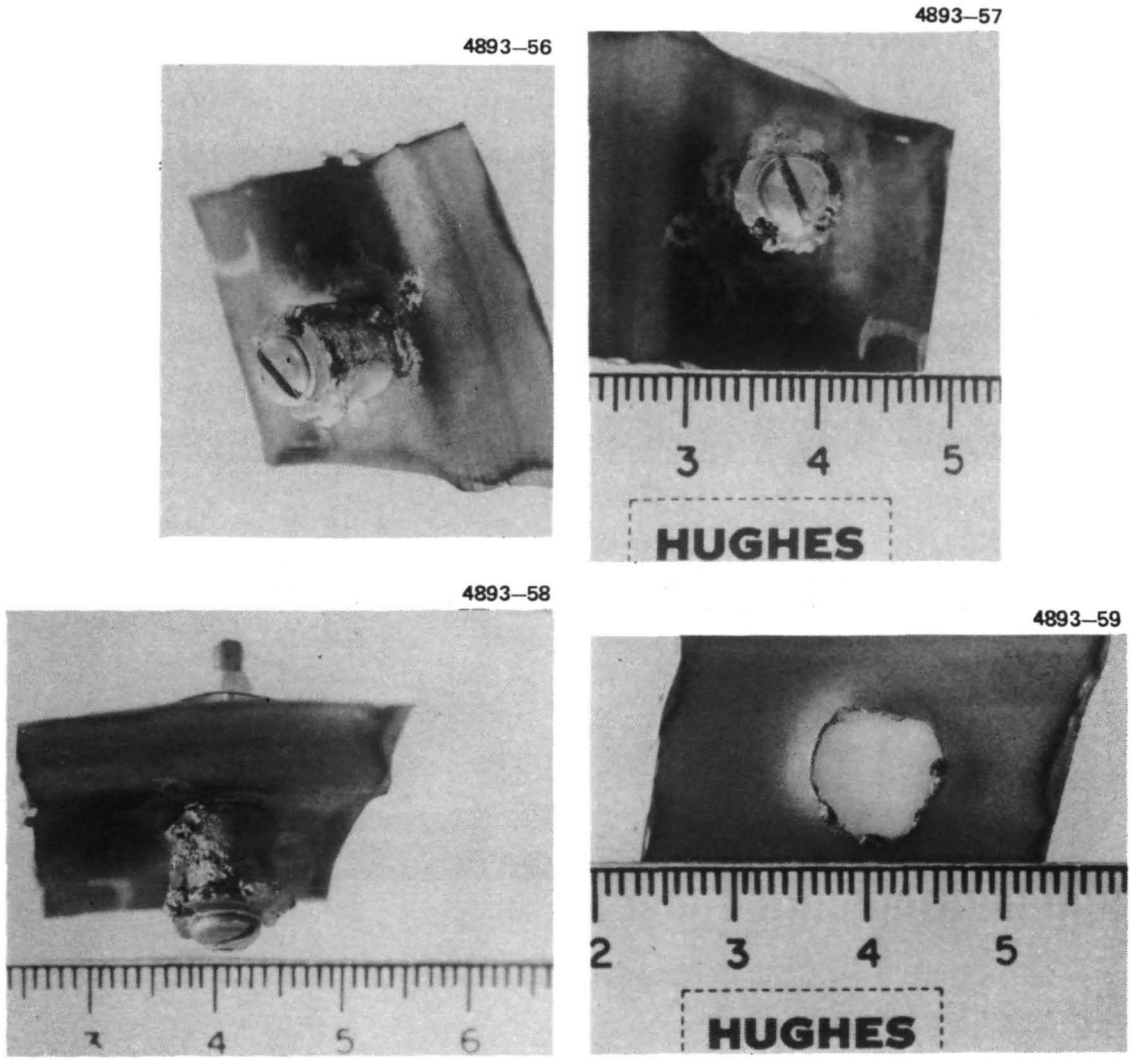

Figure A-26. Damaged anode support No. 6.

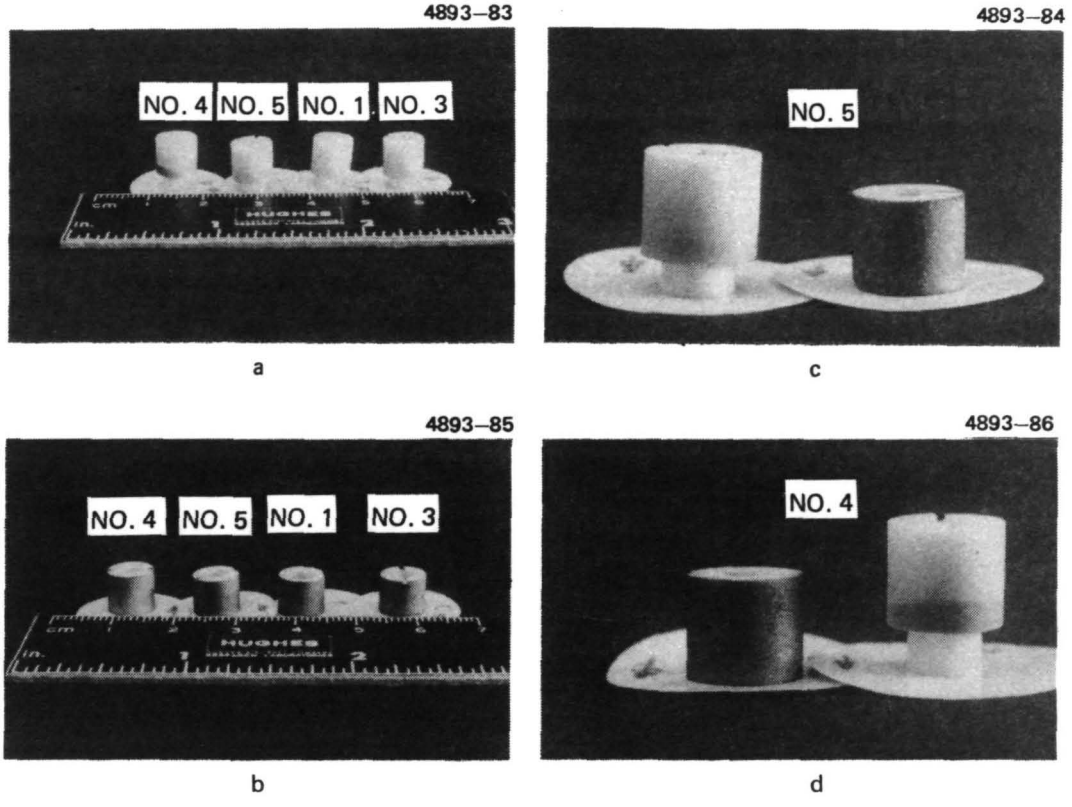

Figure A-27. Cermaic insulators from anode supports Nos. 1, 3, 4, and 5.

(downstream) of insulators No. 5 and No. 4. Note that there is no apparent difference between the coating on the upstream (No. 4) interior insulator and the downstream (No. 5) interior insulator in spite of the fact that both of the damaged anode supports occupied the upstream location (No. 2, No. 6).

Comparison of the upstream and downstream anode support locations on the interior of the discharge chamber shell and the anode reveals evidence of arc formation around the upstream insulators but not around the downstream insulators. Figures A-26, A-28, A-29, and A-30 show photographs in support of this statement. In Figs. A-26 and A-28, "arc tracks" can be seen on the discharge chamber shell around anode support locations No. 6 and No. 4, respectively. Note that in Fig. A-29, there is no evidence of arcing in the vicinity of the downstream anode support location, even though some "arc tracks" are present near the upstream anode boundary, away from the anode support. The view of the exterior surface of the anode shown in Fig. A-30 displays the difference seen in the coloration around the upstream (No. 4) and downstream (No. 3) anode support locations. Around anode support No. 3, the coloration is uniform and shows no variation around the periphery of the anode. There is a definite localized coloration in the vicinity of anode support No. 4, however, and this could be an indication of localized heating.

On the basis of the examination discussed above, it was impossible to discern what caused the damage to anode supports No. 2 and No. 6. Consequently, one of the failed insulators, No. 6, and the surviving insulator, No. 4, were encapsulated and cross sectioned as shown in Figs. A-31 and A-32 with the areas of interest identified. Magnification of Area 1 is shown in Fig. A-33(a). The screw head and washer are composed of stainless steel and the melted region contains Fe, Ni, Cr, Ti, Mn, Si, Co, and C in decreasing order of proportion as determined by SEM microprobe. It is apparent that the portion of the anode which was held between the stainless-steel washer and the ceramic has been completely absorbed in the alloy melt seen. An SEM reproduction and K_α X-ray analysis of the spatial distribution of some of these elements is included in Fig. A-34.

M11131

Figure A-28. Part of anode showing "arc tracks" around location of anode support.

M11132

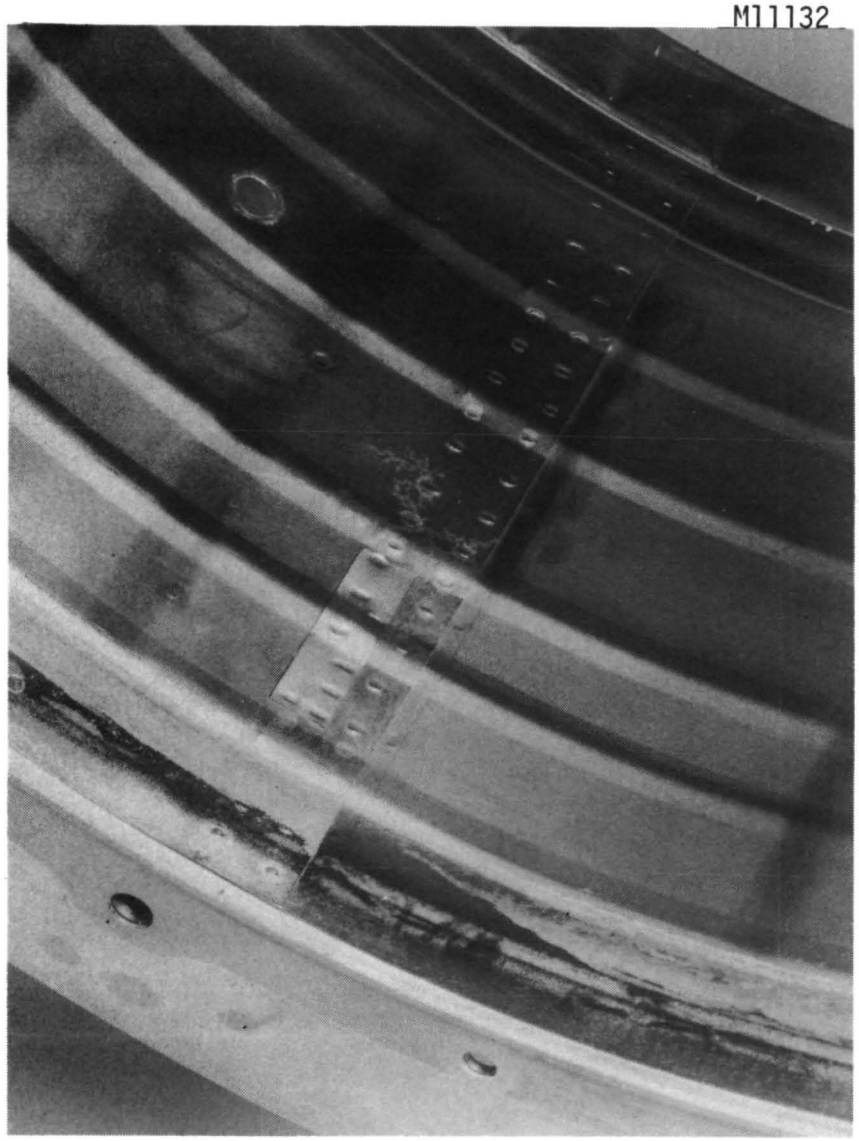

Figure A-29. Part of anode showing support location without "arc tracks."

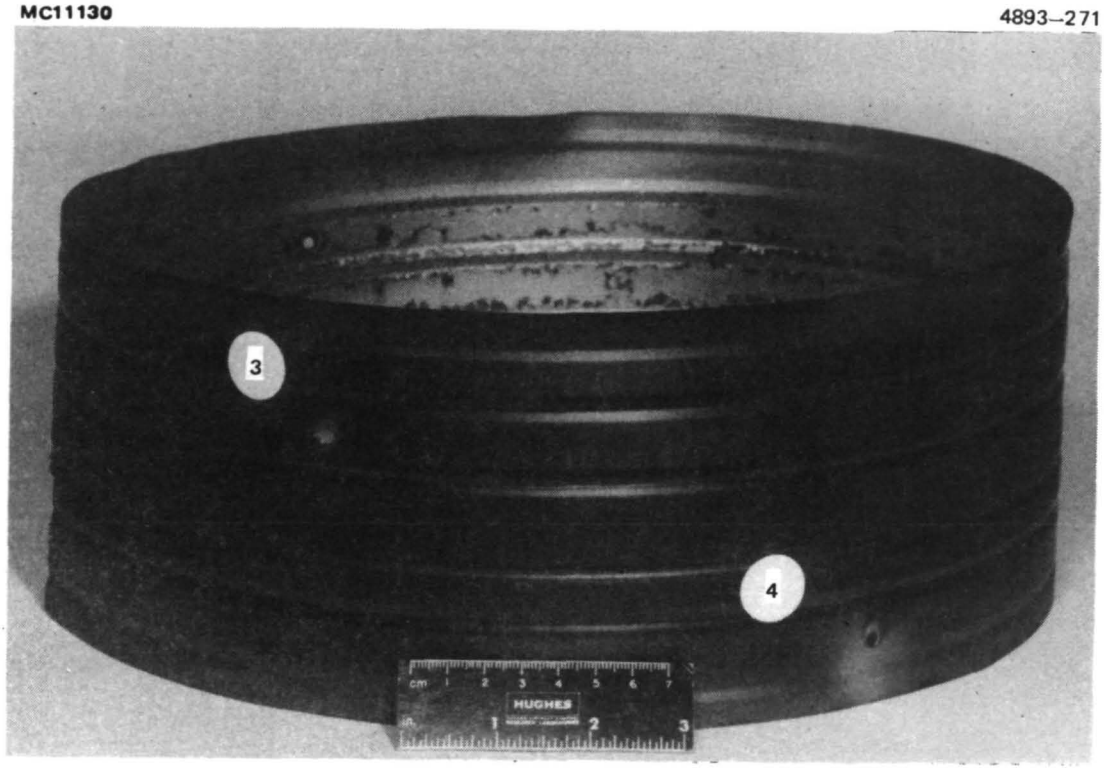

Figure A-30. Exterior surface of anode showing difference in coloration around upstream and downstream support locations.

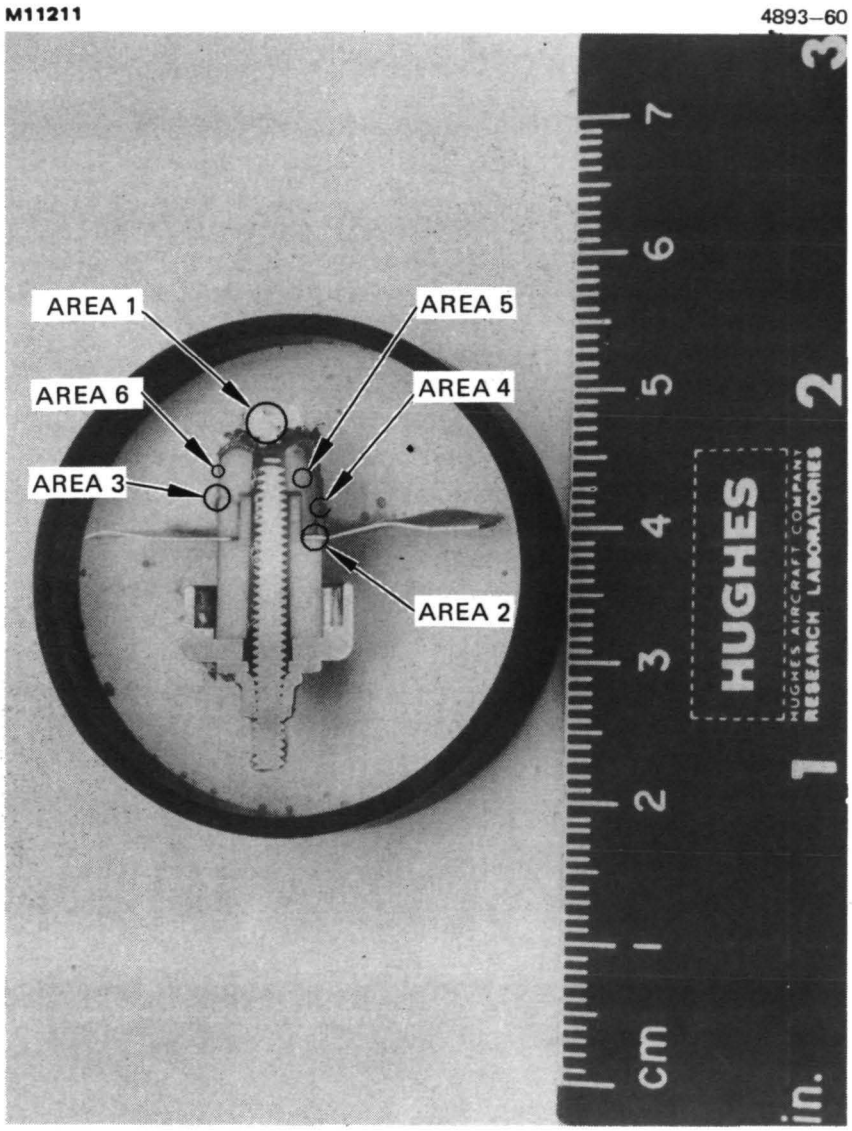

Figure A-31. Cross section of damaged anode support.

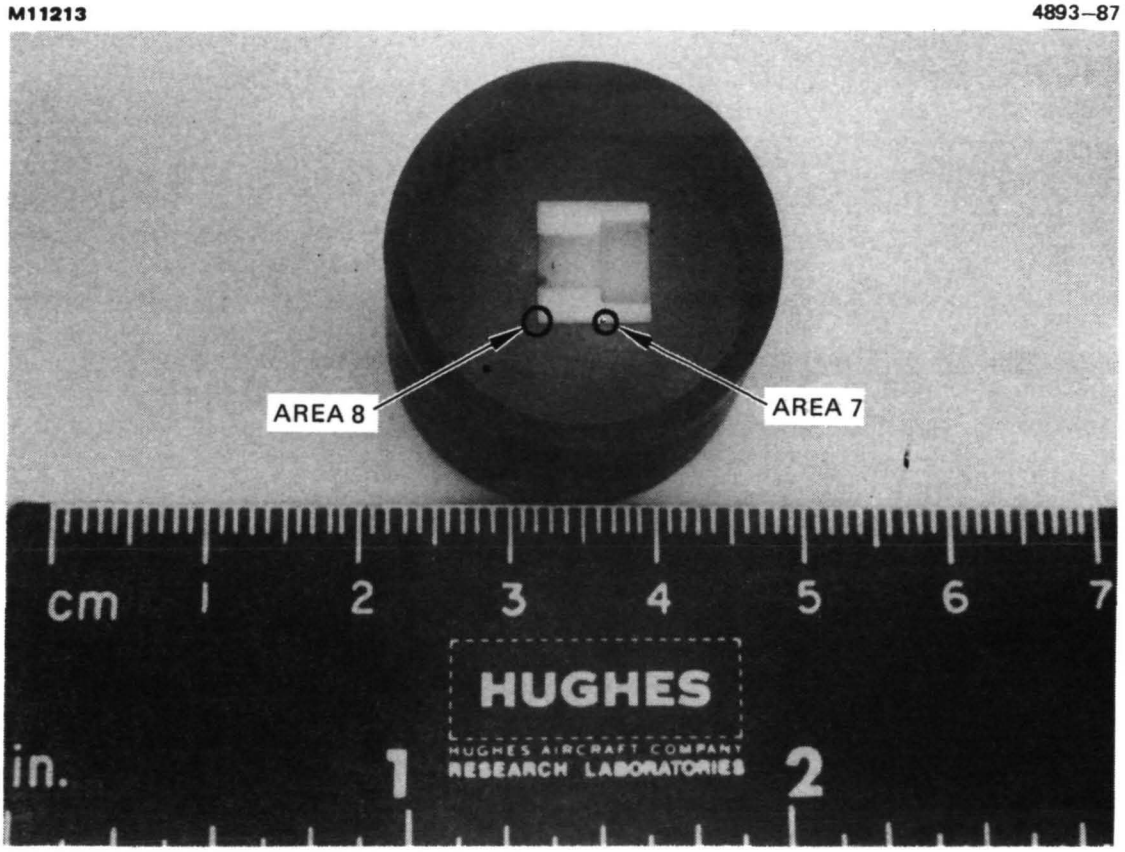

Figure A-32. Cross section of anode support insulator.

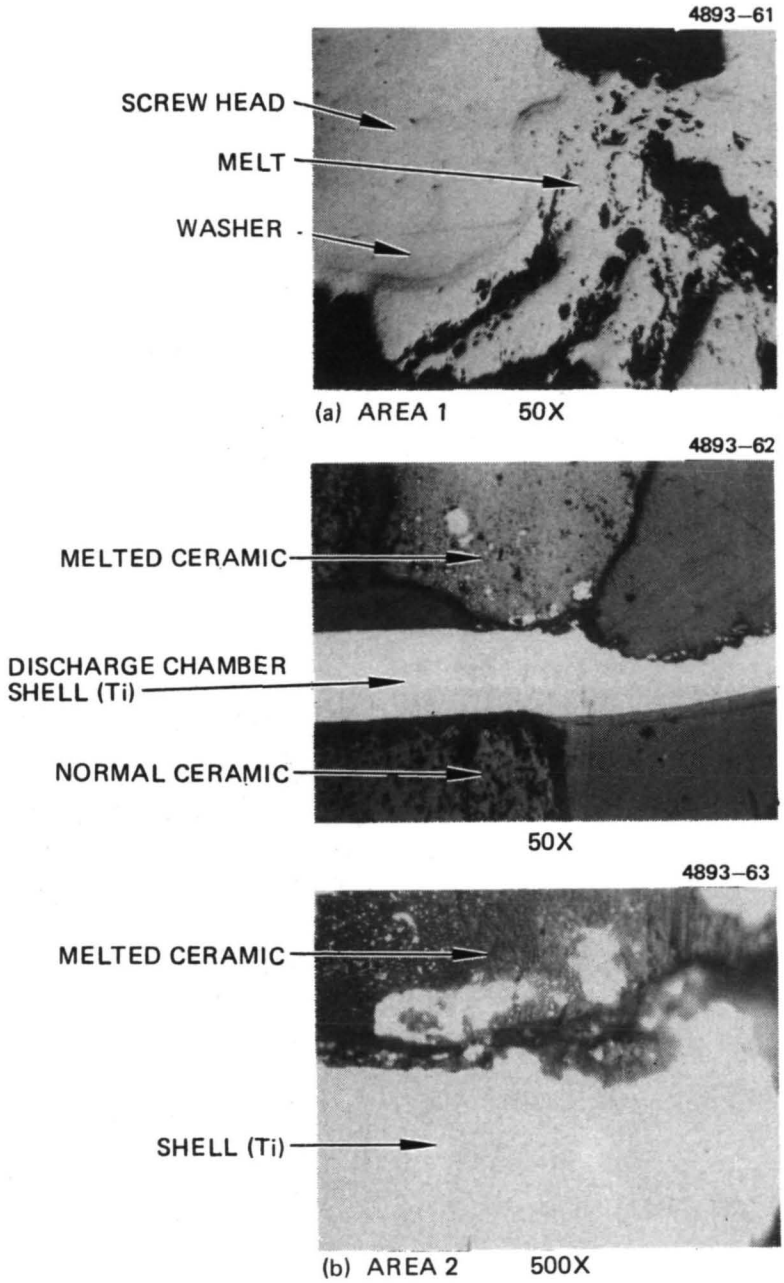

Figure A-33. Magnified view of damaged areas of anode support.

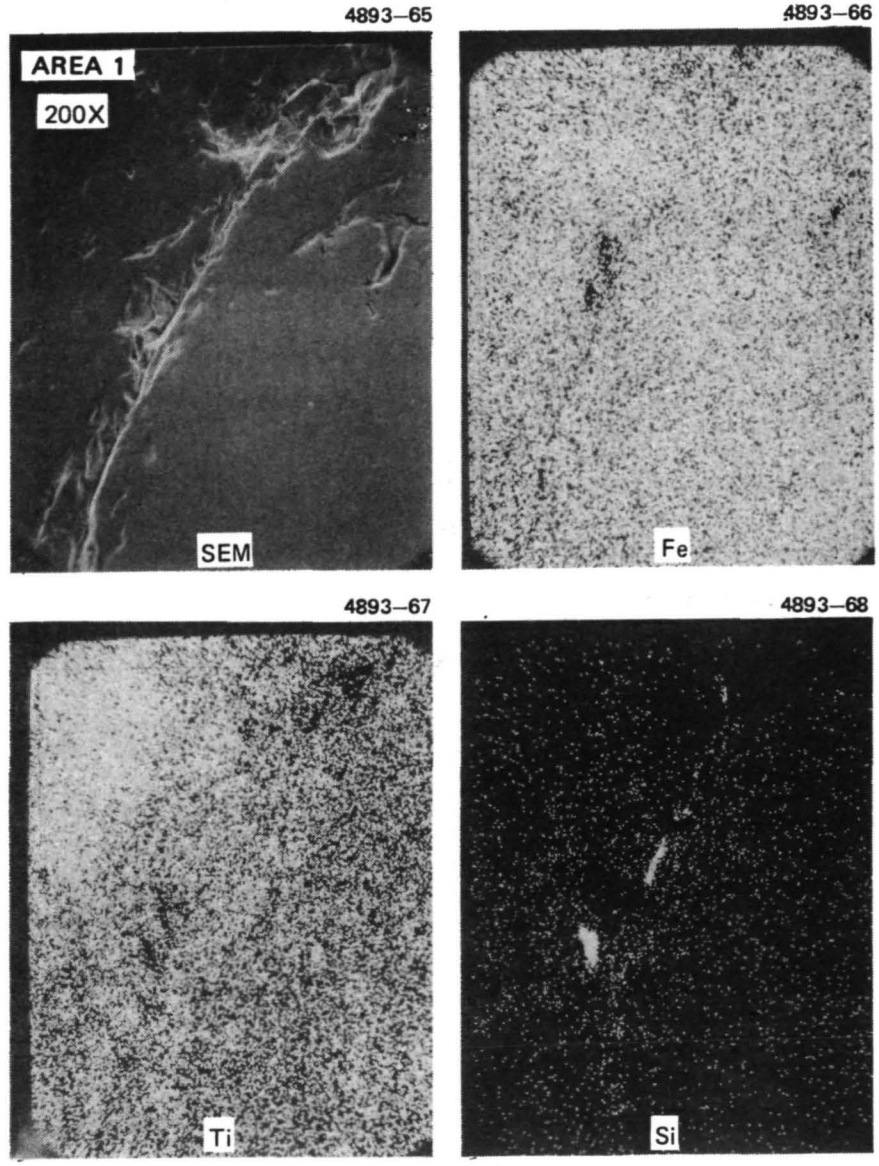

Figure A-34. Scanning electron microscope photo and K_α X-ray analysis of area 1 of anode support.

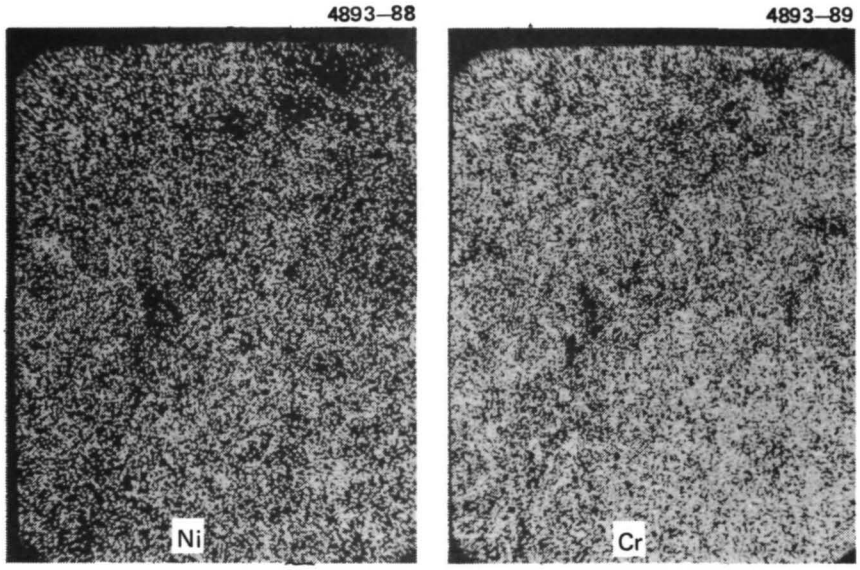

Figure A-34. Continued.

Microscopic examination of Area 2 shows that the titanium discharge chamber shell is eroded on the interior surface adjacent to the point of contact with the ceramic anode support insulator and that this ceramic has been melted in the vicinity of this point of contact (see Fig. A-33(b), 50X and 500X). Melting of the ceramic is indicated by the dendritic structure of the cross-sectioned ceramic. Titanium appears to be distributed throughout this melted region of the insulator, which would imply some sort of "wicking" or melting. This latter observation was substantiated by the SEM X-ray scan shown in Figs. A-35(a) and (b). The elements contained in this area are, in decreasing order of concentration, Al, C, O, Ti, Si, and Ca (the high percentage of C may be a consequence of the carbon coating necessary to prevent the sample from charging up in the SEM). Thus it appears that the interaction seen between the anode and the anode support elements is a consequence of melting. Considering the elements involved, the lowest melting point eutectic that could occur would be for Al and Ni at 640°C. All other binary combinations yield higher melting points. This temperature is well above ambient for any part of the discharge chamber (excluding the cathode tip). Although the presence of mercury might have some influence on the metallurgical behavior, it is considered more probable that intense heating occurs during some form of transient occurrence such as a vacuum arc across the insulator surface.

On the supposition that some form of insulator deterioration might have contributed to initiation of the phenomena that resulted in melting of the anode support insulator, the ceramic material was examined further in the areas shown as 3 through 8 in Figs. A-31 and A-32. The magnified photograph of Area 3, shown in Fig. A-36(a), seems to show a coating of about 4 μm thickness. An attempt to scan the coating in this area with the SEM microprobe showed only the elements C, Al, O, Ca, Si, and Cl. A second attempt in Area 6 produced Ti and Fe as well (SEM and the Al K_α X-ray scan are shown as Fig. A-37). Area 4 is in the damaged area, and it was thought that if the ceramic, which is predominantely Al_2O_3, was reduced to produce elemental Al, it would be possible to detect this by comparing the

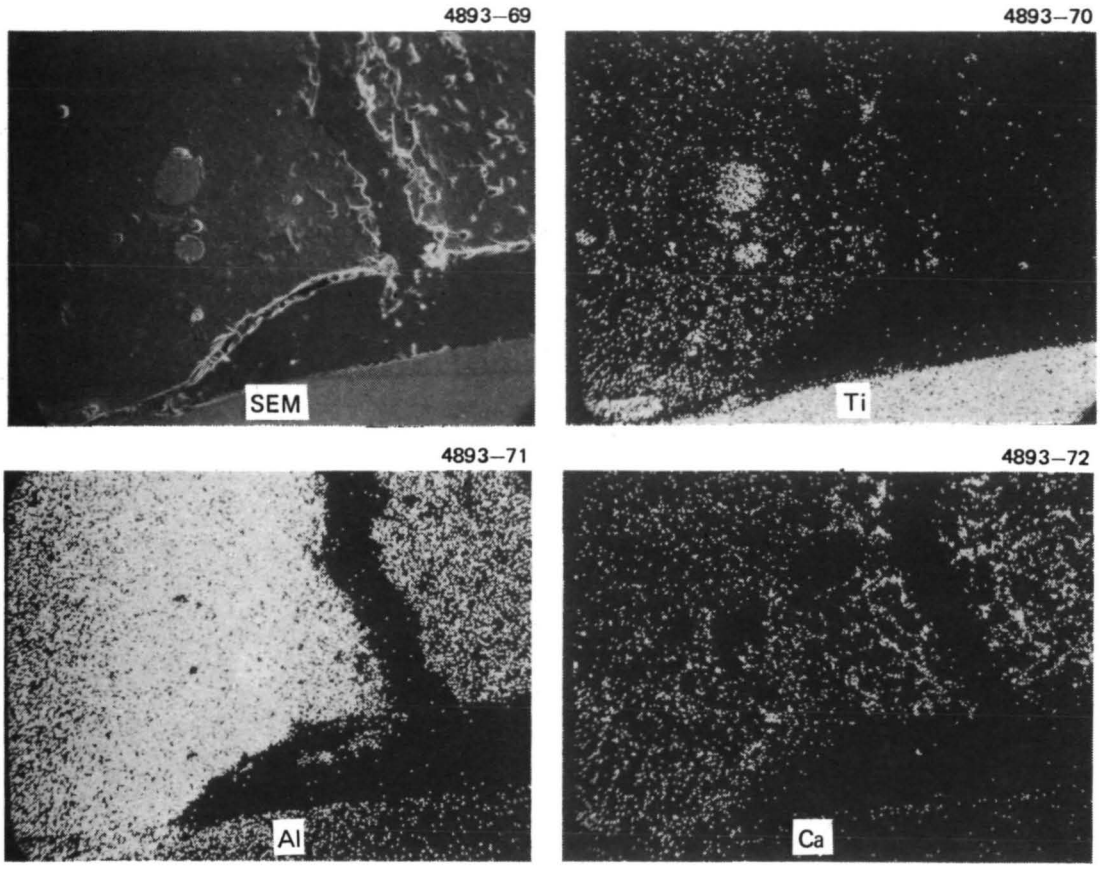

Figure A-35. Scanning electron microscope photo and K_α X-ray analysis of area 2 of damaged anode support.

AREA 2
200X

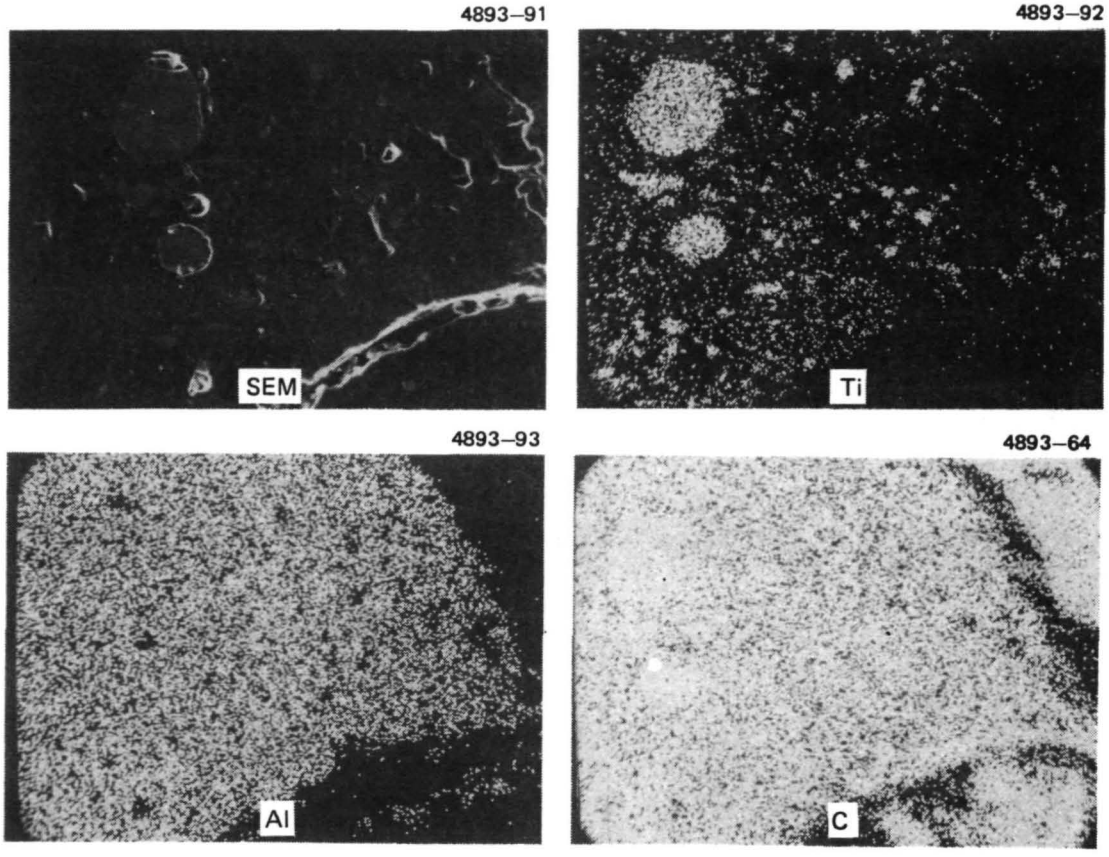

Figure A-35. Continued.

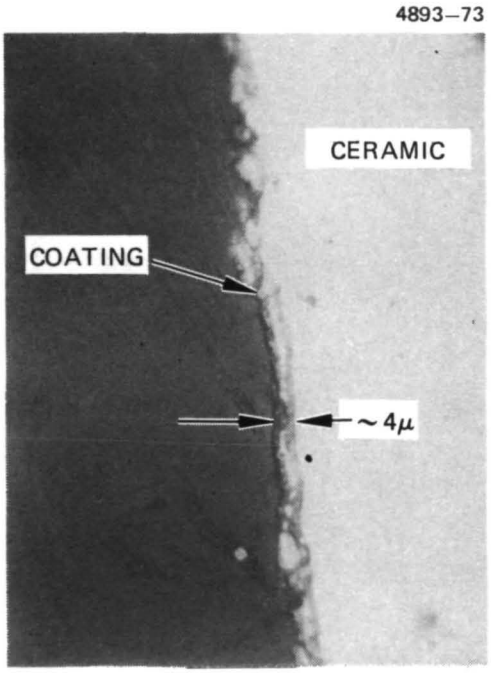

1000X

(a) AREA 3

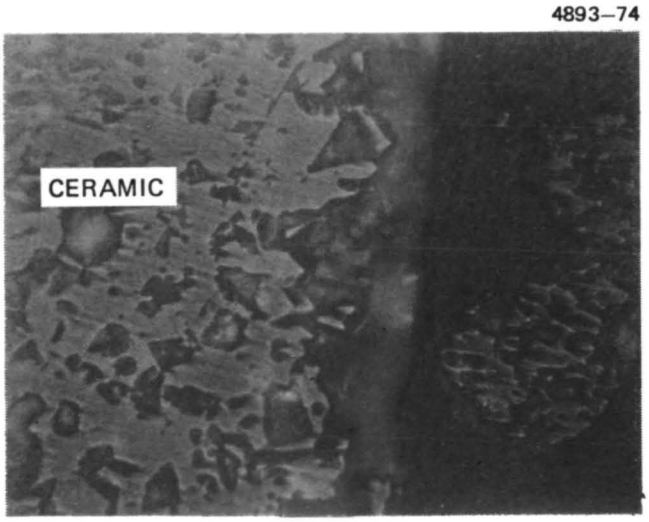

500X

(b) AREA 7

Figure A-36. Magnified view of regions 3, 7, and 8 of anode support No. 6.

4893–94

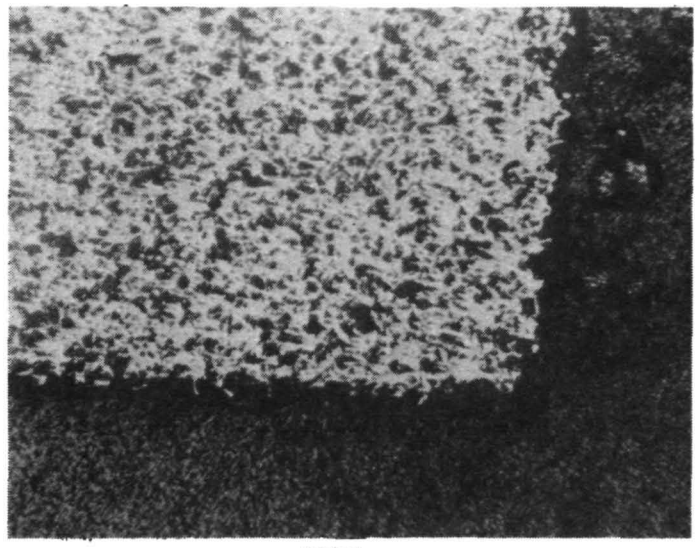

100X

4893–95

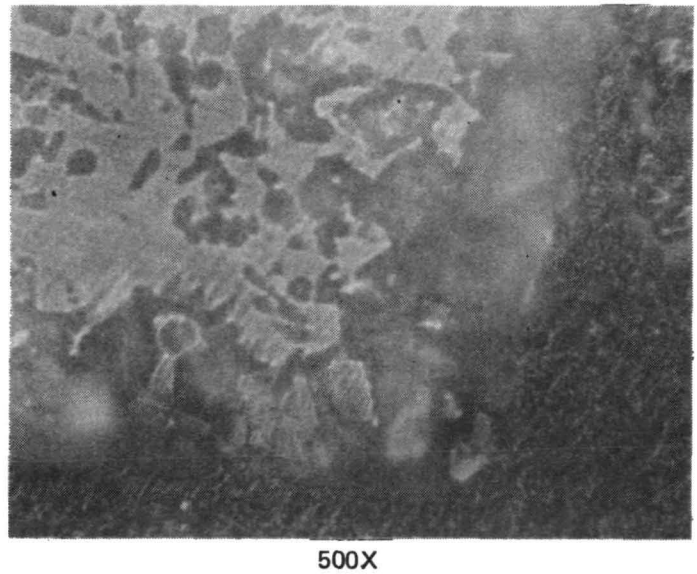

500X

(c) AREA 8

Figure A-36. Continued.

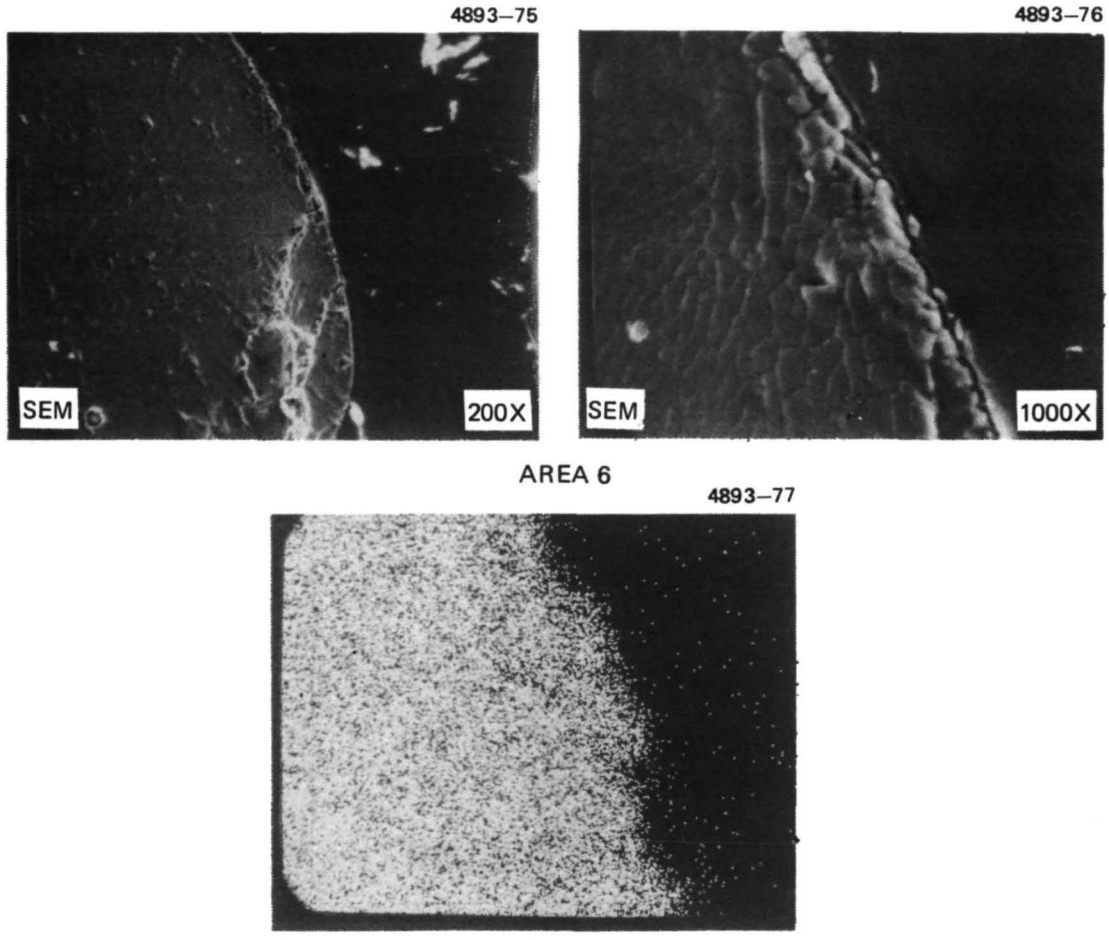

Figure A-37. SEM photo and K_α X-ray analysis of area 6 of anode support No. 6.

relative concentrations of Al and O in the damaged and undamaged areas. Figure A-38 shows an attempt to compare the Al signals from the SEM microprobe. Although it appears that the damaged area (left side of the void) has a greater concentration of Al in Fig. A-38, this is not necessarily the case, as shown by Fig. A-38 where the scan field has been shifted slightly. Thus, the apparent gradation in the concentration of Al depends more on the scan location than on the location in the material. Area 5, which is located in what is thought to be undamaged material, shows no real variation in concentration of Al, no titanium; the remaining impurities, Si and Ca, seen in Fig. A-39 are probably remnants of the polishing compound trapped in the normal voids of the Al_2O_3. Areas 7 and 8 appear identical to area 5 under the microscope, and no coating was discernible on the insulator surface. Consequently, these areas were not examined further with the SEM microprobe.

The damage to the anode support insulators is concluded to be a melting or fusion of the Al_2O_3 insulator, the Ti anode, and the stainless steel machine screw. On the basis of the observable evidence, the only logical explanation of this melting is that local high temperature produces some alloying of the Ti and Al to form a moderately low temperature eutectic ($\sim 600^{\circ}$ to 800°C). On the basis of the "arc tracks" visible on the thruster shell, formation of a vacuum arc breakdown in the vicinity of the insulator seems to be the best explanation which can be offered for generation of these temperatures. Except for the coating seen on the insulator surface, there does not appear to be any deterioration of the bulk material. Because of the relatively low voltage applied to the anode, formation of an arc by the discharge supply might be considered unlikely, unless the applied voltage appears across a very small gap. This condition could be established if a conductive coating covered the entire anode support insulator except for a small gap between the anode and the insulator as shown in Fig. A-40. The coating and gap are shown on an exaggerated scale to illustrate the conjecture being developed here. The insulator surface would most probably charge to thruster shell potential because the thruster shell is clamped firmly between two mating

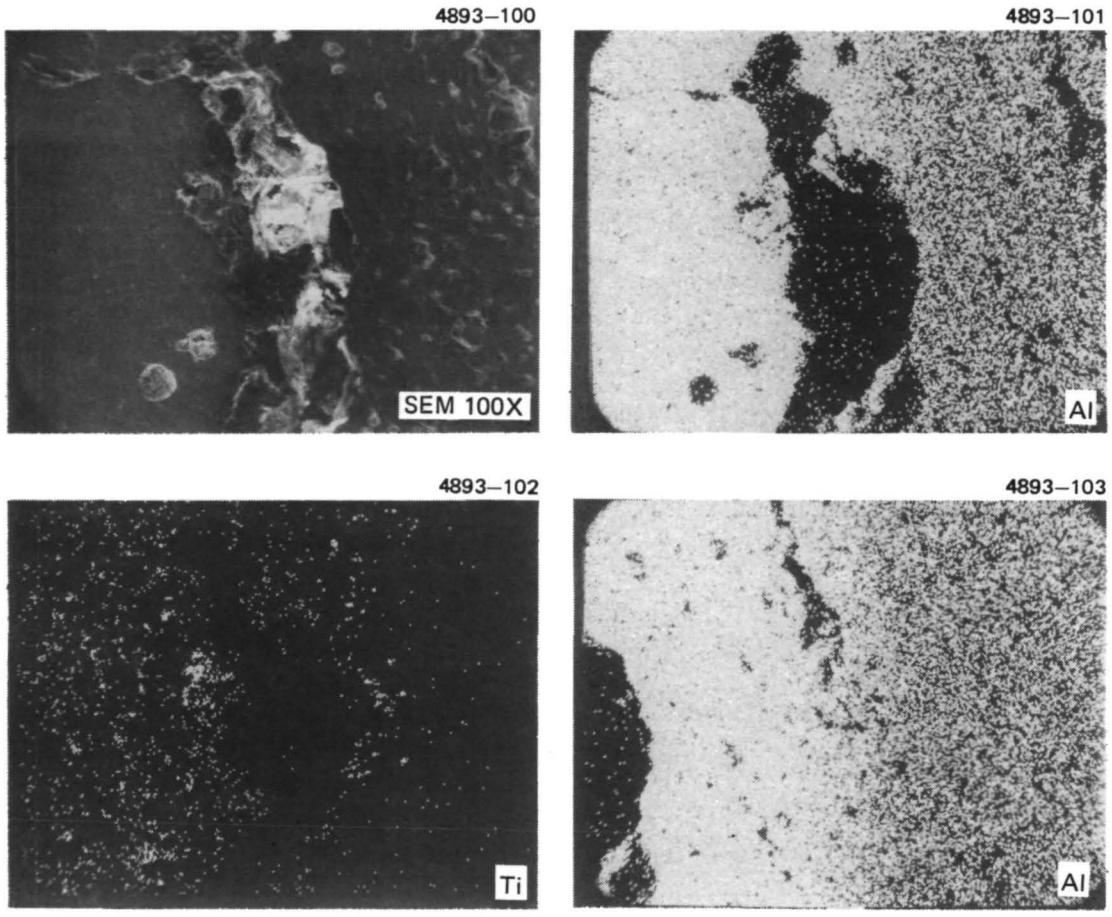

Figure A-38. SEM photo and K_α X-ray analysis of area 4 of anode support No. 6.

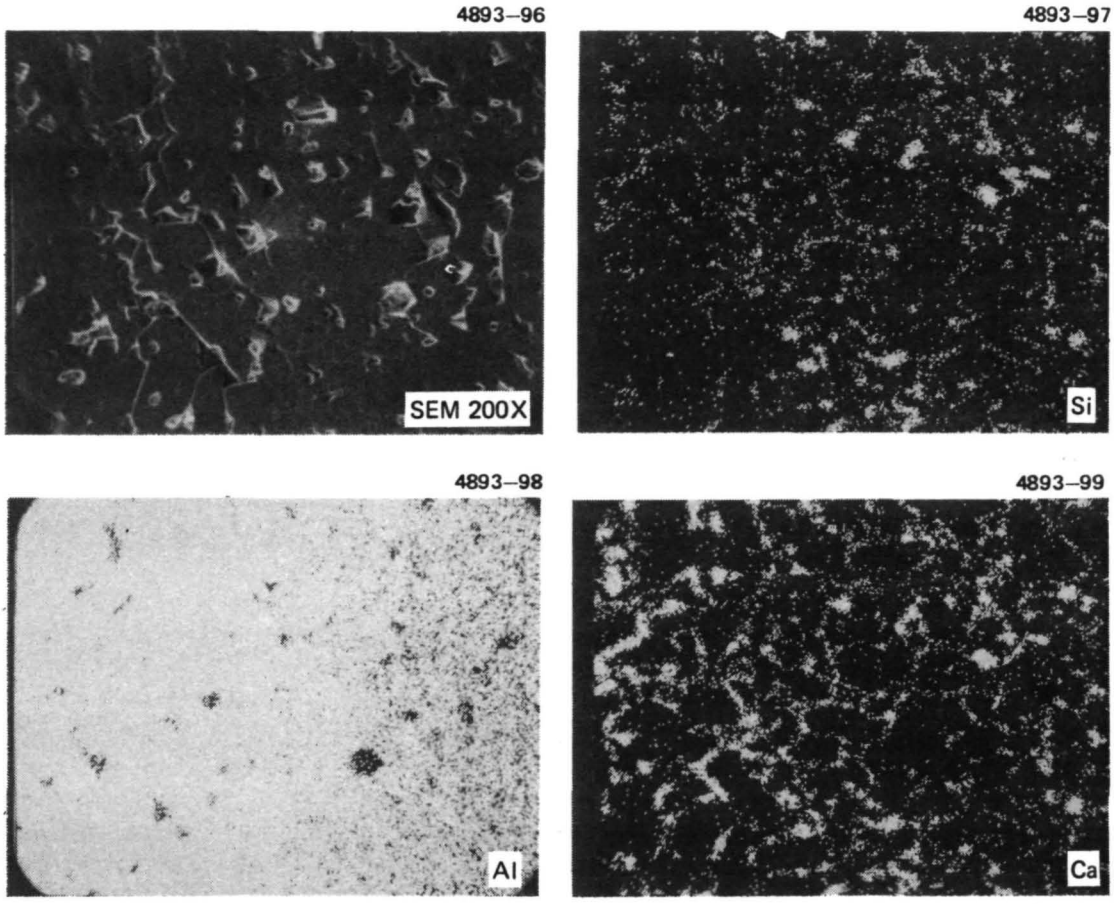

Figure A-39. SEM photo and K_α X-ray analysis of area 5 of anode support No. 6.

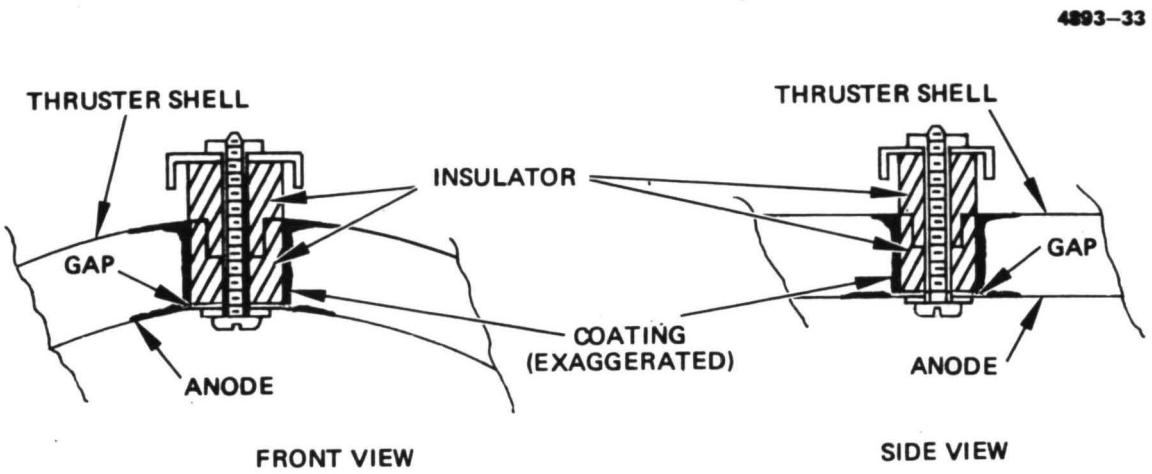

Figure A-40. Drawing illustraing possible explanation of cause of anode support damage.

ceramic parts, one being the coated insulator. The anode, on the other hand, is backed by a washer, smaller in diameter than the ceramic, and this does not assure positive contact between the anode and the insulator at the edges. Moreover, the anode support insulator has a "pumpout slot" ground into the surface that mates with the anode. Consequently, a coating on the insulator would tend to form a "spark gap" as shown instead of merely providing a resistive path from shell to anode. The downstream anode supports cannot quite satisfy this condition because one of the anode stiffening ribs interferes with the insulators, requiring special grinding on the insulator. This probably improves the anode-insulator contact such that the insulator coating makes contact with the anode and no arcing occurs, (see Fig. A-29). Insulator Number 4, the upstream insulator which showed no damage, could have also benefitted from improved anode contact because of the orientation of the "pumpout slot" with respect to the anode curvature (see Fig. A-30). While this explanation is highly speculative, it is the only one available that fits all the observations.

Thus, it has been concluded that the observed damage to the anode insulators is a direct result of the deposition on the insulators, and that damage of the type sustained by insulators number 2 and 6 may be avoided by shadow shielding the insulators to prevent deposition from reducing the insulator length.

The propellant distribution plenum is the final component to be discussed in this section. Figure A-41 shows views of the discharge and propellant sides of the plenum after its removal from the backplate, enlargements of the screen covering the plenum ports, and the discharge chamber backplate with the plenum removed. Careful examination and measurement of the plenum revealed no evidence of deposit or erosion on either the downstream surface or the screens covering the ports (compare Figs. A-41(c) and (e)). Neither was it possible to obtain a measurable coating sample from the discolored areas seen on the back-plate in Fig. A-41(d), (where the plenum is normally situated). Deposits were found on the plenum's inner mounting plate and inner wall (Fig. A-41(a)). Although these deposits were not analyzed, they are assumed to have the same constituents as samples A and B listed in Table A-4.

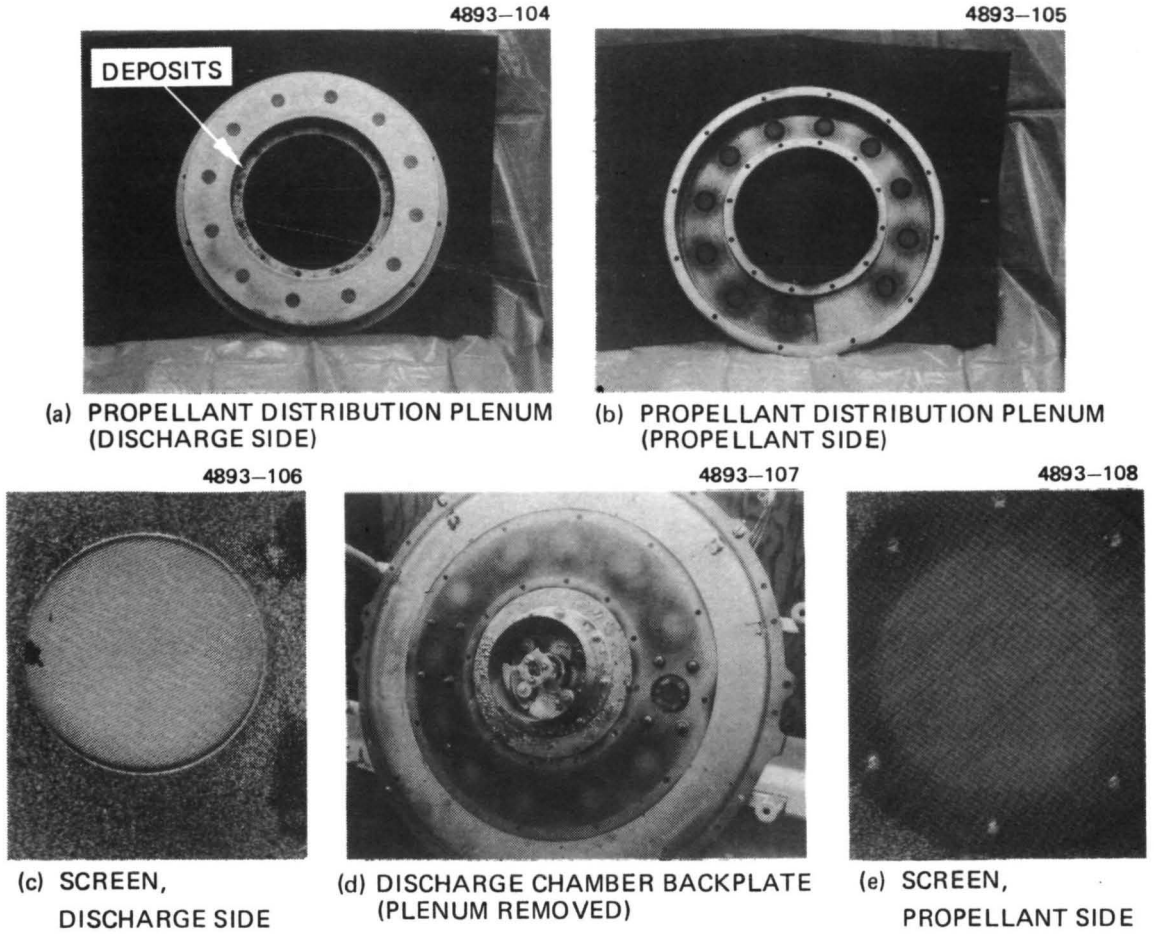

Figure A-41. Discharge and propellant sides of plenum and screen which covered plenum ports.

Although some concern has been expressed by Hughes and NASA metallurgists with respect to embrittlement of titanium by mercury, there was no evidence of embrittlement in the plenum or other discharge chamber components after 10,000 hours of exposure to mercury vapor. This is to say that no titanium part cracked in the manipulation which was necessary to disassemble the thruster components, and the sheet metal parts (such as the plenum and anode) seemed as flexible as new parts. No tests were made to determine hardness or yield strength since these quantities are not considered of primary importance to thruster operation after a thrust system achieves orbit.

C. Cathode Pole Piece/Magnetic Baffle Assembly

The principal components of the cathode pole piece/magnetic baffle assembly are the following:

- Cathode pole and mounting flange
- Baffle
- Baffle control coil and its terminal insulators
- Keeper electrode and its support insulators
- Cathode subassembly.

This assembly and some of its components are the most severely worn of the thruster parts and exhibit radical modification of component dimensions, as indicated earlier in comparing Figs. A-14 and A-15. The extensive wear seen on these components is considered to be a consequence of ion sputtering, presumably dominated by doubly charged ions. Close-up photographs of this assembly illustrating the damage are presented in Figs. A-42 to A-45. By referring back to Fig. A-15, most of the component damage is obvious in these photographs. Some of the less obvious wear or damage is pointed out specifically in Figs. A-44 and A-45. One point of interest to be noted here is that the baffle coil sheath and the cathode radiator are eroded while the keeper electrode and most of the other cathode potential surfaces in their vicinity are

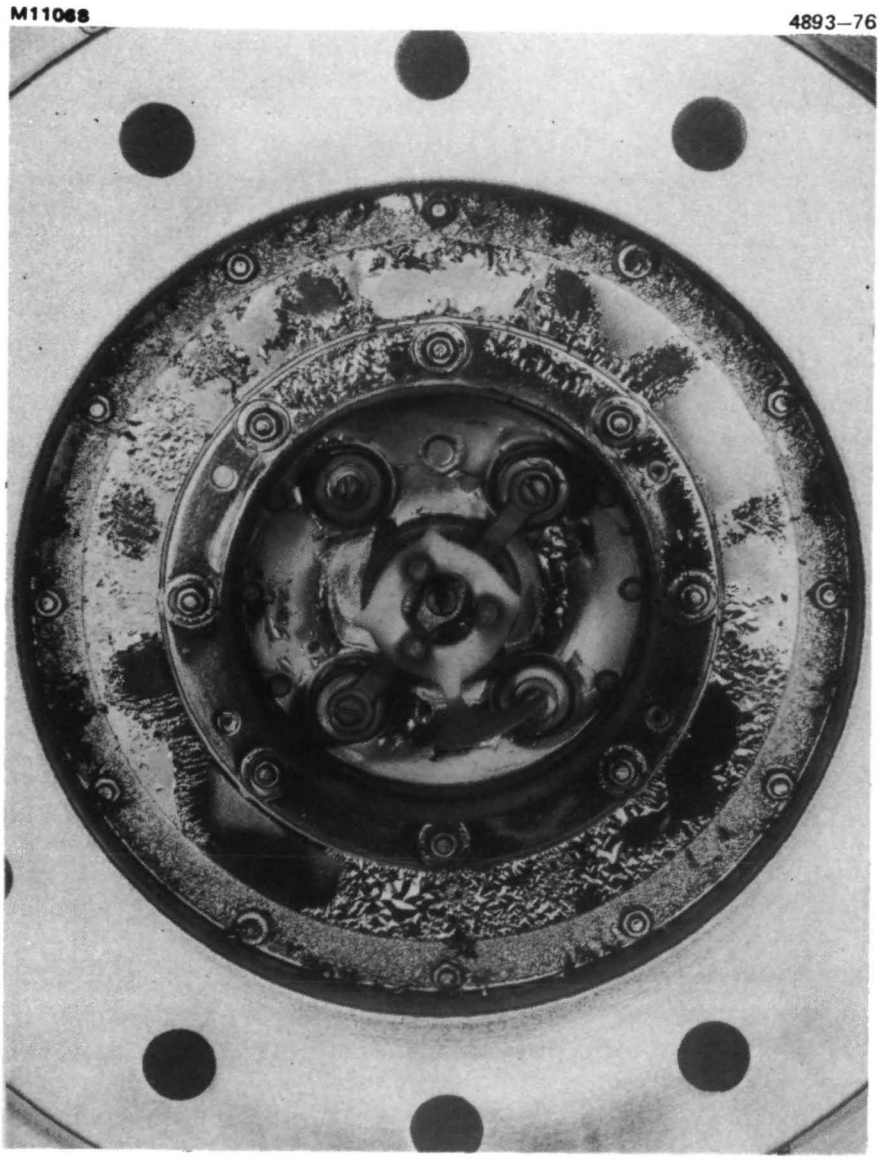

Figure A-42. Cathode pole piece/magnetic baffle assembly.

M11066

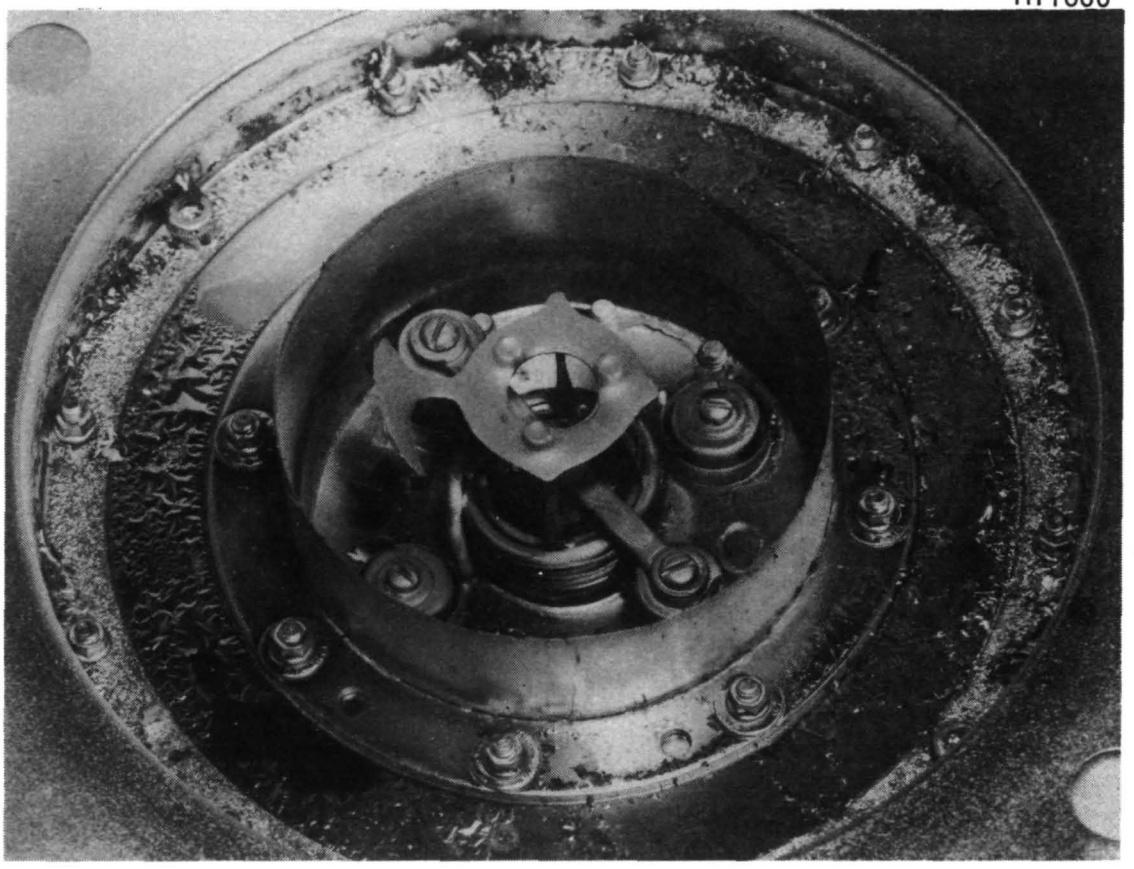

Figure A-43. Cathode pole piece/magnetic baffle assembly.

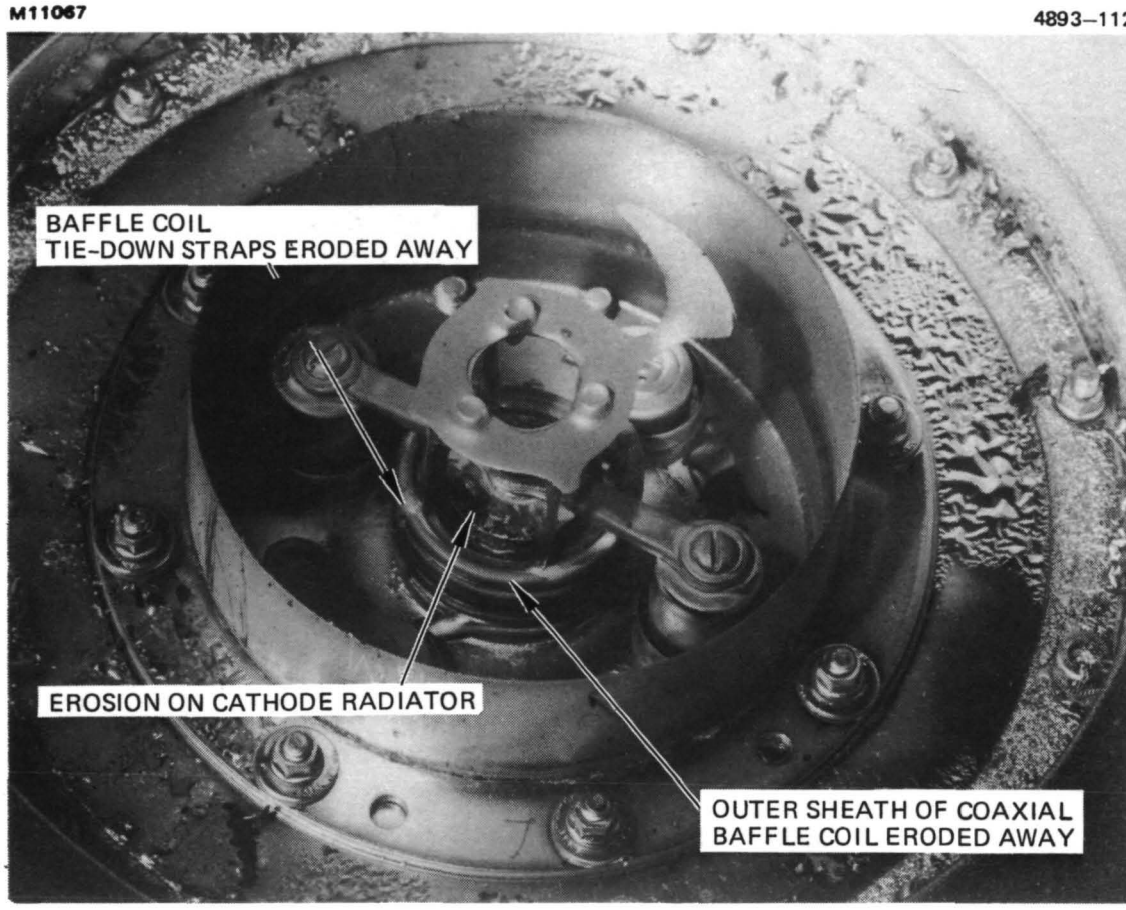

Figure A-44. Cathode pole piece/magnetic baffle assembly.

4893–109

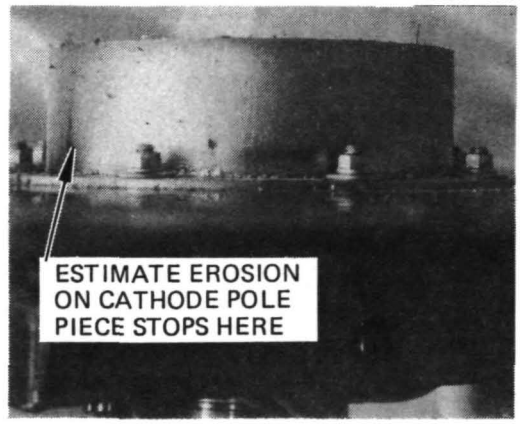

4893–110

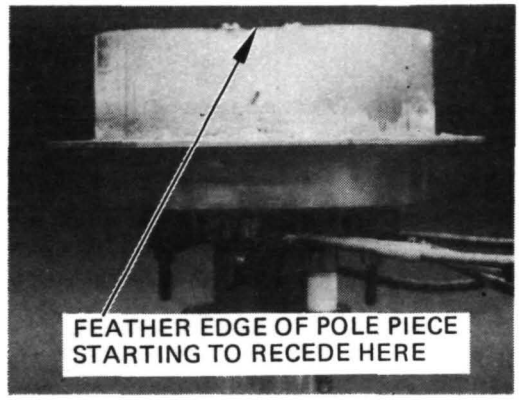

4893–111

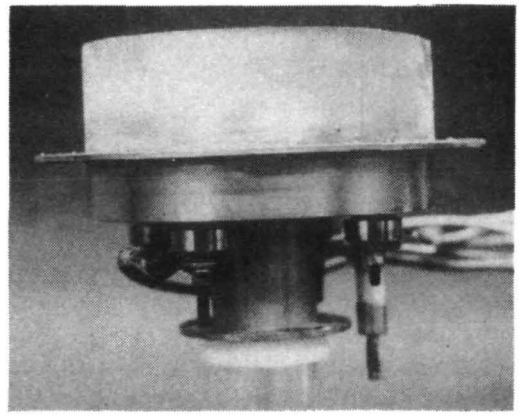

Figure A-45.
Cathode pole piece/magnetic baffle assembly.

heavily deposited. The erosion patterns have an imperfect symmetry that seems related to the orientation of the baffle coil terminations. The outer conductor of the coaxial baffle coil is seen to be eroded away in Fig. A-44, exposing the insulator over a relatively large area, while the counterpart of the coil seen in Fig. A-43 shows penetration of the coils outer sheath over a relatively smaller area. Similarly, a remnant of the baffle coil tie-down strap can be seen on the downstream side of the coil in Fig. A-43, whereas the counterpart strap is seen in Fig. A-44 to be completely eroded away on the downstream end and barely visible on the upstream end. It has not been possible to formulate a cohesive explanation for the erosion seen on the baffle coil and cathode radiator. The generally accepted model of the discharge chamber plasma potential distribution would place the plasma potential within the cathode pole piece at approximately the keeper voltage. Thus, no doubly charged ions should be formed in the region and singly charged ions should not be capable of causing damage. It is possible that this erosion is entirely a consequence of exposure to high-energy ions from the discharge chamber after the baffle was eroded away. However, taking note of the pattern of baffle wear in these photographs, it is apparent that remnants of the baffle show a "spoke-like" configuration and these remaining elements are aligned with the four baffle support members. This could be interpreted as a shielding of the baffle from ions originating within the support structure or as a magnetic field effect. No conclusive evidence exists to determine whether the erosion pointed out in Fig. A-44 is "typical" or a consequence of operation without the baffle.

Similarly, in examining the erosion of the baffle and cathode pole piece, it has not been possible to determine where the eroding particles originate. The cylindrical pole piece is worn to a "feather" edge on the downstream side, and, as shown in Fig. A-45(b), this wear has begun to reduce the pole piece length. The erosion seems to end upstream of the region indicated in Fig. A-45(a).

Closer examination of the keeper electrode disclosed heavy deposition on the upstream surface, light deposition on the downstream side, and slight erosion around the keeper orifice on the downstream side. Illustrations of this deposition and erosion are seen in Figs. A-46 through A-48. The deposition seen increased the weight of the keeper by 0.545g (about 12% of the keeper weight) and the keeper thickness by 0.02 in. (0.05 cm). The coating is very adherent and shows no tendency to form "flakes," although protrusions that have the appearance of "flakes or chips" embedded in the coating can be seen in Fig. A-46. Erosion of the keeper aperture is apparent in Fig. A-46(b) also. The keeper aperture diameter measured before the test was 0.184 in. (0.467 cm) and the asymmetric increase in diameter noted is considered inconsequential to thruster operation. Consequently, the keeper electrode is considered to have been relatively unaffected by the 10,000 hours of testing.

It was thought that a detailed analysis of the keeper deposits might offer some explanation of the erosion process or history and the sectioned keeper was analyzed using the E-beam microprobe. The "layered" appearance of the upstream coating seen in Fig. A-48(a) can also been seen in the SEM photograph and to some extent in the elemental analysis scans of Fig. A-49. The elements found were Fe, Ta, Ni, Cr, and K. Since the distribution was more or less uniform throughout the coating, it was not possible to establish a time history based on an abrupt appearance of one of the elements. The Fe, Ni, and Cr are thought to originate in the stainless-steel baffle coil sheath and tie-down straps, while the Ta originates in the cathode radiator. Next, an attempt was made to relate the layer thickness to test events as indicated in Table A-5, starting the layer formation at either the start of the test or at the appearance of the hole in the baffle. Changes in thruster beam current were selected as the test events for correlation. As shown in Table A-5, there is no significant relationship between the selected test events and the layer structure (thickness).

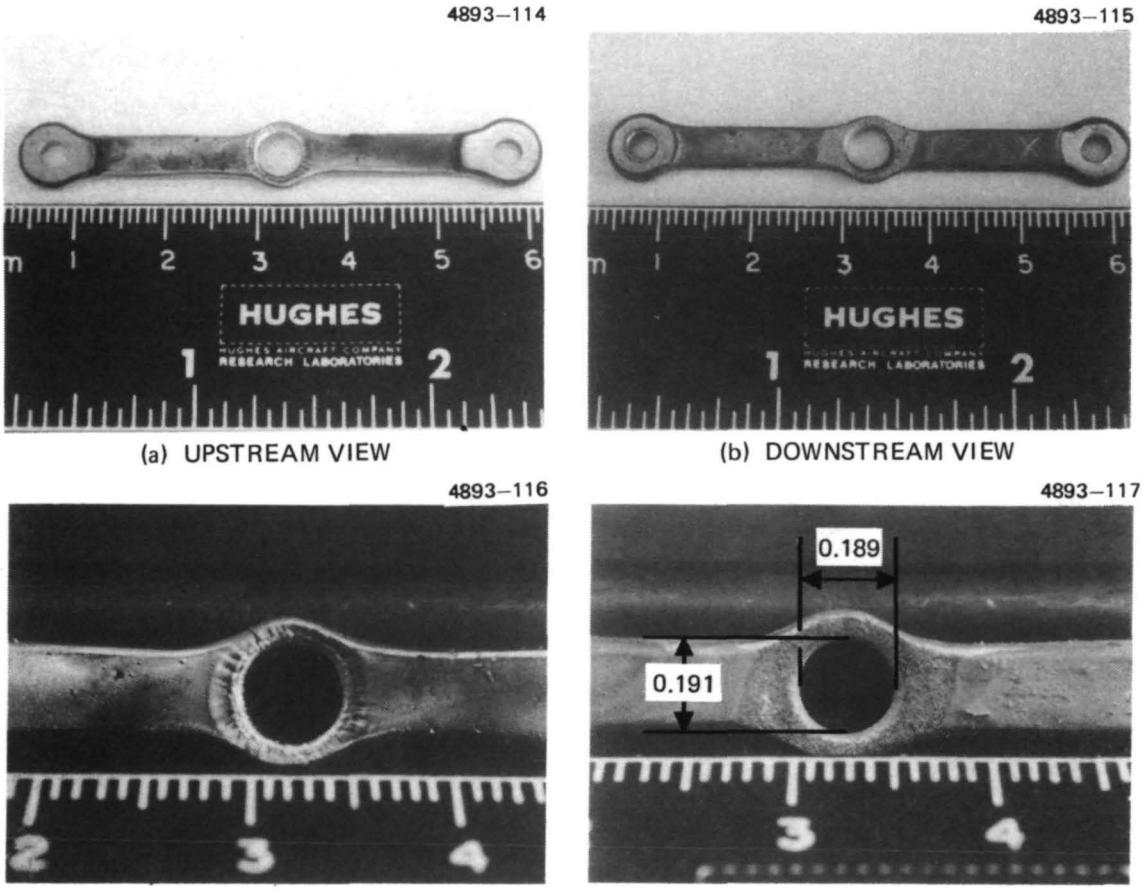

Figure A-46. Cathode keeper.

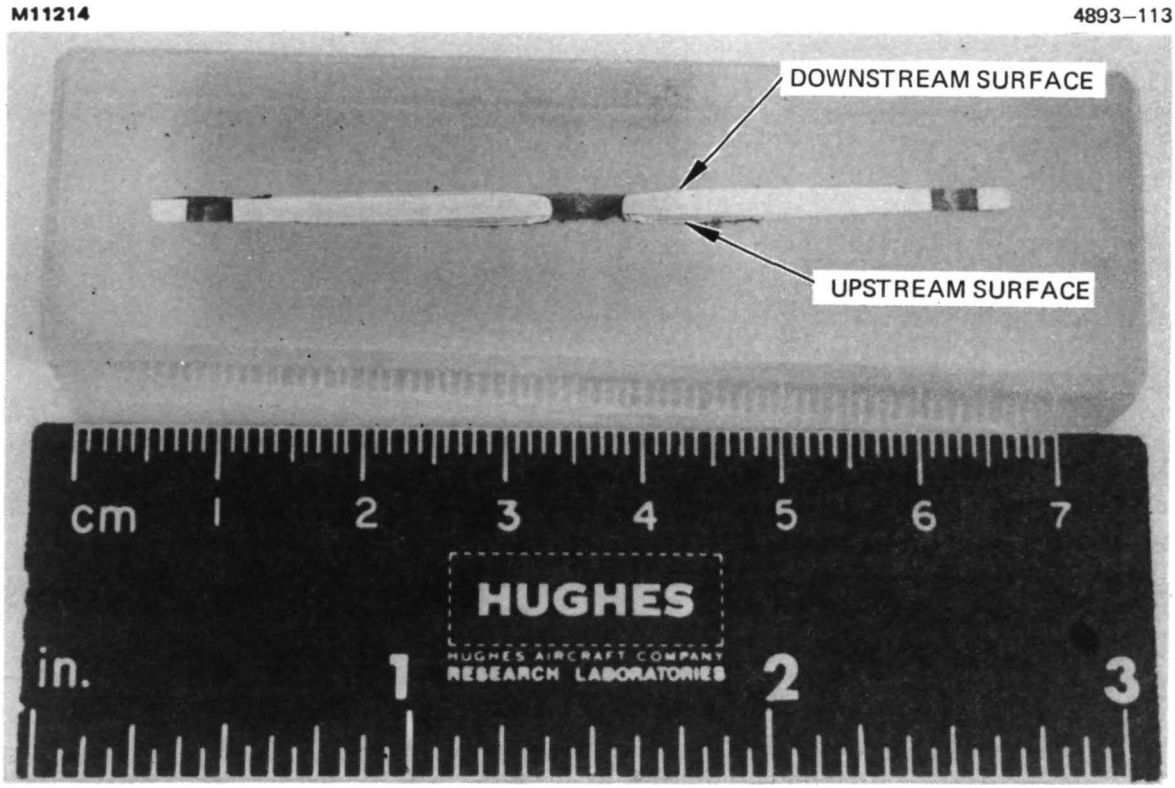

Figure A-47. Cathode keeper.

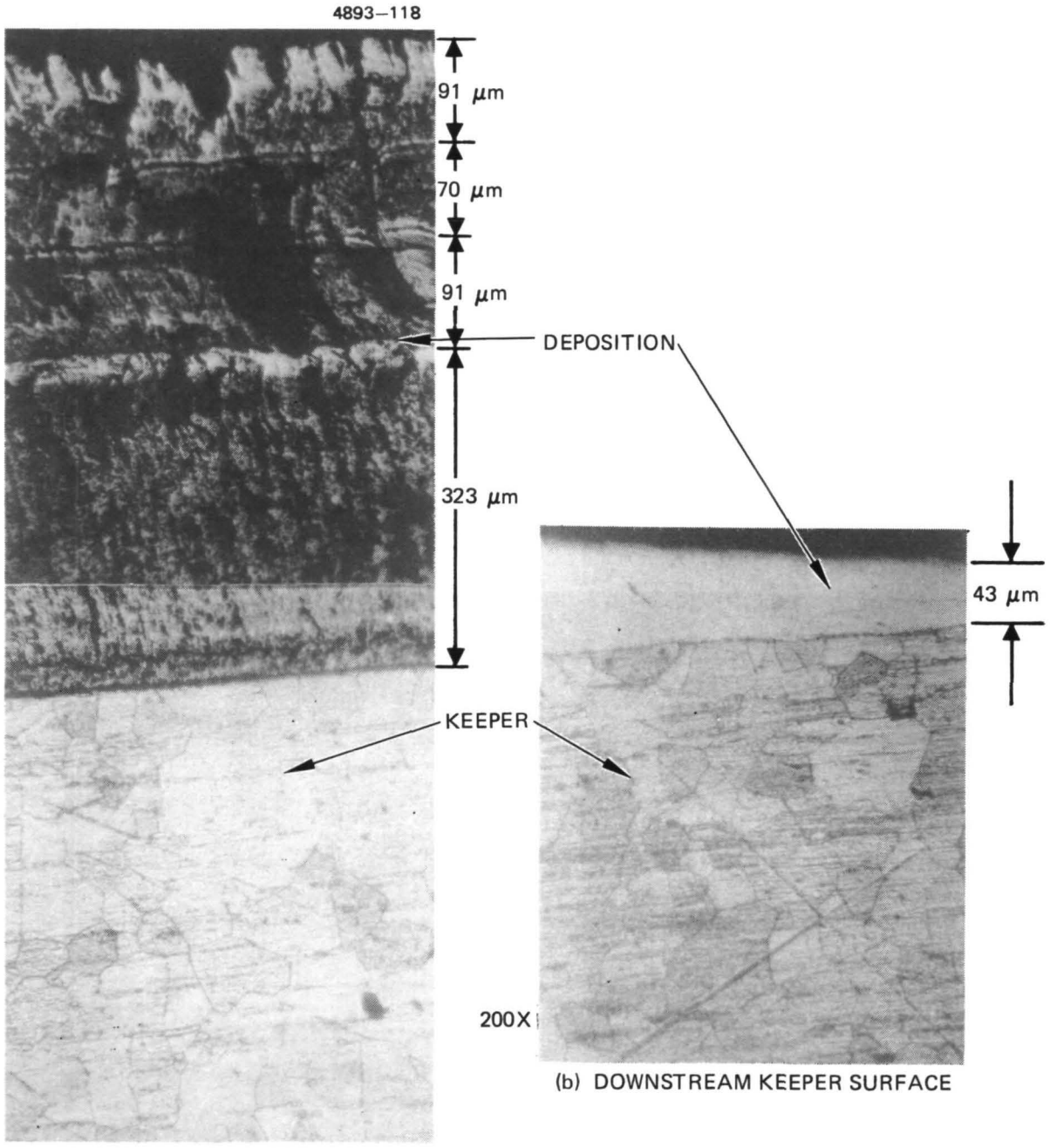

Figure A-48. Magnified views of cathode keeper.

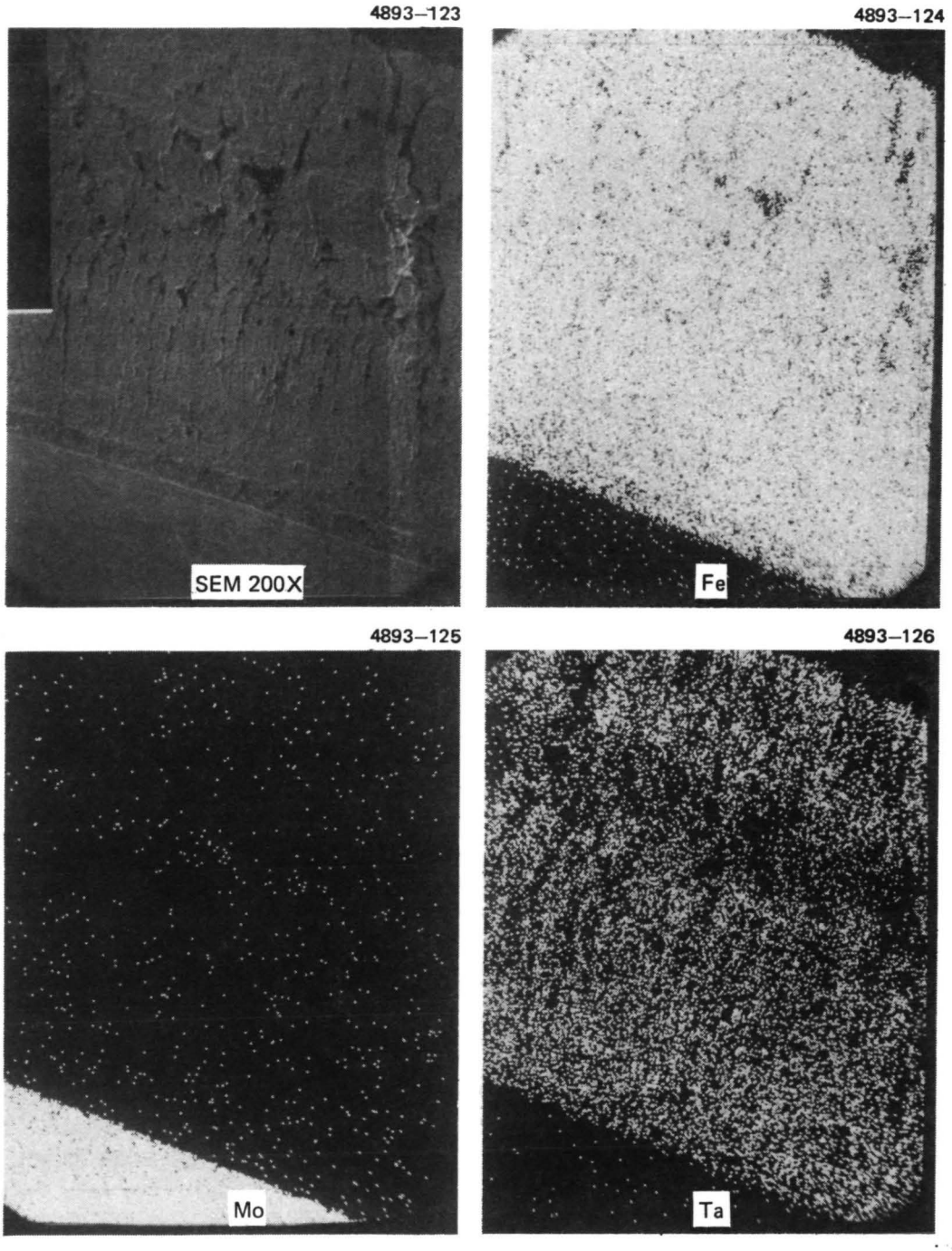

Figure A-49. SEM photo and K_α X-ray analysis of upstream keeper coating.

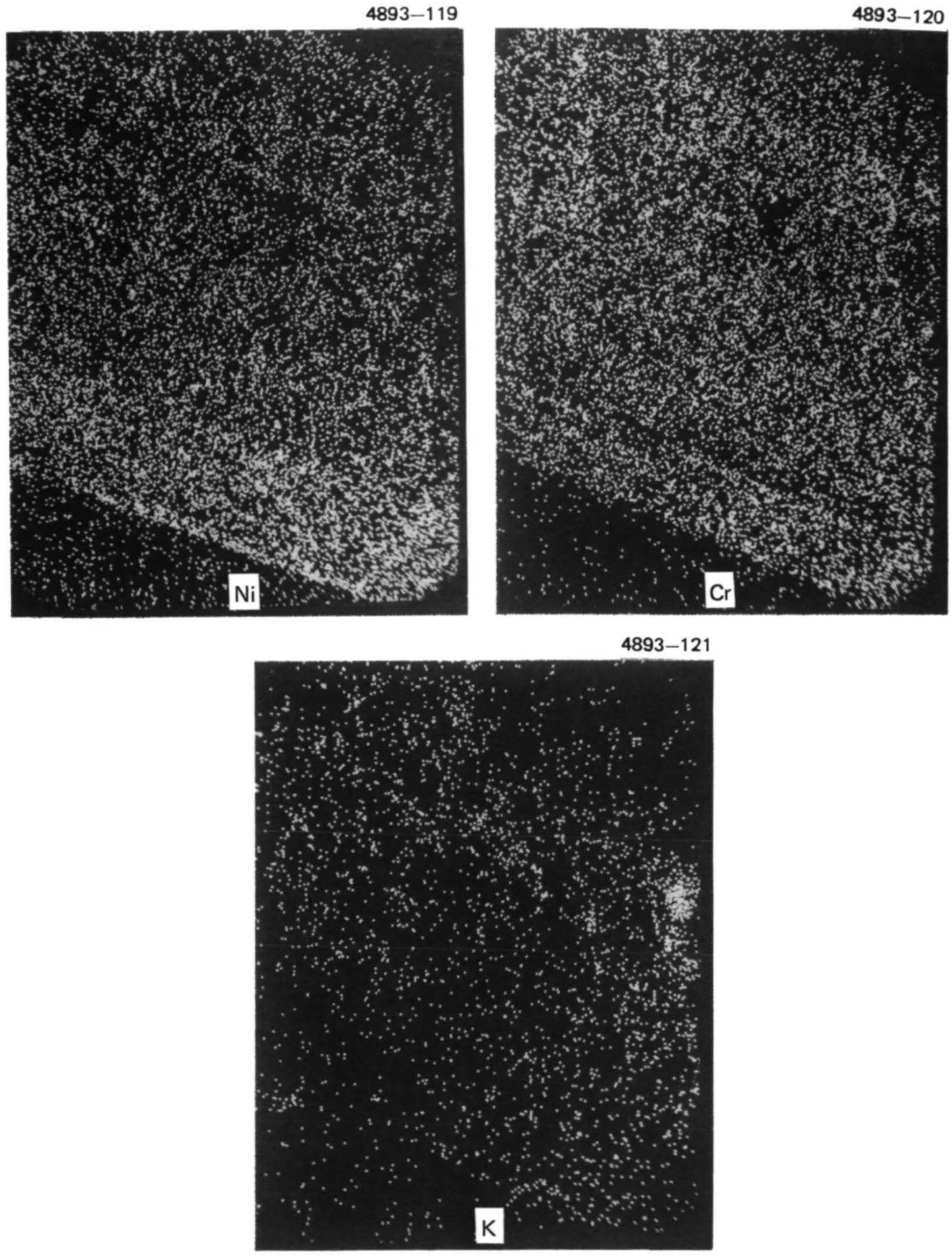

Figure A-49. (Continued).

Table A-5. Comparison of Endurance Test Events and Hypothetical Events Based on Keeper Deposit Layers

Endurance Test Events		Layer Thickness Assumed Linearly Proportional to Hours or Ampere-Hours			
Test Hour	Test Ampere-Hour	Hours	Ampere-Hour	Hours	Ampere-Hours
0	0	0	0		
2,100	3,150				
2,800	4,270				
3,000	4,610				
		5,617	7,912		
5,845 (A)	9,589 (A)			5,845(0)	9,589(0)
6,100	10,035				
			10,141		
7,200	11,685	7,200			
			11,856	8,179	
		8,761			12,114
				8,836	12,826
9,300				9,300	13,376
	13,685				
10,000	14,085	10,000	14,085	10,000	14,085

All test events correspond to beam current changes except (A) which is the test time that the hole in the baffle was noted.

T1856

The coating on the downstream surface of the keeper does not have the same sort of layer structure and the composition of the deposit is slightly different. This coating is predominantly iron, presumably from the baffle support, with some Ta and Cr. There seems to be one thin line in the E-beam scan for Mo (see Fig. A-50) that appears to be richer in Mo. Except for this unexplainable observation, the coating on the downstream surface of the keeper provides little or no new information.

It is apparent in Figs. A-43 and A-44 that removal of the machine screws which secure the baffle to its support is a questionable operation because of the erosion of the baffle supports, which weakens the structure, and because the heads of the screws are eroded to the extent that they cannot be gripped by any tool. After several unsuccessful attempts at removing these screws, the entire support was removed with a high speed abrasive wheel. Several photographs showing the structure as it was removed in several views and variations in focus are included in Fig. A-51. Note that the erosion on the baffle fastening screws is predominantly on the inner side. It is also of interest to note that a thin lip of the baffle remains extending beyond the outer diameter of the baffle support, as if the baffle had been shielded from internally generated ions by the baffle support (further evidence to support the concept of erosion by ions from the cathode plasma). The wear on this structure is documented and recorded in Fig. A-52 by dimensional measurements at the locations indicated. The most wear occurred on Member C, in agreement with the asymmetry in wear seen on the baffle itself and the pole piece.

Having documented the support structure in this manner, a second attempt at removing the baffle fastening screws proved successful, but the baffle still could not be removed and was found to be securely "welded" in place. The assembly was then sectioned as shown in Fig. A-53, and the "welded" region was identified as a nickel "braze" by means of the E-beam microprobe analysis shown in Fig. A-54. It is thought that the nickel coating placed on the mild steel parts to prevent oxidation is responsible for the "welding" of these parts. It is

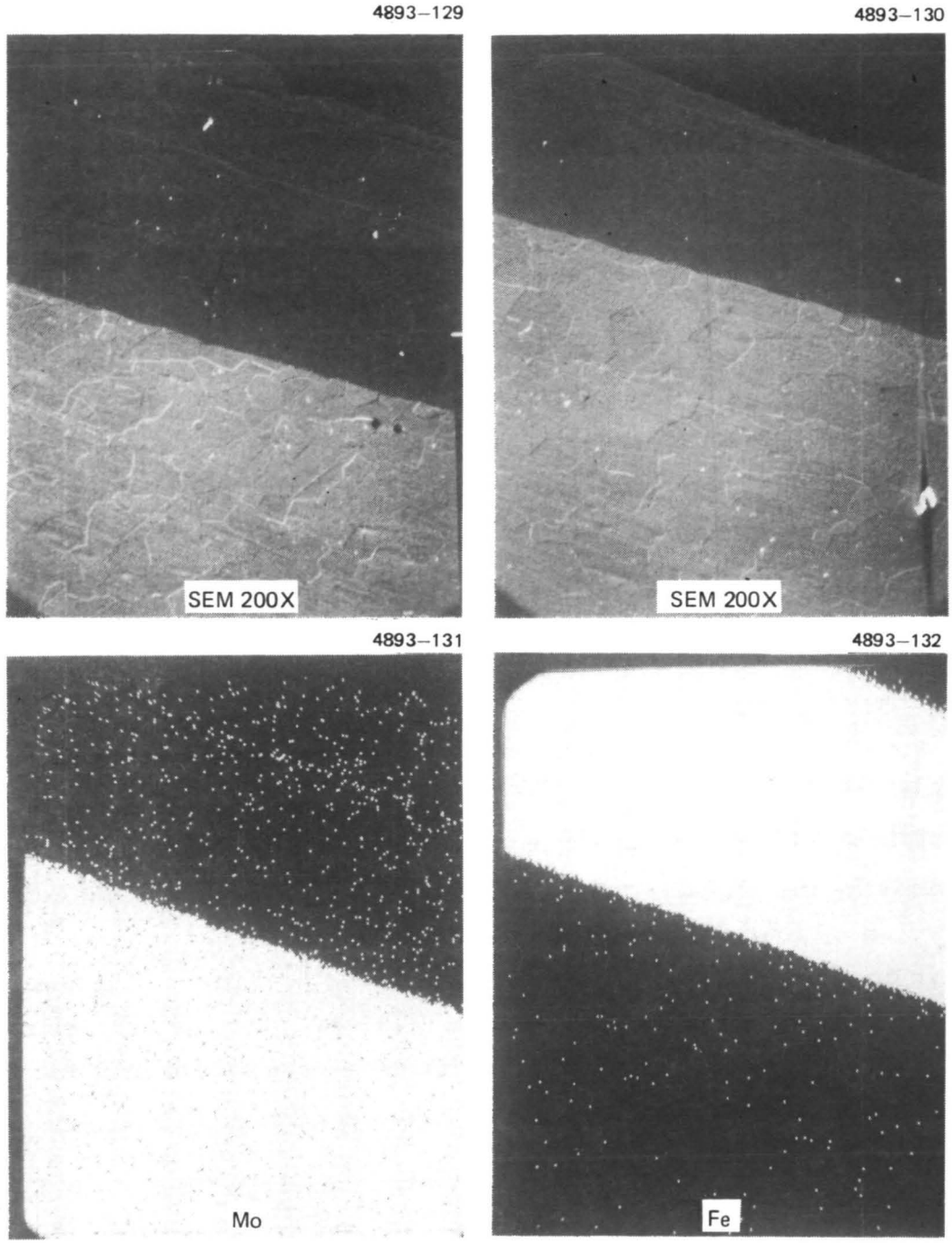

Figure A-50. SEM photo and K_α X-ray analysis of downstream keeper coating.

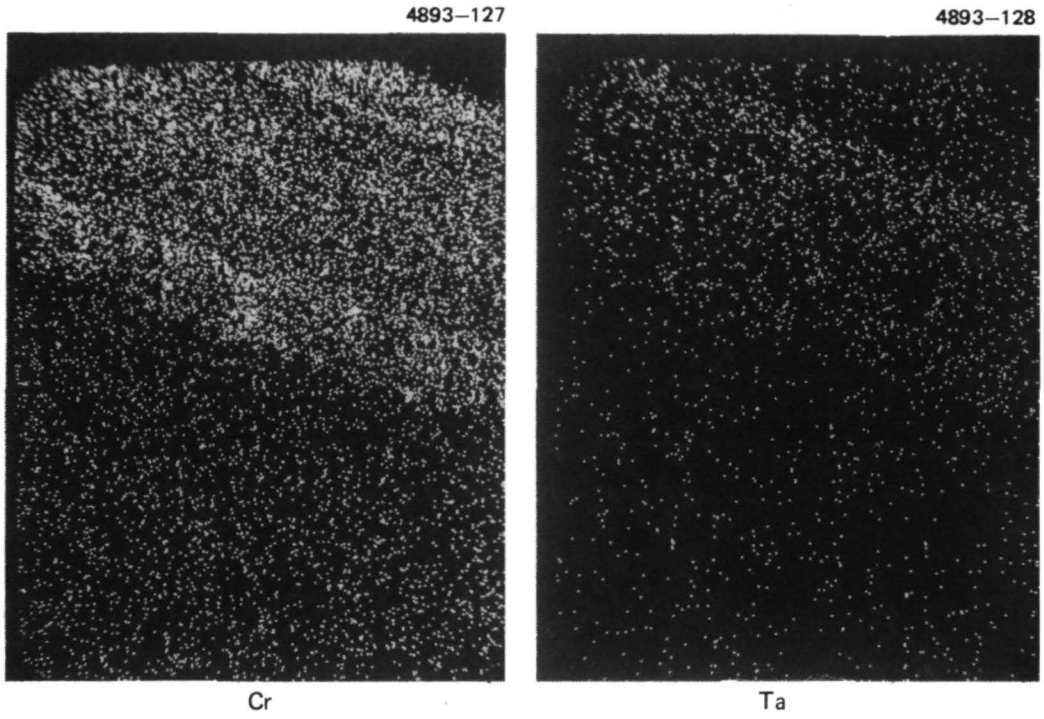

Figure A-50. Continued.

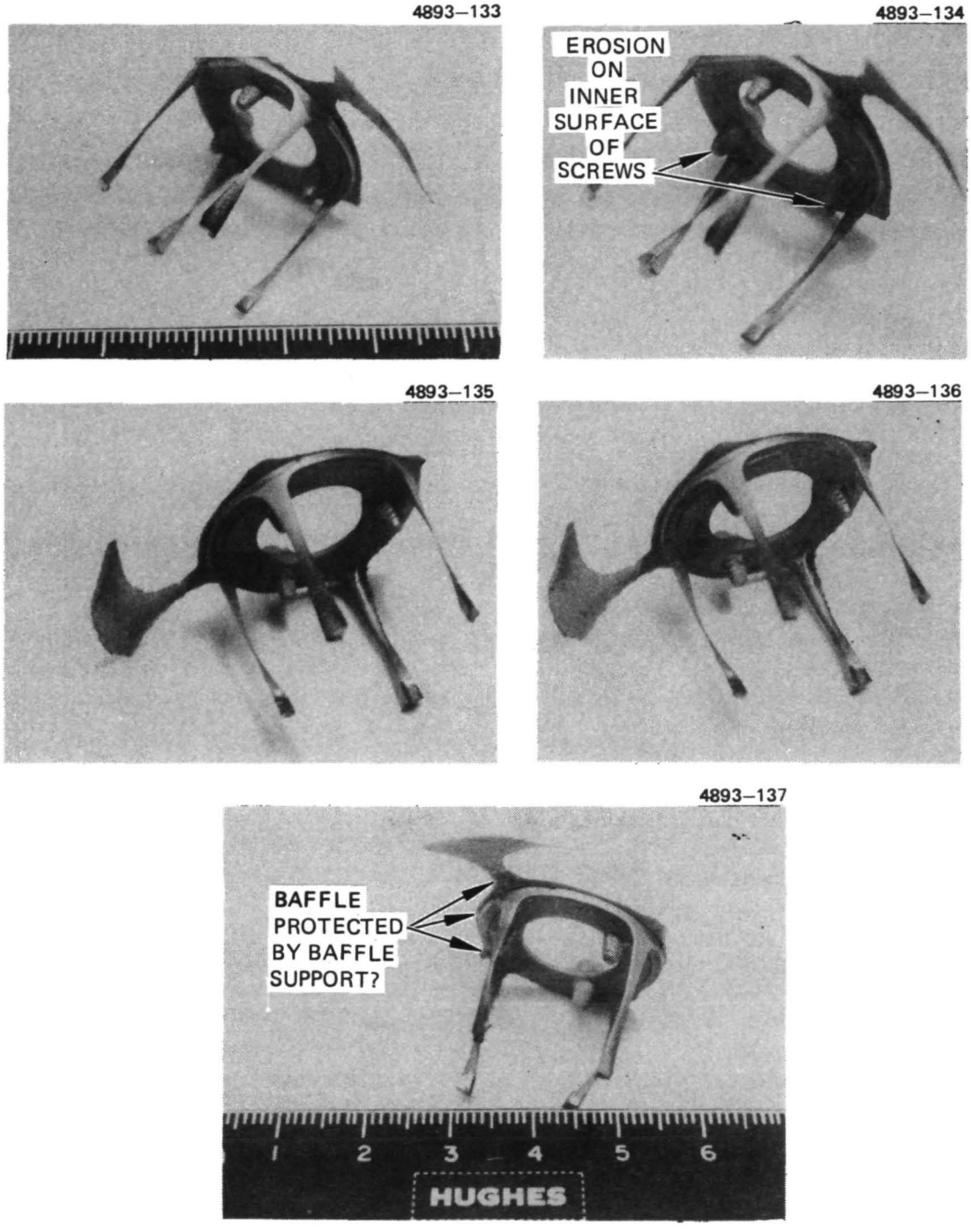

Figure A-51. Baffle support.

4893–34

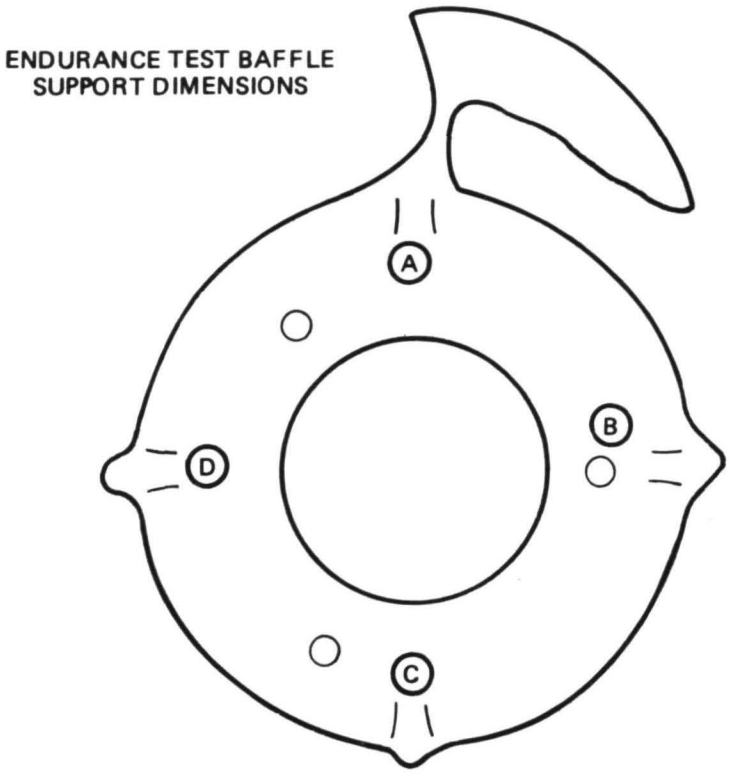

	A	A′	B	B′	C	C′	D	D′
1	0.135	0.053	0.132	0.057	0.131	0.052	0.134	0.054
2	0.082	0.047	0.084	0.048	0.081	0.037	0.090	0.043
3	0.080	0.029	0.062	0.030	0.052	0.021	0.070	0.030
4	0.030	0.008	0.055	0.020	0.019	0.003	0.052	0.017
5	0.057	0.021	0.072	0.030	0.037	0.020	0.068	0.027
6	0.086	0.047	0.090	0.047	0.077	0.045	0.089	0.045
7	0.102	0.050	0.106	0.051	0.102	0.049	0.108	0.045

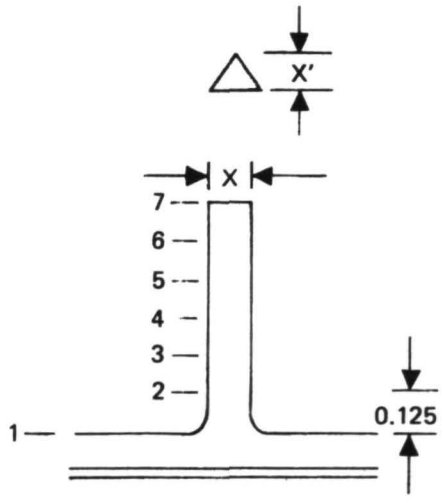

Figure A-52. Endurance test baffle support dimensions.

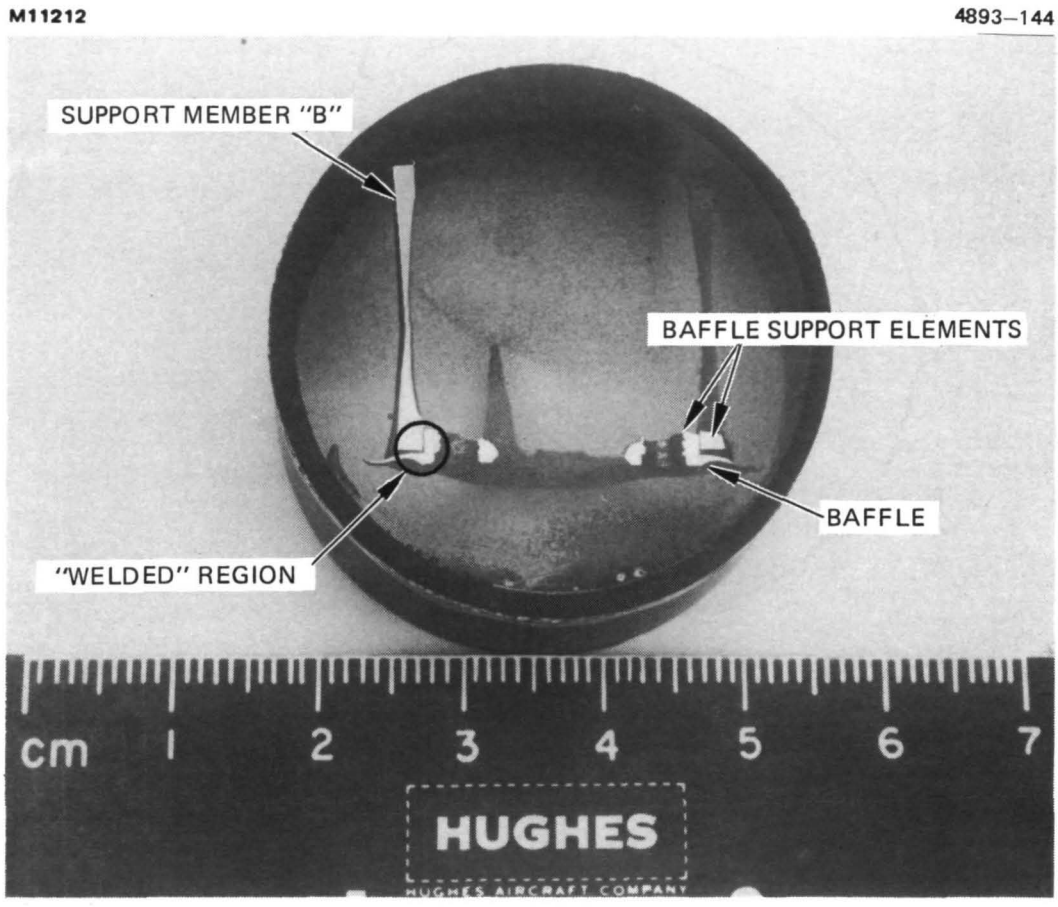

Figure A-53. Magnified view of baffle support cross section.

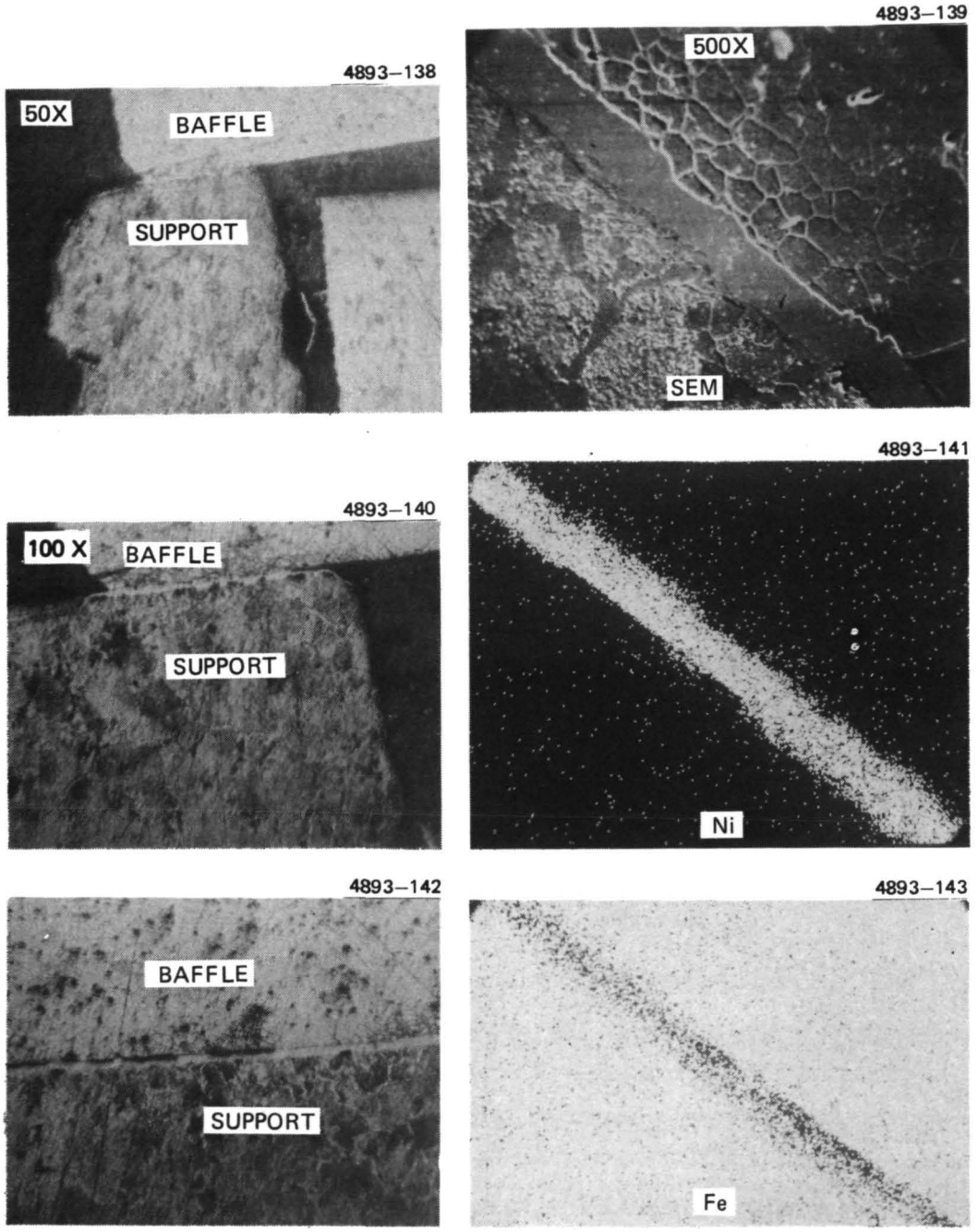

Figure A-54. SEM photo and electron beam microprobe analysis of "welded" region of baffle support.

not known whether the fusion of these nickel coatings occurred by cold flow under the pressure of the fastening screws, or whether it was aided by an abnormally high temperature. Thus, the one part of the thruster that was extensively documented prior to the test — the baffle — could not be similarly analyzed in the post-test examination.

Other observations that were made in examining this assembly are documented in Figs. A-55 and A-56. Deposition on the keeper support insulator and shield and on the baffle coil termination insulators and shield is shown in Fig. A-55. This deposition did not cause any problems in the test, but suggests a need for double shielding of the insulators and surface treatment on the shields to prevent formations of sizeable "flakes." Baffle coil termination will be made outside the discharge chamber in subsequent thrusters. A portion of the flake removed from the keeper insulator (Fig. A-55(b) was 0.0015 in. thick (0.004 cm) and would be extremely hazardous to thruster operability if it lodged between the ion optics grid. Figure A-56 shows the cathode subassembly as it appeared after removal (the threaded rods seen were used to facilitate handling). The discussion of cathode condition is deferred to a later section; however, the erosion on the cathode radiator that was visible in Figs. A-43 and A-44 can be seen more readily here. This damage is considered of little importance to either the operation or lifetime of the cathode.

In summary, the major wear to the cathode pole piece/baffle assembly was sustained by the cylindrical pole piece, the baffle, and the baffle support members. These components are considered near end of life after 10,000 hours (14,000 ampere-hours) of testing. The wearout process is thought to be ion sputtering but it has not been possible to determine the details of the process by examination of the eroded parts. The maximum erosion rate, by whatever process, is derived from the penetration time (5845 hr) of the baffle (0.029 thick) and is 9.4 μin. per hour (0.12 μm/hour). This quantity can be expressed in terms of ampere hours as 3.02 μin. per ampere-hour (0.08 μm/amp-hr). To achieve long thruster lifetime, this erosion rate must either be reduced appreciably or these eroded components must be

4893–145

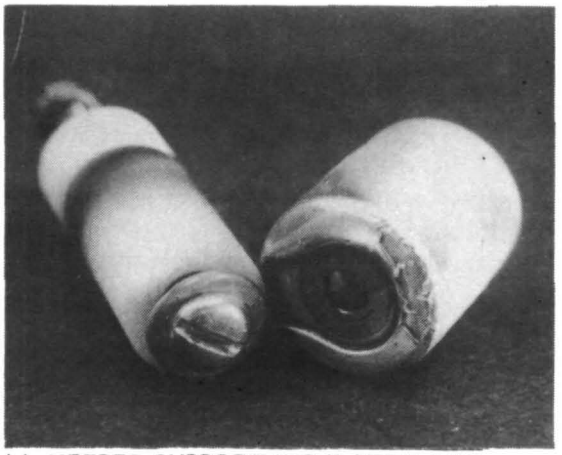

(a) KEEPER SUPPORT INSULATOR AND SHIELD

4893–146

(c) BAFFLE TERMINAL INSULATOR AND SHIELD

4893–147

(b) KEEPER INSULATOR SHIELD

4893–148

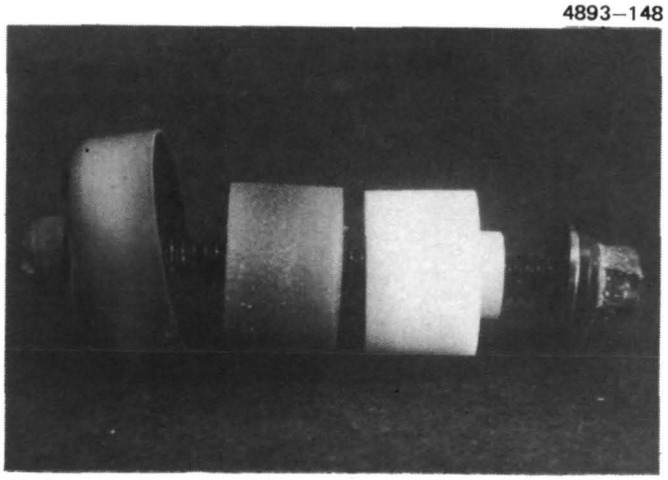

(d) BAFFLE TERMINAL INSULATOR AND SHIELD

4893–149

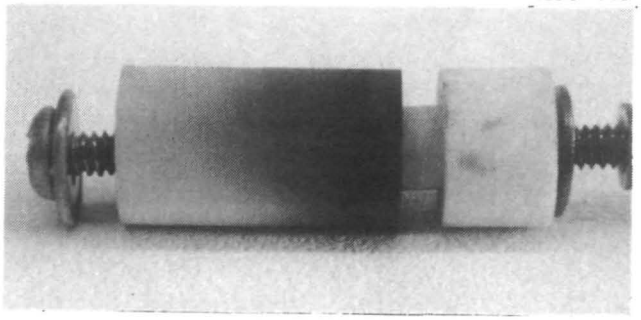

(e) KEEPER SUPPORT INSULATOR

Figure A-55. Cathode keeper supports and baffle terminal supports.

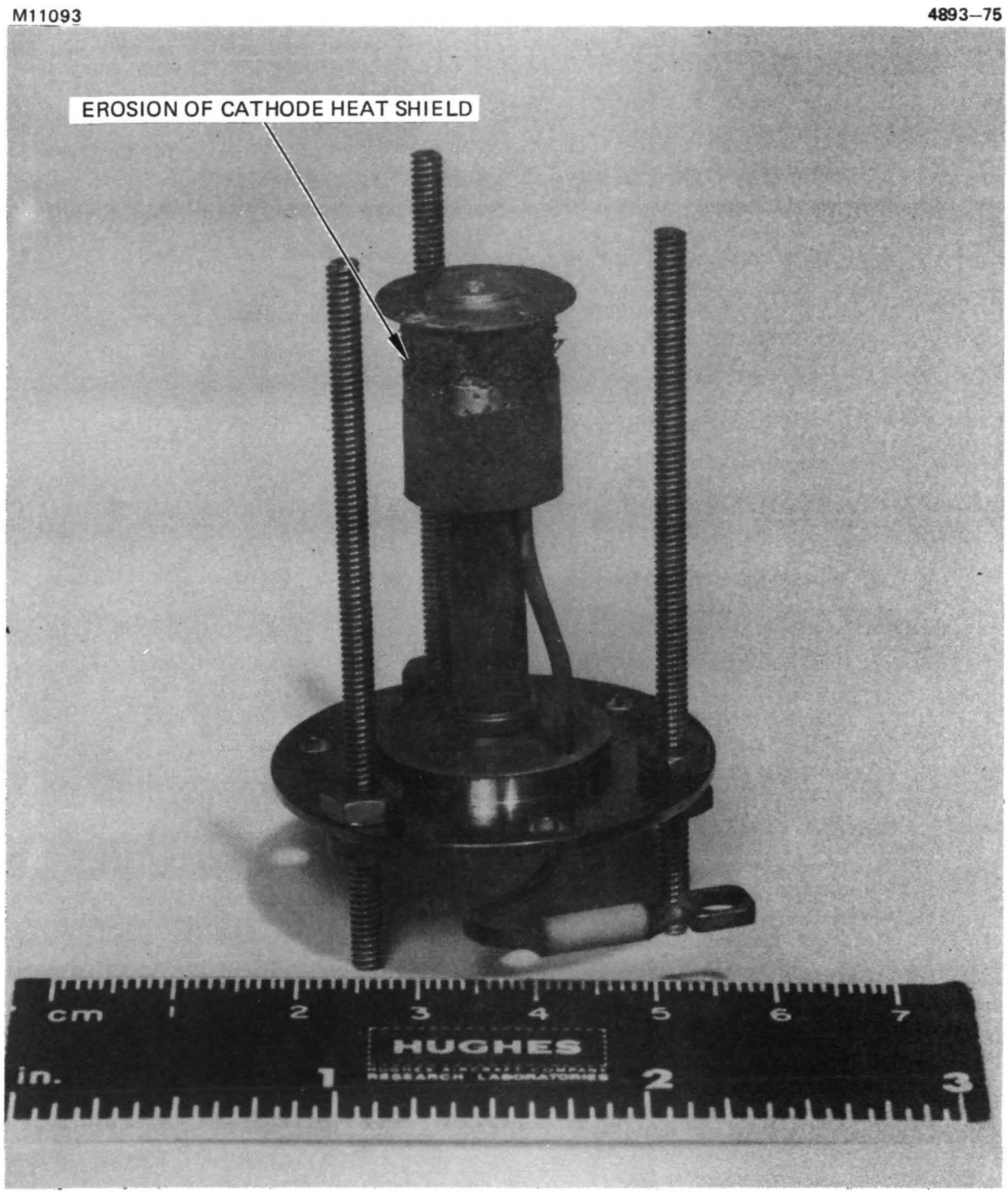

Figure A-56. Thruster cathode.

adequately protected. Diagnostic work in the area of discharge chamber sputter erosion and deposition has also been reported in references 4 and 5.

D. Ion Optics Assembly

The ion optics assembly is perhaps the most important single subassembly to the operational characteristics of the ion thruster. Its principal components as discussed here are:

- The accelerator electrode
- The screen grid electrode
- The electrode support assembly.

Before discussing the component parts individually, several measurements and observations concerning the complete assembly will be presented. After completion of the 10,000 hours of testing, the ion optics assembly was removed from the life test thruster, photographed, and measured to determine whether the inter-electrode grid spacing had changed. Tables A-6 and A-7 give the electrode specifications and spacing measurements recorded before and after testing. There appears to be a tendency for the spacings to be somewhat smaller in Table A-7 but the change is considered relatively insignificant. The grids were next cleaned as carefully as possible (to remove the flakes) and mounted on thruster SN 301B, which is the laboratory prototype version of the 700-series design. Thruster operation with the optics assembly was normal except for an extremely high arc rate. The grid set was capable of operation at ever increasing arc rate up to 1 A of beam current, but the arc rate was too high to obtain any meaningful performance or optics perveance data. It is not known whether this condition was a consequence of flake material which had not been adequately removed from the grids or whether the electrodes lose structural stability because of wear.

Wearout of the accelerator electrode by charge exchange ion erosion has in the past been considered a critical, if not the major, factor in determining thruster lifetime. This type of wear was not the major factor in this test. The most severe damage to the accelerator

Table A-6.

30 cm OPTICS ASSEMBLY RECORD
SCREEN ACCELERATOR SPACING CHART

DATE: 2/19/74
TECH: Brian J. Reeves

MOUNTING RING ASSEMBLY S/N 648
ACCELERATOR ELECTRODES S/N 648
NOTES:

SCREEN ELECTRODES S/N 648
NOTES:

TYPE	Dished .830
DRAWING NO.	D1026138-92
APERTURE dia	.060
SPACING CTR/CTR	.087
THICKNESS	.020
DRAWING NO.	D1026137-93
APERTURE dia	.075
SPACING CTR/CTR	.087
THICKNESS	.015
REDUCTION (%)	

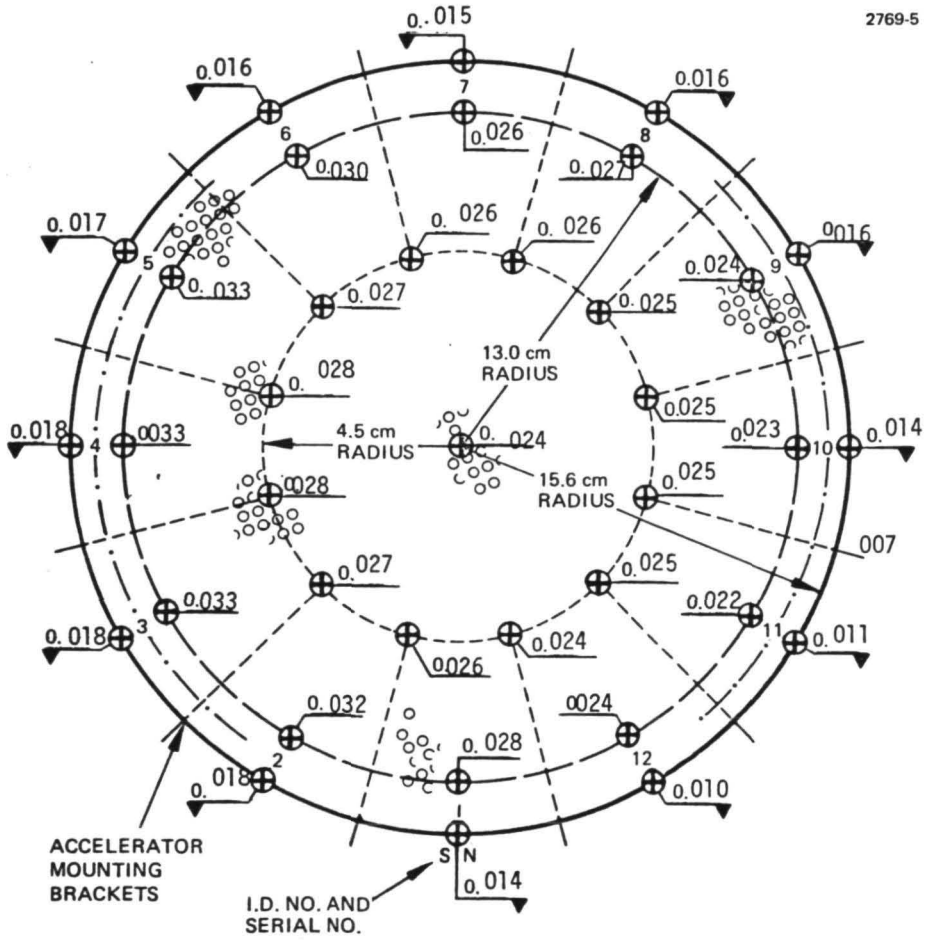

Table A-7.

30 cm OPTICS ASSEMBLY RECORD
SCREEN ACCELERATOR SPACING CHART

DATE: 6/4/75
TECH: H.T.

MOUNTING RING ASSEMBLY S/N 648
ACCELERATOR ELECTRODES S/N 648
NOTES: _____

SCREEN ELECTRODES S/N 648
NOTES: _____

TYPE	.830 Dished
DRAWING NO.	D1026138-92
APERTURE dia	.060
SPACING CTR/CTR	.087
THICKNESS	.020
DRAWING NO.	D1026137-93
APERTURE dia	0.075
SPACING CTR/CTR	0.087
THICKNESS	0.015
REDUCTION (%)	0.4%

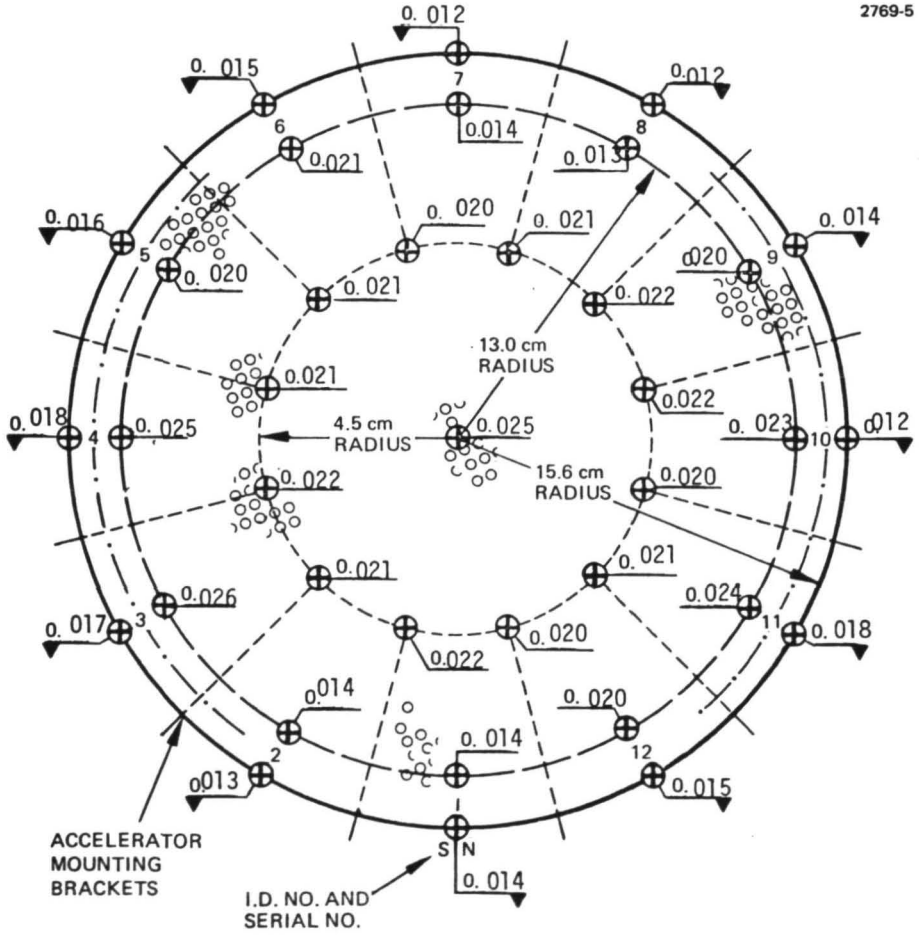

electrode was caused by direct interception of high-energy ions which were deflected or defocused by flakes of material partially covering screen grid apertures (as seen earlier in Figs. A-1 and A-12). Several examples of damage of this type are pointed out in Fig. A-57. The typical pattern of "pits" and grooves caused by charge exchange ions is also seen. Photographs comparing the downstream side of the accelerator electrode before and after testing are shown in Figs. A-58 through A-67. By careful examination of these photographs (or the actual electrodes under a microscope), it is seen that the ion machining damage is randomly distributed and irregular in form. The erosion caused by charge exchange ions, on the other hand, is quite uniformly distributed and exhibits a well defined pattern. This pattern is oriented to the hexagonal aperture array but does not show any region of accelerated wear that would indicate the neutralizer location. Thus, the major difficulty observed in the SERT II tests is not at all in evidence here.

Some selected areas of damage are shown magnified in Fig. A-68. Note that in the views shown as (b) and (f), some webs of material between the apertures have been cut through completely by beam ions. View (e) shows a flake lodged in the electrodes and the resultant damage. Views (a), (b), and (c) illustrate the change in orientation of the charge exchange erosion patterns that can be seen as a function of thruster radius. The orientation of these photographs places the center of the electrode at the top of the page and view (a) is nearest the center, while view (c) is nearest the edge. It is apparent that the erosion is deepest near the electrode center, view (a), and that the erosion pattern is centered on and symmetric with the aperture pattern. Nearer the edge, as in Fig. A-68(c), the erosion is less and the pattern is shifted towards the grid center. This offset in the erosion pattern occurs because the beamlets formed at the edge apertures are by grid design deflected radially inward to counteract the divergent effect introduced by grid curvature and therefore the charge exchange ions are also focused towards the grid center.

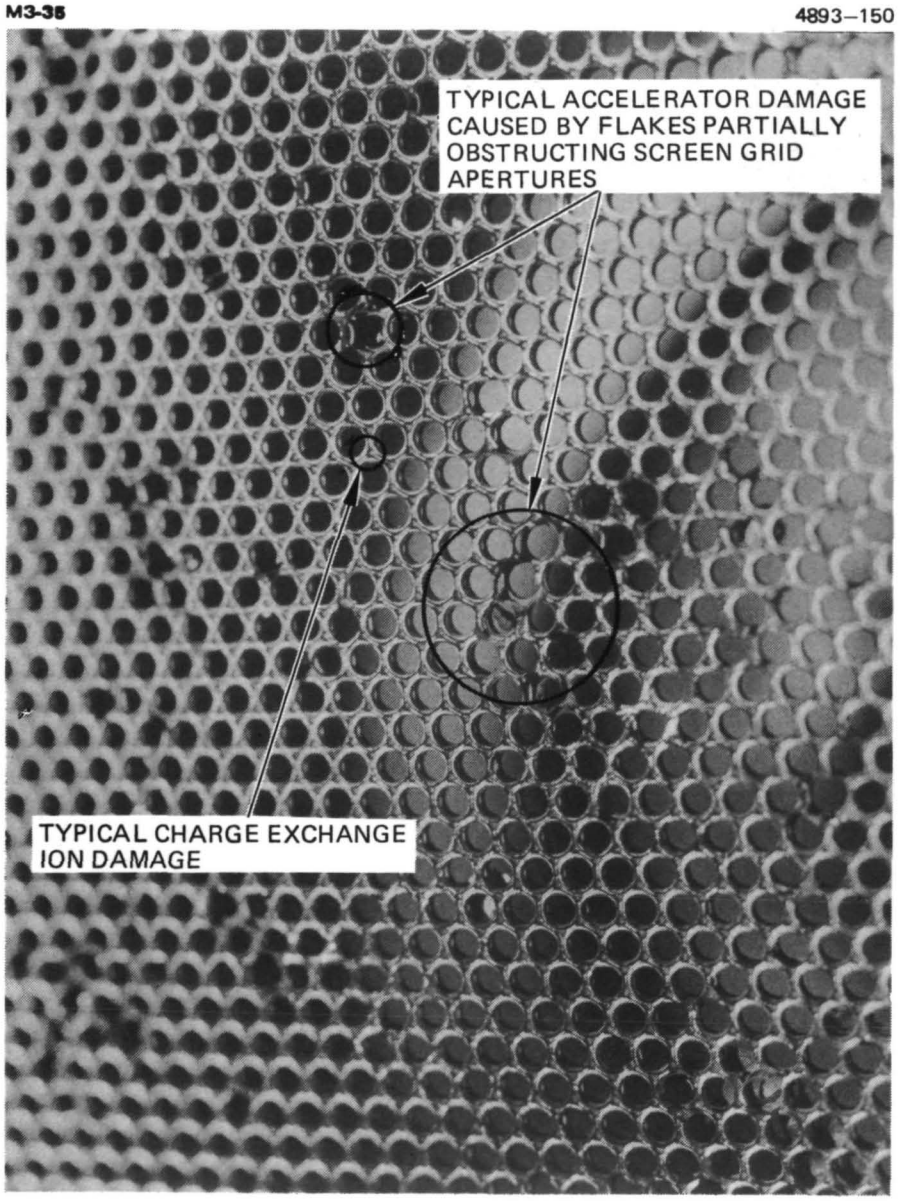

Figure A-57. Accelerator electrode, downstream view.

M10067 4893-260

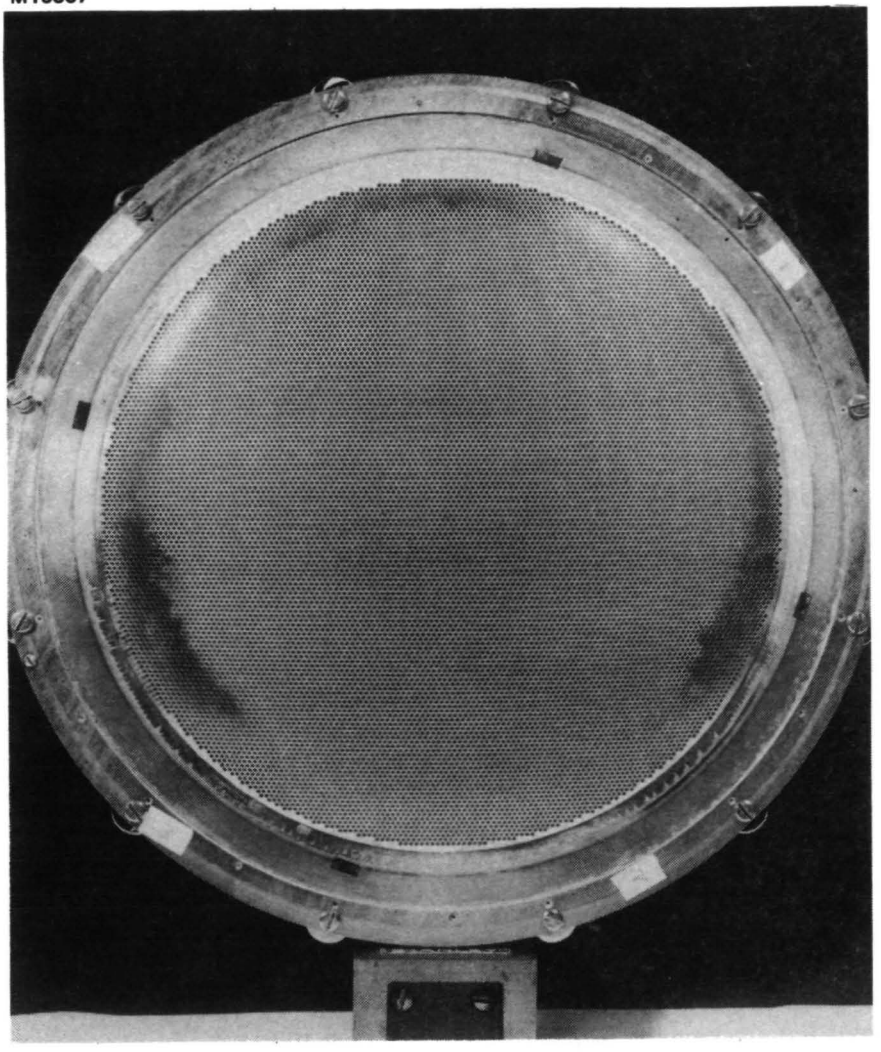

Figure A-58. Ion optics assembly SN648 downstream view before test.

M11056

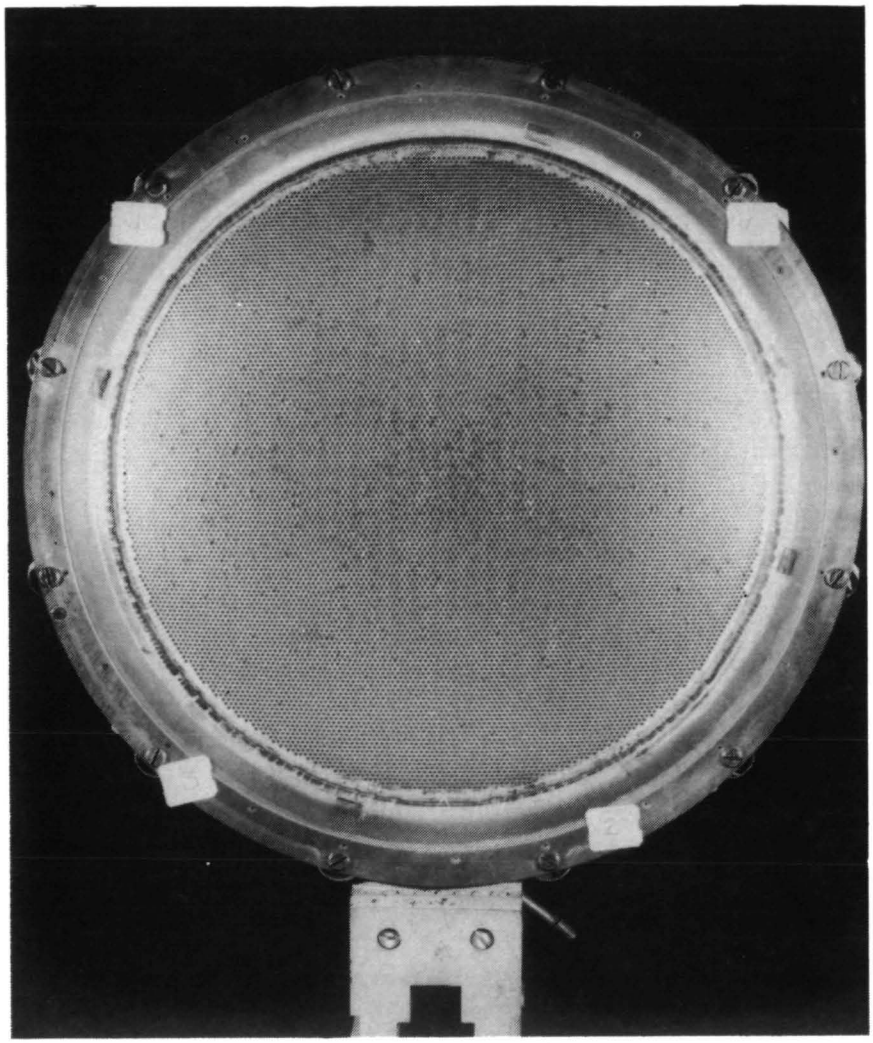

Figure A-59. Ion optics assembly SN648 downstream view after test.

M10068

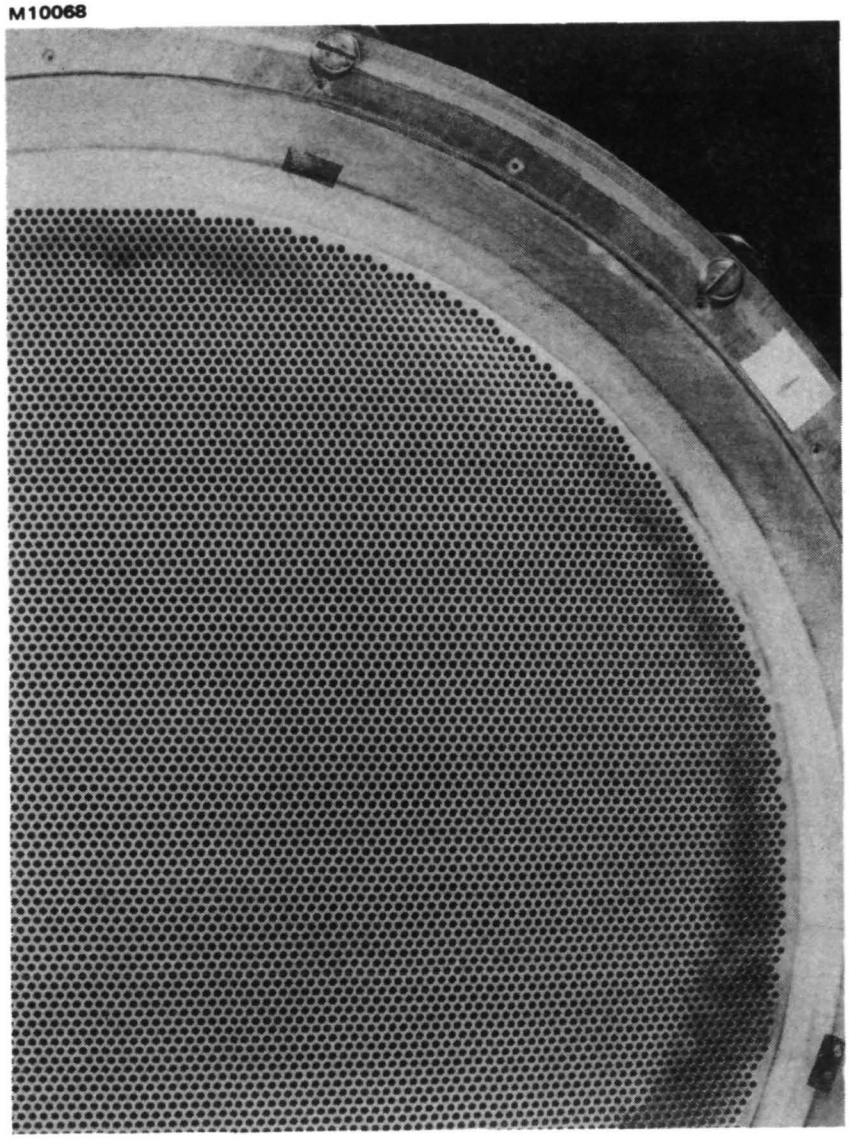

Figure A-60. Accel before test.

M11060 4893–151

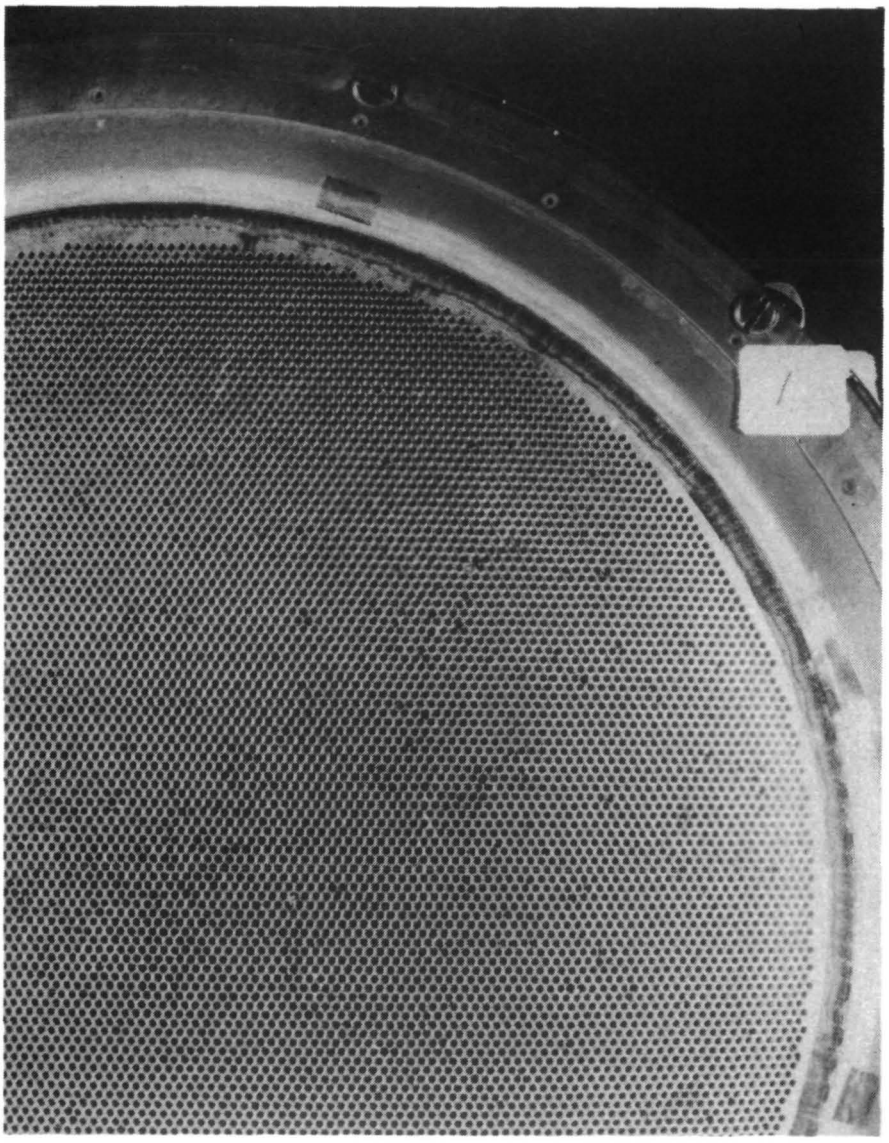

Figure A-61. Accel after test.

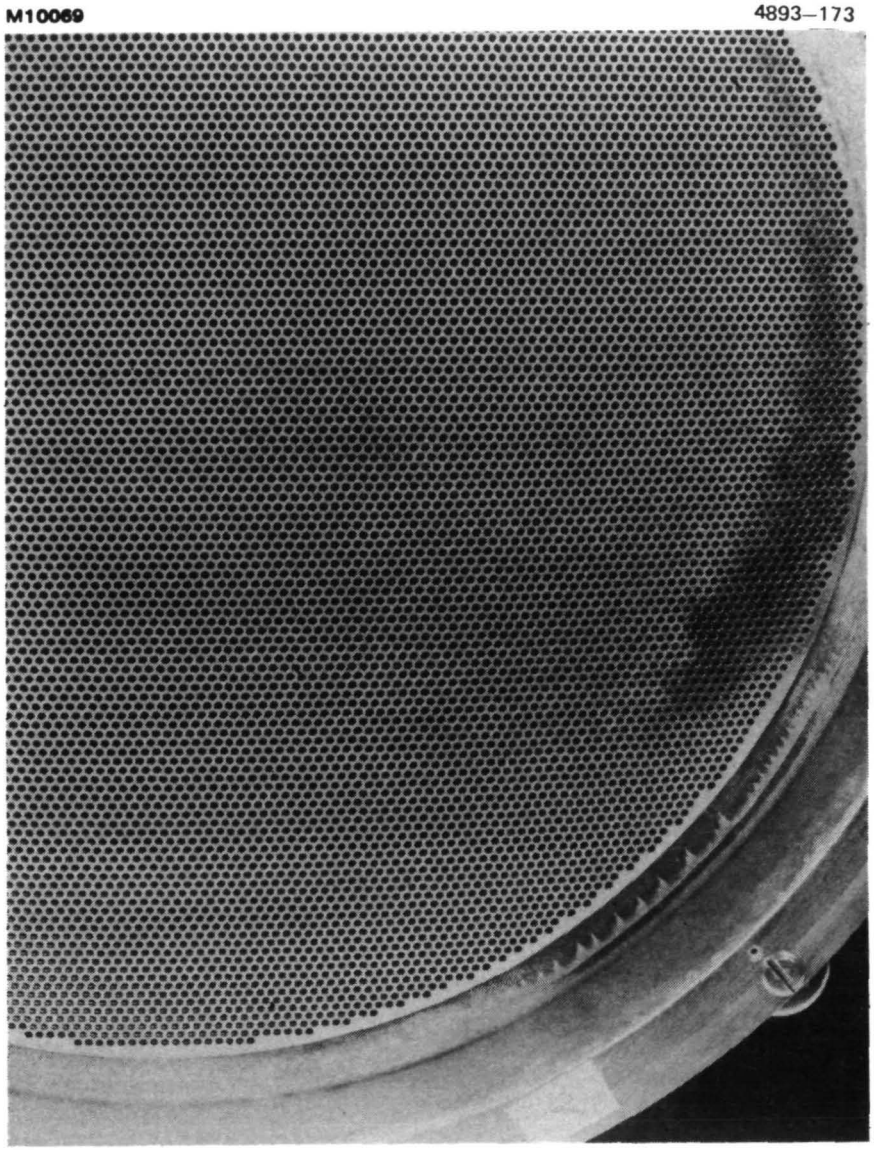

Figure A-62. Accel before test.

M11059

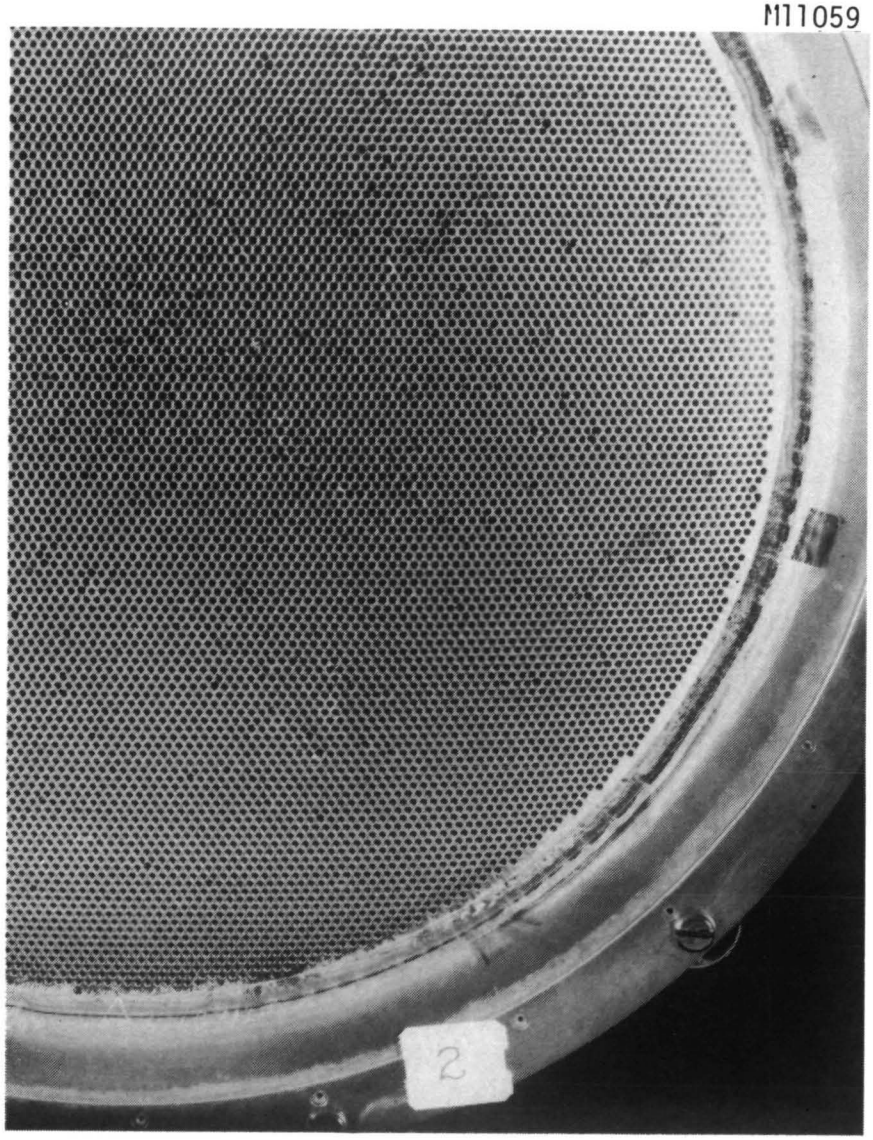

Figure A-63. Accel after test.

M10070

Figure A-64. Accel before test.

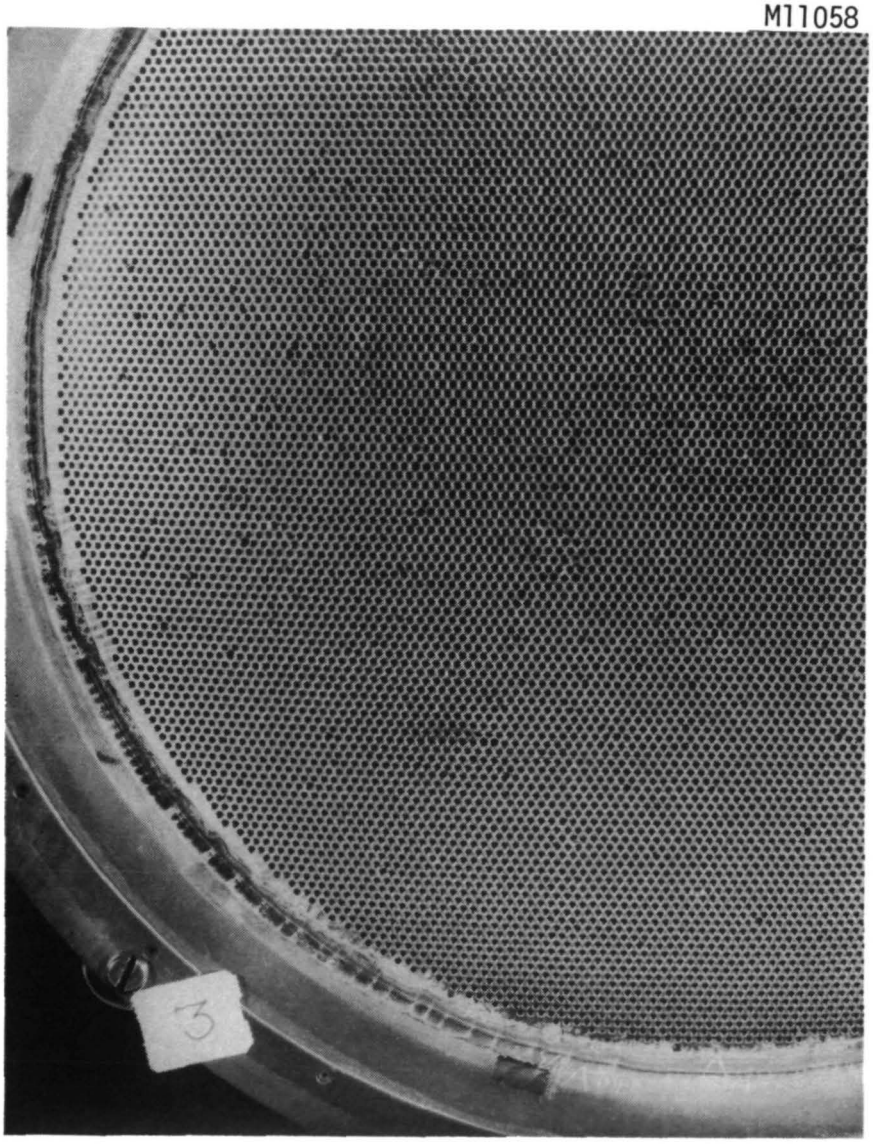

Figure A-65. Accel after test.

M10071

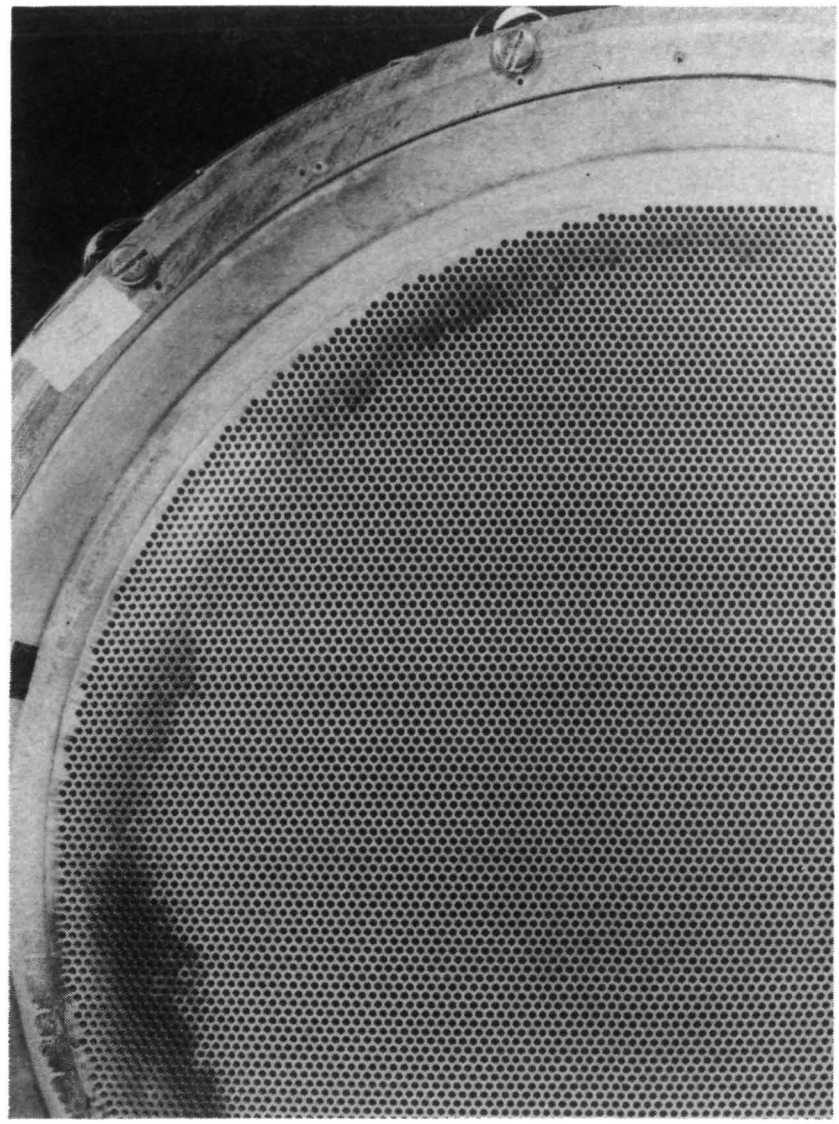

Figure A-66. Accel before test.

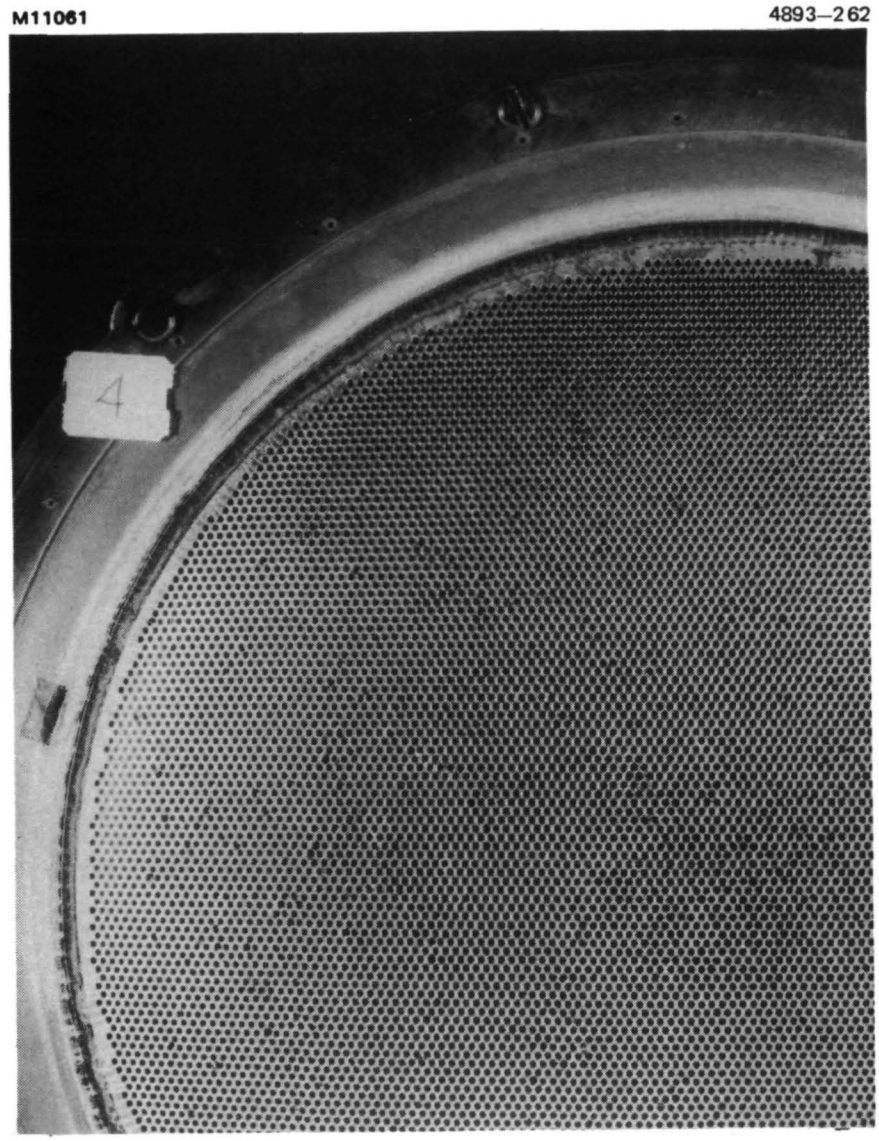

Figure A-67. Accel after test.

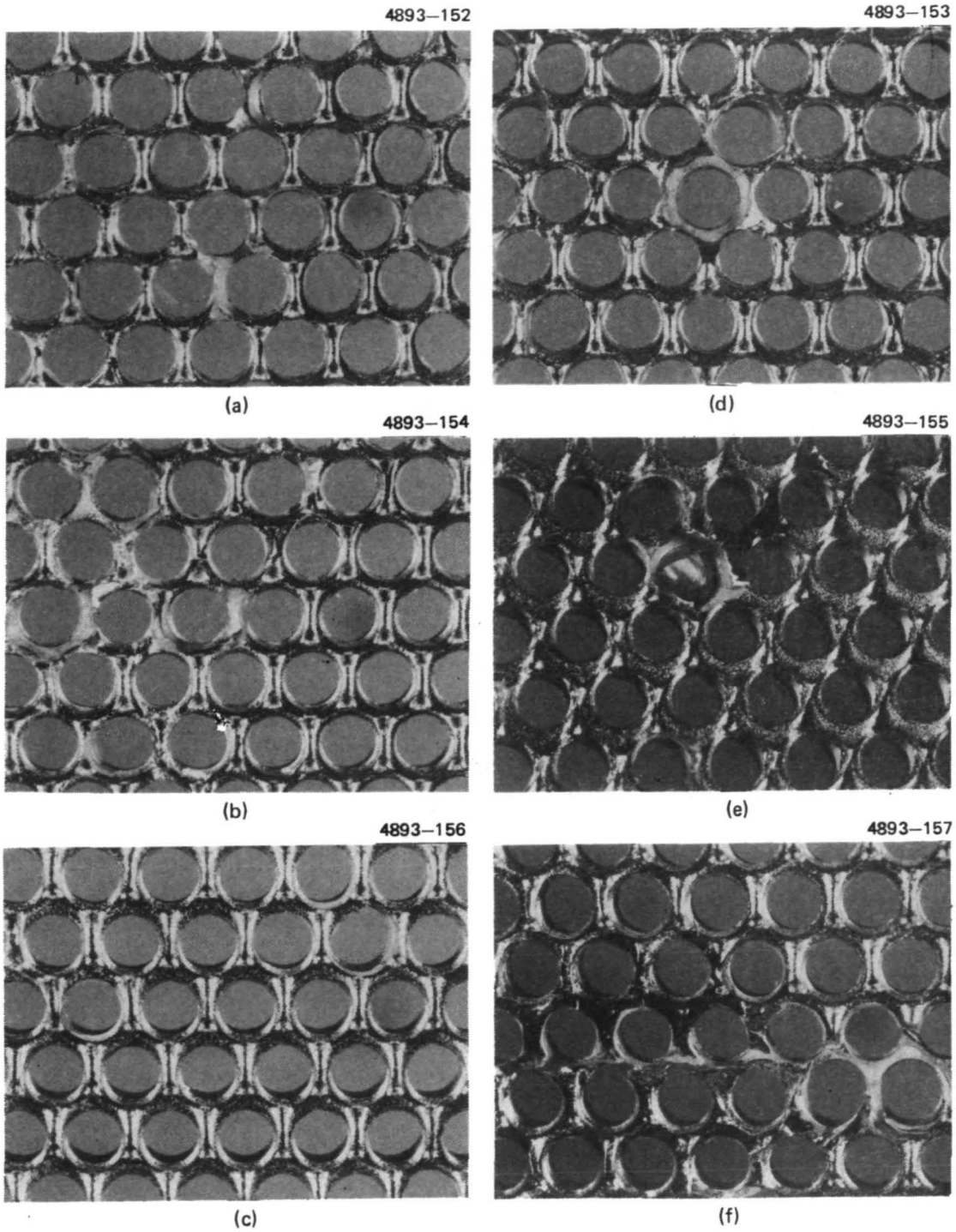

Figure A-68. Selected areas of downstream surface of accel electrode.

The depth of the charge exchange erosion was investigated carefully, both by microscopic examination and by cross-sectioning segments of the electrode taken from the center and the edge of the grid. The "pits" are seen as triangles (Fig. A-68) in the center of the web of material common to any three apertures. These pits vary but are usually almost conical in shape with a very small cross section at the deepest point. They vary in depth from a maximum of 0.013 in. (0.033 cm) near the center to being immeasurable near the edge. The pits are connected by grooves, which are a maximum of 0.006 in. (0.015 cm) deep at the mid-point between pits. The depth and shape of the pits and grooves eroded by charge exchange ions appears to also be influenced by their proximity to defocused beam ion damage. In areas where there is extensive ion machining damage, the pits and grooves are shallower and broader. Figure A-69 shows some selected cross-sections of the accelerator electrode near the center and the edge. The difference in the views shown reflects the location and angle of the cut through the material. The views shown as Fig. A-69(a) and (b) represent a cut along the groove and through the pits, the depth of the pit shown being approximately 0.012 in. (0.030 cm). It is thought that the sample in (b) has been polished to nearly pass through the center of the pit. A survey of pit depth was made using a microscope at high magnification (1000X) and measuring the travel required to focus on the bottom of the pit as compared to focusing on the undamaged edge. A plot of representative pit depth variation is shown in Fig. A-70.

To illustrate that there is no uniform erosion or thinning of the accelerator grid, Table A-8 shows electrode thickness measurements as measured with a micrometer for the endurance test electrode and for a new electrode. Note that there is some variation in thickness over the electrode but this variation does not appear to be systematic. The only explanation that can be offered for the thickness variation is that either the original material was not uniform or the electropolish was uneven. Accelerator aperture wear, except for damaged apertures, appears only slightly related to thruster radius. A comparison of the endurance test accelerator aperture measurements is made with those of a new accelerator grid in Table A-9. The relatively small changes in accelerator

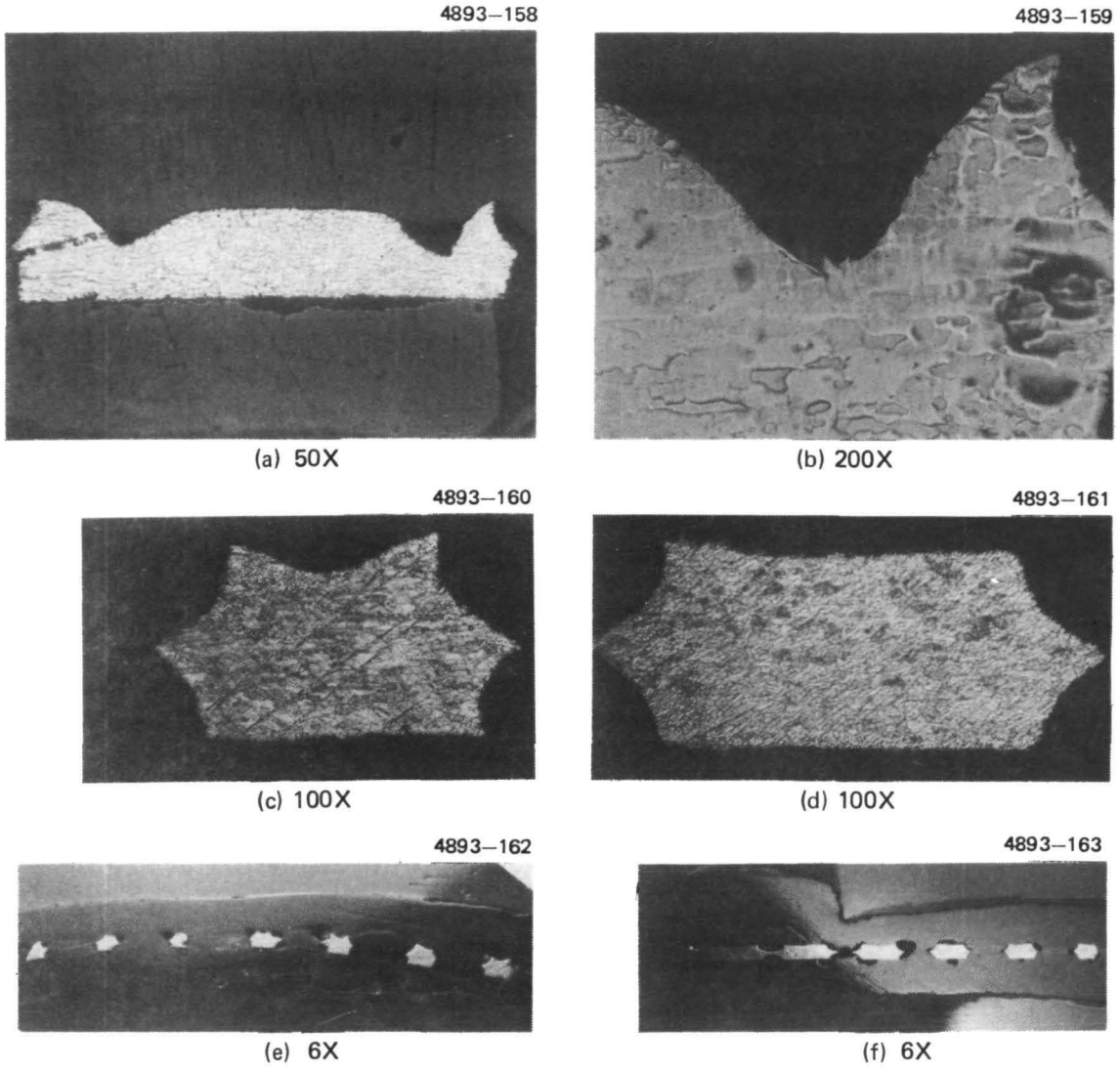

Figure A-69. Selected cross sections of accel electrode.

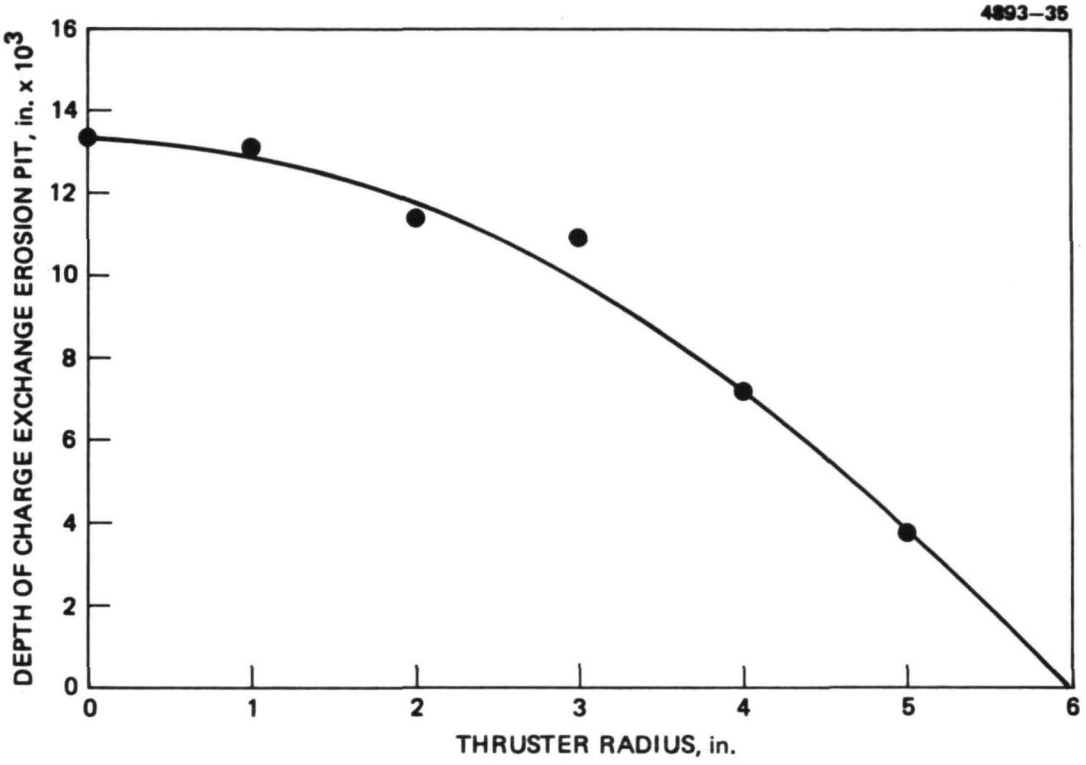

Figure A-70. Depth of charge exchange ion erosion pits as a function of thruster radius on accelerator grid SN648 after 10,000 hour endurance test.

Table A-8.

Comparison of Electrode Thickness Versus Radius for Endurance Test Accelerator Electrode (SN 648) and New Electrode (SN 803) Measured Along a Different Radii								
Radius in.	Electrode Thickness							
	SN 648 in. x 10^3				SN 803 in. x 10^3			
0	18.7 Ⓐ	19.2	19.2	19.2	19.5	19.5	19.5	19.5
1	19.9	19.5	18.7	17.7	19.5	19.4	19.2	19.4
2	17.5	16	18	17.5	18.9	18.9	18.7	18.8
3	19.9	19.2	17	16.5	18.3	18.2	17.6	17.5
4	18.3	17.2	17.2	16.5	18.5	18.4	17.8	17.9
5	18	17.2	17	17.0	18.6	18.5	18.1	17.8
Ⓐ Entries in this column measured with microscope								

T1857

Table A-9.

Comparison of Accelerator Electrode Aperture Diameter Versus Radius for the Endurance Test Electrode (SN 648) and a New Electrode (SN 653) Measured Along Different Radii						
Radius in.	Electrode Thickness					
	SN 648 in. x 10^3				SN 653 in. x 10^3	
0	63	63	62.5	63	60	60
1	62	62	60	52	60	59
2	61	61	60	61	60	59
3	61	61	60	61	59	59
4	60	60	58	60	59	59
5	59	60	58	59	59	59

T1858

electrode thickness and aperture diameter as indicated in Tables A-8 and A-9 are not considered significant to thruster lifetime or operation.

Photographs of the upstream surface of the accelerator are shown in Figs. A-71 through A-75. Careful examination of these pictures reveals several features that have been magnified and included in Fig. A-76. View (a) shows an area that is relatively undamaged but has a "matte" finish that may be the result of low energy ion erosion. Figure A-76(b) shows a typical area in which deflected beam ion erosion has occurred causing "scythe" shaped markings on the grids. This type of damage is rather widespread and, in areas where flakes remained on the screen grid for long time periods, the damage progresses as shown in view (d). View (c) is rather unusual in that the small triangular areas seen in the location that is usually occupied by charge exchange ion erosion pits on the downstream surface is actually a deposition here on the upstream surface. In addition, the edges of the apertures seen in view (c) appear rounded in a chamfered fashion, which is not typical of most other areas on the electrode. No explanation can be offered for the wear seen in view (c). In considering the relatively large number of high voltage overload recycles which occurred during the test, it was thought that arc damage might be distinctly visible on the upstream surface of the accelerator electrode. It has not been possible to identify any damage seen on this electrode with the appearance of damage that is seen when grids are purposely short circuited and the shorting material is then removed by capacitive discharge. This statement does not imply that such damage did not occur, but only that it cannot be conclusively identified.

The screen grid electrode has not in the past been of great concern as a factor limiting thruster lifetime. It will be seen in the following paragraphs that appreciable concern is justified. Proceeding in the same manner as above for the accelerator electrode, Figs. A-77 through A-86 compare photographs of the upstream surface of the screen grid before and after testing. It is difficult to detect any differences in the appearance of the screen grid. There appears to be a slight rounding of the aperture edges as seen in views (a) and (b) of the magnified photographs shown in Fig. A-87. These views are representative of the appearance of the center of the electrode, while view (e) shows that such

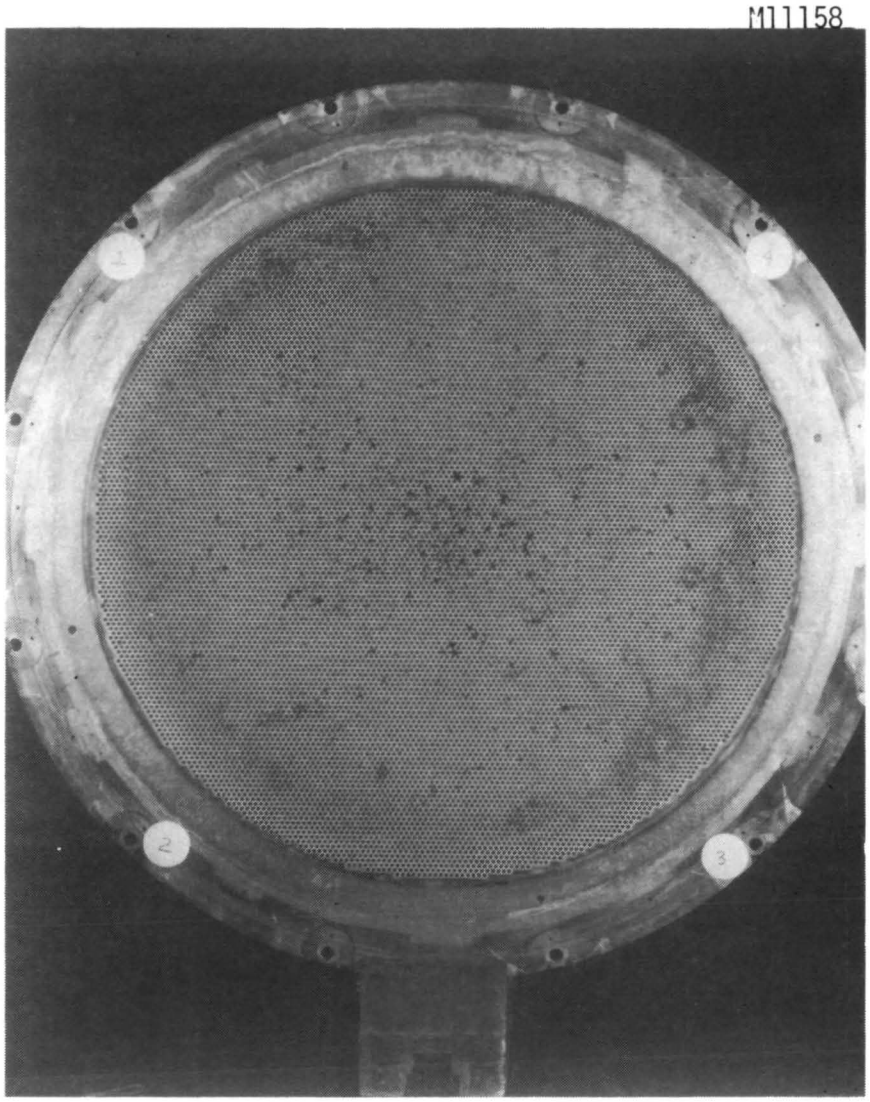

Figure A-71. Accel after test, upstream side.

M11161

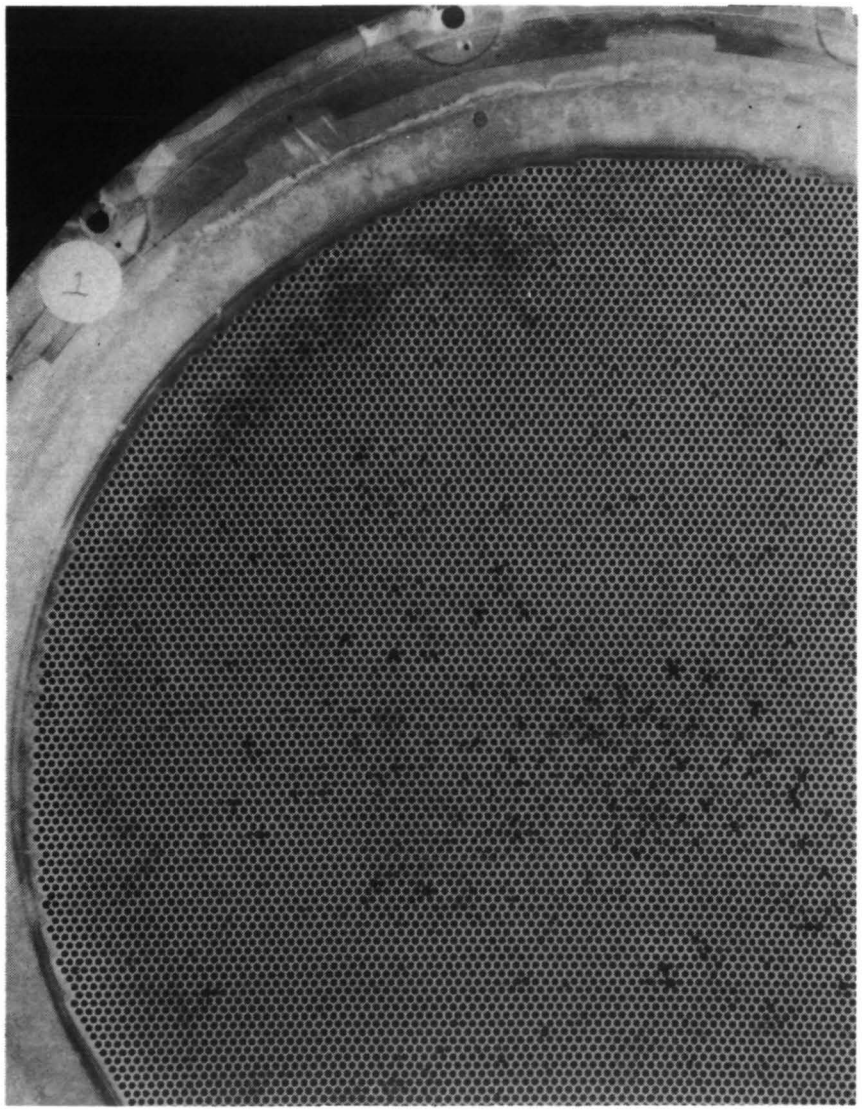

Figure A-72. Accel after test, upstream side.

M11160

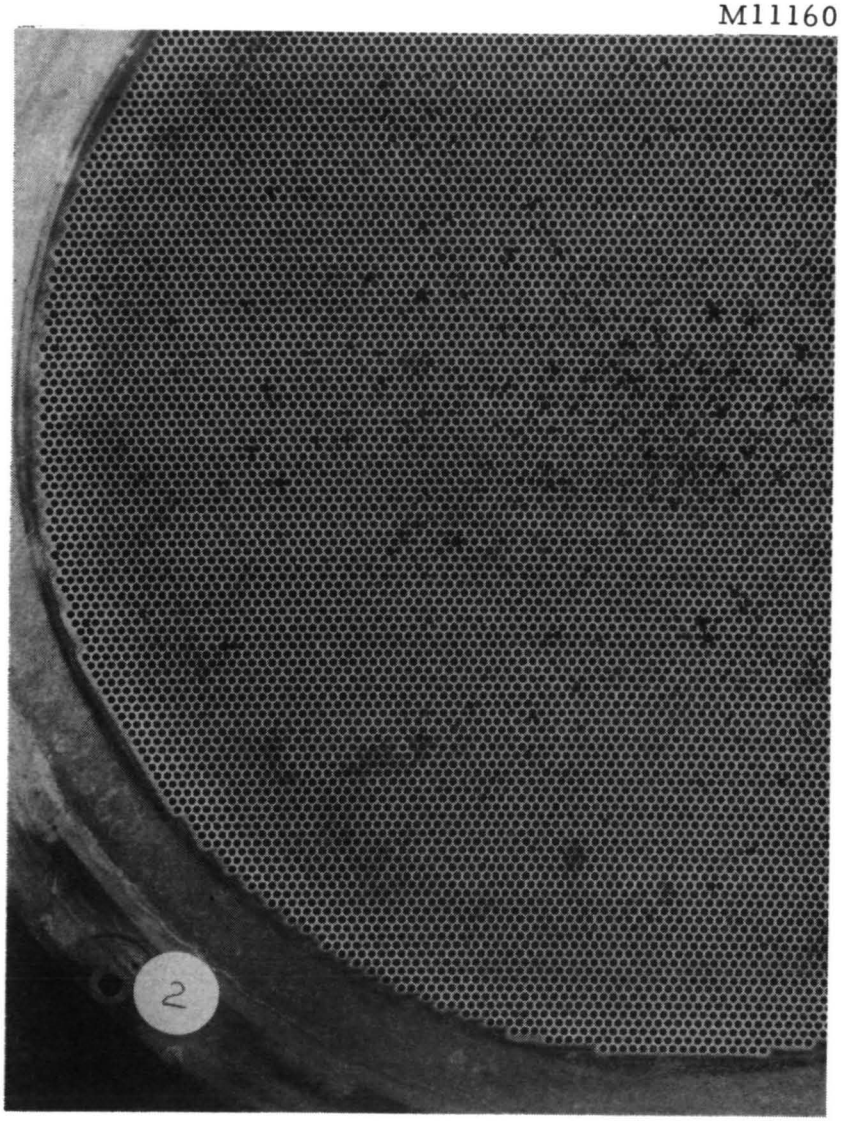

Figure A-73. Accel after test, upstream side.

M11156

Figure A-74. Accel after test, upstream side.

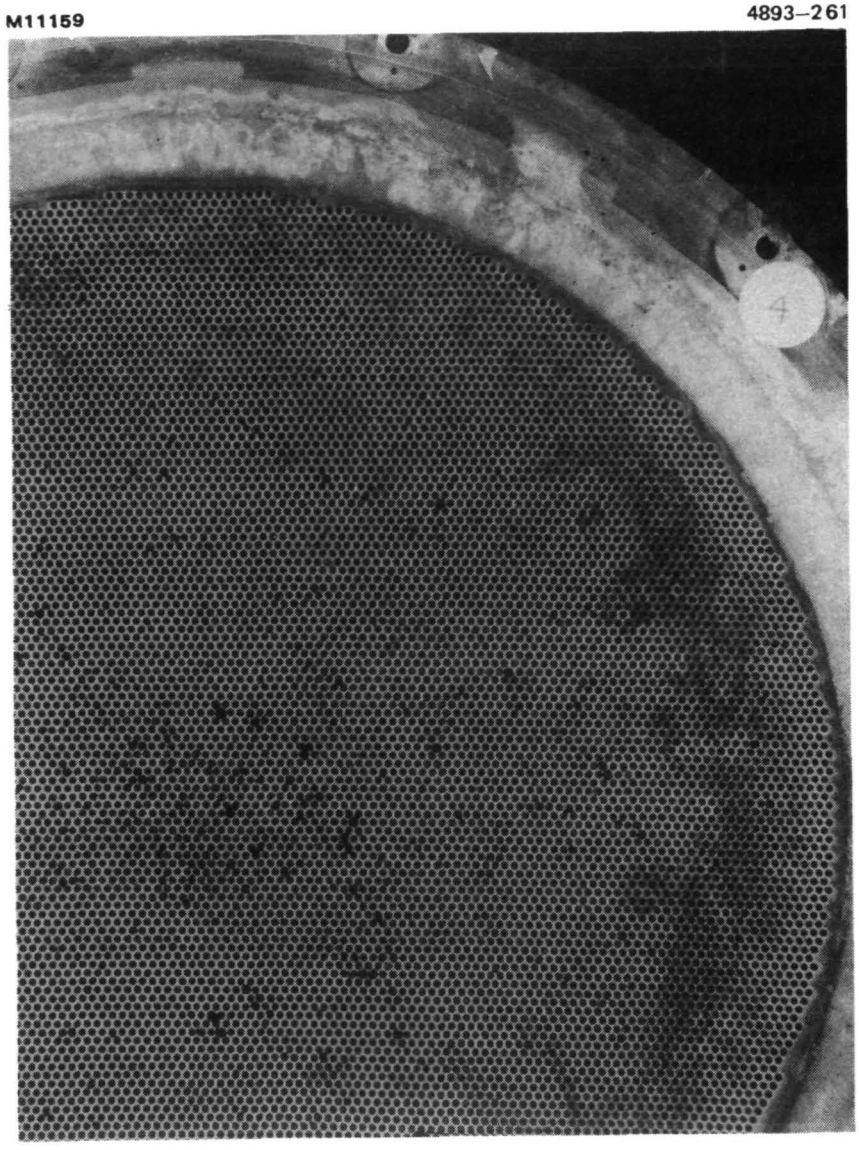

Figure A-75. Accel after test, upstream side.

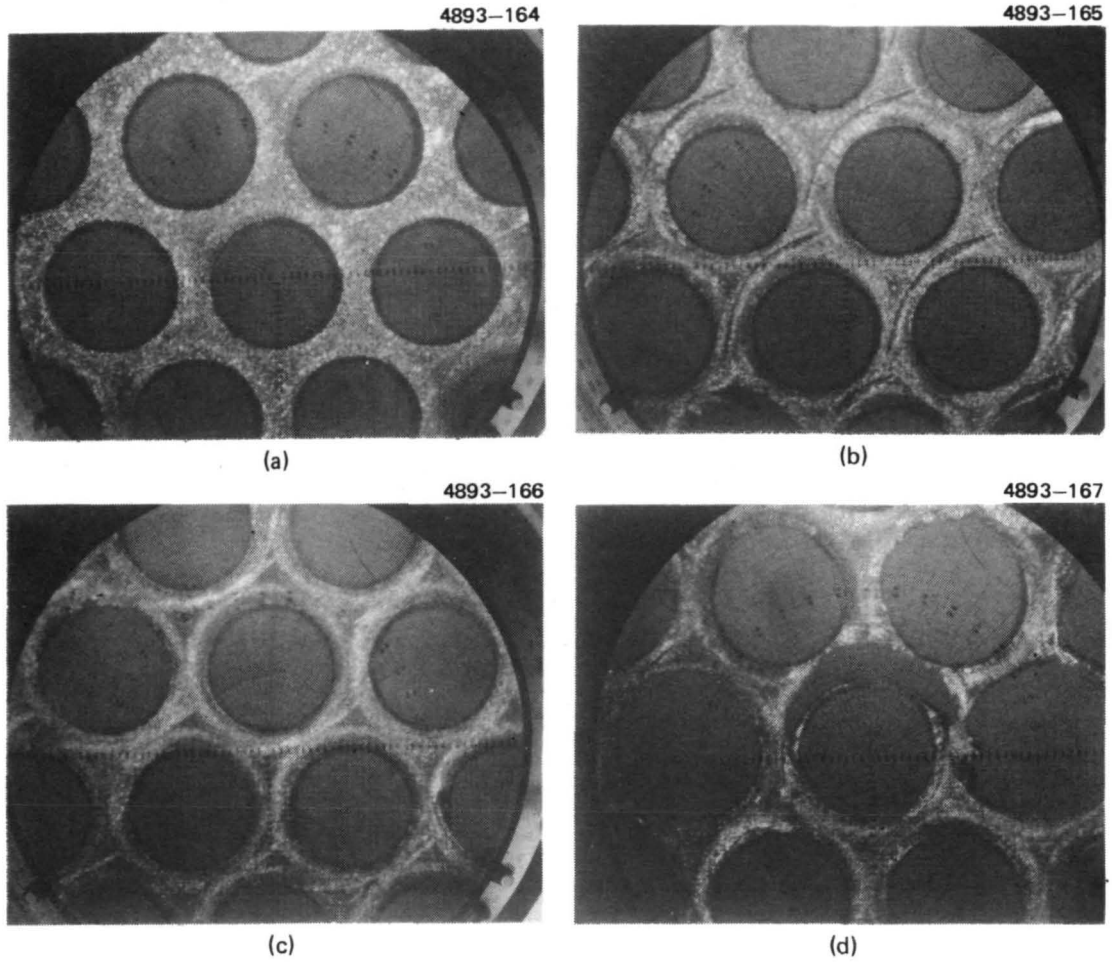

Figure A-76. Magnified view of selected areas of upstream surface of accel electrode.

M10072 4893-269

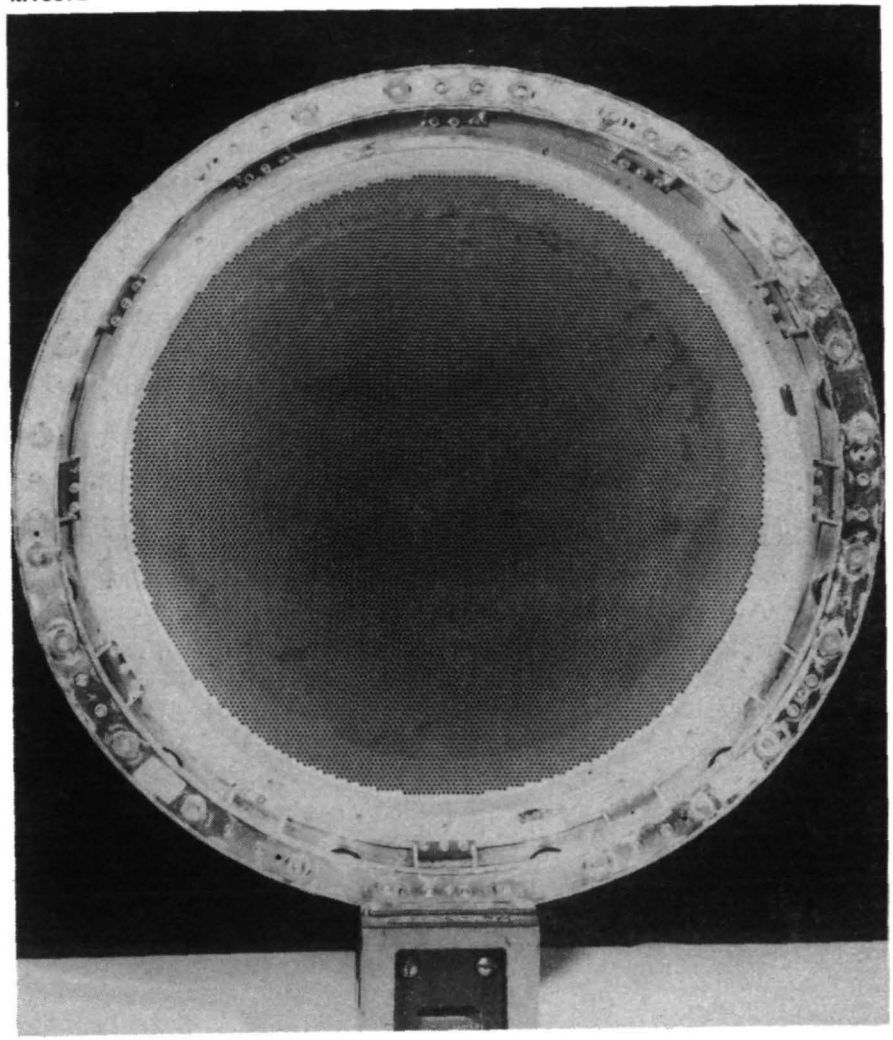

Figure A-77. Screen electrode, before test.

M11057

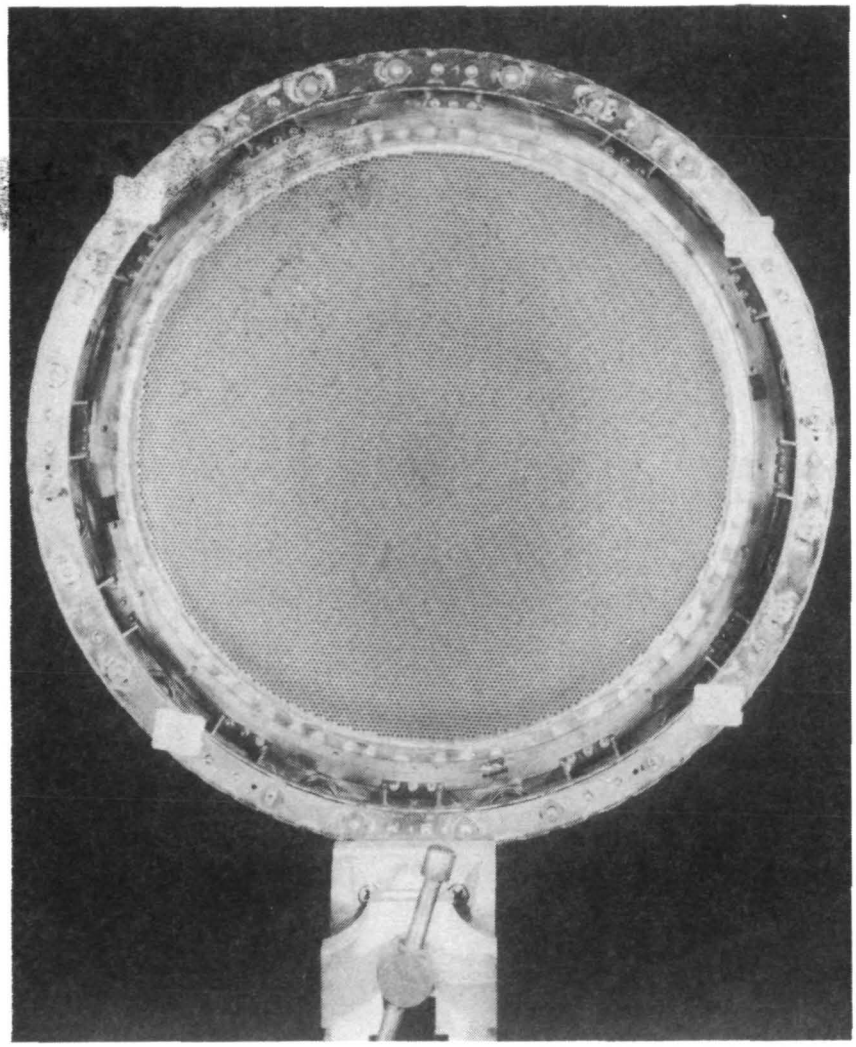

Figure A-78. Screen electrode, after test.

M11073

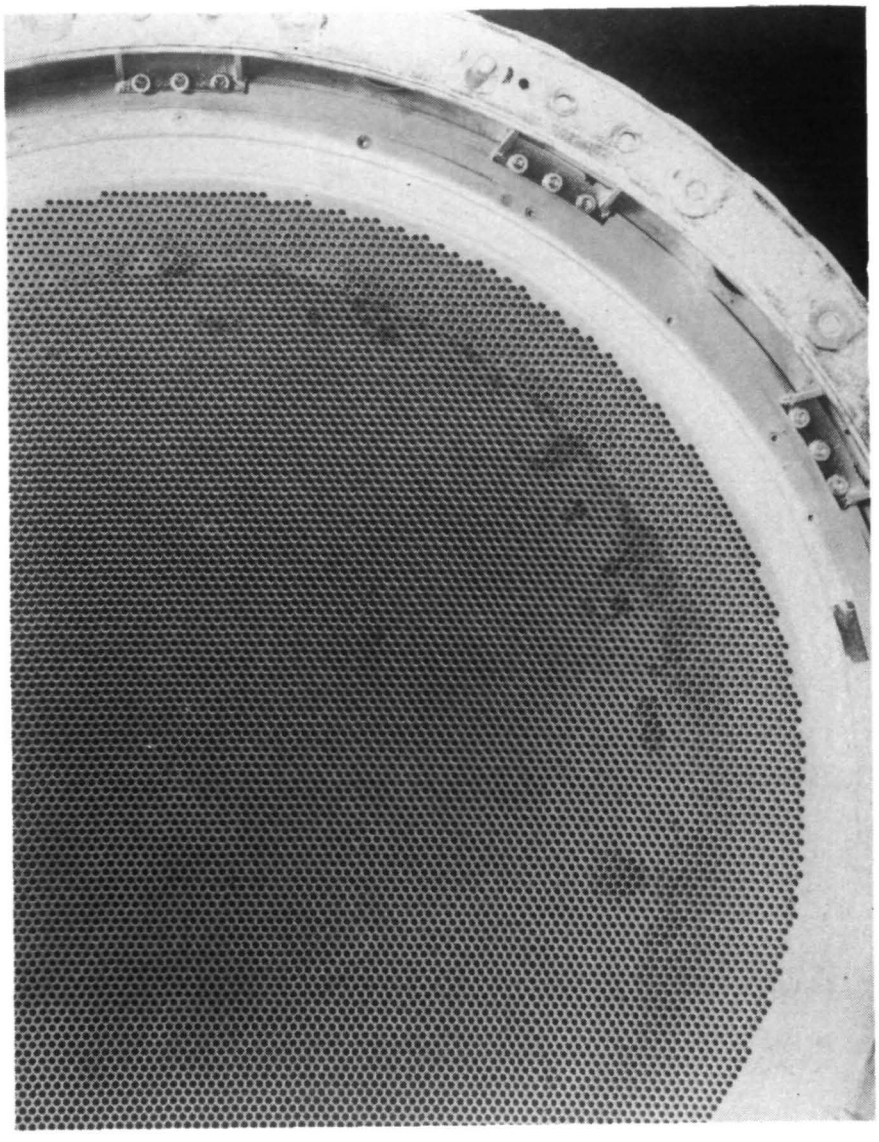

Figure A-79. Screen electrode, before test.

M11065

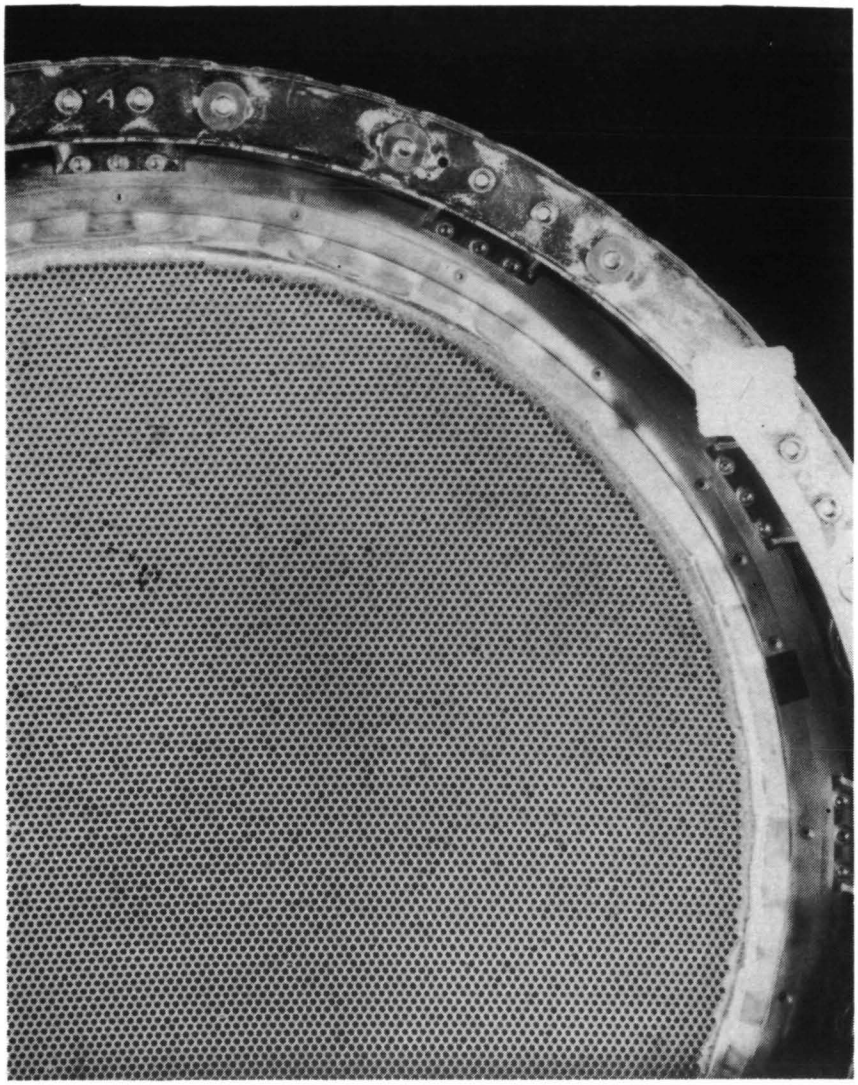

Figure A-80. Screen electrode, after test.

M10074

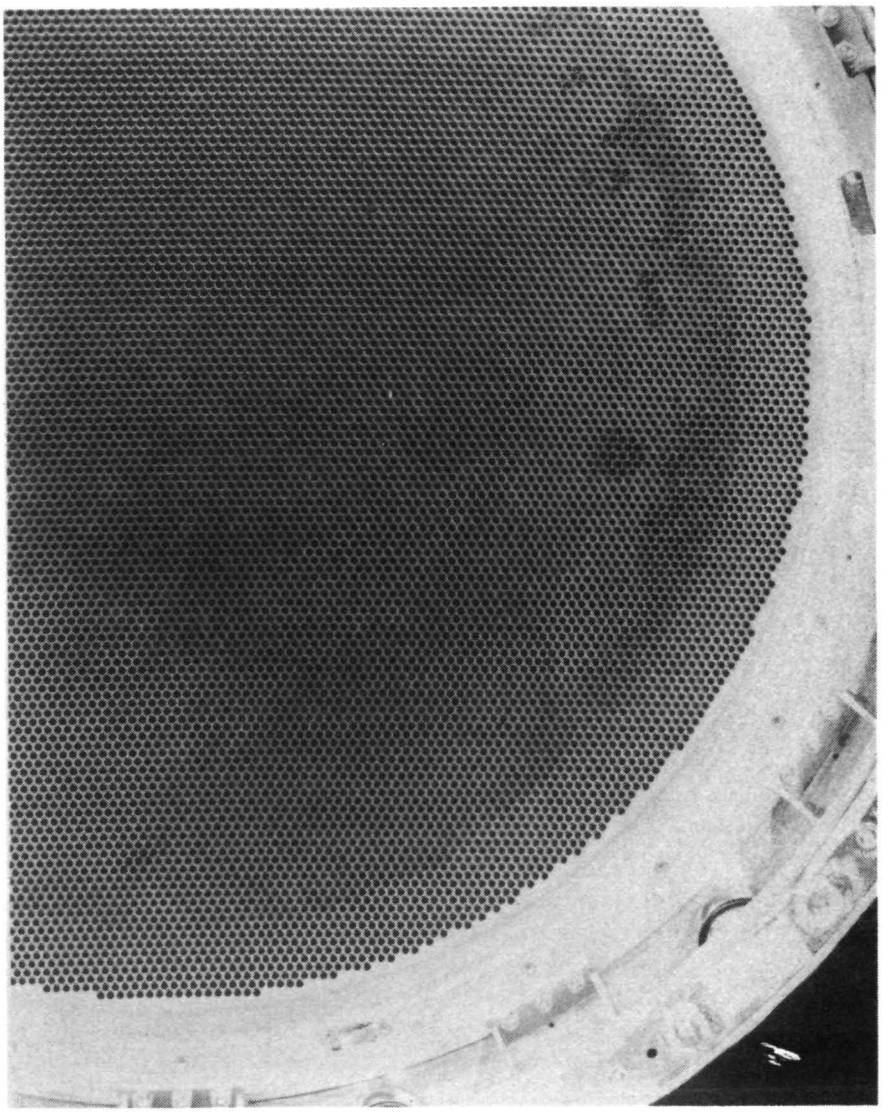

Figure A-81. Screen electrode, before test.

M11064

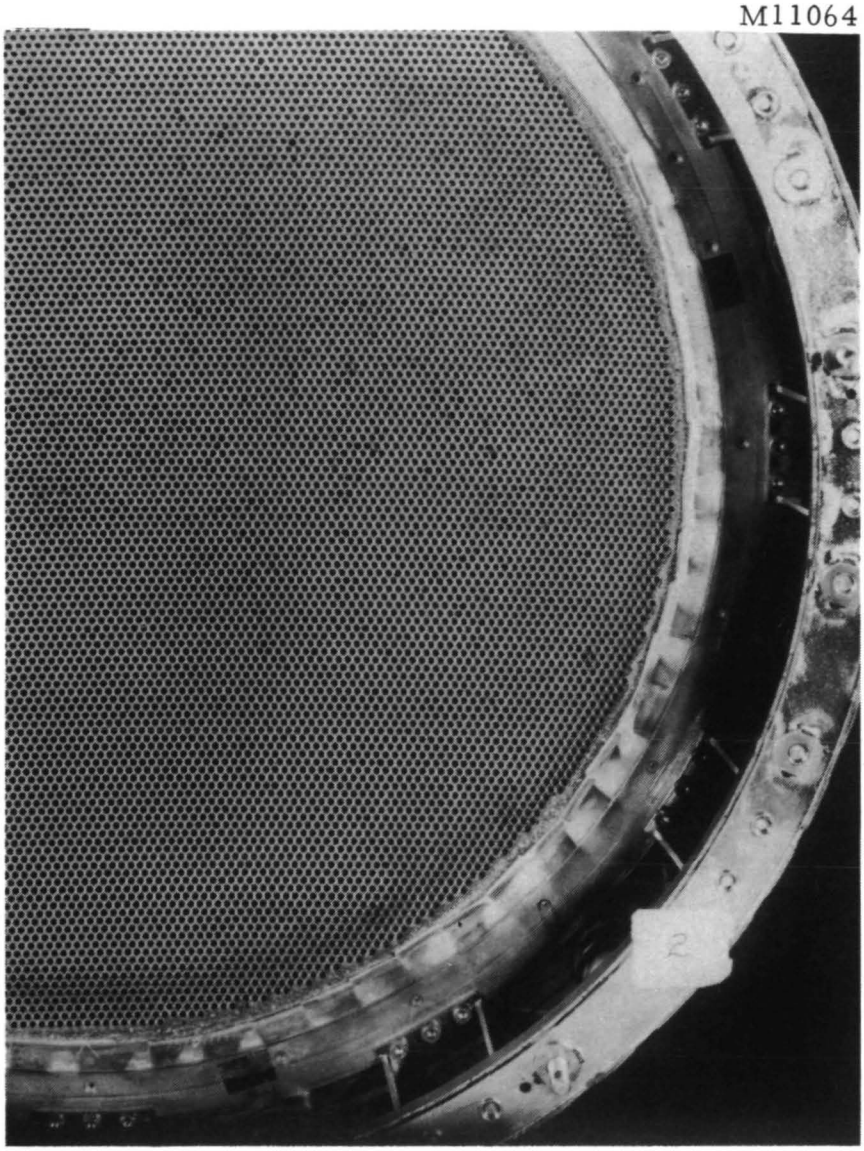

Figure A-82. Screen electrode, after test.

M10075

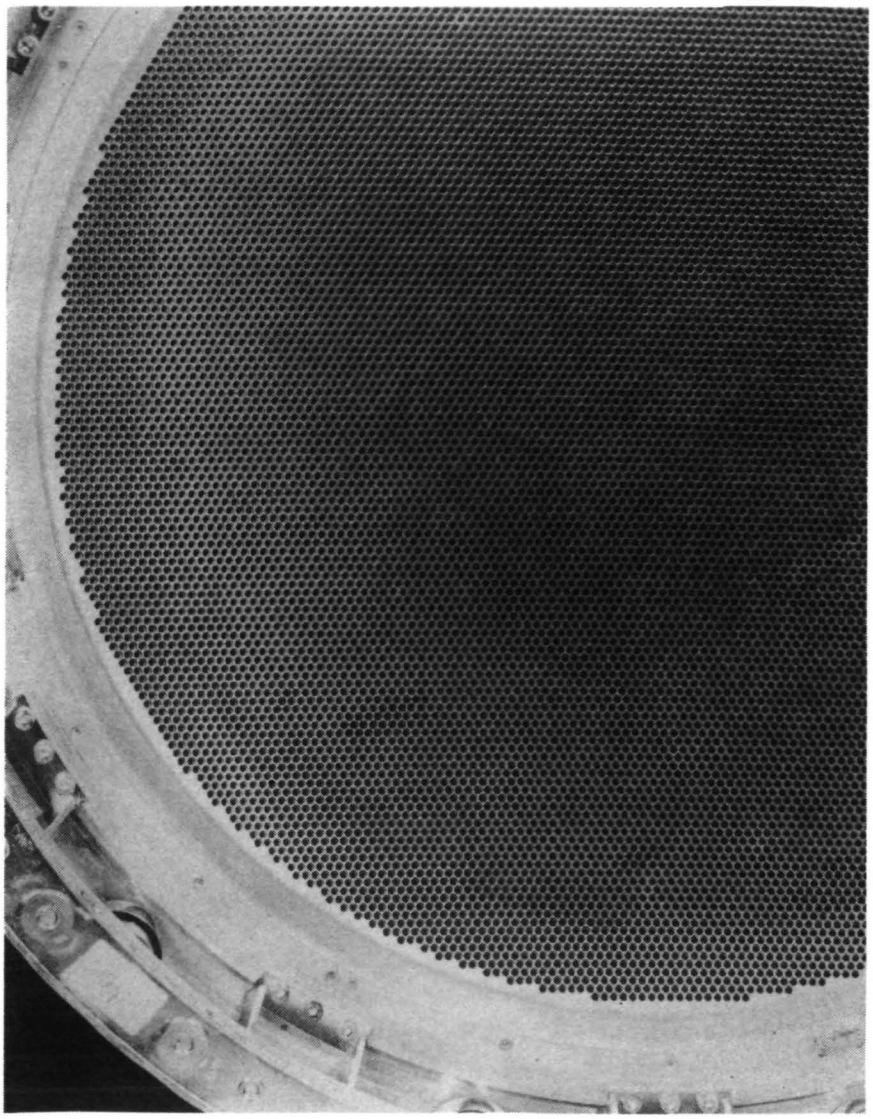

Figure A-83. Screen electrode, before test.

M11063

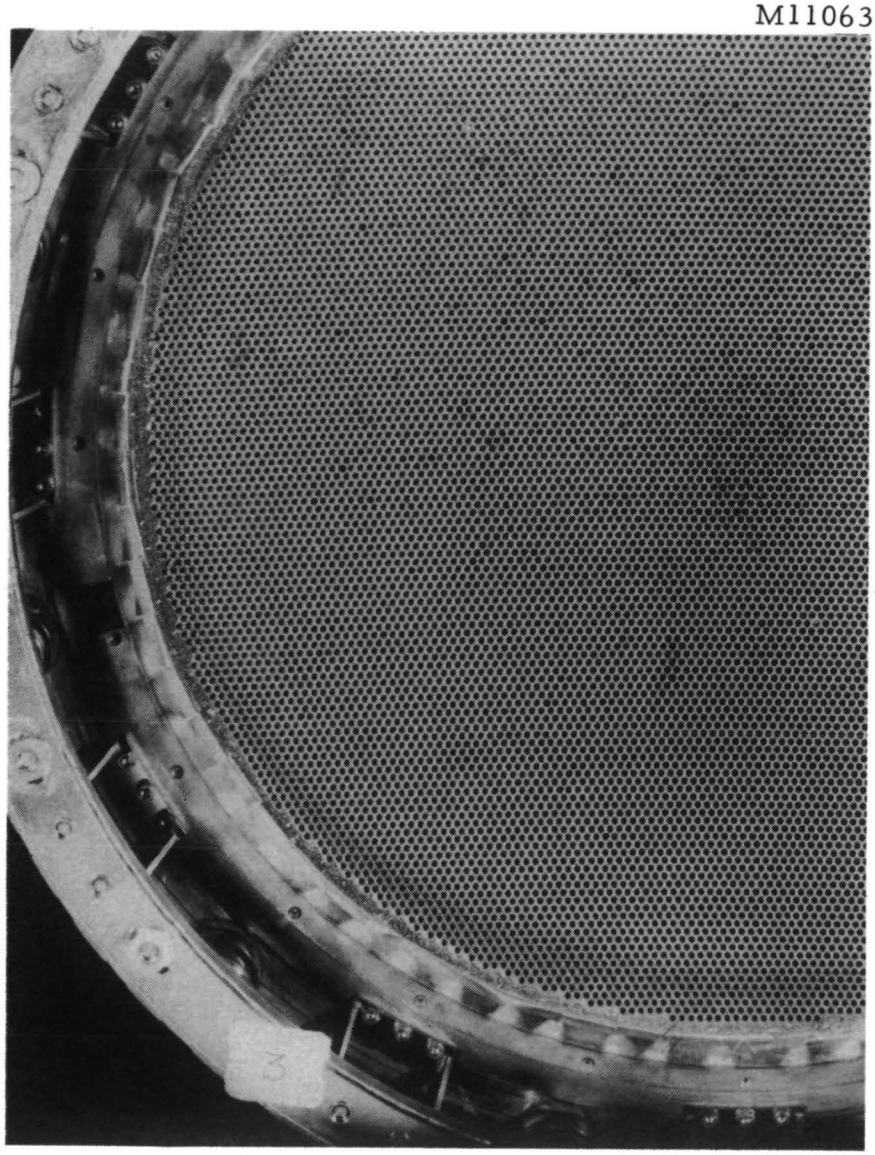

Figure A-84. Screen electrode, after test.

M10076

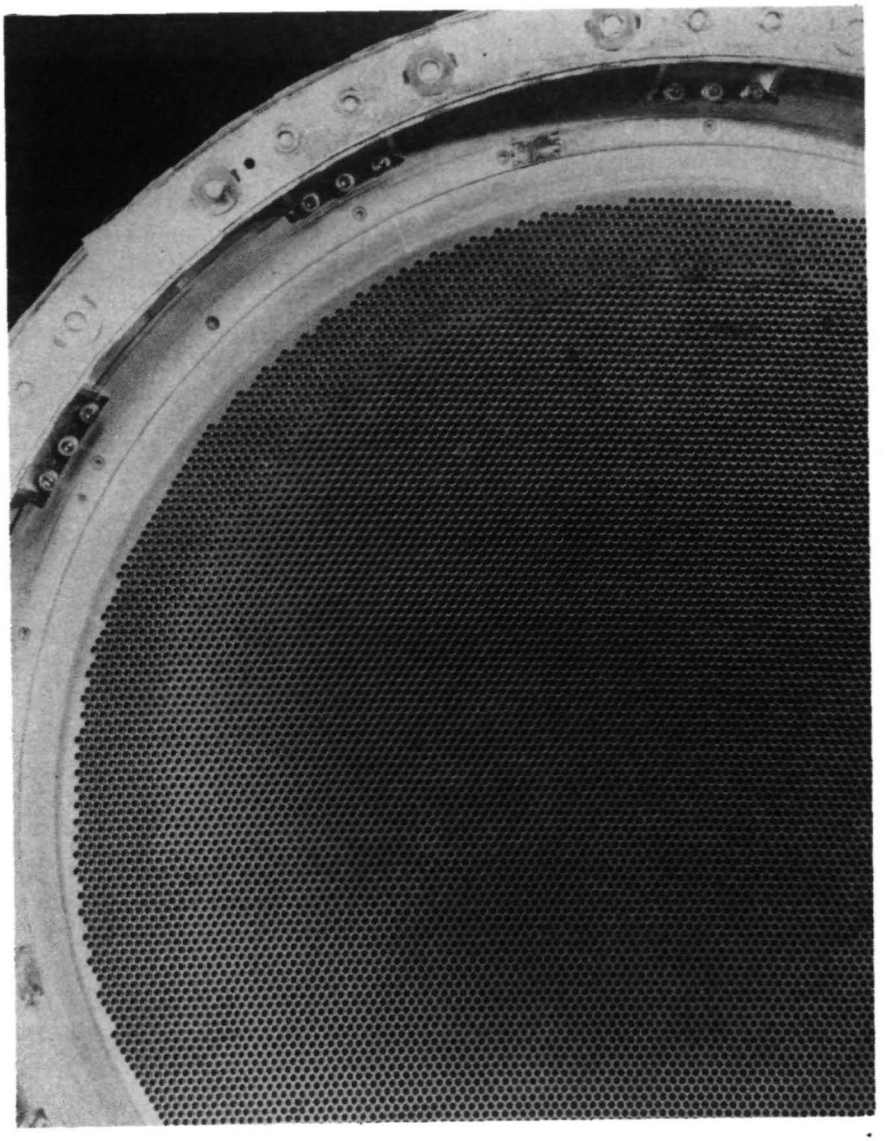

Figure A-85. Screen electrode, before test.

M11062 4893-264

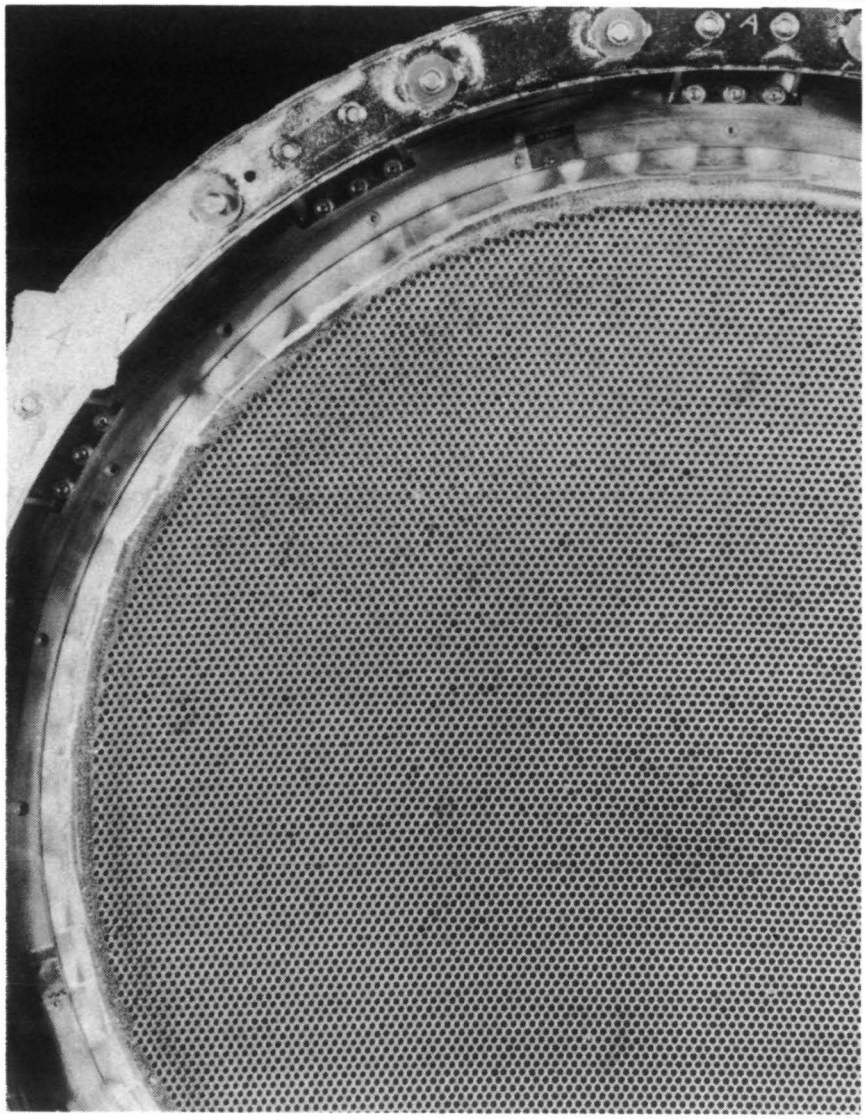

Figure A-86. Screen electrode, after test.

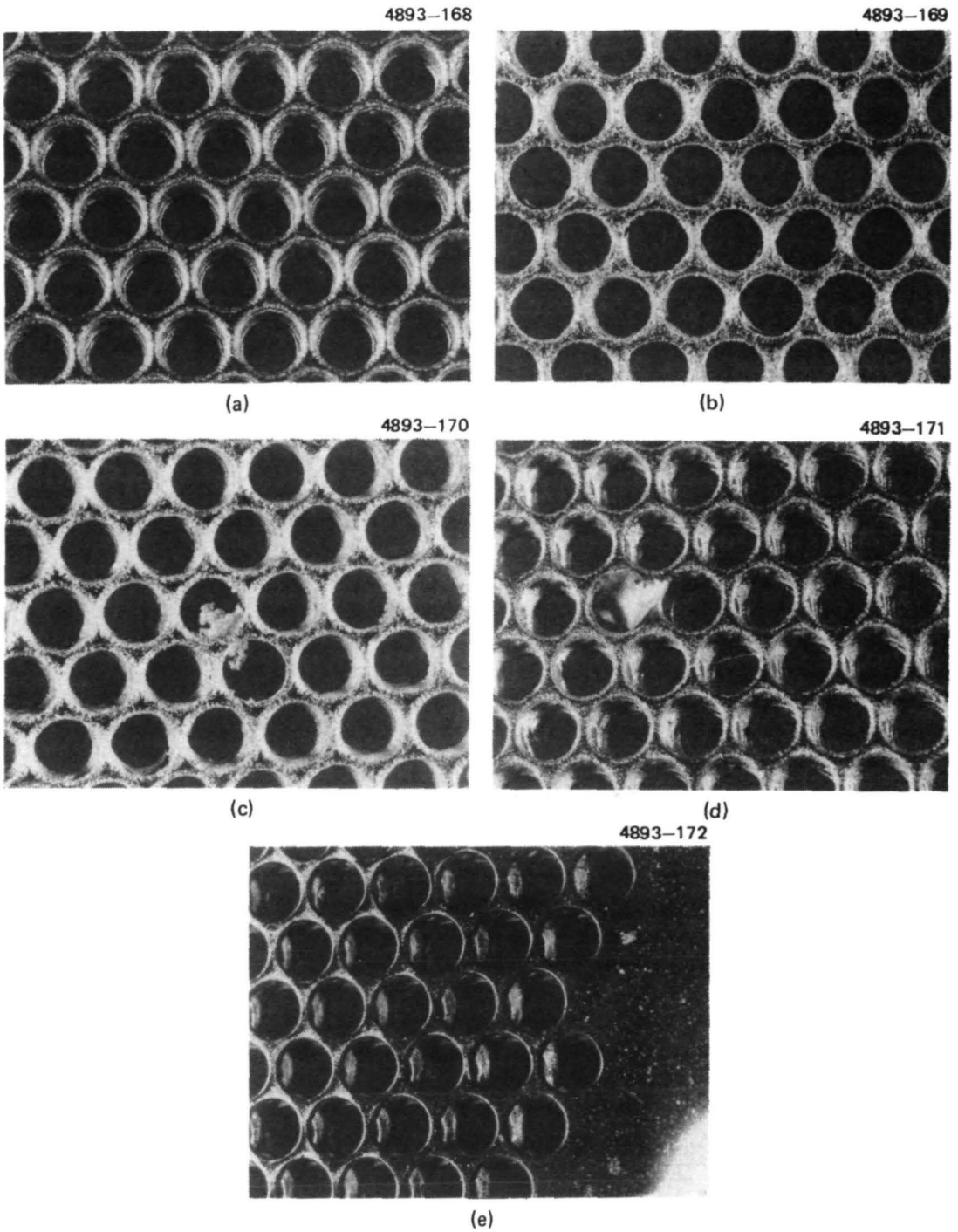

Figure A-87. Selected areas of upstream side of screen electrode.

chamfering is not present near the electrode edge. Figure A-87(c) and (d) are located about mid radius and show residual flakes on the grid. It was thought at first that the screen grid electrode apertures were slightly enlarged nearer the center of the grid. Table A-10 gives measurements of the aperture diameters for the endurance test screen grid electrode. It is apparent that most apertures are smaller than the nominal 0.075 in. (0.191 cm) dimension specified by the design.

Table A-10.

Screen Grid Electrode Aperture Diameters Measured Along Several Radii of Endurance Test Grid SN 648				
Radius in.	Aperture Diameter[A] in. x 10^3			
0	74	—	—	—
1	75	76	74	76
2	72	73	72	74
3	73	73	73	73
4	72	75	73	72
5	73	72	73	73
(A) Print Specifies 75 ±1 x 10^{-3} in.				

T1859

Measurement of the electrode thickness showed the grid to be appreciably eroded and reduced in thickness nearer the center as documented in Fig. A-88. Measurements were performed using the same technique on a slightly used electrode (SN 645) which had been fabricated from the same material lot during the same time period as the endurance test electrode; these values are included in Fig. A-88 for comparison. The erosion seen, like that of the cathode pole piece and baffle, is thought to be a consequence of ion sputtering, predominantly by doubly charged ions. Figure A-89 shows unequivocally the extent of this erosion by comparing cross sections removed from the edge of the grid, in view (a), with several others taken from the center of the grid (views b, c, and d). The minimum thickness of the section shown in Fig. A-89(d) is only about 0.006 in (0.015 cm) thick as compared to the 0.010 in. minimum thickness shown in Fig. A-88 (measured with micrometer). The difference in these values can be explained by the depression seen in view (d) and a coating on the downstream side of the grid that is about 0.001 in. thick. The coating on the downstream side of the screen grid electrode is readily seen in the magnified views shown in Fig. A-90. Figure A-90 also presents the electron beam microprobe scans which identify the elements composing the deposited layer. The molybdenum, iron, chromium, and mercury are expected constituents, while the silicon, aluminum, and potassium originate in the glass used as a "potting" agent (to maintain sharp edges of the sectional sample). The origin of the barium and the chlorine is uncertain, however. Photographs of the entire downstream surface of the screen grid electrode are shown as Figs. A-91 through A-95. It is difficult to see any flakes or deposition in these photographs without magnification. Figure A-96 shows magnified views of what can be seen over the grid surface. Most of the electrode appears as shown in view (a) with a few "patchy" areas like the one shown in view (b). The electrode surface was examined for evidence of arcs, as was done with the accel, but the only marking found that has the appearance of damage caused by clearing a metallic flake is shown as view (c), (circled area). As a consequence of this relatively complete absence of grid damage like that

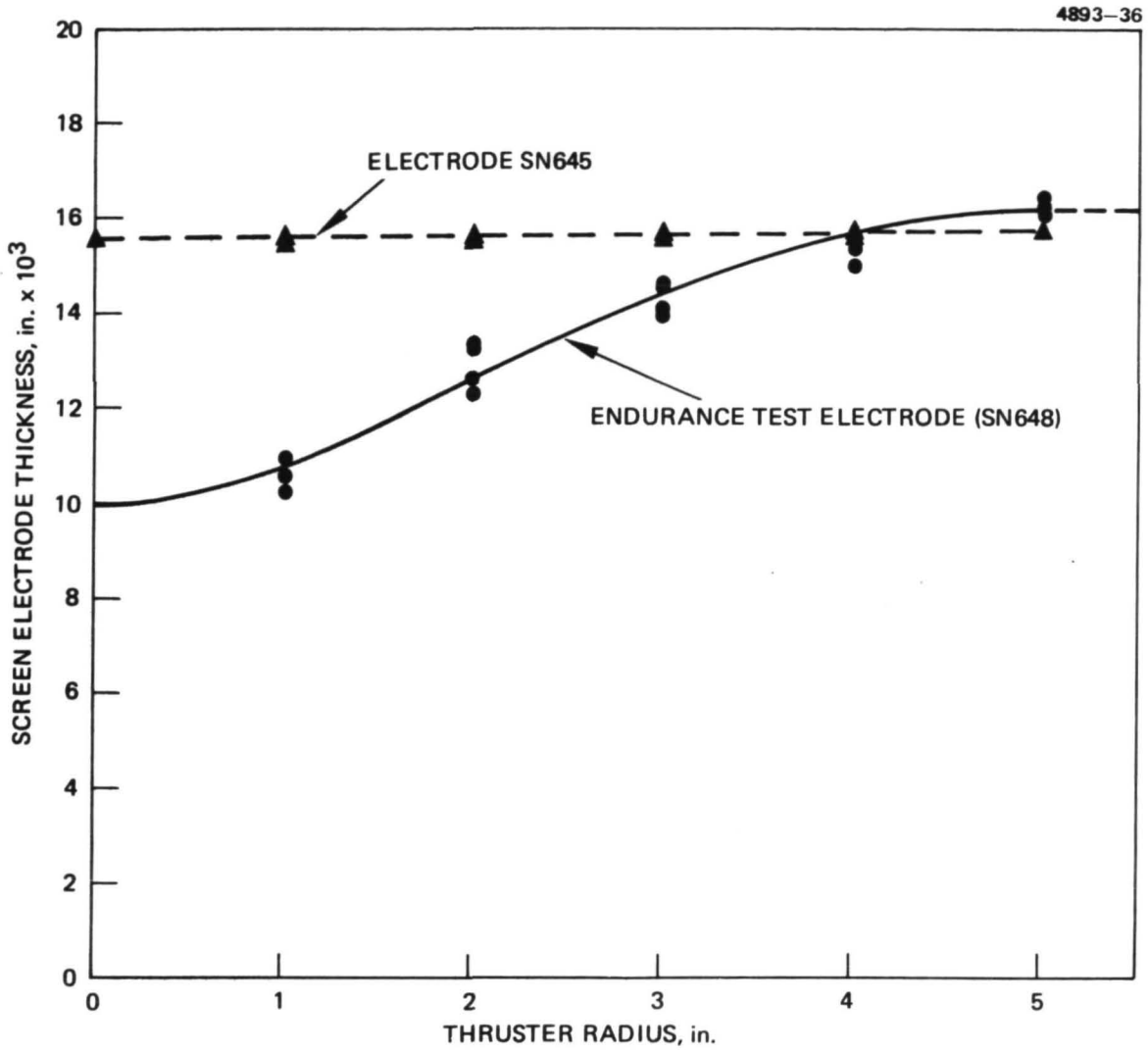

Figure A-88. Comparison of screen electrode thickness vs thruster radius for endurance test electrode (SN648) after 10,000 hours operation and slightly used screen electrode (SN645).

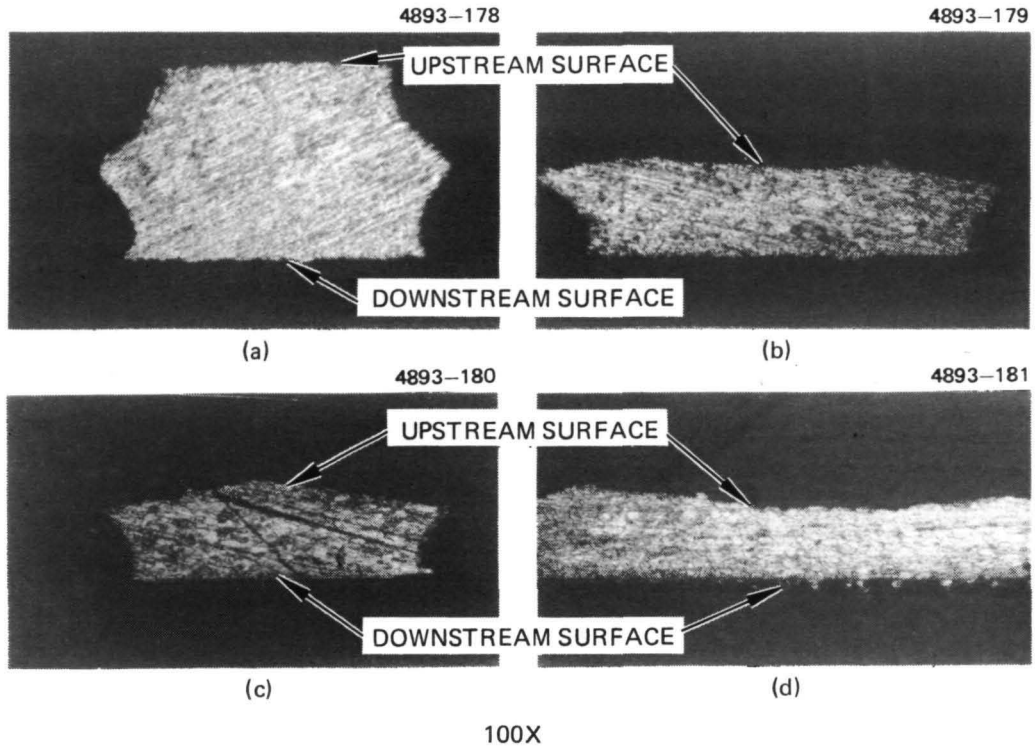

Figure A-89. Cross sections of screen electrode (a) edge of electrode; (b), (c), and (d) center of electrode.

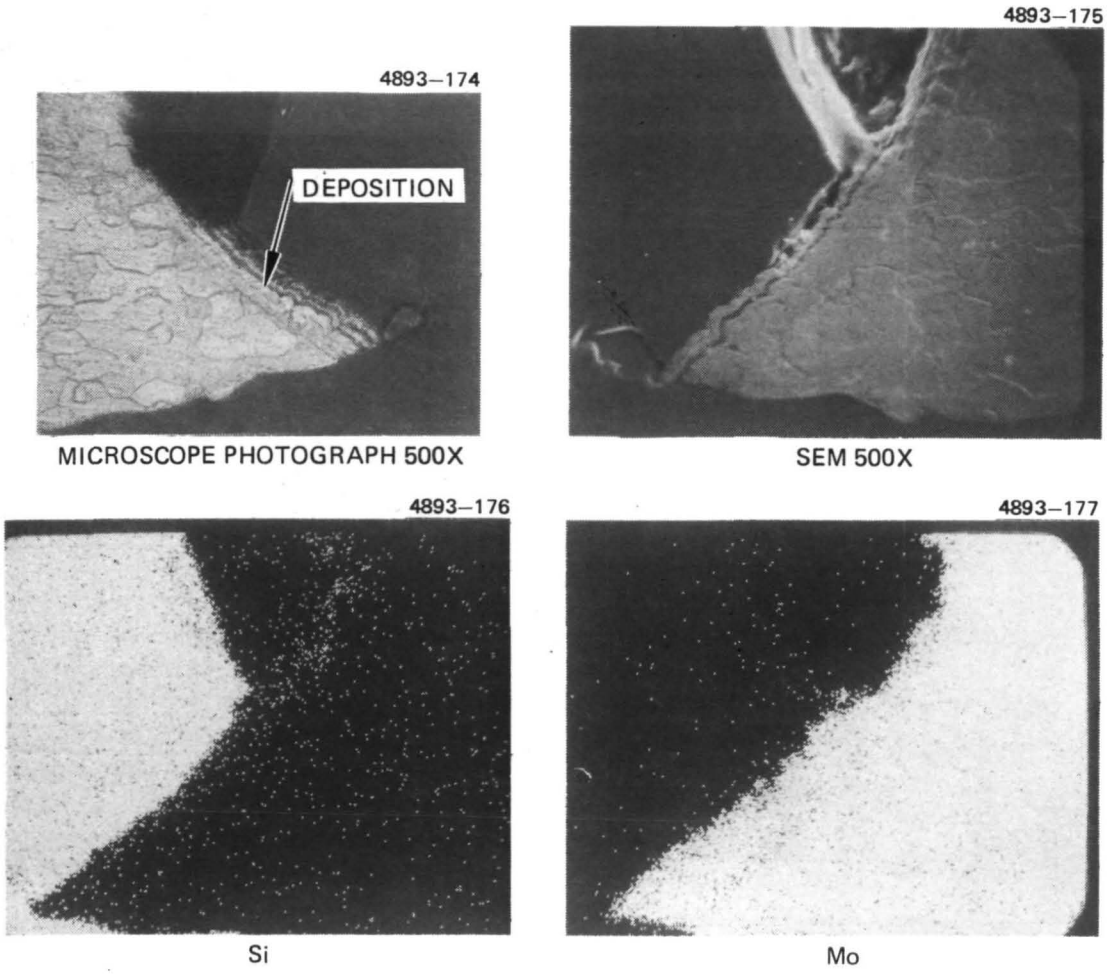

Figure A-90. Microscope photo, SEM photo, and E-beam microprobe analysis of screen electrode downstream coating.

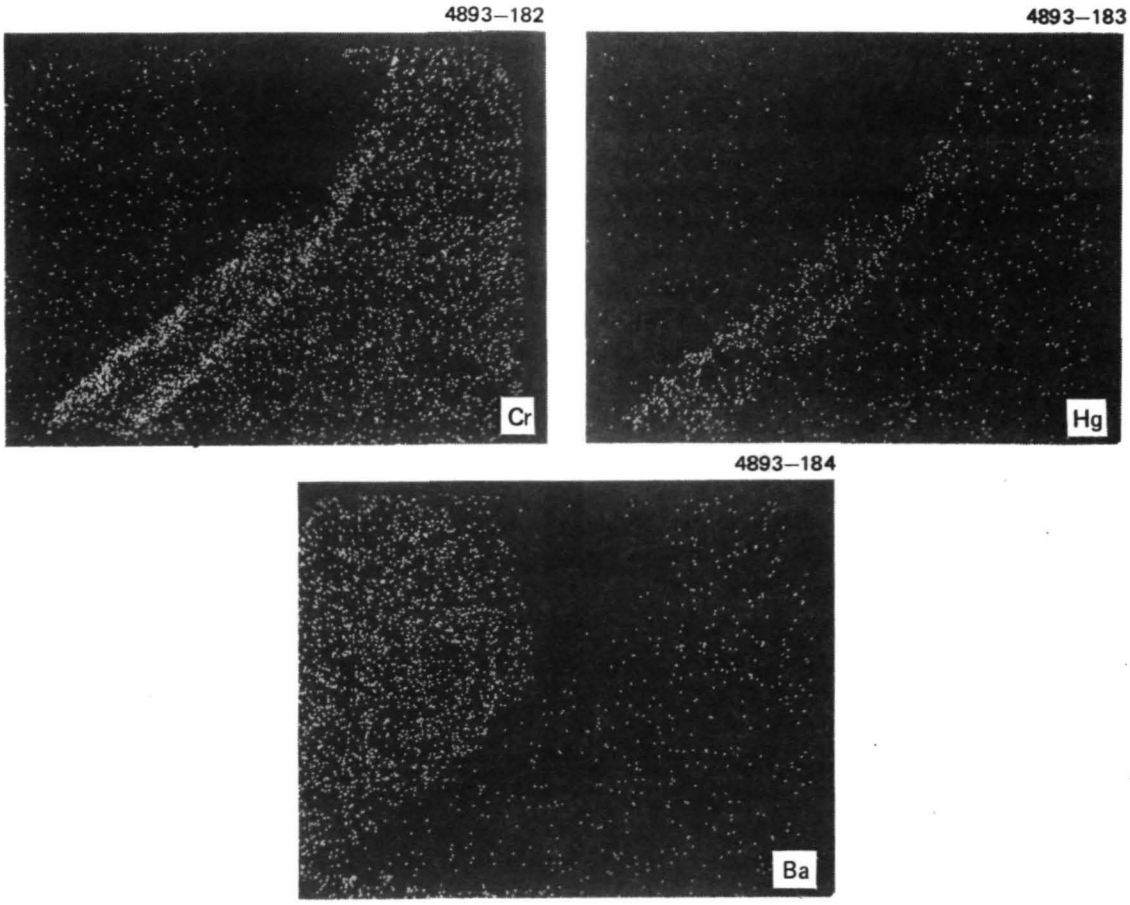

Figure A-90. Continued.

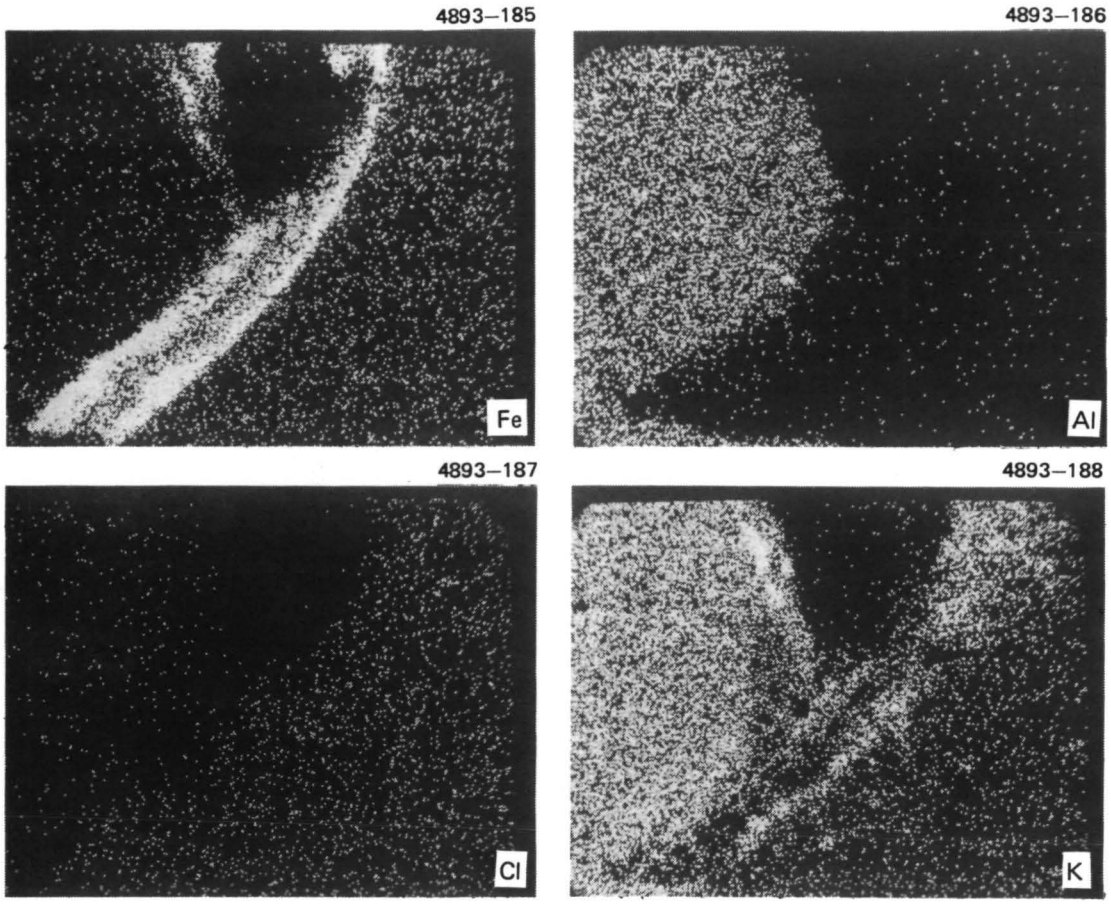

Figure A-90. Continued.

M11162

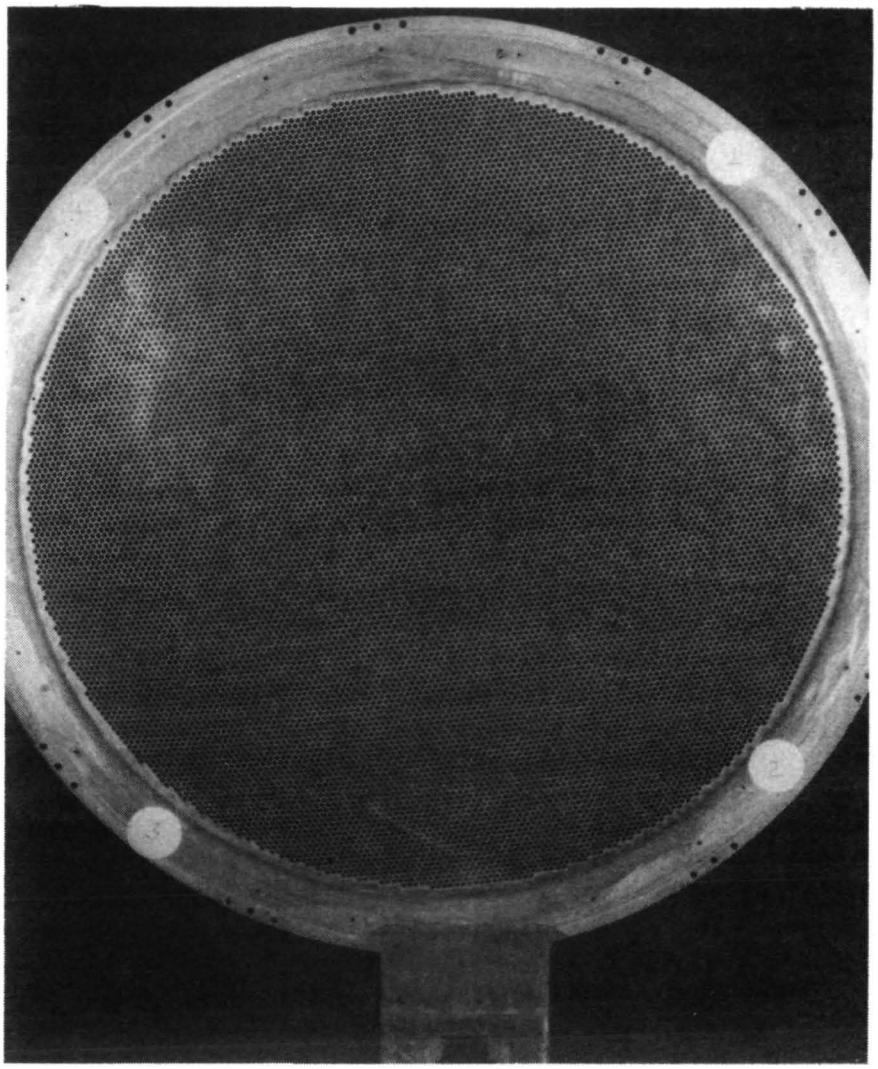

Figure A-91. Screen electrode, downstream side.

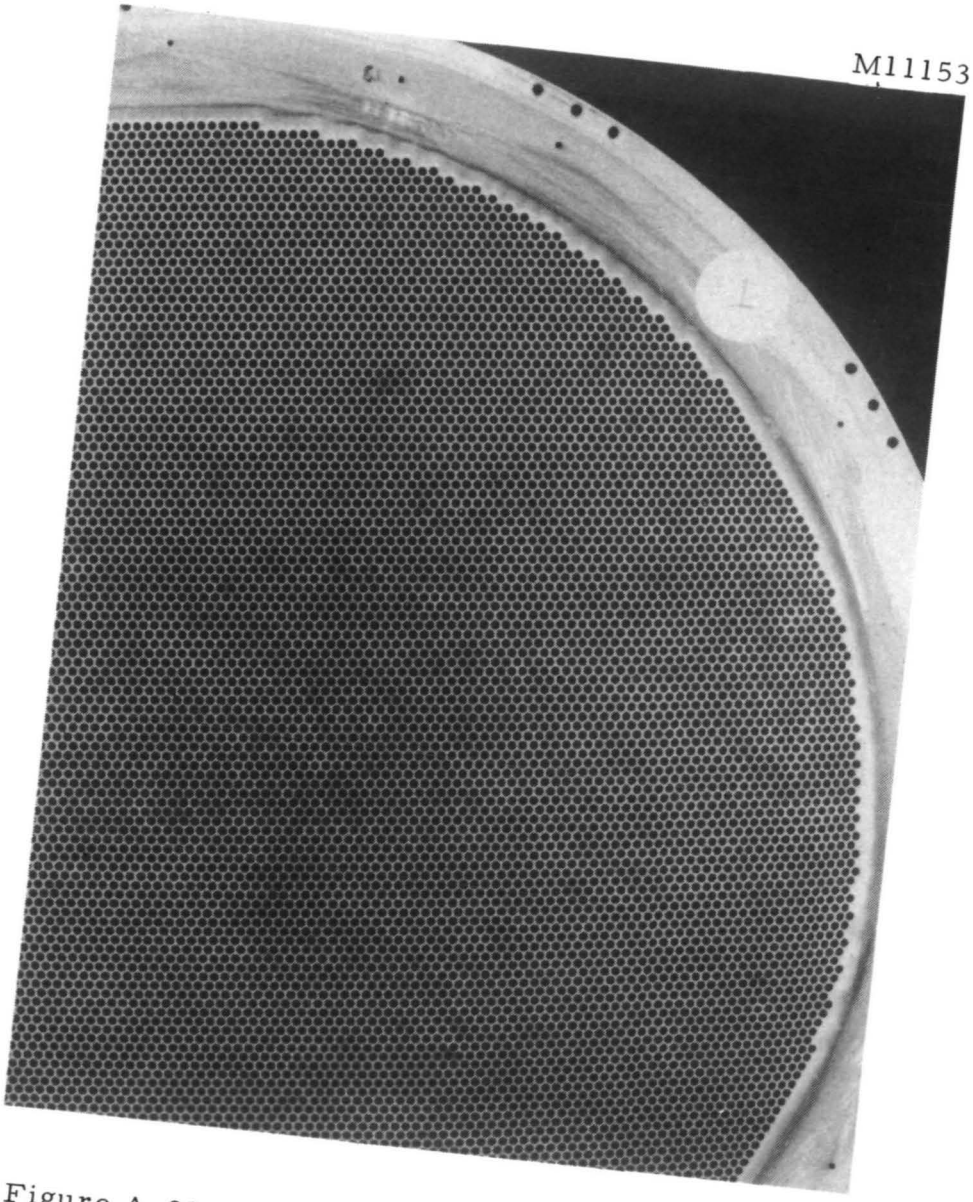

Figure A-92. Screen electrode, downstream side.

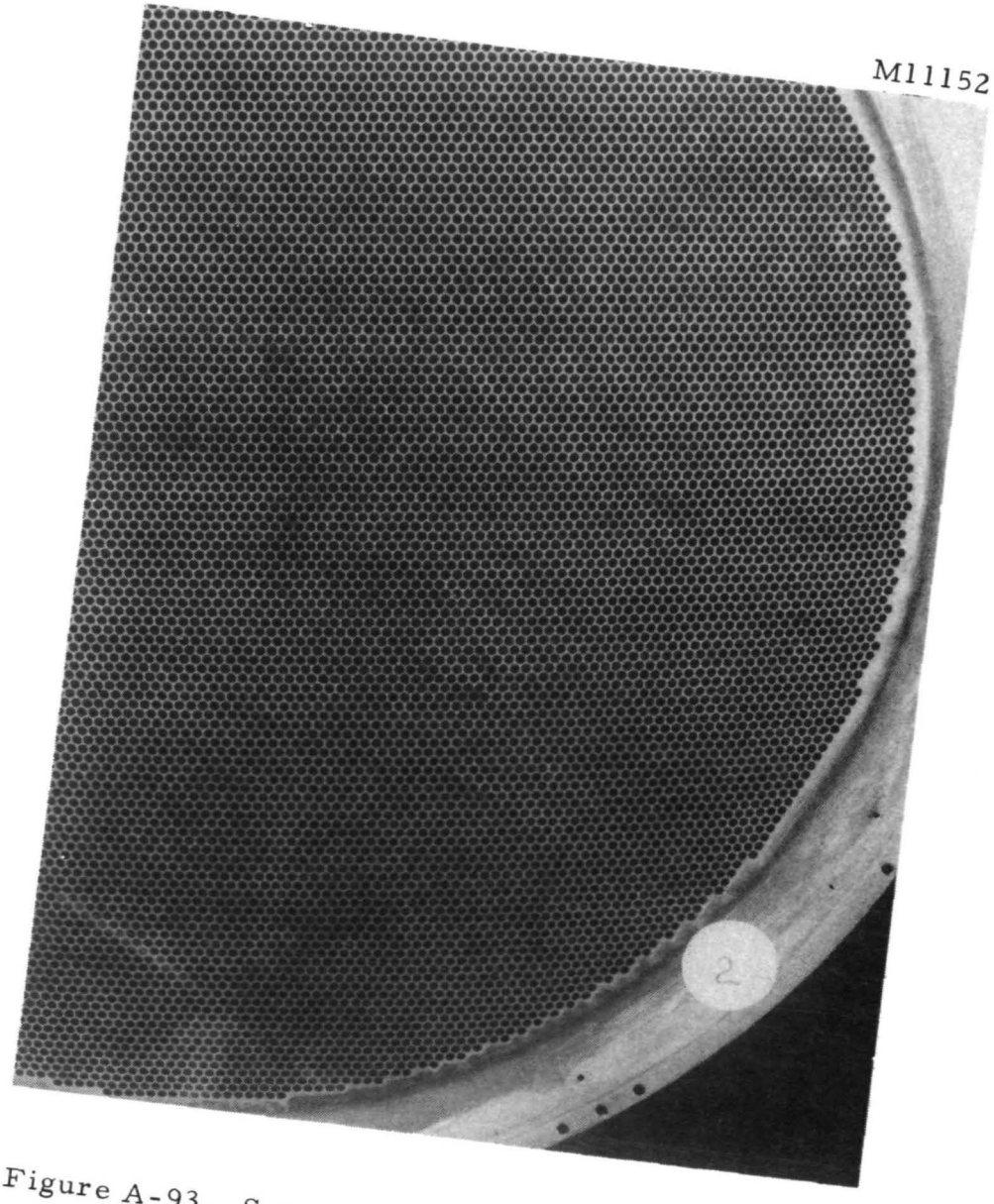

Figure A-93. Screen electrode, downstream side.

M11151

Figure A-94. Screen electrode, downstream side.

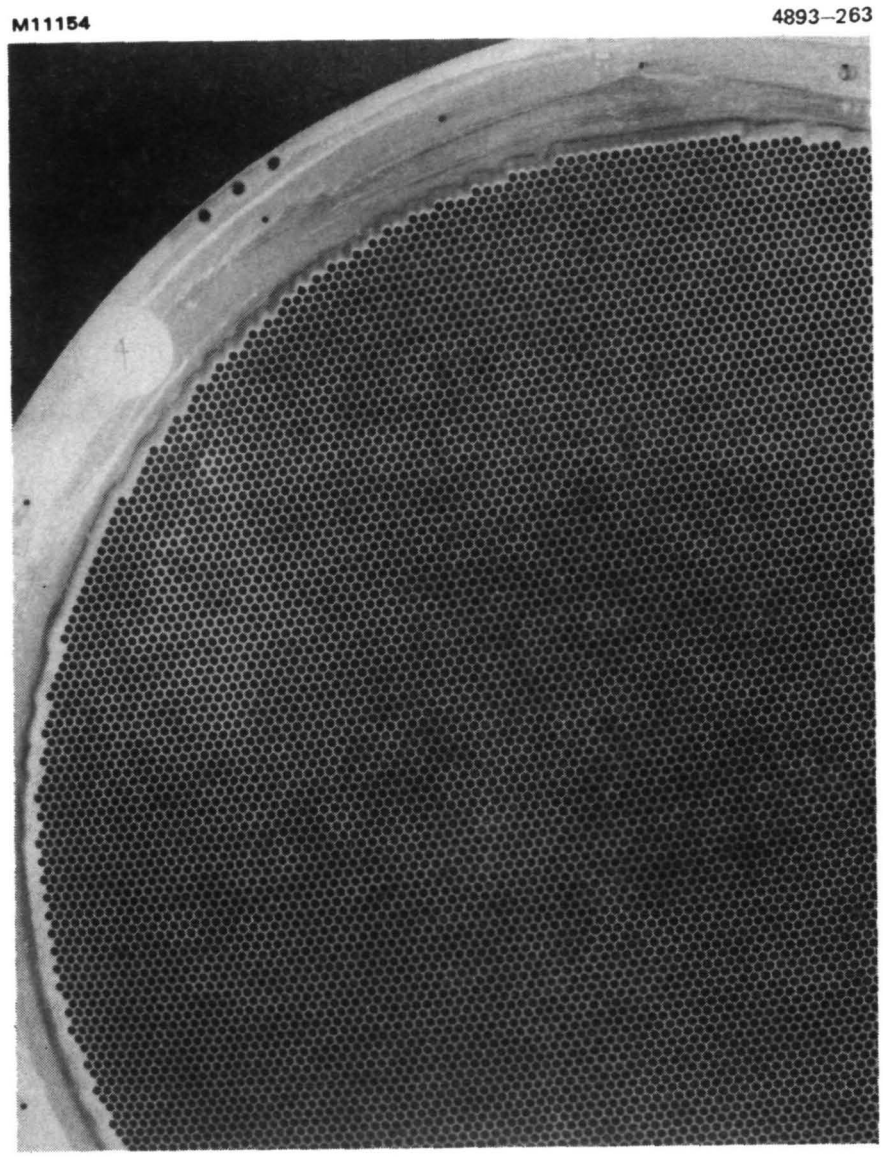

Figure A-95. Screen electrode, downstream side.

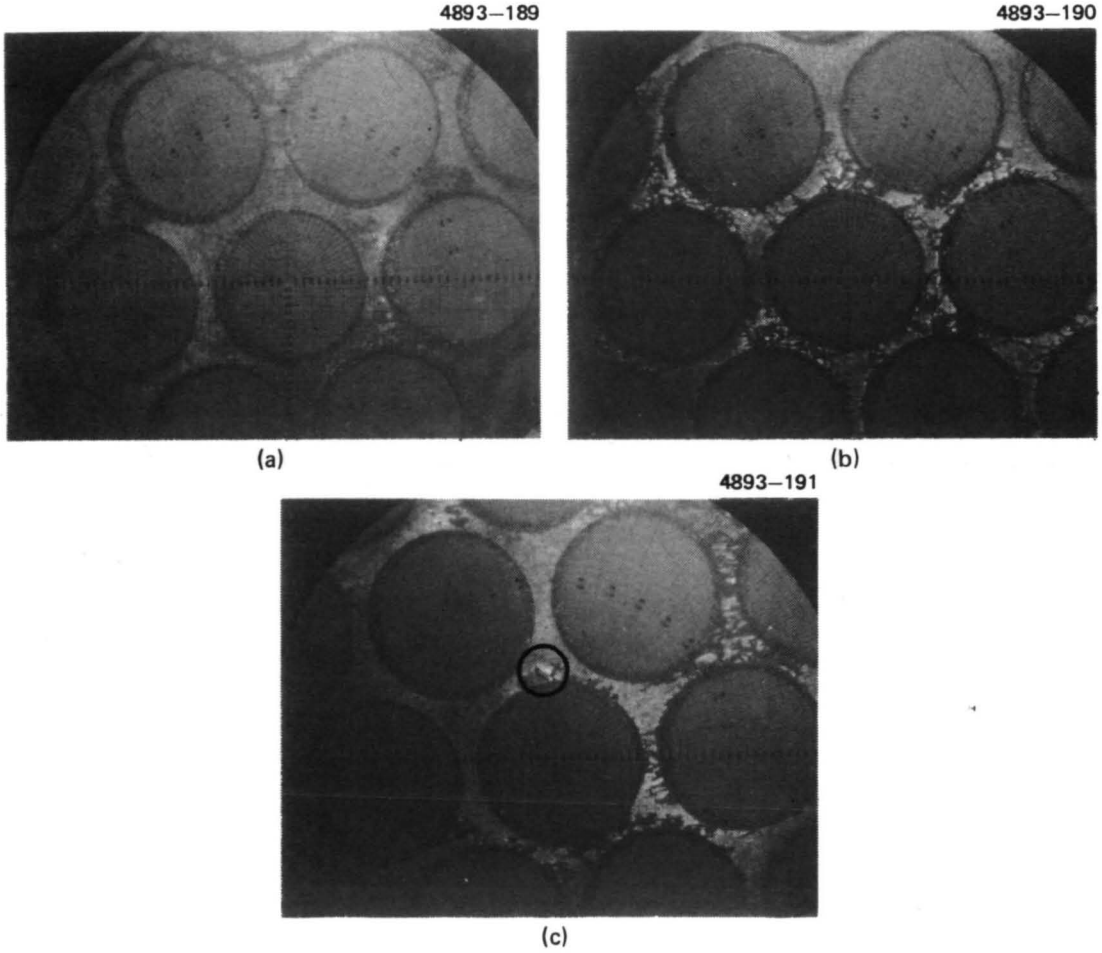

Figure A-96. Magnified view of selected areas of downstream surface of screen electrode.

usually caused when metallic shorts are removed by capacitive discharge, it is concluded that insignificant damage is caused by discharging a 1 μF capacitor charged to beam voltage (0.6 J) through a metllic grid short.

The ion optics electrode support structure used in this test has been replaced by a design that can be fabricated more readily. Consequently, only a few observations are commented on here. The primary purpose of this structure is to maintain a stable, uniform separation of the electrodes, establishing a voltage insulation to at least 2 kV. This structure demonstrated this property very well. One cause for concern is a series of markings seen on the insulator shields. These markings can be seen in Figs. A-97 through A-100 (arrows). Although there is no real damage seen, it has not been possible to offer a convincing explanation of the origin of these marks. Presumably, the markings have been made by ions accelerated to these accelerator potential surfaces. It is possible that they were made during early testing before the installation of the tantalum gasket that prevents a direct path from the discharge chamber to these surfaces. If this is not the case, then some ion "leakage" from the discharge may still be occurring. The design of the support assembly which replaces the assembly tested here should eliminate most possible paths (unless the ions leak out between the optics electrodes).

The final figure presented in this section shows the support assembly with the grids removed (see Fig. A-101). Note the pristine condition of the insulators. It would be impossible to differentiate this assembly from one that had been tested only a few hours.

In summarizing this section on the ion optics assembly, the following major conclusions can be drawn:

- There is no evidence of excess charge exchange ion erosion associated with the neutralizer.
- Charge exchange ion erosion of the accelerator is a secondary factor in life limitation.
- Screen grid erosion by discharge ions is a significant factor in thruster wearout lifetime.
- Grid damage by sparks from metallic shorts is not a serious concern.

M11072 4893–192

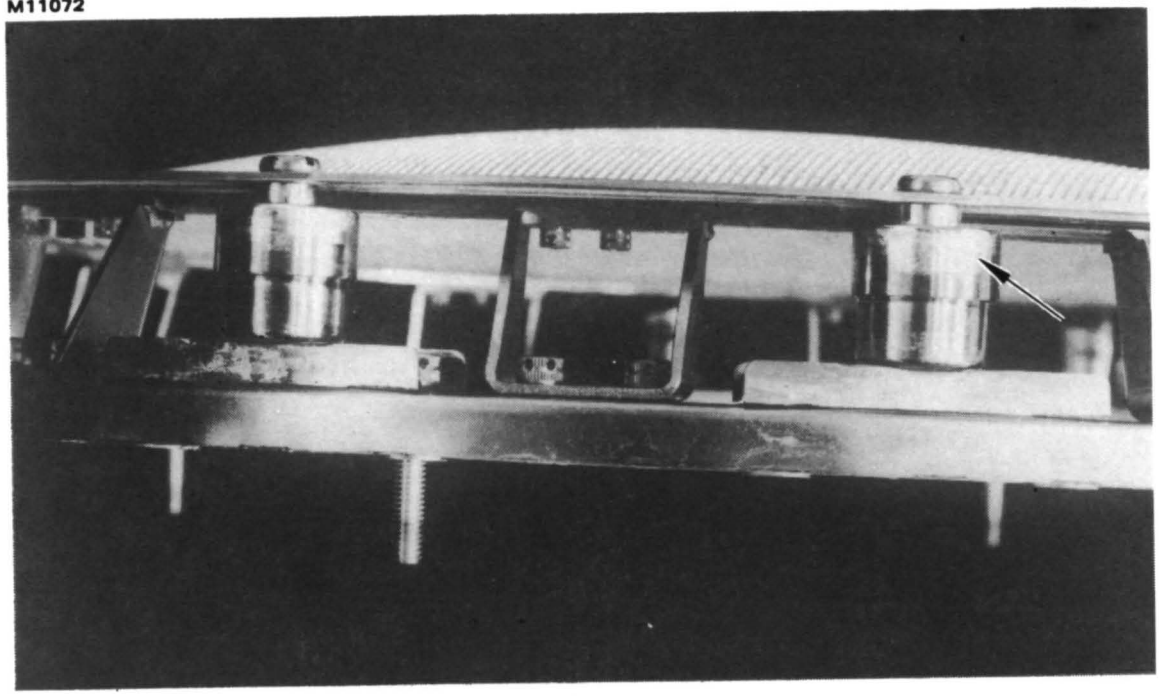

Figure A-97. Optics showing markings on insulator shields.

M11071 4893–193

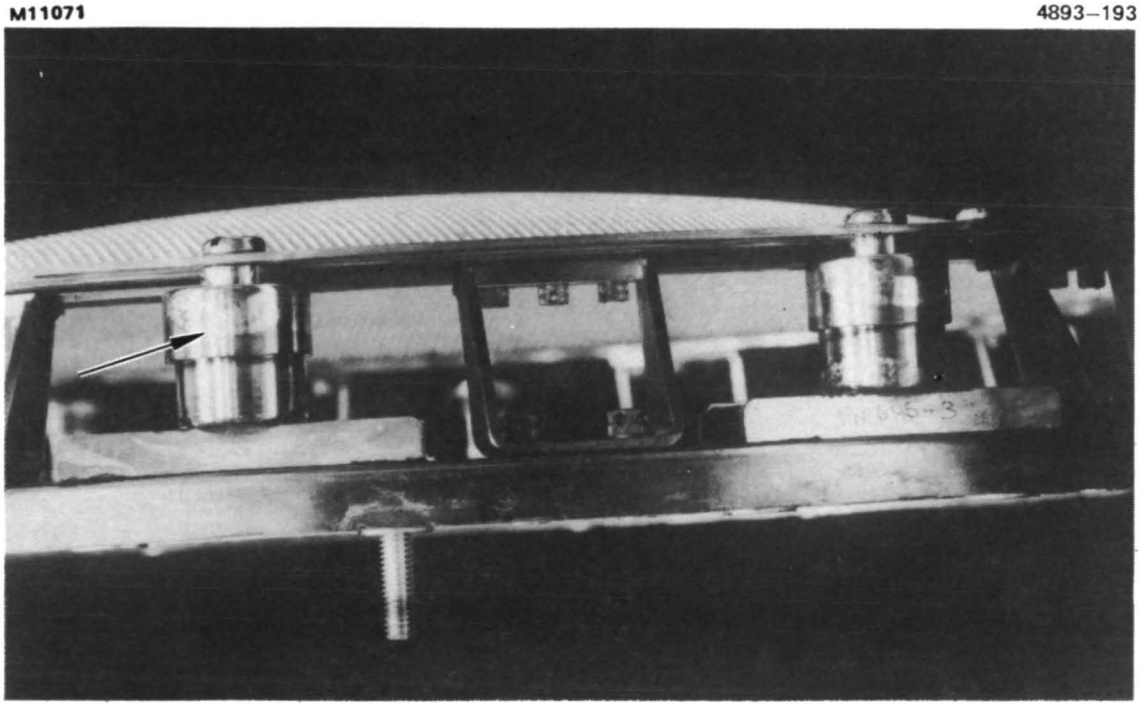

Figure A-98. Optics showing markings on insulator shields.

M10070 4893–195

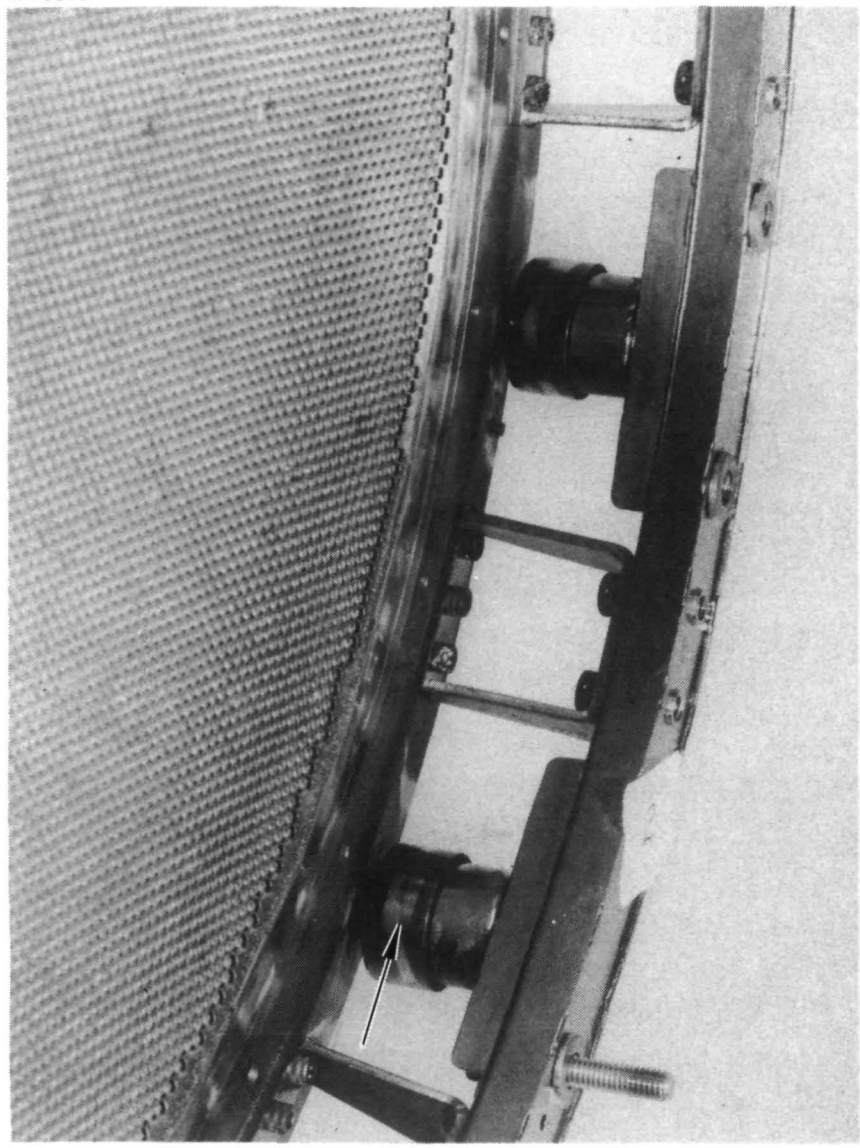

Figure A-99. Markings on optics insulator shields.

M11069 4893–194

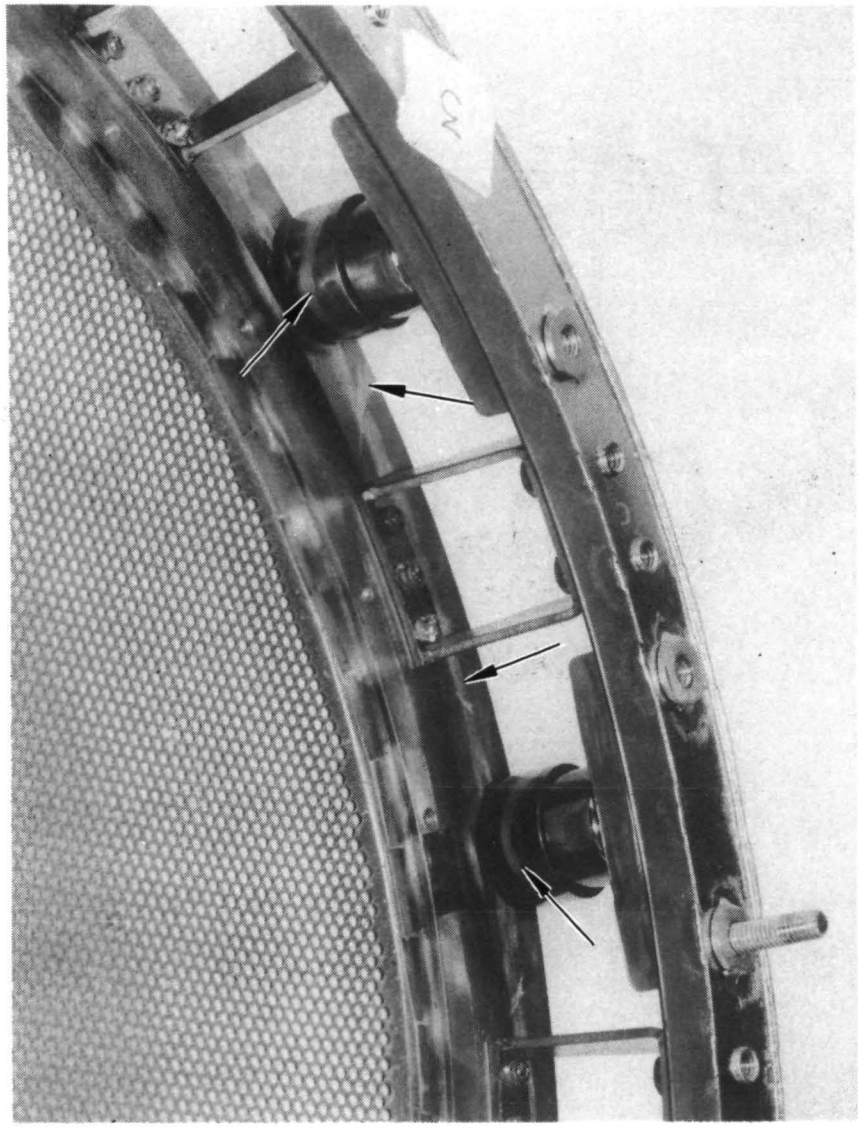

Figure A-100. Markings on optics insulator shields.

M11157

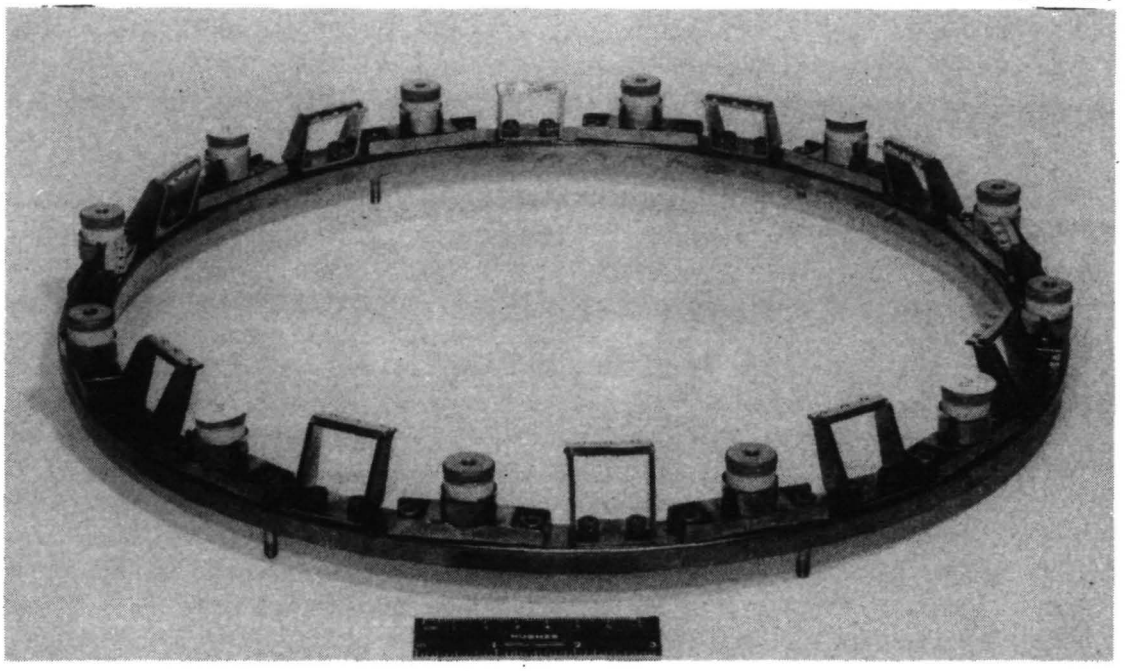

Figure A-101. Optics support assembly.

- Coating formation on the screen grid electrode (downstream side) may require special surface treatment of the electrode.

E. Neutralizer Assembly

Two neutralizer assemblies were mounted on thruster SN 701 during the 10,000 hour test but only one, SN 701, was operated as a part of the test. The other neutralizer, SN 415, was included as a back-up and was operated only for brief intervals both before and after the test to demonstrate that it was capable of operation. The components of the neutralizer that are of interest in this discussion are

- The outer covering
- The keeper electrode
- The keeper and NIV support insulation
- Electrical wiring and terminals
- The neutralizer isolator vaporizer subassembly (NIV).

Figures A-102 and A-103 show the portions of the neutralizer SN 701 outer covering that is of interest here. Note that there is no evidence of deposition and that the keeper cover is in fact eroded away at the downstream most inboard surface. In contrast to this, Fig. A-104 shows that several surfaces of the neutralizer SN 415 outer cover are coated with both metallic deposits and finely divided mercury. Thus it appears that the active neutralizer is eroded while the inactive neutralizer has accumulated deposits. Figure A-105 compares dimensional parameters for the two neutralizers. Energetic ions with trajectories at angles up to 75° have been measured under the 2.5 kW Advanced Technology Ion Thruster Program (NAS 3-17831) and simulated by trajectory computations through variations in the shape of the neutralization plane. Consequently, it is concluded that the presence of erosion on the active neutralizer is related to the shape of the neutralization plane in the vicinity of the active neutralizer. A more definitive explanation would require further study of the observed high angle ion trajectories.

M3-5A 4893-267

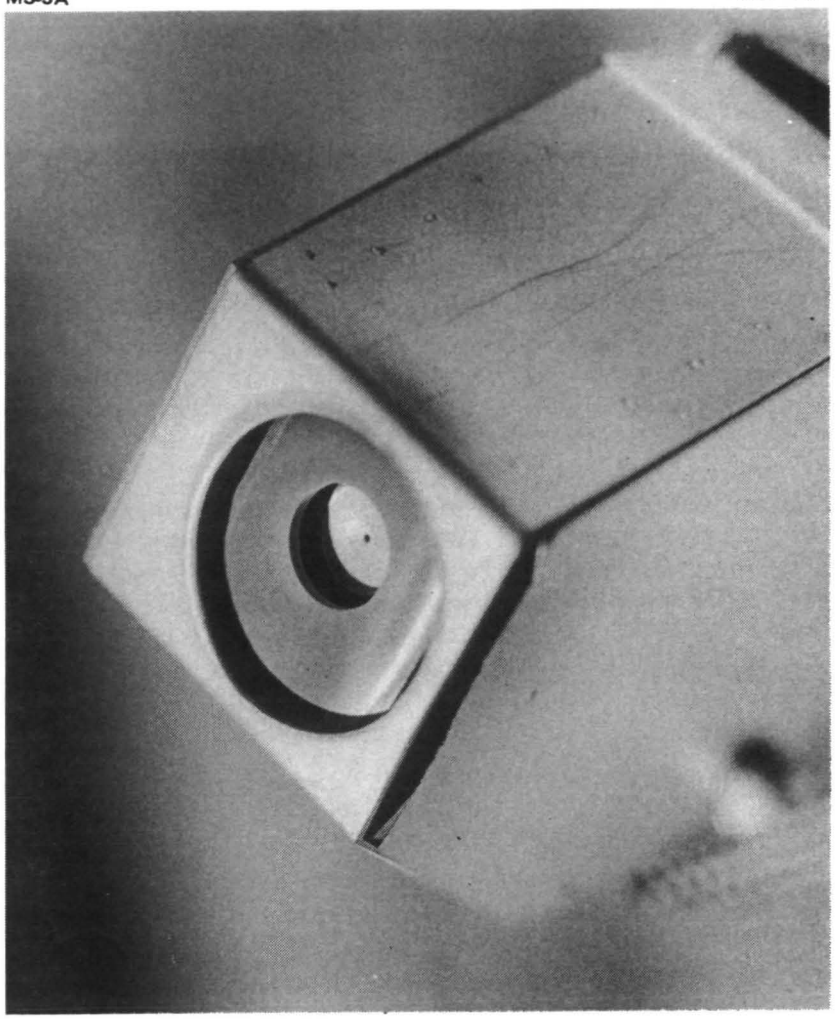

Figure A-102. Neutralizer 701 cover.

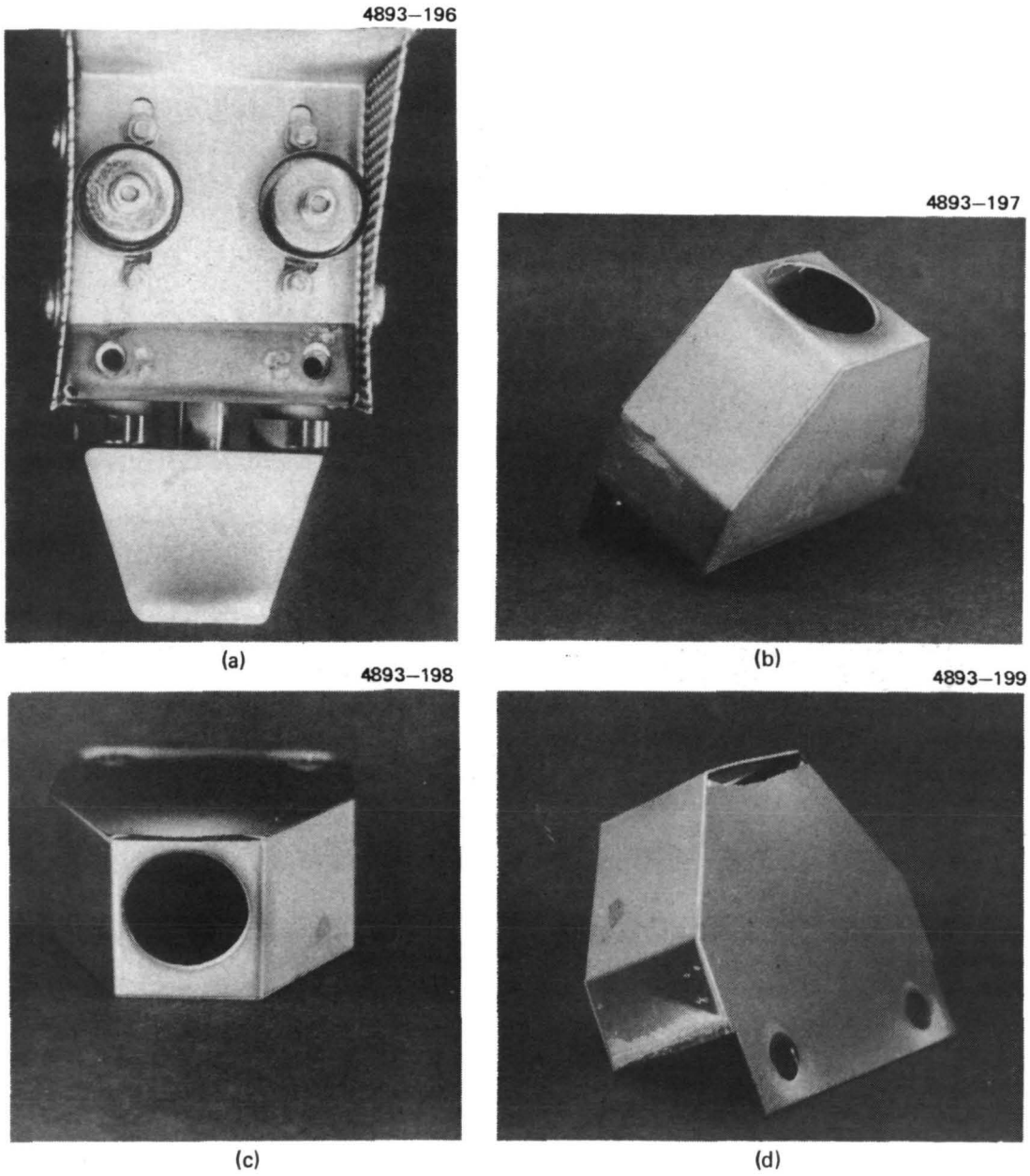

Figure A-103. Neutralizer 701 and keeper cover from neutralizer 701.

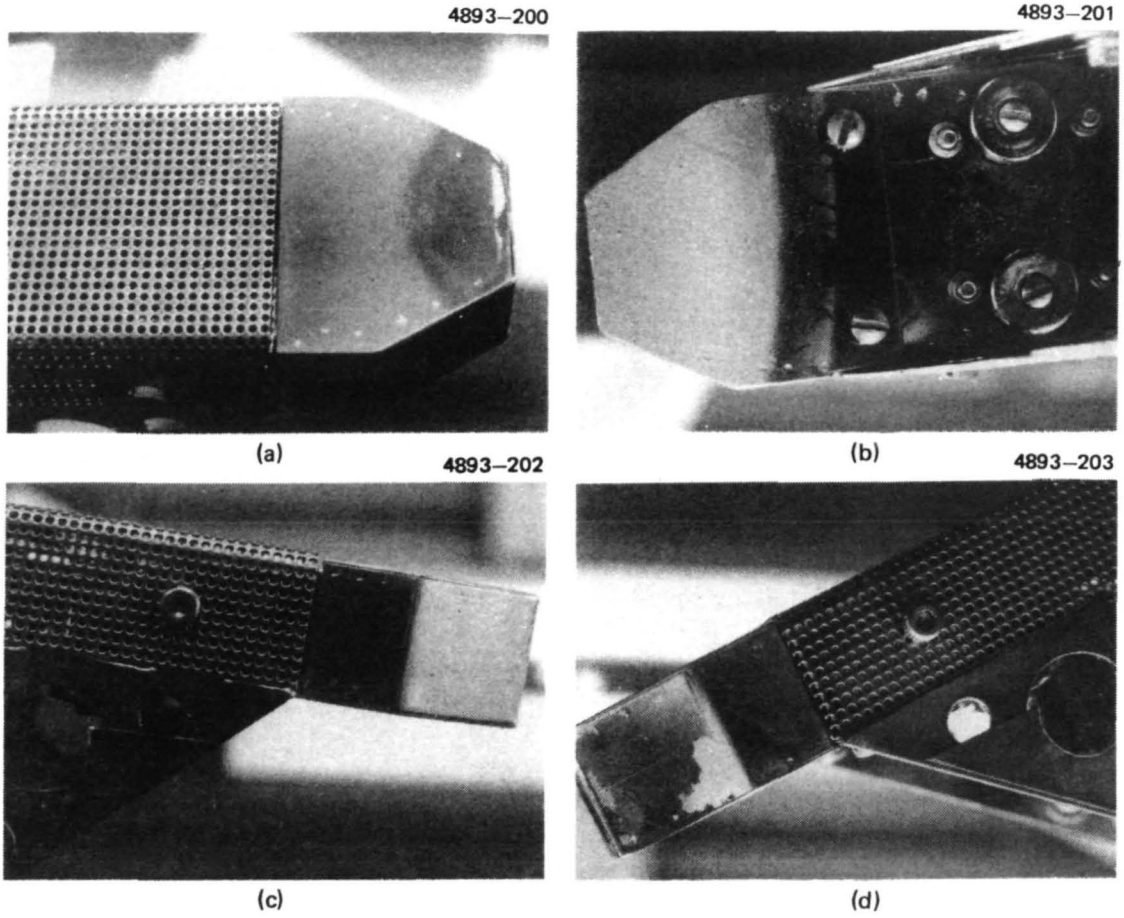

Figure A-104. Neutralizer 415.

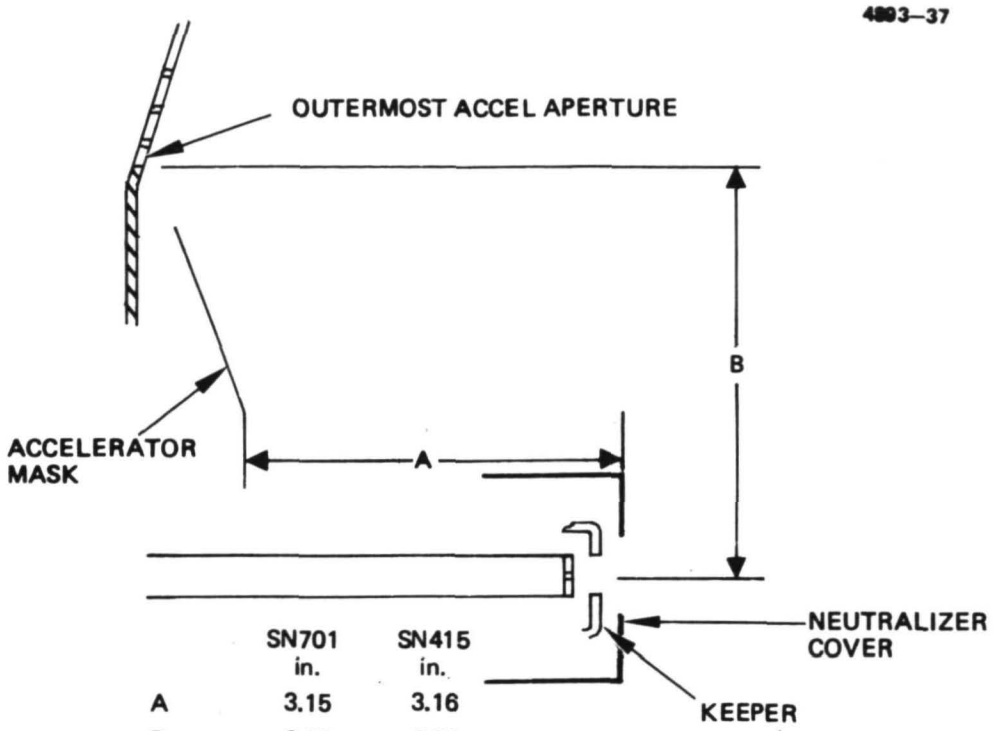

	SN701 in.	SN415 in.
A	3.15	3.16
B	3.25	3.25

a) NEUTRALIZER LOCATION

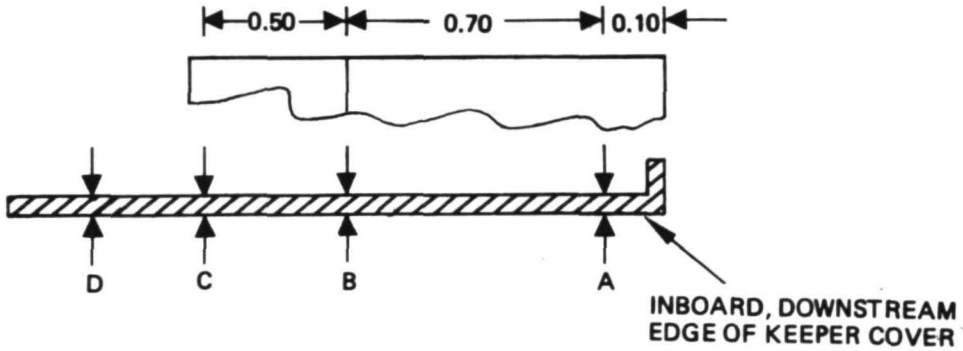

	SN701 in.	SN415 in.
A	0.004	0.018
B	0.017	0.019
C	0.019	0.020
D	0.023	0.022

b) NEUTRALIZER KEEPER COVER (SHIELD) CROSS SECTION DIMENSIONS

Figure A-105. Comparison of post test dimensions of neutralizers 701 and 415.

Figures A-106 and A-107 compare the appearance of the keeper electrodes on the active (SN 701) and reserve (SN 415) neutralizers. The SN 701 keeper electrode shows some discoloration on its exterior, but no substantial deposition such as that seen on SN 415. Both the weight and dimensions of the SN 701 keeper were unchanged (within measurement accuracy). Some copper colored deposition is also present on the inside of the SN 701 keeper electrode. This is thought to originate in the copper braze (now missing) of the tip heater support. A leakage resistance of 1 to 5 MΩ is present across the keeper support insulators for both assemblies. It is apparent in both Figs. A-107(a) and A-108(a) and (b) that the unshielded support insulator located inside the neutralizer housing has been coated over. Loosening of the fastener holding the keeper lead wire for neutralizer SN 701 increased the leakage resistance from 1 MΩ to greater than 2000 MΩ. In either case, the neutralizer keeper insulator leakage was not a source of difficulty during the test. The remaining discussion in this section relates to 700-series design components.

Figure A-108 shows neutralizer SN 701 with the outer covering removed. Note the deterioration of the wiring and the discoloration of the insulators. Figure A-109 shows matching discoloration on both the interior and exterior surfaces of the outer covering parts. It is apparent that at least parts of the discoloration has its origin inside the neutralizer cover, and, based on the decomposition seen in the wiring, the wiring insulation is a probable source. Thus, future designs should make better provision for routing polymide insulated wire such that high temperatures and consequently deterioration are avoided.

If the neutralizer is to be truly isolated from the spacecraft, then surfaces of the insulators that support the NIV, and the keeper electrode must be kept in good condition, in the same manner as the propellant isolator ceramics. Figure A-110 shows considerable darkening of the unshielded portions of all of these insulators. Note that the double-shielded portion of the support insulator, shown in Fig. A-110(d), is clean. The NIV isolator (Fig. A-110(a), (b)) had a leakage resistance of 5 MΩ as measured with all leads disconnected.

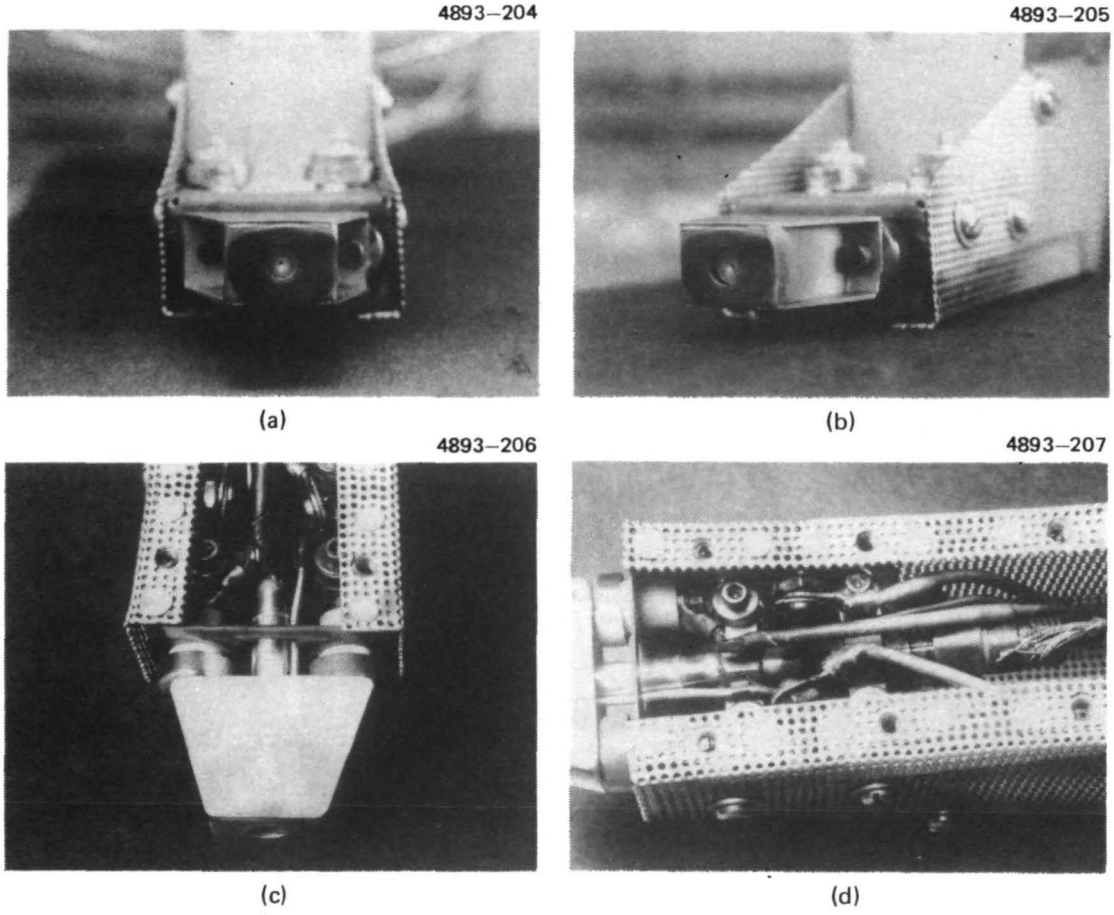

Figure A-106. Neutralizer 701.

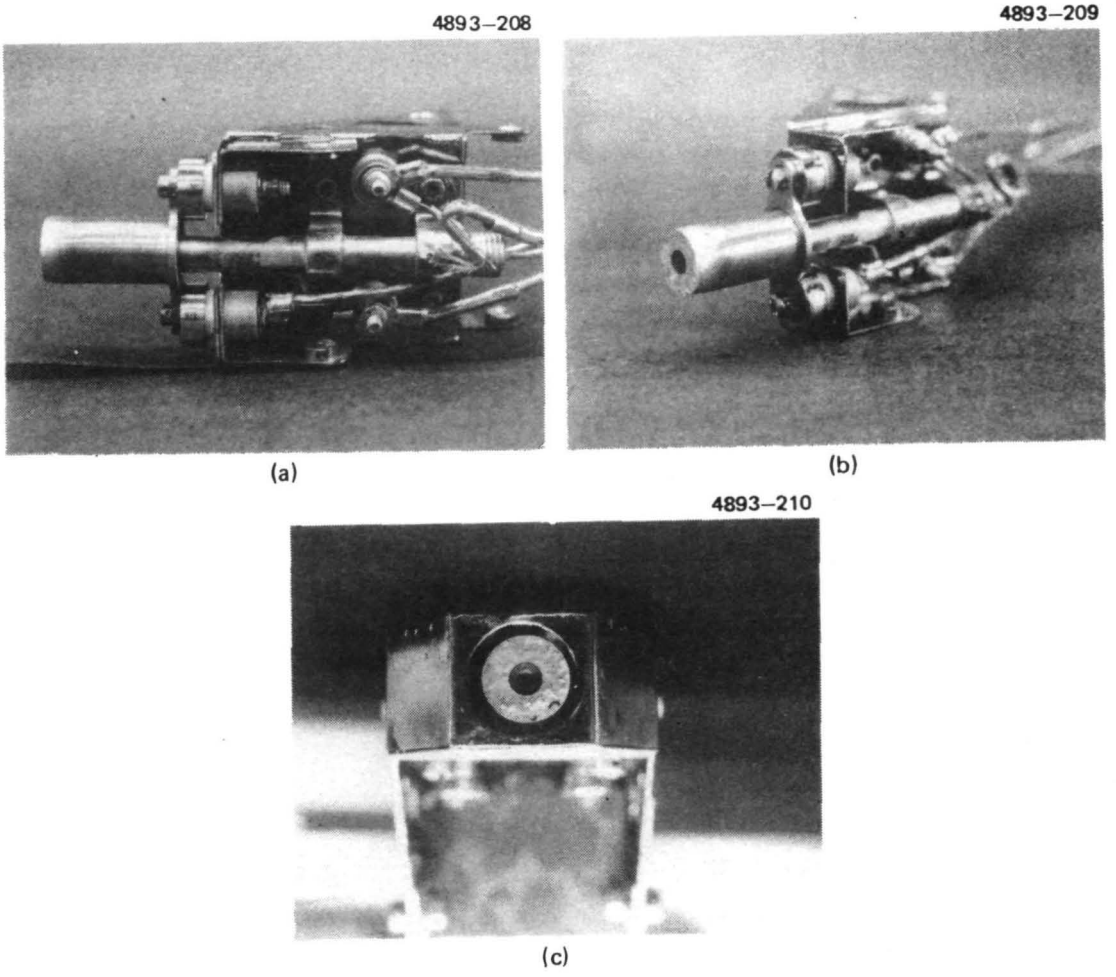

Figure A-107. Neutralizer 415.

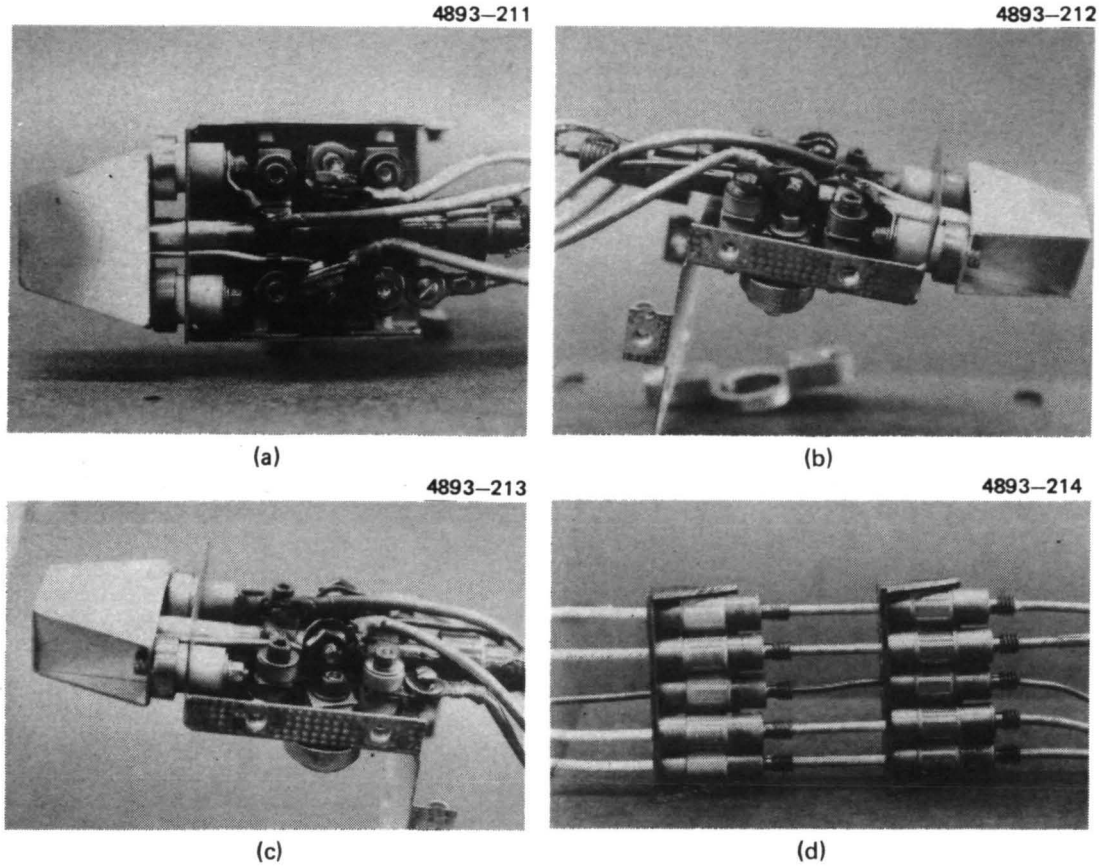

Figure A-108. Neutralizer 701.

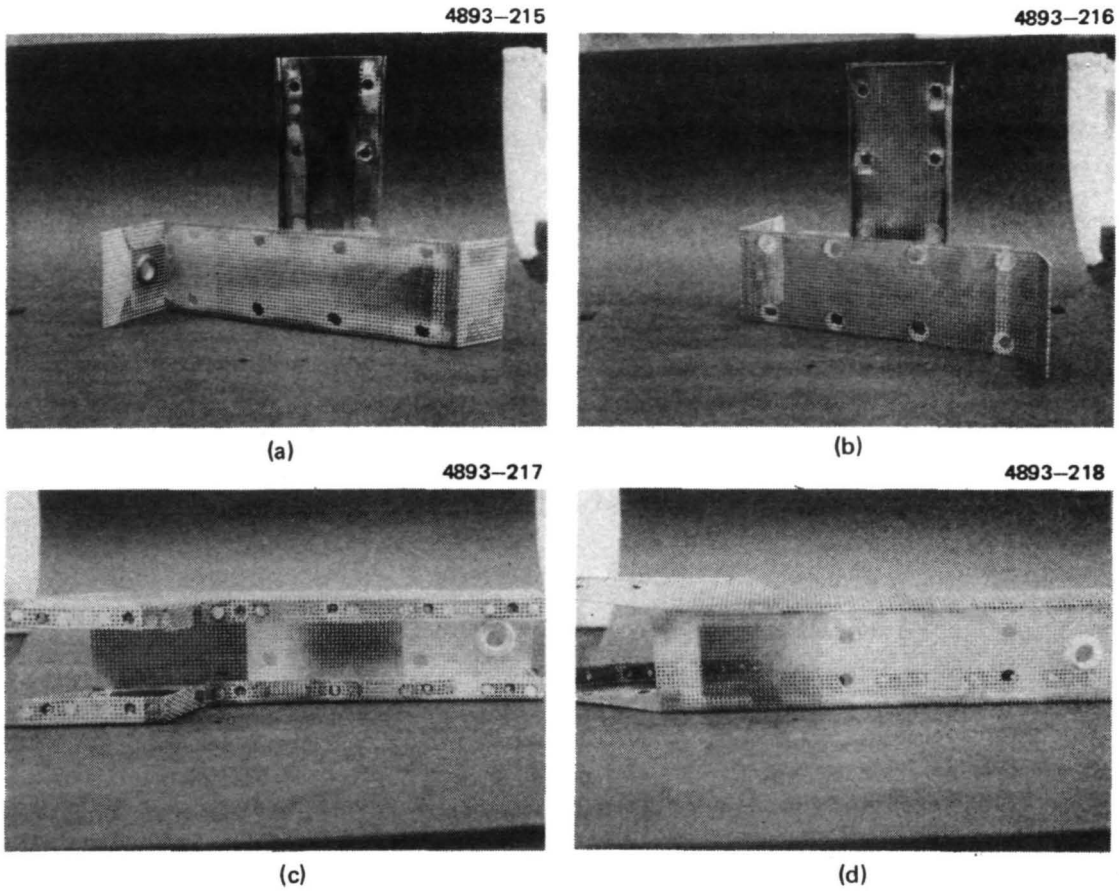

Figure A-109. Cover from neutralizer 701.

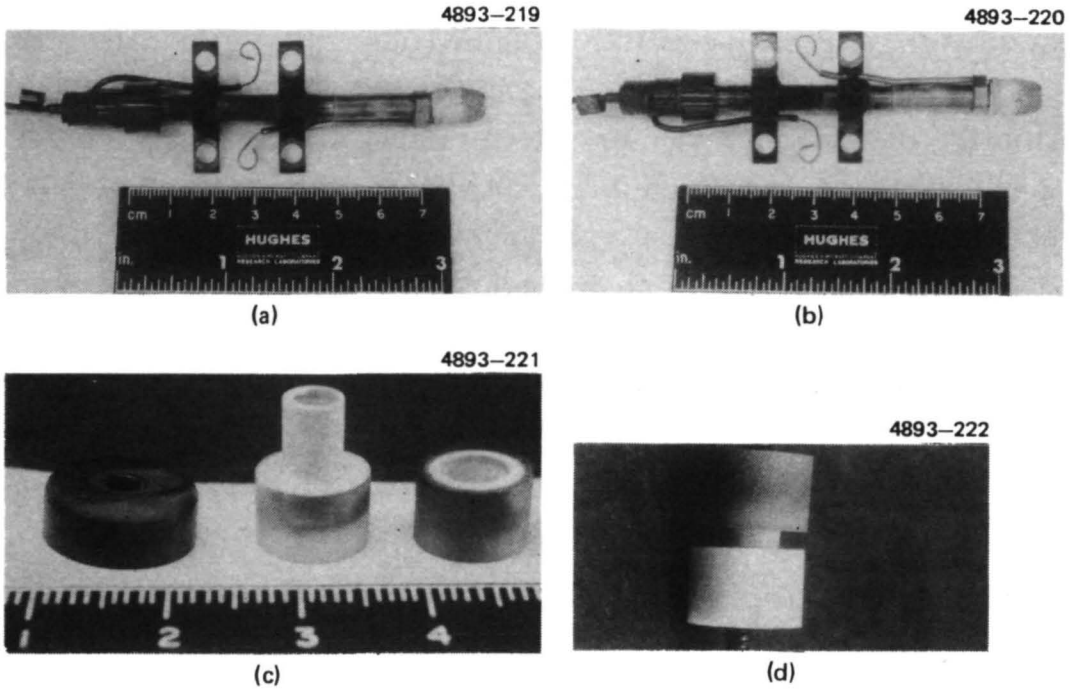

Figure A-110. (a) and (b) NIV 701; (c) and (d) neutralizer 701 keeper insulators.

The neutralizer assembly, as examined here, is considered to have no major wear problems. Erosion of the keeper cover would be corrected most efficiently by eliminating or reducing the high angle trajectory ion flux. Otherwise, increasing the thickness of the cover would suffice to compensate for the erosion. Insulator deterioration can be readily eliminated by shielding of the exposed ceramic surfaces. Although the cathodes are discussed in detail in the following section, it is appropriate to note here that neutralizer cathode wear is relatively insignificant. Some operational anomalies observed during the test have resulted in a design change for the cathode insert, however.

F. Discharge and Neutralizer Cathodes

The hollow cathodes which serve as the electron sources for the discharge chamber and the neutralizer are considered to be critical components in determining thruster lifetime. Satisfactory cathode operation depends on the properties of three major elements:

- Cathode orifice dimension
- Cathode insert
- Cathode tip heater.

Cathode orifice dimensions govern the internal mercury vapor pressure for a given flow rate and thereby control the operational characteristics. Small changes in dimensions are tolerable and do not significantly affect the overall performance or operational characteristics of either the discharge chamber or the neutralizer. Measurement of the discharge cathode orifice using wire gauges shows that the orifice diameter decreased slightly from 0.028 in. (0.071 cm) before testing to 0.026 in. (0.066 cm) after the test. Figure A-111(a) through (d) compares photographs of the discharge cathode orifice and radiator taken before and after the test in views (a) through (d). It is apparent that the surfaces of the cathode and radiator have been eroded by ion sputtering. Cross sections of the cathode shown in Fig. A-111(e) and (f) indicate that the material removed is negligible. Figure A-111(f) shows evidence of a coating in the orifice region. The erosion seen is not considered

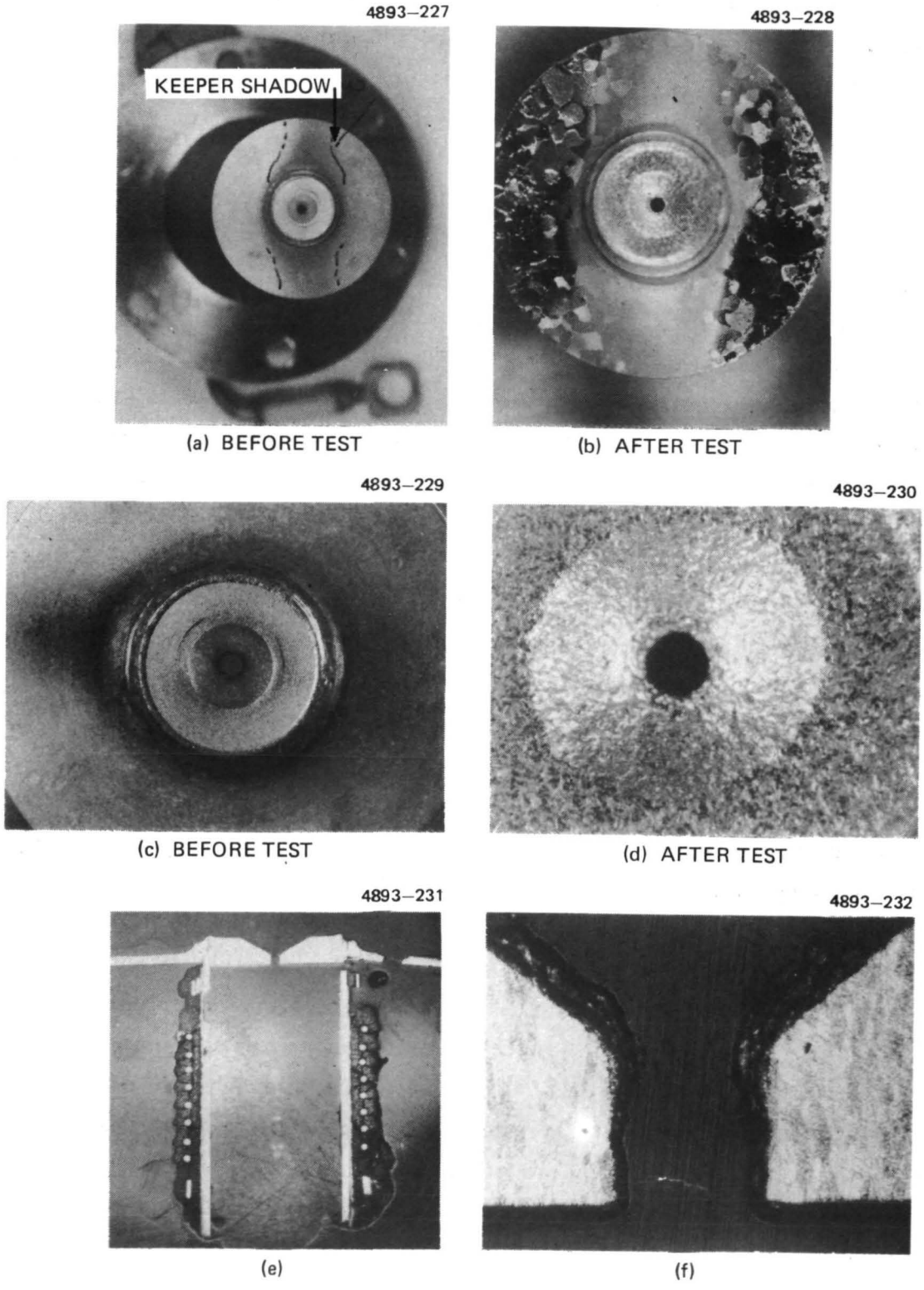

Figure A-111. Cathode radiator and orifice before and after test.

to be a life limiting factor at this time. This cross section does not pass exactly through the cathode center, and consequently determination of the orifice diameter should not be attempted using Figs. A-111(e) and (f). The length of the orifice channel should be to scale, however, and is seen to be only 0.016 in. (0.041 cm), which is slightly smaller than the 0.020 ±0.003 in. (0.051 ±0.008 cm) dimension specified. It is not known whether the initial dimension was low or whether this difference represents the erosion on the cathode face.

The neutralizer cathode orifice dimensions were not modified significantly during the test either. Figure A-112 compares photographs of the neutralizer orifice taken before and after testing in views (a) and (b). Again, some erosion by ion sputtering is evident, and the cross sections shown in Fig. A-112(c) and (d) show the extent of the dimensional changes. As in the case of the discharge cathode, these cross sections should not be used to determine the orifice diameter because the cut is neither parallel to the cathode axis nor does it pass through the orifice center. The orifice length is represented relatively accurately, however, and is seen to be reduced to 0.039 in. (0.0013 cm) by chamfering erosion as seen on the cathode face. The cathode plug still measures the original 0.051 in. (0.129 cm) at the edge. Again, the erosion seen is considered to be tolerable and both cathodes are thought capable of operating at least 10,000 hours more based on orifice wear and assuming that erosion processes are linear with time.

The cathode inserts used in this test were 0.0005 in. (0.0012 cm) thick tantalum foil coated with Baker R-500 triple carbonate mixture. Loss of the barium coating on the insert by evaporation or reaction with the tantalum has been considered a possible life-limiting factor in the operation of hollow cathodes of this type. The downstream edge of the insert was positioned 0.25 in. upstream of the orifice in the discharge cathode and 0.375 in. upstream of the orifice in the neutralizer cathode. It is thought that the operating temperature of the inserts at these locations ranges between 850°C and 950°C. In this temperature range, the rates for evaporation and reaction of barium should provide long life. It was possible to remove both cathode inserts in relatively good

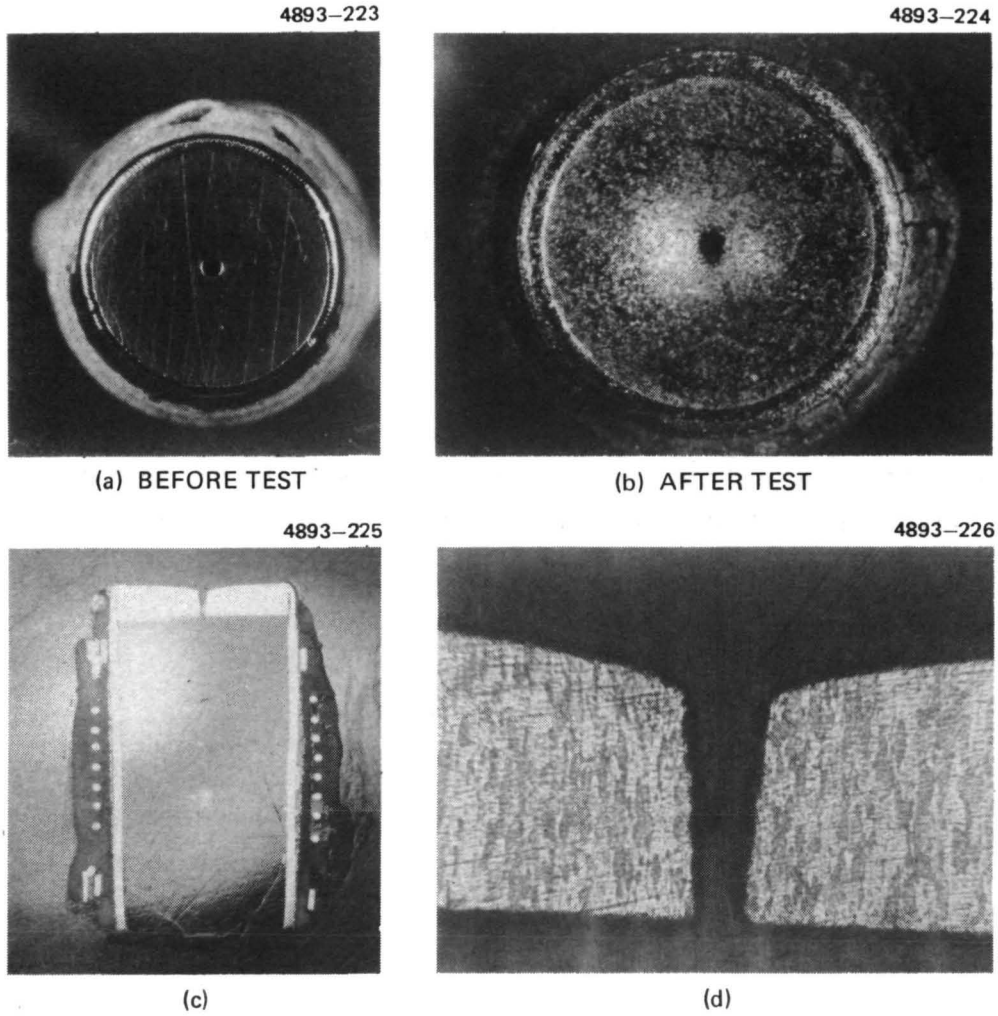

Figure A-112. Neutralizer 701 orifice before and after endurance test.

condition, although the powdery coating, thought to be the triple carbonate (or oxide) material, was extremely fragile and brushed off quite easily. The discharge cathode insert is shown in Fig. A-113 as it appeared on removal and after it was unrolled. The most in downstream edge of the insert appeared "fused" and broke off during the unrolling process. The insert material was neither extremely brittle nor ductile but was "springy" and caution was required to prevent the foild from rolling up again. The weight of the insert was 0.359 g after the test as compared to the initial weight of 0.401 g. No attempt has been made to analyze this weight loss (42 mg) since a whitish, powdery coating, presumed to be a portion of the emissive coating material is found inside the cathode and on the downstream surface of the C-IV flange (see Figs. A-114 and A-115). Moreover, the foil insert design has been replaced by a barium aluminate impregnated porous tungsten material in 800-series thruster designs. This change has been made to improve the quality control and operational control of the neutralizer. Thus, the results of further quantitative analysis relating to the foil design are considered relatively unimportant.

The neutralizer cathode insert was removed in the same manner as the discharge cathode insert. A weight measurement was not attempted here because of the relatively large quantity of the coating that fell off as the insert was pulled from the cathode. Photographs of the neutralizer cathode insert are shown in Fig. A-116. On the basis of the amount of emissive material remaining and the absence of insert embrittlement, it is concluded that considerable additional cathode lifetime could be obtained from the inserts in both the neutralizer and discharge cathodes.

The cathode heaters are required primarily to ignite the hollow cathode discharge. Once ignited, the keeper discharge imparts sufficient power to the cathode to maintain emission. The cathode heaters used in the 700-series design make use of alumina encapsulated tungsten-rhenium wire. The alumina encapsulation is accomplished by flame-spraying the material over the heater. Fabrication of these cathodes in a controlled, reproducible manner has been difficult, and a swaged heater design is being substituted for future thrusters. The cathode heaters

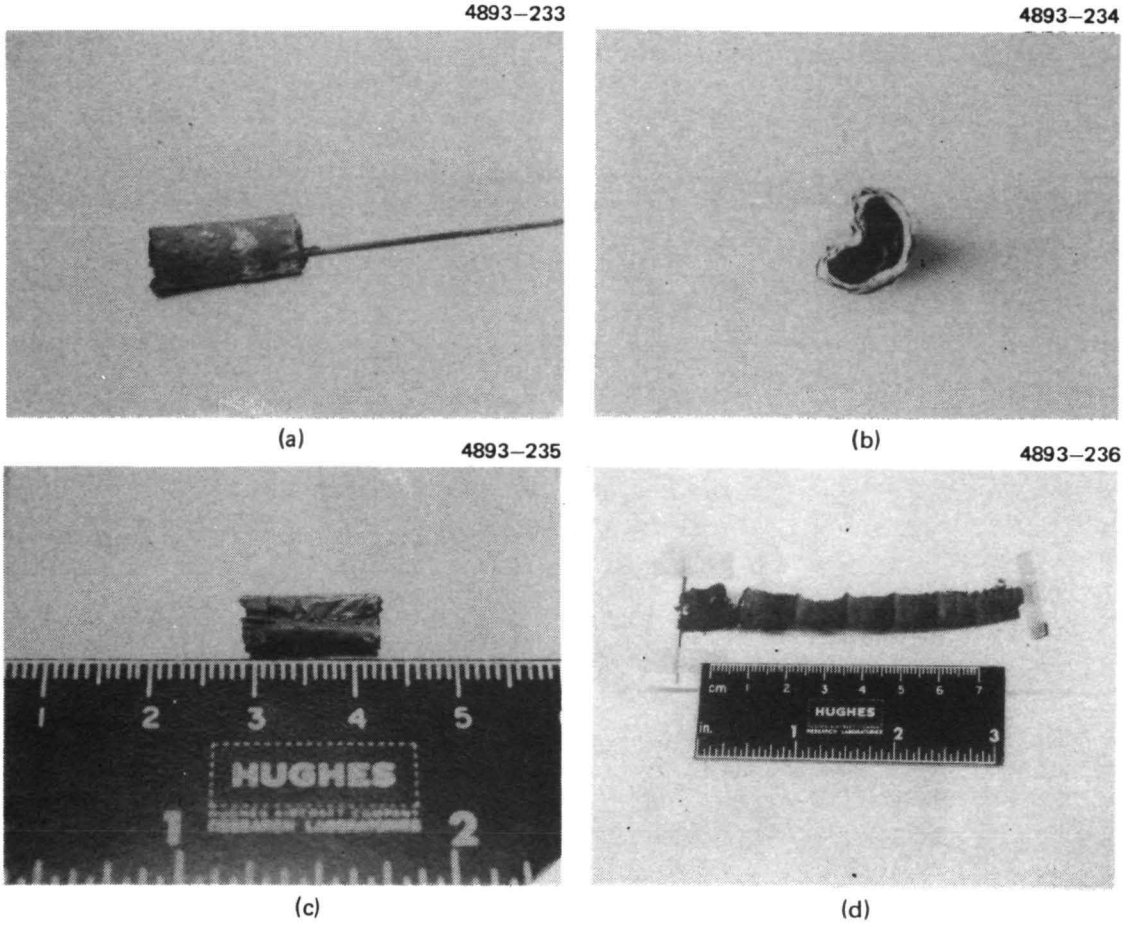

Figure A-113. Discharge cathode insert.

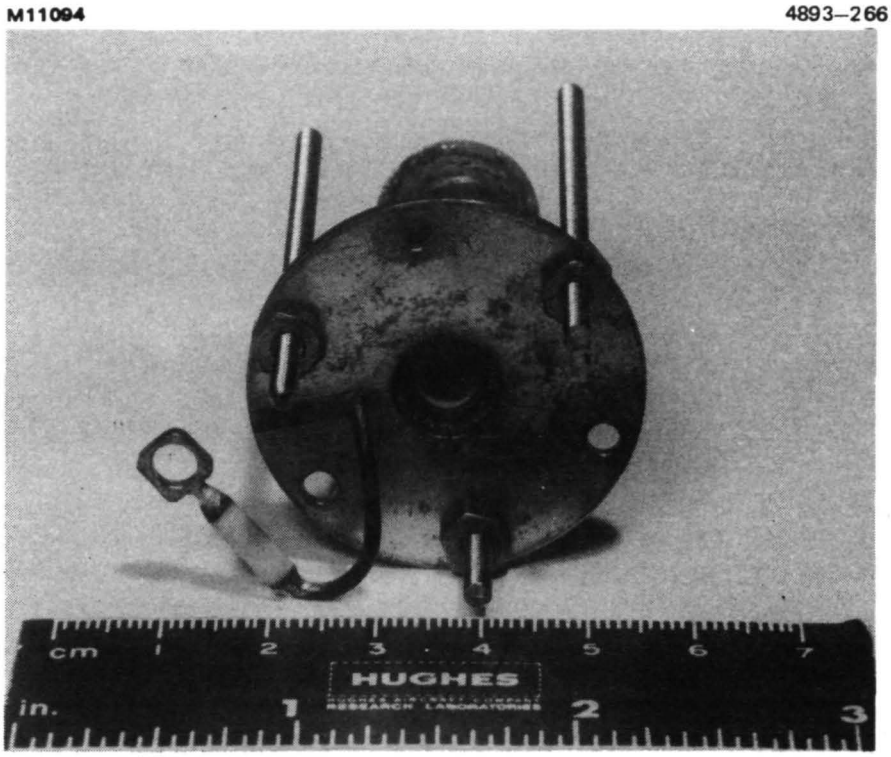

Figure A-114. Cathode assembly. Powder inside cathode is preseumed to be emissive coating from insert.

M11116 4893–268

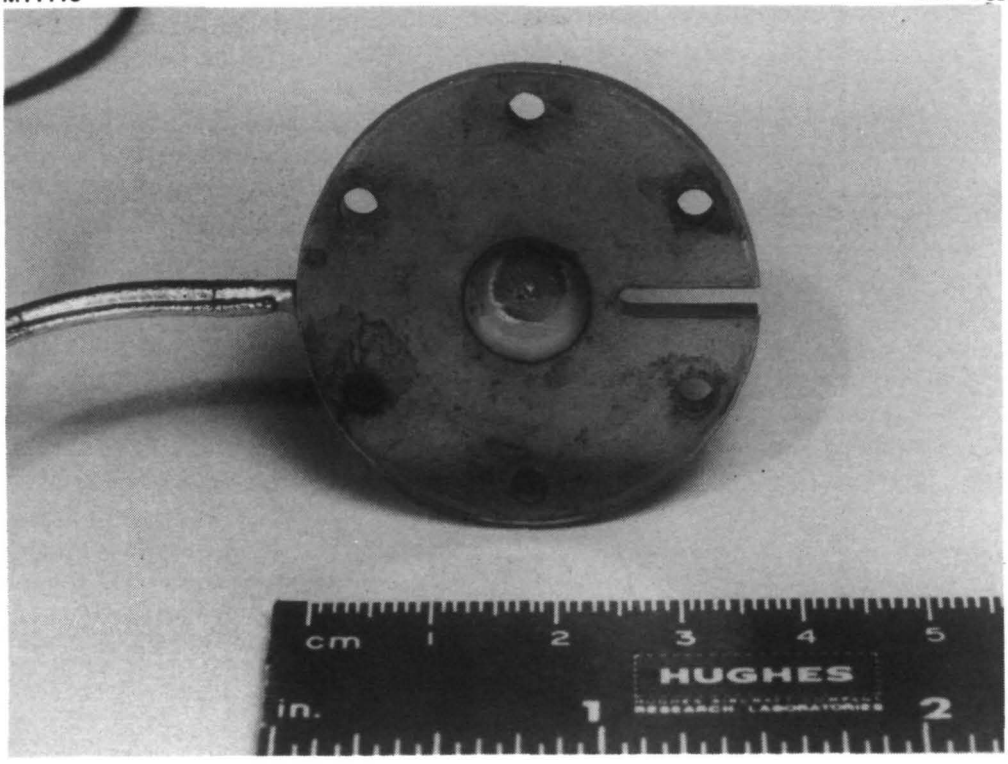

Figure A-115. Downstream surface of C-IV flange.

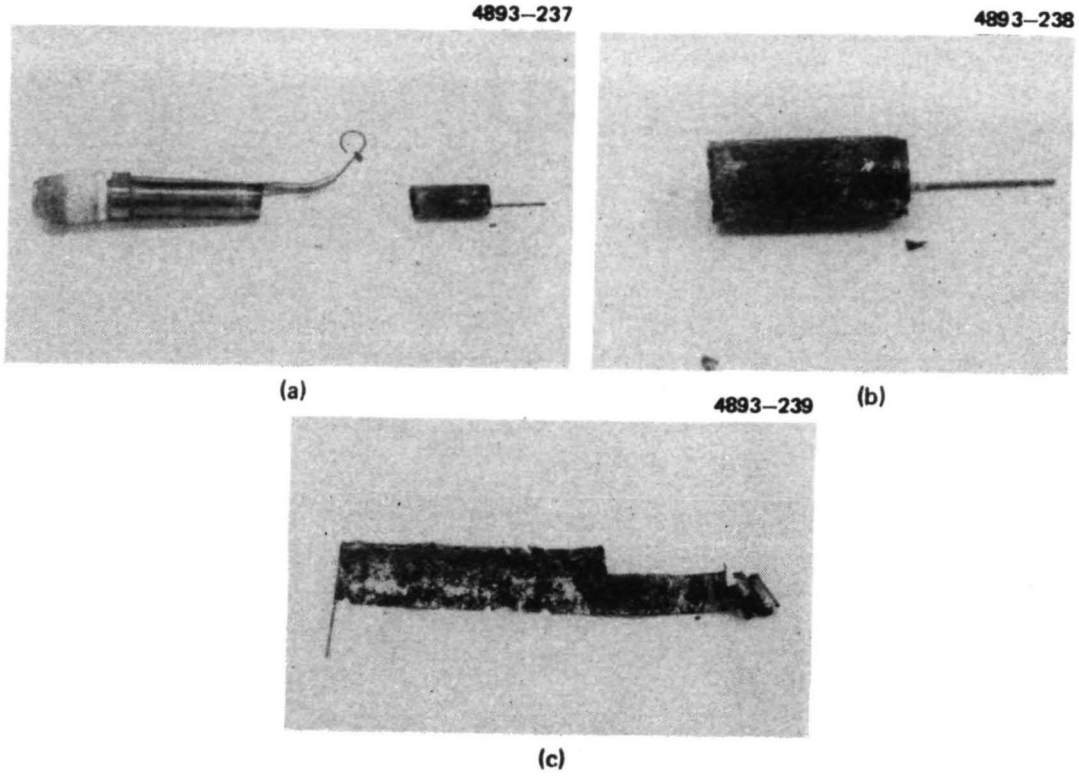

Figure A-116. Neutralizer 701 insert.

used in this test had been carefully selected as the best of a group and exhibited excellent performance throughout the test.

The discharge cathode requires heat shielding to enable the cathode to reach emissive temperature, primarily because the alumina bond between the heater coil and the cathode tube does not provide adequate thermal contact. As pointed out earlier, this heat shield was partially eroded by ion sputtering. It is thought that this ion sputtering is a consequence of operating with a damaged baffle, which permitted high-energy discharge ions to enter the cathode pole region. Figure A-117 shows the extent of the erosion of the heat shield. Three of the five layers have been penetrated (see Fig. A-118), and, if this type of erosion were continuous, the heat shield could probably furnish another 5000 hours of operation without difficulty. Figure A-119 shows the cathode heater with heat shields removed and compares the insulator as seen before and after testing. Notice that although the ceramic material is cracked, there is no loss of material or insulation between heater windings.

The neutralizer heater is shown in Fig. A-120 as seen before and after the test. Note that the cracks seen in the ceramic coating were present even before the test and the many cycles of start-up only increased the cracking somewhat. Both of these heaters performed excellently during the 10,000 hour test, without any change in power requirements.

To summarize, it is concluded that both the discharge chamber and neutralizer hollow cathodes have demonstrated the capacity for 10,000 hour operation without degradation and could be operated for substantially greater periods before wearout.

G. Isolator-Vaporizer Assemblies

There are three isolator-vaporizer assemblies in the 700-series EM thruster design which supply mercury vapor to the discharge cathode (C-IV), the discharge chamber (MIV), and the neutralizer cathode (NIV). The neutralizer isolator has been discussed earlier and will not be

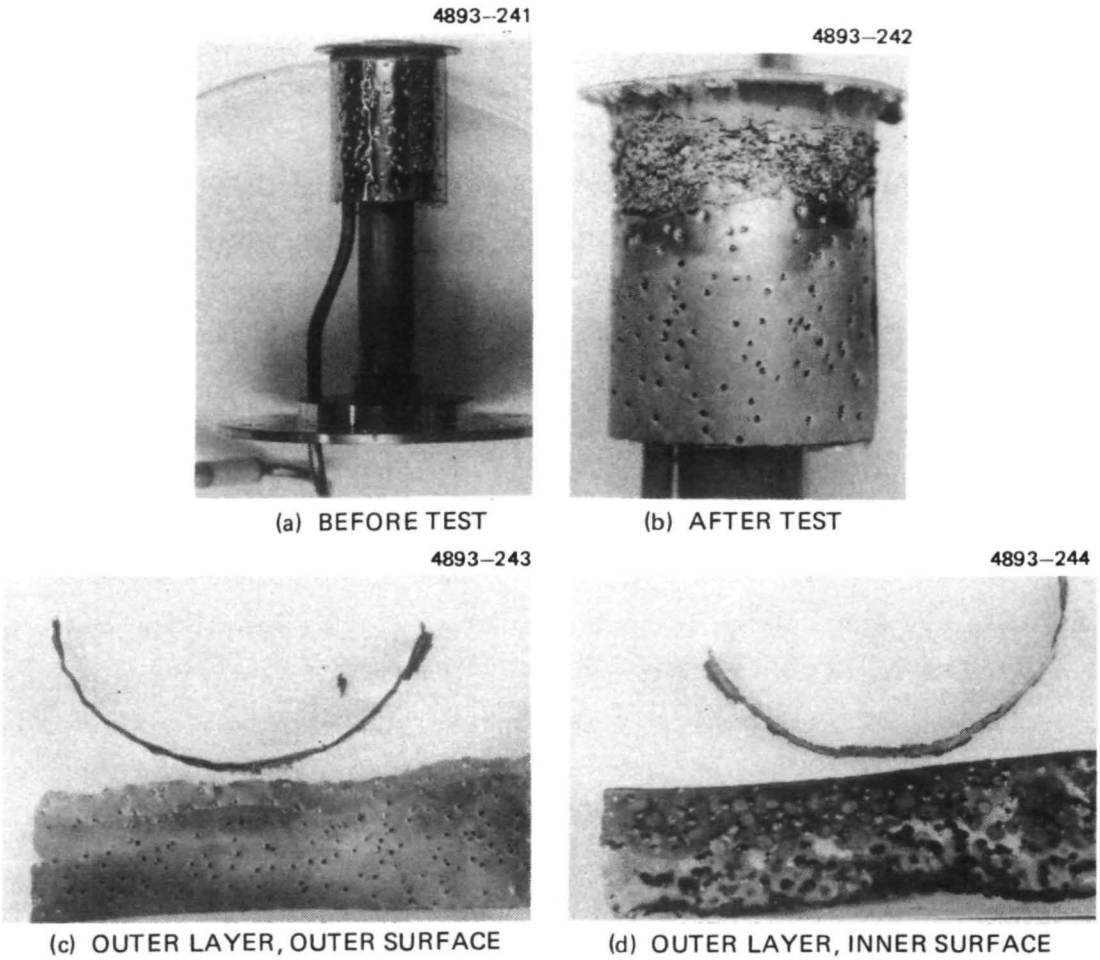

Figure A-117. Cathode heat shield before and after endurance test.

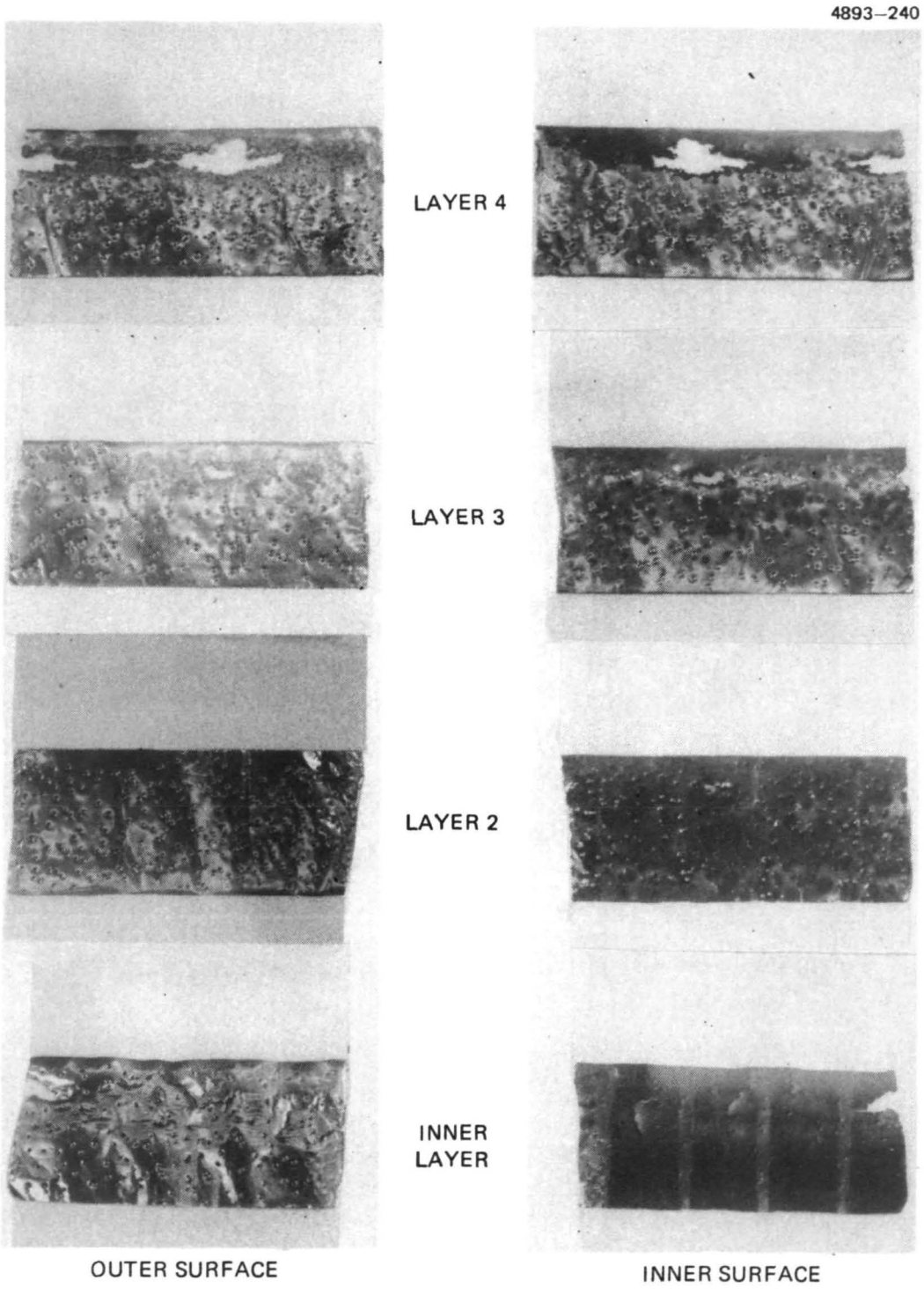

Figure A-118. Cathode heat shield after endurance test.

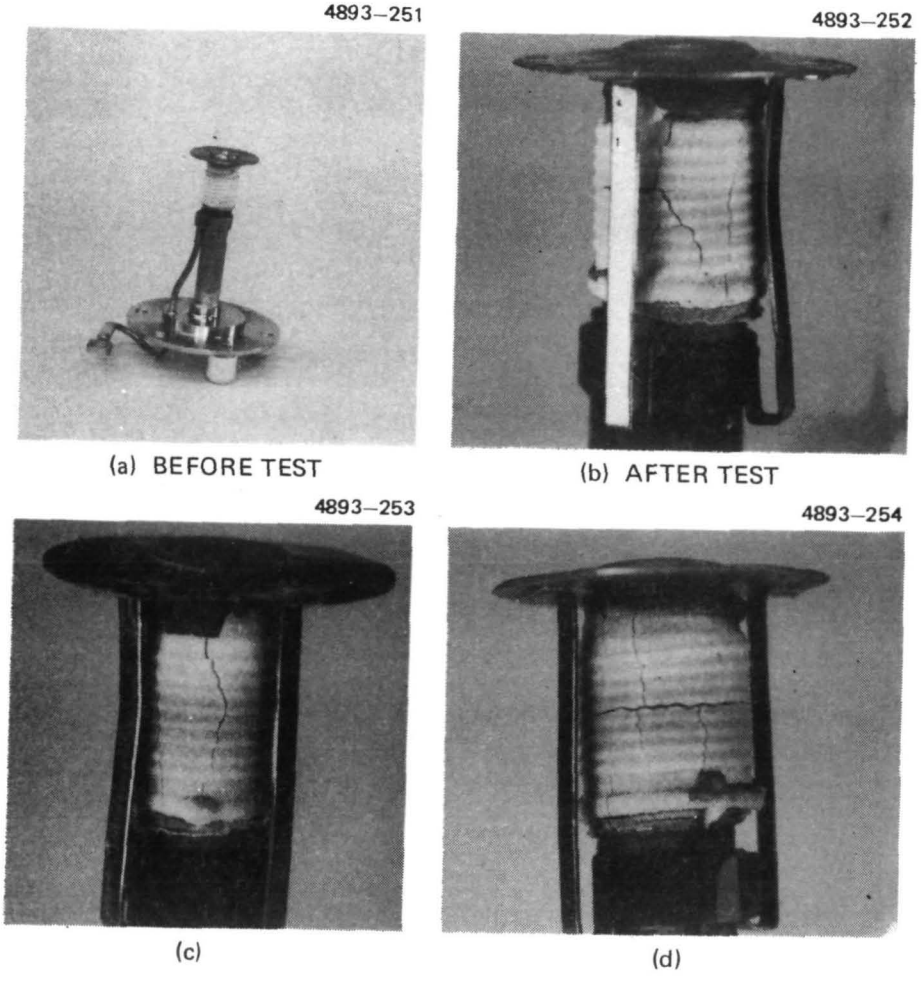

Figure A-119. Cathode tip heater before and after endurance test.

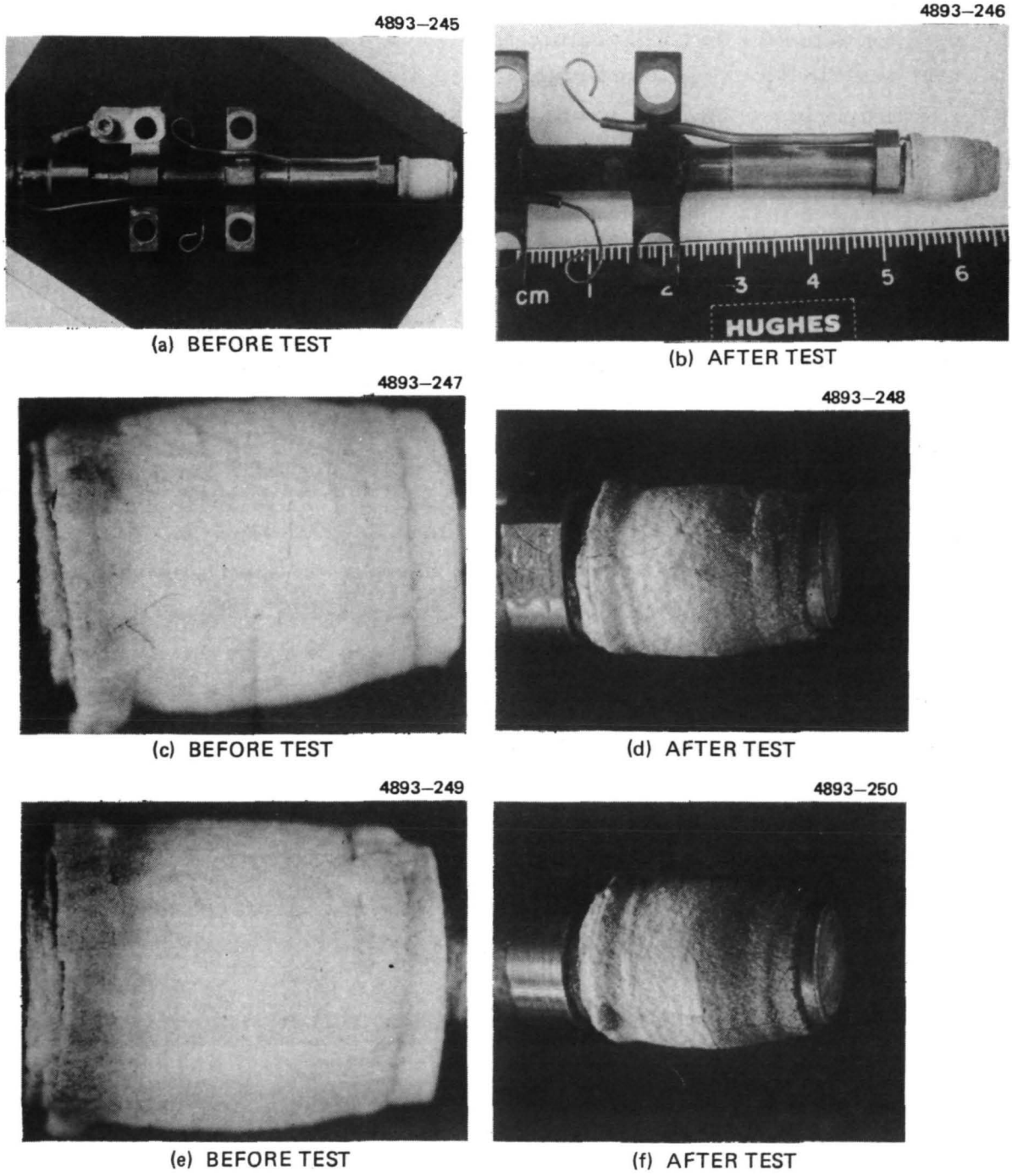

Figure A-120. Neutralizer 701 tip heater before and after endurance test.

considered further here. These assemblies functioned according to specification throughout the test. Except for the NIV, which has conductive deposits on the ceramic insulator of the isolator, the post-test examination disclosed nothing that indicates wear or any form of life limitation. Thus, a problem area that existed earlier in endurance testing of a 400 series thruster design (insulation deterioration in the isolators) has been eliminated in the 700 series design. Photographs of the C-IV and MIV assemblies are included in this section to complete the post-test documentation.

Figure A-121 shows the C-IV as it appeared before the start of the test with the ceramic insulator shadow shields in place. Figure A-122 shows the same view after testing. Note that there is a slight darkening of the entire assembly. One can speculate that this slight deposition could cause insulator deterioration if the insulator were not protected by the re-entrant shadow shields. Figure A-123 shows the bottom side of the assembly; note the deposits in the transition that mates with the cathode assembly. Figures A-124 and A-125 compare the assembly before and after testing as seen without the protective shield that covers the ceramic insulator. Except for a few minute spots the insulator (as in Fig. A-125 shows) is as clean as any new assembly.

Post-test photographs of the MIV assembly are shown in Figs. A-126 through A-128. As in the case of the cathode isolator assembly, there is no evidence of anything that could be considered a life limiting factor. Further analysis of these assemblies is considered unnecessary.

M10066

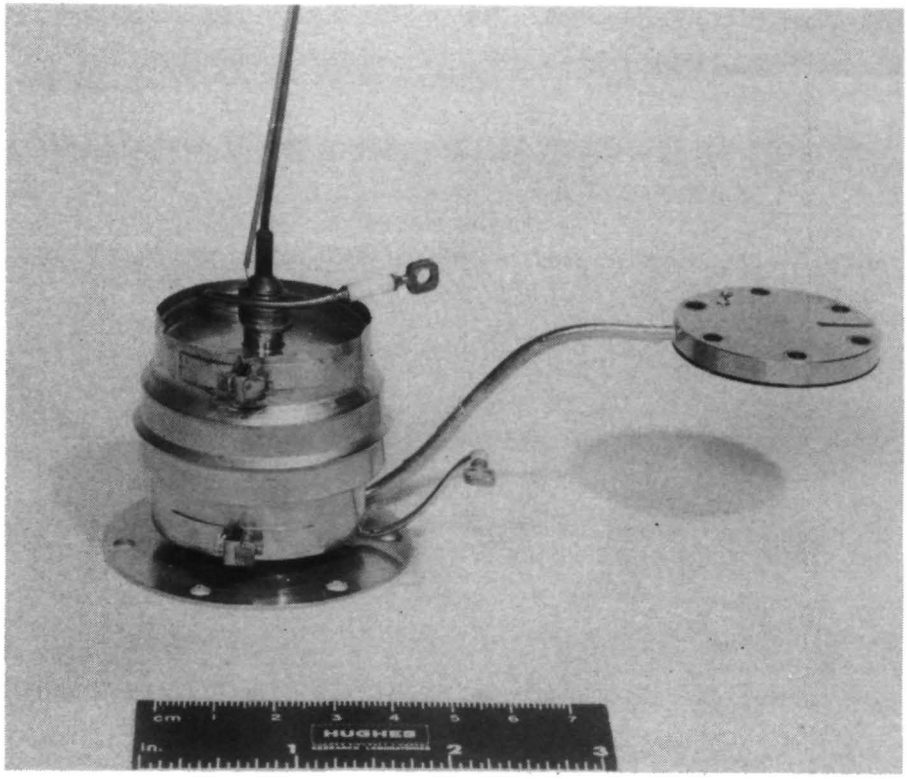

Figure A-121. C-IV before test.

M11118

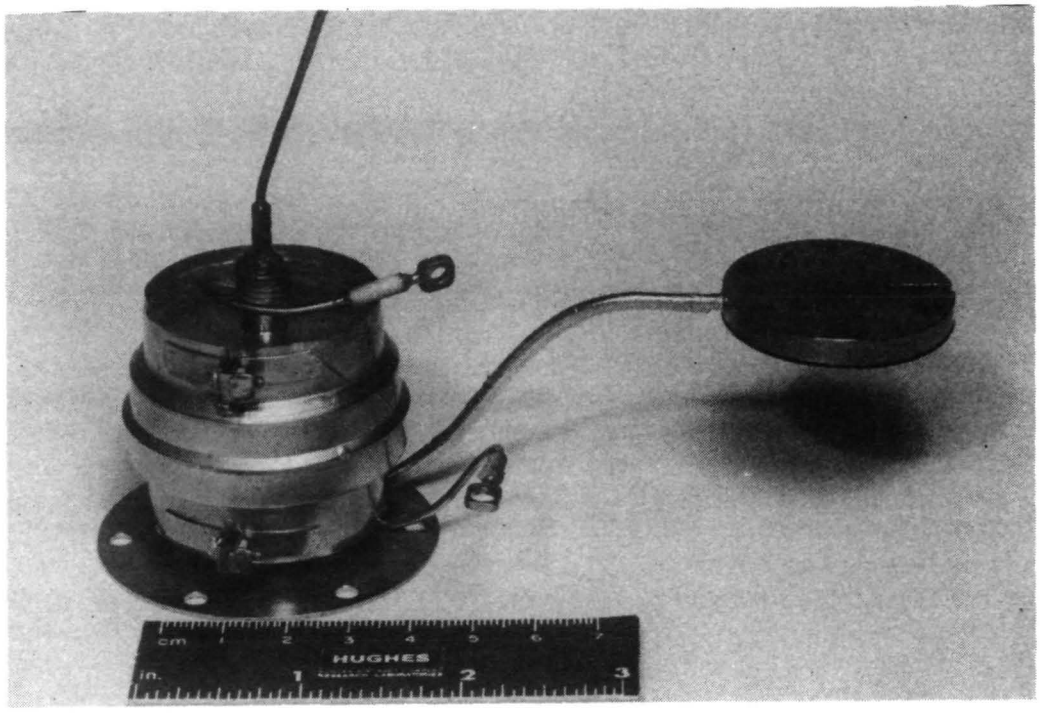

Figure A-122. C-IV after test.

M11117 4893–265

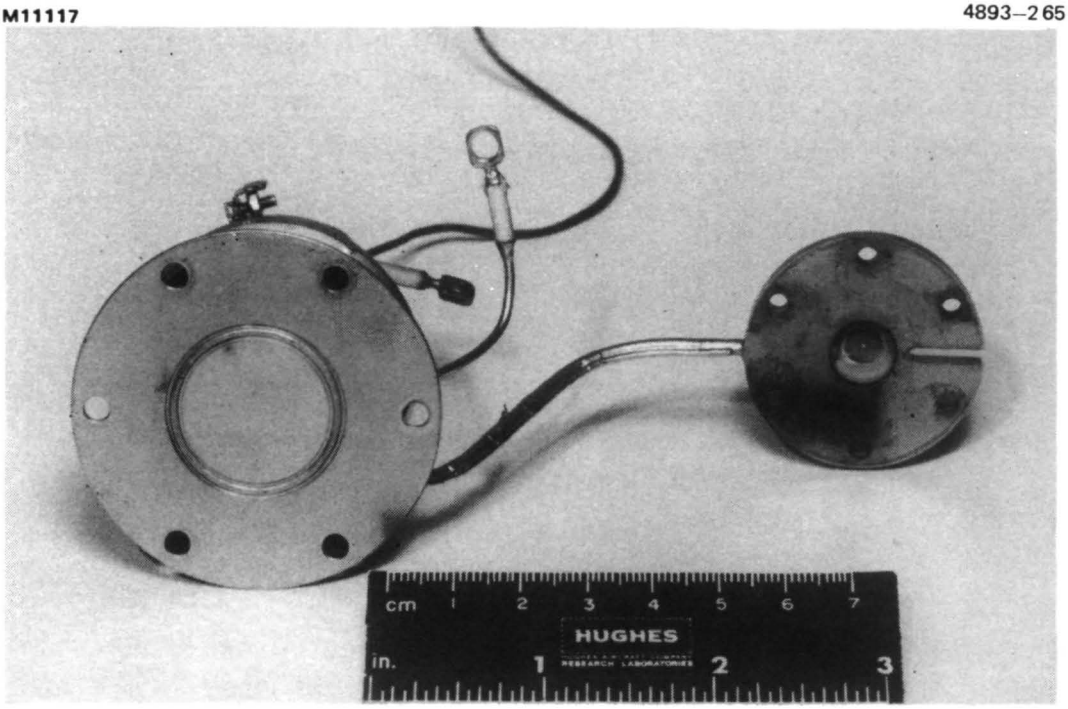

Figure A-123. Bottom of C-IV assembly after endurance test.

4893–255

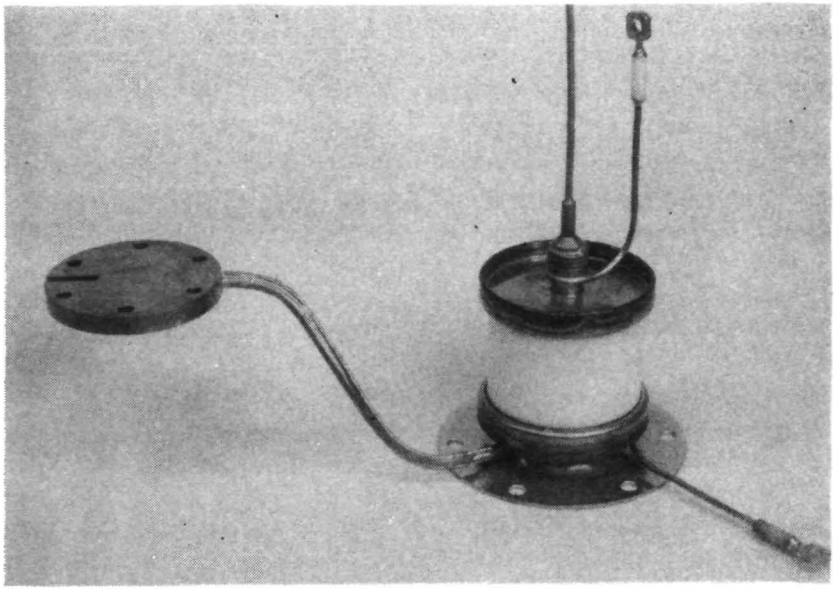

4893–256

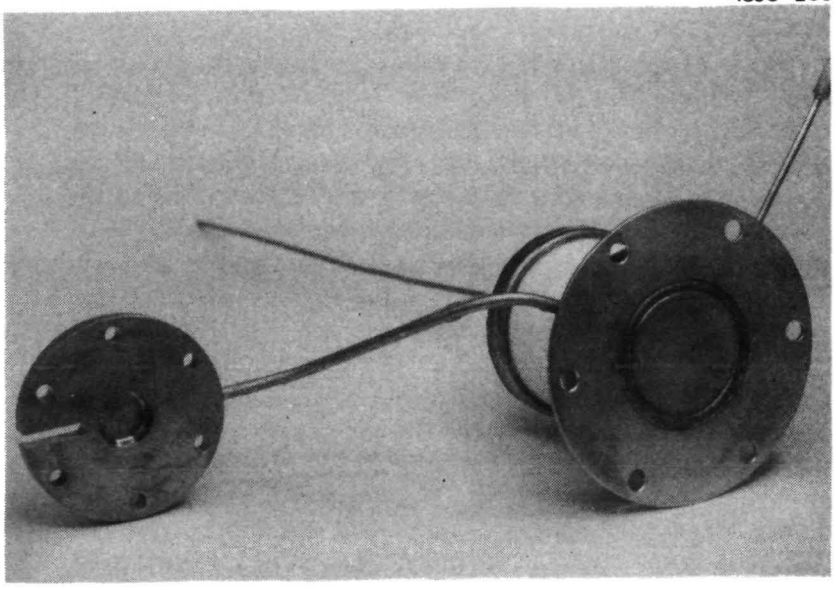

Figure A-124. C-IV before test.

M11143

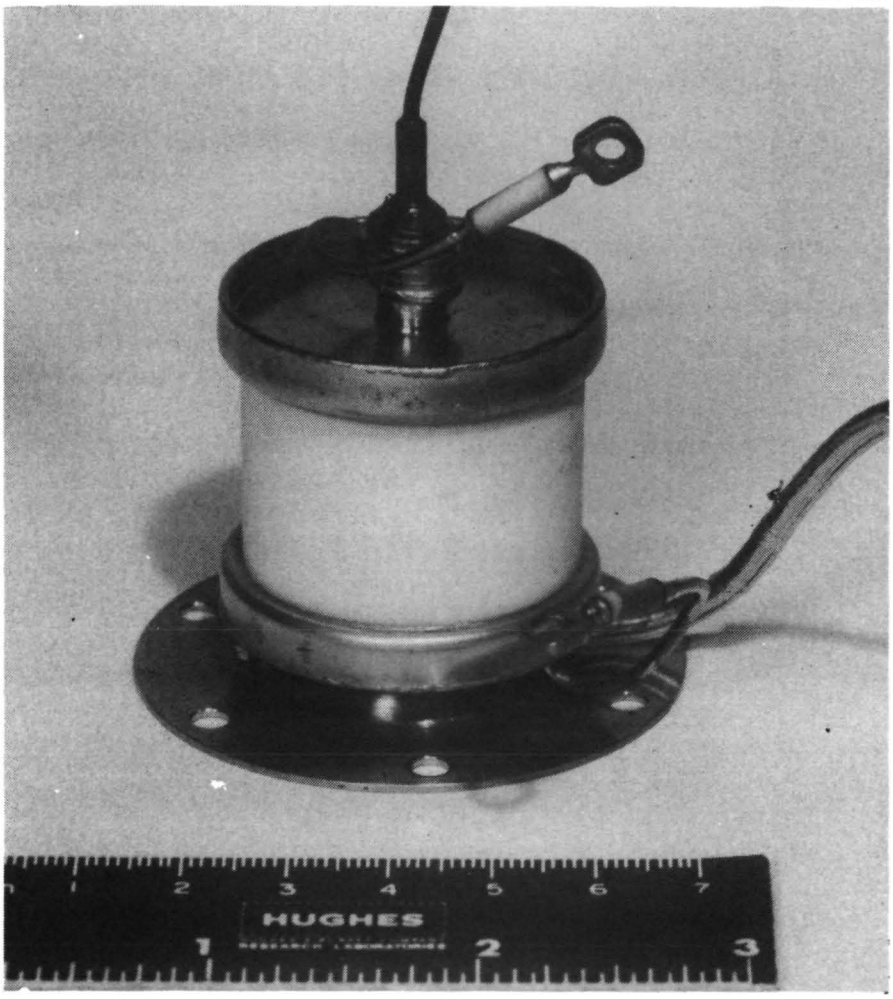

Figure A-125. C-IV after test.

M11114

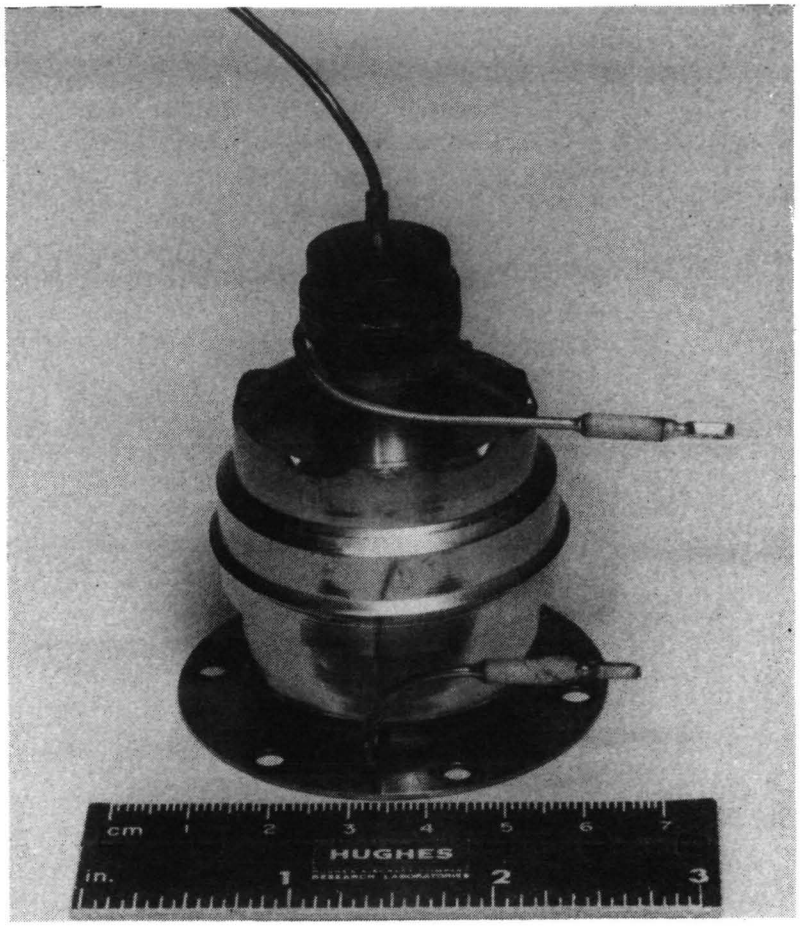

Figure A-126. MIV assembly after endurance test.

M11115

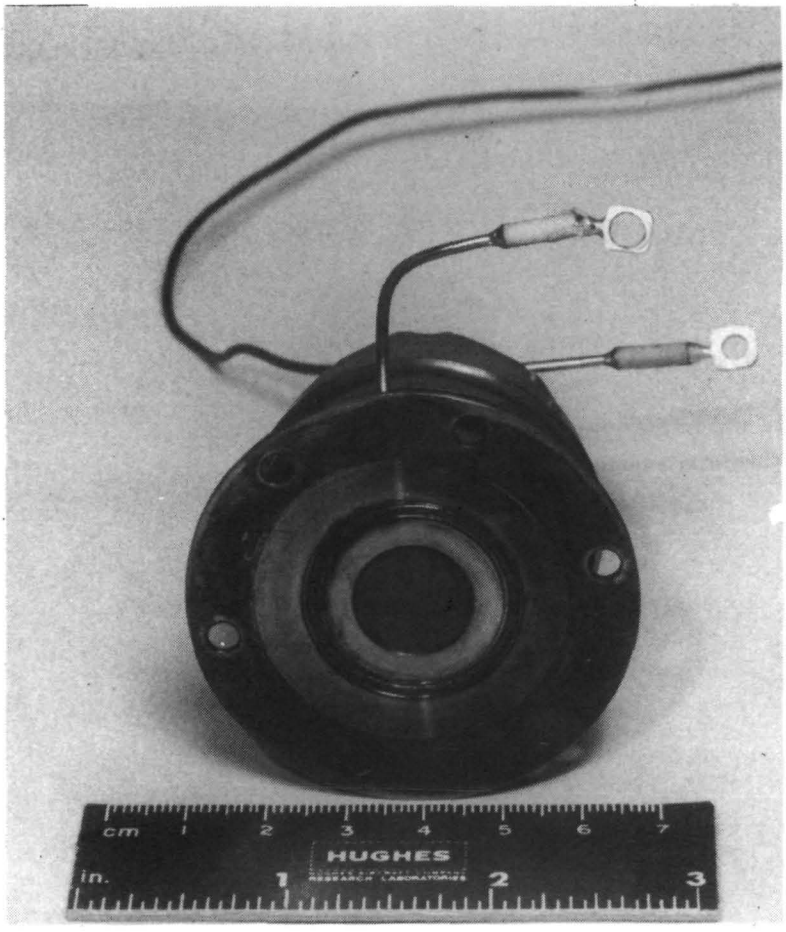

Figure A-127. MIV after endurance test.

MC11144

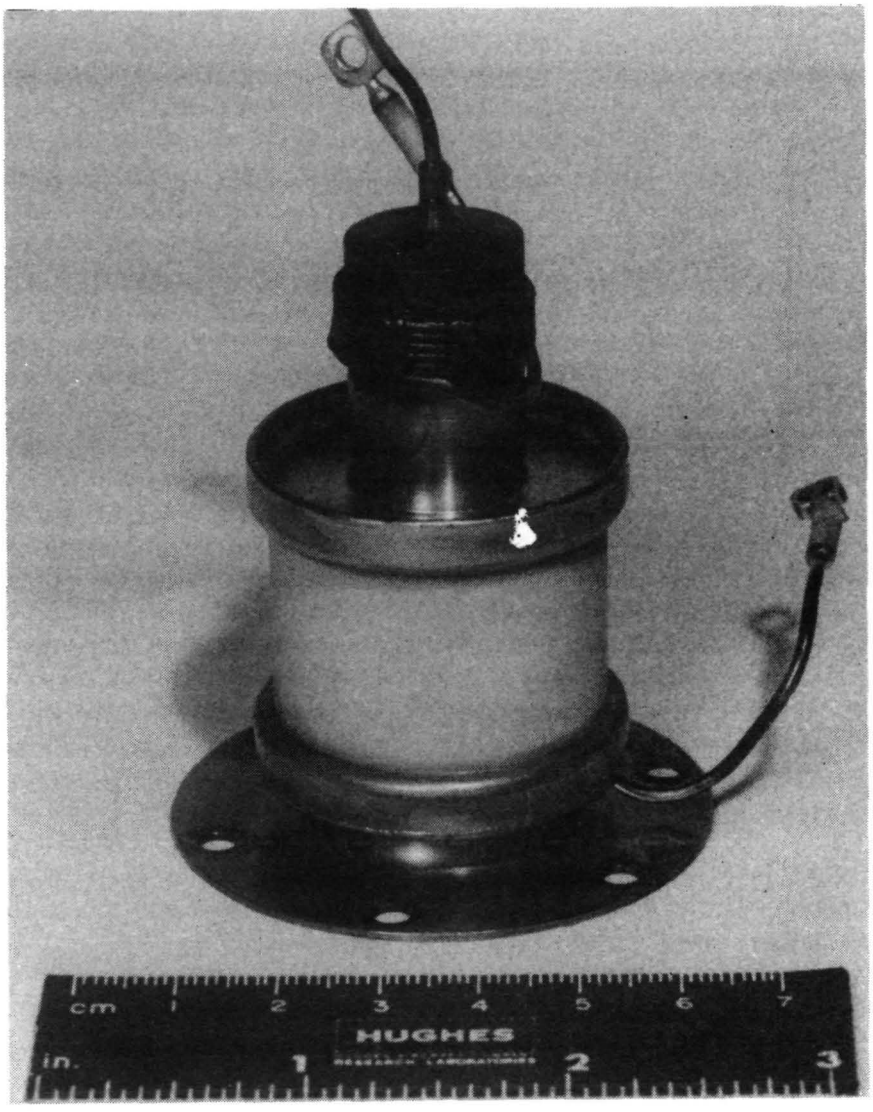

Figure A-128. MIV after endurance test.

REFERENCES

1. H. J. King et al., "Low Voltage 30 CM Thruster," NASA CR-120919, February 1972.

2. A. J. King et al., "Low Voltage 30 CM Ion Thruster Development," NASA CR-134731, October 1974.

3. D.E. Schnelker and C.R. Collett, "30-cm Engineering Model Thruster Design and Qualification Tests, AIAA Paper 75-341, March, 1975.

4. J.L. Power, "Solutions for Discharge Chamber Sputtering and Anode Deposit Spalling in Small Ion Thrusters," AIAA Paper 75-399, New Orleans, La., 1975.

5. M.A. Mantenieks and V.K. Rawlin, "Studies of Internal Sputtering in a 30-cm Ion Thruster," AIAA Paper 75-400, New Orleans, La., 1975.